196(1), 2024

COMBUSTION ENGINES

AVL

Reimagining Motion

For a greener, safer, better world of mobility.

We are driven by a passion to examine the science, mechanics and philosophy of movement. By using all our imagination, creativity and pioneering spirit, we create a world that is climate neutral and one that makes safe, comfortable, green mobility a reality for everyone.

Some will call it a distant dream.
We call it **Reimagining Motion.**

www.avl.com

Due to the dynamic development of machine and vehicle powertrains, the "Combustion Engines" scientific journal, while retaining its historical title, currently publishes works related not only to internal combustion engines, but also other powertrains, including hybrid drives, electric drives and fuel cells.

PTNSS Supporting Members
Członkowie wspierający PTNSS

BOSMAL Automotive Research and Development Institute Ltd
Instytut Badań i Rozwoju Motoryzacji BOSMAL Sp. z o.o

Motor Transport Institute
Instytut Transportu Samochodowego

Institute of Aviation
Sieć Badawcza Łukasiewicz – Instytut Lotnictwa

Automotive Industry Institute
Sieć Badawcza Łukasiewicz – Przemysłowy Instytut Motoryzacji

Sieć Badawcza Łukasiewicz – Poznański Instytut Technologiczny

AVL List GmbH

Air Force Institute of Technology
Instytut Techniczny Wojsk Lotniczych

Military Institute of Armoured & Automotive Technology
Wojskowy Instytut Techniki Pancernej i Samochodowej

Toyota Motor Poland Ltd. Sp. z o.o.

RADWAG Balances and Scales
RADWAG Wagi Elektroniczne

MS Mechatronic Solutions Group

FOGO Sp. z o.o.

COMBUSTION ENGINES

A Scientific Magazine

2024, 196(1)

Year LXIII

PL ISSN 2300-9896
PL eISSN 2658-1442

Publisher:

Polish Scientific Society of Combustion Engines
60-965 Poznan, pl. M. Skłodowskiej-Curie 5, Poland
tel.: +48 61 6475966, fax: +48 61 6652204
E-mail: sekretariat@ptnss.pl
WebSite: http://www.ptnss.pl
Papers available on-line: http://combustion-engines.eu

Contents

Publisher:

Polish Scientific Society of Combustion Engines
60-965 Poznan, pl. M. Sklodowskiej-Curie 5, Poland
tel.: +48 61 6475966, fax: +48 61 6652204
E-mail: sekretariat@ptnss.pl
WebSite: http://www.ptnss.pl

Subscriptions
Send subscription requests to the Publisher's address.
Cost of a single issue PLN 100.

Preparation for print
ARS NOVA Publishing House
60-782 Poznan, ul. Grunwaldzka 17/10A

Circulation: 60 copies

Printing and binding

Zakład Poligraficzny Moś i Łuczak, sp. j.,
Poznań, ul. Piwna 1

The journal is under the patronage of the Transport Committee of the Polish Academy of Sciences

The journal is registered and listed in the Polish and international database

Papers published in the
Combustion Engines
quarterly receive 70 points as stated by the Notification of the Minister of Science dated 5 January 2024.

Declaration of the original version
The original version of the Combustion Engines journal is the printed version.

Cover
I – 2.4-litre twin-turbo four-cylinder diesel Mitsubishi engine *(www.drive.com.au)*; background *(light lines background, motion concepts, abstract brown – www.peakpx.com)*
IV – Electrically assisted turbocharging *(link.springer.com)*

Article citation info:
Wróbel R, Sroka Z, Sierzputowski G, Dimitrov R, Mihaylov V, Ivanov D. Driving protocols: the possibility of using routing protocols in autonomous transport. Combustion Engines. 2024;196(1):3-9. https://doi.org/10.19206/CE-170418

Radosław WRÓBEL
Zbigniew SROKA
Gustaw SIERZPUTOWSKI
Radostin DIMITROV
Veselin MIHAYLOV
Daniel IVANOV

Combustion Engines
Polish Scientific Society of Combustion Engines

Driving protocols: the possibility of using routing protocols in autonomous transport

ARTICLE INFO

Received: 11 May 2023
Revised: 28 July 2023
Accepted: 3 August 2023
Available online: 6 November 2023

Removing the human factor from transport (in the direct sense) is still a plan, reaching into the future. However, this plan does not require so much imagination – autonomous vehicles can already be found on the roads. Currently, they are not only autonomous but also independent, i.e. decisions about traffic parameters are made in the vehicle. In the future, with more autonomous vehicles, there will be a need to connect them with a communication network, which will eliminate a number of telematic problems. It remains an open question how to make this network? Is it based on the modern Internet network? What and which data will be necessary to achieve the "right relations" between autonomous vehicles (hosts of network)? The article presents one aspect of the mentioned problem; the amount of data generated by an autonomous vehicle is presented in light of the processing capabilities of modern ICT systems.

Key words: *autonomous vehicle, transport protocols, routing protocols, transport of the future, telematics*

1. Introduction

The automobile market is facing (as it typically does) new challenges and its evolution is accelerating. One of the new challenges is the idea of autonomous vehicles. The main aim behind attempts to replace human drivers with machines is to minimize or even eliminate human error (but still meet emission standards [2]). According to WHO, 1.25 million people die annually in road accidents around the world. While full statistics on road accidents are not available in developing countries, data show that over 80% of collisions and accidents in developed countries are caused by humans [2]. A key requirement for a driver is to have high mental ability to accurately evaluate the situation on the road and make responsible decisions. Motor skills are equally important, as they allow the precise execution of the intended maneuvers. Research indicates that road accidents are mainly caused by young drivers (aged below 25) and by people older than 60 years [3]. However, the reasons for the accidents were different for the two groups: the older people have lowered motor skills, while the younger people show impulsive behavior, aggression or even a pathological fear of driving a vehicle. Although the poor condition of roads and vehicles is (often) mentioned as the main cause of accidents and collisions, research shows that such events are most frequently caused by an inappropriate response from the driver. The problem of high car accident rate can be solved by increasing the skills of the driver (requires stricter traffic regulations), improving the condition of the infrastructure, validating vehicles or delegating control over the vehicle to a unit which is capable of minimizing the number of driving errors, i.e. by fully automating the driving process (the driver only defines the destination).

2. Last-mile transport in Personal Rapid Transit networks

Over the years, scientists and engineers have been pursuing options to shift the responsibility for driving a car from humans to machines. The idea dates back to the 1920s [2]. The motivation behind the early attempts made in the U.S. has not changed – to improve safety and reduce the number of fatal accidents. Currently, car manufacturers compete in developing self-driving technologies in order to gain prestige which allows them to draw specific clients and offer them services not offered by the competition.

The first automated guided vehicle (AGV) was the Guide-O-Matic, which was able to follow a wire path and which was constructed in the 1950s by Arthur „Mac" Barrett, owner of Barrett Electronics [5]. Another modification is an inertial navigation system (INS) with reference points, coordinates, a gyroscope and sensors for detecting the position – following the idea that a modification of the route consists of the modification of the reference points. Despite making the impression of intelligence, such vehicles still only move along a predefined track and are not able to independently plan actions and make autonomous decisions. They perform carefully planned movements in a limited space, owing their increased popularity largely to high efficiency and precision, as well as to the fact that they can be used in working conditions harmful to humans.

The PRT system is a modern type of urban transportation (typically electric). Its basic elements are small vehicles capable of transporting a limited number of passengers and moving autonomously in a designated aerial space or in a dedicated traffic lane [5, 6].

In its current form, PRT can provide transport in an on-demand mode or supplement local transportation systems in which no intermediate points exist between the starting point and the finish point and in which the infrastructure comprises redundant tracks, allowing an optimal route choice depending on the conditions.

In September 2019, an autonomous bus manufactured by EasyMile transported passengers to the local ZOO in Gdansk, Poland, as part of the Sohjoa Baltic program titled: "Transformation to ecological and autonomous last-mile

public transport in the Baltic region" [8]. This experiment may be considered the first widely available public PRT application in Poland. For passenger safety, the operator present in the vehicle was required to react in case of problems, and the bus moved along one, dedicated lane of Karwieńska street – the lane was closed to other vehicles.

Although all vehicle manufacturers agree about the CASE standard (connected, autonomous, safe, and efficient – the last one being frequently understood as electric) they rather disagree on the technical details of this system. The 2019 CASE agreement was signed by Aptiv, Audi, Baidu, BMW, Continental, Daimler, FCA, HERE, Infineon, Intel and VW [16]. The above car manufacturers work independently, focusing on building advantage over their competition and providing their cars with cutting-edge equipment. However, their ultimate goal will be to develop a uniform and complex system that will be implemented by all of the manufacturers and which will serve as a basis for designing equipment used in autonomous vehicles. Failure to adhere to such defined standards will result in a significantly increased road-accident risk.

The Society of Automotive Engineers (SAE) identifies six levels of driving automation, with level 0 representing no driving automation and level 5 – full driving automation [2]. Levels 1–4 are intermediate, with gradually increasing driver support during maneuvers and analysis of the situation on the road and around the vehicle.

Level 3 raises the greatest controversy, as numerous experts believe that it should be completely eliminated. In this level, the vehicle completely controls the surrounding area and moves with no need for the attention of the driver. The controversy is related to the fact that the car may inform the "passenger" about the need to regain control of the vehicle, and if the human using the "autopilot" and not focusing on the road is suddenly interrupted, they may pose a threat to themselves and other road users. Modern trucks frequently meet the requirements of level 2 – they offer adaptive cruise control and lane centering on highways. They are also able to connect in a convoy using the V2V technology in order to continue a part of a journey synchronously. Trucks in such convoys travel with constant speeds and with fuel consumption reduced by approximately 4–5 liters per 100 km [18], resulting in higher efficiencies, lower operating costs and lower emissions of harmful gasses into the atmosphere. Although the 2016 European Truck Platooning Challenge tests of autonomous synchronized driving in a convoy were successful [2], the main goal of the international EU-supported ENSEMBLE program (introducing truck platoons to selected European public roads before the end of 2021) has not yet been accomplished. The remaining problem is for truck manufacturers to agree on standards which would allow the safe and effective multi-brand platooning.

Over the years, scientists and engineers have been pursuing options to shift the responsibility for driving a car from humans to machines. The idea dates back to the 1920s [2]. The motivation behind the early attempts made in the U.S. has not changed – to improve safety and reduce the number of fatal accidents. Currently, car manufacturers compete in developing self-driving technologies also for prestige which allows them to draw specific clients and offer them services not offered by the competition. The first automated guided vehicle (AGV) was Guide-O-Matic, which was able to follow a wire path and which was constructed in the 1950s by Arthur „Mac" Barrett, owner of Barrett Electronics [5].

3. Routing Protocols in Transport ("Driving Protocols")

The topology of transportation roads can be compared to a map, in which "streets" represent physical communication paths (routes), "signs" represent the result of the involved protocols (routing), and "addresses" represent a particular location. From the perspective of information technology, the analogy to the global network (the Internet) is eclectically similar, if each autonomous vehicle (AV) is understood to be in fact a host. Each device connected to the global network needs to acquire a unique IP address, and the rapid growth of the number of devices operating within the Internet of Everything (IoE) necessitates the use of the IPv6 protocol as the communication tool.

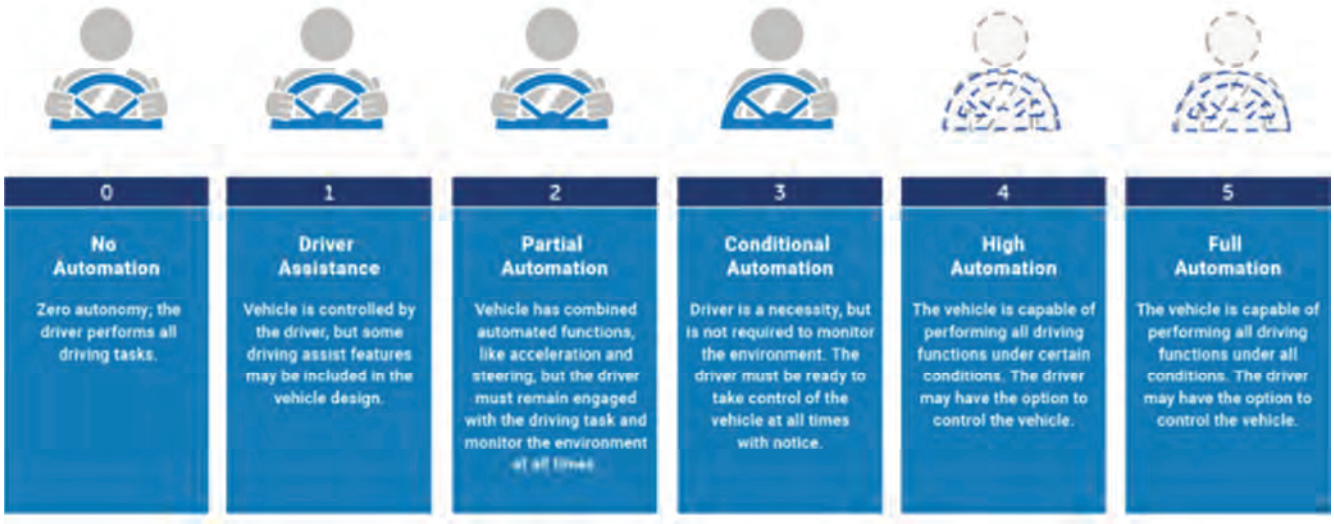

Fig. 1. Driving automation levels as defined by SAE [17]

In order for AVs to reach global markets on a mass scale, the number of available IP addresses should be sufficient both at present and in the future perspective. The IPv6 is additionally advantageous in that it allows the connected devices to be configured automatically, thus effectively limiting the number of potential mistakes and enabling an unambiguous identification of each machine [19].

Each AV regularly generates a finite portion of data, which are then processed locally and later sent to the server for interpretation. The acquired information can be classified by its usage method as:

- technical data
- crowdsourced data
- personal data.

The technical data, acquired from the sensors and preprocessed in order to remove faulty or incomplete electronic measurements, allows the vehicle to analyze its surroundings. The implementation of artificial intelligence which identifies the source of each piece of information and fuses the information in real time into one coherent and valuable unit will allow highly "intelligent" (autonomous) vehicles which will be capable of making "conscious" decisions on the road.

The crowdsourced data are acquired from the collectively shared information and will allow optimal planning of the occupied space and effective management of the road traffic. To date, such data were collected only from measurement points installed along the road infrastructure, which thus needed modification. The typical solutions include induction loops, vision cameras and microwave devices. Additional data, albeit less reliable, are also collected from commercial services based on sensor readings from fleet vehicles. Additional sensors installed in autonomous vehicles will allow the acquisition of very precise data directly from the machines. As a result, the vehicles will be able to communicate with each other in a complex, ant-robot manner, following the concept of miniature, intelligent electronic devices which act as autonomous individuals but cooperate to accomplish a set goal [20].

In the context of AVs, the above concept will lead to full cooperation between the machines and to the definition of a hierarchy between the road users (hosts). This phenomenon will be of particular importance in the transition period, when AVs will have to coexist with other "less intelligent" machines. The analysis of data incoming from other road users will allow a reduction in the number of dangerous road accidents.

Personal data are packages of information most closely related to the vehicle user. In the first stage, they will serve only to identify the user, and in the next stages – also to increase the travel comfort by means of personalization, such as selecting the preferred route or following further points on the agenda of the user.

The above solutions imply a substantial amount of data generated by an AV. It is impossible for the vehicles to exchange complete information within the autonomous system. In the case of "conscious transport" (in which AVs know about each other by exchanging information), the vehicle should be treated as a (mobile) host, (not a node!) in an ICT network. The problem of routing between hosts has already been solved in IT. A number of the so-called routing protocols have been designed to allow the exchange of information between nodes (intermediate points) following the "best" path (route) between two points. The intermediate points use the routing protocol to indicate the optimal path for the host (vehicle). The protocol running in the node calculates the "best path" by including a number of variables, such as distance, traffic intensity, blockades or priorities. The following is a short description of the three most popular open-source protocols: RIP, OSPF and EIGRP.

Routing Information Protocol

The first version of Routing Information Protocol (RIP) is described in document RFC 1058, which dates back to June 1988 [10]. To date, new versions have been published: RIPv2 – the second version, working with IPv4 [22] and RIPng – a version dedicated to IPv6 [24]. RIP selects the route based on the best path. In the case of RIP, the best path is the one with the smallest hop count (this metric is calculated with the graph-based Dijkstry algorithm – the best path has the smallest count, as it requires the smallest number of hops – intersections).

OSPF protocol

OSPF (Open Shortest Path First) is a protocol more complex than RIP – it is used in autonomous systems operating in a medium having different bandwidths (road capacity). The first document describing the OSPF protocol was published in 1989. It is currently available in two versions: OSPFv2 for IPv4 [21] and OSPFv3 for IPv6 [10]. The protocol divides the network of local routers into areas, i.e. groups of nodes, and employs the flooding technique to inform the neighbors (nodes) about changes in the topology. Each node (router) in the OSPF network maintains a routing table for its area. Border routers – which are part of one area but neighbor another area – additionally have the routing table for the neighboring area. The OSPF protocol uses an additional designated router to store all local routes.

EIGRP protocol

EIGRP (Enhanced Interior Gateway Routing Protocol) is a hybrid protocol which combines the features of the above-described protocols. Therefore, it is theoretically the most "intelligent" protocol of the three. Unfortunately, its more advanced algorithm causes this protocol to use more node resources. EIGRP was developed by Cisco, and its description can be found in RFC [13]. It employs a highly specialized transport protocol called RTF (Reliable Transport Protocol). The EIGRP algorithm searches for the best path to the destination using a mathematical function with variables such as bandwidth, reliability, delay, and load (in terms of transport: road capacity, current traffic intensity, accident statistics, and speed statistics, respectively).

4. Estimation of computing power demand from PRT

To analyze the amount of continuously flowing data generated by a vehicle, Intel "froze" their static fragment. This approach allows the application of current knowledge

to the theoretical investigation of the problem. Based on the average time spent in the car by the user, Intel predicts that a single autonomous vehicle will generate approximately 4 TB of data [11].

The Mobileye autonomous vehicle has been provided with 12 cameras, 6 lidar sensors, 6 radars, a sonar and a GPS receiver, and the total amount of the generated data is provided in Table 1.

Table 1. Theoretical amount of data (optimistic variant) generated by Intel Mobileye

Optimistic variant – vehicles generate a minimum expected amount of data				
Source	per sec	[–]	Data sent over 1.5 h [MB]	Data sent over 1.5 h [GB]
Cameras	240	MB	1296000	1265.63
Radar	60	kB	316.41	0.31
Sonar	10	kB	52.73	0.05
Lidar	60	MB	324000	316.41
GPS	50	kB	263.67	0.26
				SUM TOTAL: 1582.65 GB

Table 2. Theoretical amount of data generated (pessimistic variant) by Intel Mobileye

Pessimistic variant – vehicles generate a maximum expected amount of data				
Source	per sec.	[–]	Data sent over 1.5 h [MB]	Data sent over 1.5 h [GB]
Cameras	480	MB	2592000	2531.25
Radar	600	kB	316.06	3.09
Sonar	100	kB	527.34	0.51
Lidar	420	MB	2268000	2214.84
GPS	50	kB	263.67	0.26
				SUM TOTAL: 4749.96 GB

Even in the optimistic approach, in which the amount of data is three times lower than in the pessimistic scenario, the 3 trillion vehicles estimated to be on the roads in 2050 will generate at least 12 yottabytes of information per day – a value comparable to the content of the entire Internet. The above estimation indicates a necessity for implementing driving protocols that will enable fully automated autonomous transportation.

The decision can be postponed in waiting for improved transmission medium and server solutions to be ready to accommodate the above-mentioned load. However, this progress will simultaneously apply to the equipment installed in intelligent vehicles: engineers will hesitate to implement additional modules as they will be expected to generate increased amounts of data. The potential of AVs can be fully utilized only if the scalability of this solution is increased, as optimization seems to be the missing link on the road to the global implementation of this technology [4]. Unfortunately, the current problems include the need to define which sources of data the machine will need at a particular moment or which information will enable the effective management of transportation. Therefore, all available data must be initially acquired to enable efficient management of the tested AV fleet [7]. The properly identified transmission priorities will allow a decision on which information should be sent to the server cyclically as the car is in motion, and which information can be sent later. The data for immediate transmission include GPS coordinates which allow the analysis of the local traffic and enable the cooperation with regular vehicles. The information needed by the AV to make independent decisions on the road can be given a lower priority.

5. Potential to compress the AV data – lidar, GPS, video

Lidar sensors emit waves continuously or cyclically, and the scattered light beams are reflected from obstacles. The analysis of the intensity of the wave recorded by the optic system allows a precise estimation of the distance to and the shape of the objects. The cloud point thus generated offers a highly accurate representation of the geometry of the surrounding objects. Unfortunately, the specific character of lidar data disqualifies them as the only source of information for an autonomous vehicle – although lidar sensors are very precise, they are sensitive to weather conditions: the signal is "lost" not only in the presence of fog and clouds, but also when touching the asphalt. The combination of lidar and other sensors will eliminate dead zones, i.e. fragments of the surroundings not visible to the vehicle from the available perspective. It will also allow an advanced correction of the measurement errors and provide information about important object features such as convexity and speed, enabling the vehicle to predict events and plan maneuvers with appropriate response time. Tests [12, 14, 15] have demonstrated that with the algorithm correctly adjusted to the type of the surroundings the file size can be considerably reduced. In urban traffic conditions, the original amount of data could be reduced by 75% without any significant loss of data quality.

Table 3. Theoretical amount of data (optimistic variant) generated by vehicle

Optimistic variant – vehicles generate a minimum expected amount of data				
Source	per sec.	[ ]	Data sent over 1.5 h [MB]	Data sent over 1.5 h [GB]
Cameras	240	MB	1296000	1265.63
Radar	60	kB	316.41	0.31
Sonar	10	kB	52.73	0.05
Lidar	15	MB	81000	79,10
GPS	50	kB	263.67	0.26
				SUM TOTAL: 1345.34 GB

Table 4. Theoretical amount of data (pessimistic variant) generated by vehicle

Optimistic variant – vehicles generate a minimum expected amount of data				
Source	per sec.	[ ]	Data sent over 1.5 h [MB]	Data sent over 1.5 h [GB]
Cameras	240	MB	1296000	1265.63
Radar	60	kB	3164.06	3.09
Sonar	100	kB	527.34	0.51
Lidar	105	MB	567000	553.71
GPS	50	kB	263.67	0.26
				SUM TOTAL: 3088.82 GB

Although it is very useful for the driver today, the 2D GPS (Glonass, Galileo) map is not a sufficient source of information for an autonomous vehicle – the data that an AV requires must be of accuracy and precision level sufficient to allow the vehicle to make a proper decision on the road. Being provided with advanced electronic systems and software, AVs will be able to use the 3D map technology.

The 3D map is a series of repeatedly taken photographs or 3D lidar scans which serve to construct a point cloud comprising objects present in the particular space. Each object has an assigned depth which is used to determine its distance from the road axis.

In order to increase precision or eliminate occlusion, the data are subjected to additional operations and subsequently to compression with the aim for the "view to be presented from the center of the roadway in perpendicular to its edge" [9]. In the DNA Roadmapping project, TomTom attempted a digital mapping solution with a positioning accuracy of up to 5 cm with respect to the road lane [25].

The basic elements of the system comprise the following layers:

- RoadDNA – a detailed point cloud for a particular location
- vertical traffic signs and horizontal lines on the roadway – adjusted to enable the positioning of a vehicle on the basis of data from its cameras
- radar – supplementary positioning data enabling the continuous view of objects scanned by sensors
- lamp posts along the road, which facilitate the positioning of a vehicle with the use of data from radar or lidar sensors, as well as from cameras
- road surface, using the reflectivity of the lidar laser beam.

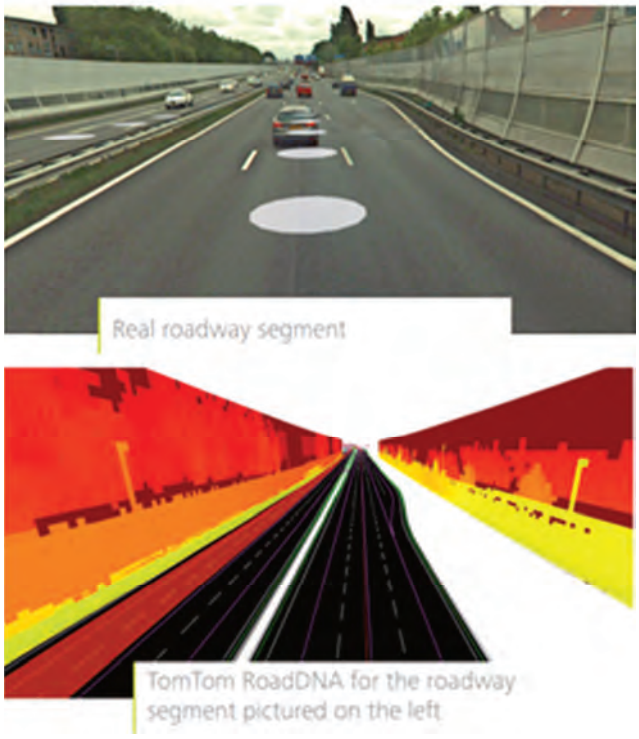

Fig. 2. RoadDNA technology developed by TomTom [25]

Intel estimates the amount of data sent by the GPS module at approx. 50 kbps and the main purpose of providing AVs with such a receiver is to build a traffic map and to analyze data for the informed development and management of the road infrastructure. However, the effectiveness of GPS can be increased by expanding its functionality with the option to read additional parameters directly from the vehicle.

Table 5. Impact of GPS data compression (Albatross) on the amount of generated data

Optimistic variant – vehicles generate a minimum expected amount of data				
Source	per sec.	[–]	Data sent over 1.5 h [MB]	Data sent over 1.5 h [GB]
Cameras	240	MB	1296000	1265.63
Radar	60	kB	316.41	0.31
Sonar	10	kB	52.73	0.05
Lidar	15	MB	81000	79.10
GPS	0.2	kB	1.05	0.001
				SUM TOTAL: 1345.09 GB

Table 6. Impact of GPS data compression (Albatross) on the amount of generated data

Pessimistic variant – vehicles generate a maximum expected amount of data				
Source	per sec.	[–]	Data sent over 1.5 h [MB]	Data sent over 1.5 h [GB]
Cameras	480	MB	2592000	2531.25
Radar	600	kB	3164.06	3.09
Sonar	100	kB	527.34	0.51
Lidar	105	MB	567000	553.71
GPS	0.2	kB	1.05	0.001
				SUM TOTAL: 3088.57 GB

With high-resolution (UHD or 4K) devices, the imaging ("video") function will allow a 360-degree representation of the surroundings and a full view of the situation on the road. Proper recognition of the color space ensures that objects are correctly identified in different light conditions, and a high frame-per-second rate reduces the response time of the vehicle. However, the disadvantage of modern solutions lies in the size of the output file, which may hinder the effective transmission of the material to the server. A proper video compression may facilitate the information transmission over the network. However, video compression, based on a series of the so-called codecs and continuously developed protocols, will not be able to meet the demand resulting from the amount of data generated by new versions of imaging technologies. The above problem is of significance, as this type of sensors is currently the basis for the local autonomy of vehicles (although not all of the information needs to be transmitted).

We cannot forget about possible additional diagnostics, which will result from the vehicle's supply method (e.g. control of electricity flow in the vehicle [23]) and the use of this information to place the vehicle in the charging queue.

6. Conclusions

Although intelligent transport systems are still in the test phase, public administration should already regulate and support the development of new standards by building a uniform digital infrastructure for numerous and various economic entities. The purpose of tests performed across the world is not only to prepare societies for the broad deployment of autonomous vehicles but most importantly to identify the potential problems and eliminate them at an early stage. From this perspective, Sweden is the leading country, with a range of legal acts regulating the use of AVs and their tests on public roads.

To date, discussions on the future of vehicles and their propulsion systems have focused on two aspects: either the type of motor or the emissivity [1]. Vehicle autonomy seems an underestimated issue, regarded as a curiosity rather than a (practically certain) direction of development. Research units and the automotive industry view vehicle autonomy from the perspective of its commercial potential – as an opportunity to demonstrate their ability by creating a mechatronic device with a certain autonomy. However, several completely new problems have meanwhile appeared: how to control a group of AVs in an autonomous system? How to process the amount of data generated by AVs over a single day – an amount equivalent to the content of the entire Internet? Should such data be processed locally or globally? The above questions can be answered from the perspective of the current IT resources: the technology will not be able to accommodate the traffic generated by the AV fleet.

The problem has not yet been addressed on a wide scale (except stress tests by Intel), while the challenges posed by the autonomous transport of the future include not only the propulsion system and the emissivity.

Nomenclature

AGV	Automated Guided Vehicles
AV	Autonomous Vehicle
EIGRP	Enhanced Interior Gateway Routing Protocol
GPS	Global Positioning System
ICT	Information and Communication Technologies
INS	Inertial Navigation System
IoE	Internet of Everything
IPv4	Internet Protocol version 4
IPv6	Internet Protocol version 4
IT	Information Technology
LiDAR	Light Detection and Ranging
OSPF	Open Shortest Path First
PRT	Personal Rapid Transit
RFC	Request for comments
RIP	Routing Information Protocol
RTF	Reliable Transport Protocol
WHO	World Health Organization

Bibliography

[1] Andrych-Zalewska M. Research of pollutant emissions from automotive internal combustion engines in conditions corresponding to the actual use of vehicles. Combustion Engines. 2023;193(2):64-70. https:// doi.org/10.19206/CE-162621

[2] Andrych-Zalewska M, Chłopek J, Merkisz J, Pielecha J. Investigations of exhaust emissions from a combustion engine under simulated actual operating conditions in real driving emissions test. Energies. 2021;14:1-20. https://doi.org/10.3390/en14040935

[3] Barker K, Cioara J. TCP/IP IPv6 – Networking Training. CBT Nuggets; 2019.

[4] Caillet P, Dupuis Y. Efficient LiDAR data compression for embedded V2I or V2V data handling. Arvics 2019.

[5] Choromański W, Grabarek I, Kozłowski M, Czerepicki A, Marczuk K. Pojazdy autonomiczne i systemy transportu autonomicznego. PWN, Warsaw 2020.

[6] Dimitrakopoulos G, Tsakanikas A, Panagiotopoulos E. Autonomous Vehicles Technologies, Regulations, and Societal Impacts. Elsevier 2021. https://doi.org/10.1016/C2020-0-02875-6

[7] Gościewski D. Application of RLE recompression to reduce the size of grid files (in Polish). Technical Journal of the Cracow University of Technology. 2008

[8] Igliński H. Pros and cons of autonomization of trucks (in Polish). Transport and forwarding (June–July); 2018.

[9] Intel automatic driving informations. https://newsroom.intel.com/editorials/krzanich-the-future-of-automated-driving

[10] Internet Engineering Task Force, RFC 1058. https://datatracker.ietf.org/doc/html/rfc1058

[11] Internet Engineering Task Force, RFC 2080. https://datatracker.ietf.org/doc/html/rfc2080

[12] Internet Engineering Task Force, RFC 2328. https://datatracker.ietf.org/doc/html/rfc2328

[13] Internet Engineering Task Force, RFC 2453. https://datatracker.ietf.org/doc/html/rfc2453

[14] Internet Engineering Task Force, RFC 5340. https://datatracker.ietf.org/doc/html/rfc5340

[15] Internet Engineering Task Force, RFC 7868. https://datatracker.ietf.org/doc/html/rfc7868

[16] Isenburg M. LASzip: lossless compression of LiDAR data. Photogrammetric engineering and remote sensing. February 2013.

[17] Kij M. Difficult adolescence (in Polish). Truck&Van. 2020;6.

[18] Lyamin N, Dengy Q, Vinel A. Study of the platooning fuel efficiency under ETSI ITS-G5 communications. IEEE 2016:551-556. https://doi.org/10.1109/ITSC.2016.7795608

[19] Markowski A. Psychological basis of road accidents (in Polish). Time for transportation. 2017;9.

[20] Pobocha B. Robo-ants (in Polish). Connected life (May/June). 2015.

[21] Processing in autonomous vehicles. https://www.thedrive.com/tech/20553/the-language-of-self-driving-cars-is-dangerous-heres-how-to-fix-it

[22] Statistics of Polish Police. https://statystyka.policja.pl

[23] Szałek A, Pielecha I, Cieślik W. Fuel cell electric vehicle (FCEV) energy flow analysis in real driving conditions (RDC). Energies. 2021;14:4. https://doi.org/10.3390/en14165018

[24] The first Polish autonomous public transport bus. https://www.transport-publiczny.pl/wiadomosci/gdansk-tworcy-autonomicznego-busika-spodobal-sie-62612.html

[25] Tom–Tom HD maps. https://www.tomtom.com/products/hd-map

Prof. Radosław Wróbel, DSc., DEng. – Faculty of Mechanical Engineering, Wroclaw University of Science and Technology, Poland.
e-mail: *radoslaw.wrobel@pwr.edu.pl*

Radostin Dimitrov, DEng. – Faculty of Mechanical Engineering, Technical University of Varna, Bulgaria.
e-mail: *r_dimitrov@tu-varna.bg*

Prof. Zbigniew Sroka, DSc., DEng. – Faculty of Mechanical Engineering, Wroclaw University of Science and Technology, Poland
e-mail: *zbigniew.sroka@pwr.edu.pl*

Veselin Mihaylov, DEng. – Faculty of Mechanical Engineering, Technical University of Varna, Bulgaria.
e-mail; *v_mihaylov@tu-varna.bg*

Gustaw Sierzputowski, DEng. – Faculty of Mechanical Engineering, Wroclaw University of Science and Technology, Poland.
e-mail: *gustaw.sierzputowski@pwr.edu.pl*

Daniel Ivanov, MEng. – Faculty of Mechanical Engineering, Technical University of Varna, Bulgaria.
e-mail: *dan.ivanov@tu-varna.bg*

Article citation info:
Kamiński A, Krakowian K, Skrętowicz M, Kupski M. Efficiency optimization of a vehicle combustion engine by the adjustment of the spark advance angle. Combustion Engines. 2024;196(1):10-14. https://doi.org/10.19206/CE-175071

Adam KAMIŃSKI
Konrad KRAKOWIAN
Maria SKRĘTOWICZ
Mateusz KUPSKI

Combustion Engines
Polish Scientific Society of Combustion Engines

Efficiency optimization of a vehicle combustion engine by the adjustment of the spark advance angle

ARTICLE INFO

Received: 31 May 2023
Revised: 27 October 2023
Accepted: 10 November 2023
Available online: 16 December 2023

Changing the ignition advance angle has a significant impact on the performance of a combustion engine. Optimization of ignition advance angle is a major task of adjusting the engine concerning emission standards, fuel consumption, torque value, etc. The results of the research showed that the process of optimizing the ignition advance curve can noticeably increase engine efficiency, as well as torque and power output from the engine while reducing fuel consumption as a result of lower indications of the air flow mass per second from MAF sensor (mass air flow sensor). The highest impact of the ignition advanced angle modifications can be seen in the area of the highest volumetric efficiency of the tested combustion engine. Almost no impact is observed within high engine speed levels. Simultaneously increasing engine load and rotation speed increases the possibility of engine knocking, which has a devastating effect on engine durability.

Key words: *combustion engine, ignition advance, ignition timing, efficiency, optimization*

1. Introduction

According to the latest emission standards and the power supply crisis in Europe, the efficiency of the combustion engine has increased in importance. Many vehicles in developing countries are aged. The average age of the vehicles in Poland is 14 years now. Furthermore, some of them are from the other continent, especially from North America where the exhaust emission standards differ from EU standards [3]. The growing interest in the USA import cars forces us to determine the optimum methods of readjustments and retrofitting engine control algorithms to adapt them to our environment. One of the critical parameters influencing engine efficiency is spark advance. As mentioned in articles [1, 8, 12, 13] depending on the quality of the factory ignition curve optimization process and basic emissions policies, past the process of the additional spark angle adjustments, gains in engine efficiency, can be as much as 20%. According to the study of Mobility and Vehicle Mechanics [4] if the flashpoint of fuel increases, requirements for the quality of the ignition also increase. An example of gas fuel with a higher than gasoline (480–530°C) flashpoint is CNG (545–800°C). Additionally CNG has a lower rate of flame speed propagation in relation to crank angle [10]. That phenomena induces necessity in recalibration factory settings of the powertrain control module to achieve correct efficiency. As Amr Ibrahim and Saiful Bair have shown [5] even exhaust gas recirculation strategy lowers the flame speed propagation which has to be compensated by adding spark advance, otherwise the engine will lose torque and fuel efficiency. CFD software simulations [6] confirm the increase in combustion pressure when approaching the optimum spark advance. As mentioned in [2, 7, 9, 11], increasing spark advance lowers the exhaust temperature due to a more complete burning process but simultaneously increases the NO_x emissions due to the ideal gas law which tells that an increase in pressure corresponds with a higher peak temperature.

2. Materials and methods

The experiment was performed using a car with an engine powered by gasoline and LPG fuel but for research purposes only gasoline fuel was used. A vehicle which has been chosen for the research is Ford Explorer 1996 4.0l V6 OHV, according to the high rate of popularity in Poland and officially selling the 1996 to 2001 models in Poland and Germany. Detailed vehicle specifications are presented in Table 1. Engine parameters are measured by the chassis dynamometer MAHA 4×4 (Table 2). Oil temperature is maintained around 100°C. Ambient and IAT temperature is held constantly during all tests. About the calculations of the PCM, except for dynamometer measurement of torque and power, graphs also contain the NET calculated value of torque and power by the Ford EEC V microchip. NET value is collected by the ForScan diagnosis software. The working bench diagram is shown in Fig. 1.

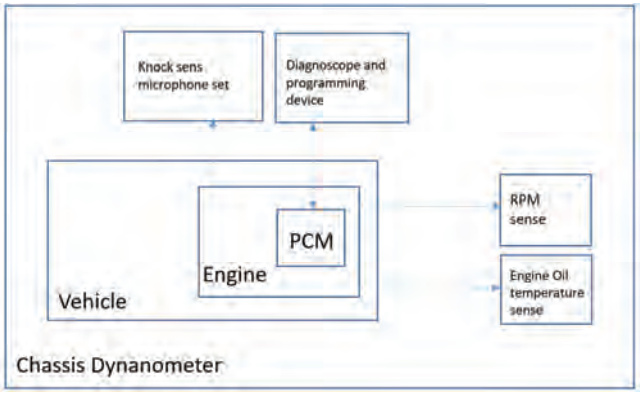

Fig. 1. Workbench diagram

Every dynamometer pull is repeated three times to calculate the correct average values. Knock detection is achieved by listening to the engine using an electronic stethoscope. Detailed names of tools used in research are

detailed in Table 3. Spark advance is limited by the knock detection or the lower reading referring to the latest pull. Optimized spark advance values are uploaded to the PCM, past every change in the software, according to the KAM memory reset, the vehicle is idling for around 5 minutes.

Table 1. Vehicle and engine specification

Vehicle system	Detail
No. of cylinders	6-cylinder
Arrangement	V-type
Valve mechanism	12-valve OHV
Combustion chamber	Ford fast-burn
Manifolds	Parallel flow
Fuel System	Ford EFI SFI
Ignition system	Ford integrated EDIS
Control system	Ford EEC-V
Displacement	245 CID
Bore × Stroke	3.95×3.31 inches
Compression ratio	9.0:1
Power	119 kW@4200 rpm
Torque	323 Nm @2400 rpm
Firing order	1-4-2-5-3-6
Spark plug gap	0.054 inches (1.37 mm)
Base EEC catchword	LID0 → YZZ2
Transmission	Automatic 4R55E electronic control

PCM strategy is changed from LID0 to YZZ2 according to better data acquisition in YZZ2 versions and the origin of the software. LID0 is the first EU calibration for the 1996 model year while YZZ2 was used as a basic US model strategy for 1996 model year. The basic settings of PCM algorithms are the same. Differences in scalars are minor and do not have any influence on the car's performance. It refers especially to the differences in the mandatory existence of on-board emissions monitors (OBD1 EU vs OBD2 USA). Due to USA calibration data acquisition is easier on YZZ2 calibration than LID0.

Table 2. Chassis dynamometer

Name	Detail
Chassis dynamometer model	MAHA MSR 4×4 MSR 500/2
Measurement error	±2% of measured power

Table 3. Measurement, diagnosis and programming tools

Purpose	Detail
Diagnosis/programming	MongoosePro Ford
Programming software	Binary Editor 5.209
Diagnosis	ForScan 2.42
Diagnosis	Ford FJDS
Programming software	Binary Editor 5.209
Knock detection	Electronic Stethoscope
AFR measurement	STAG AFR
Oil temperature measurement	MAHA MSR 4×4 integrated sensor

To ensure that the environmental conditions are correct and constant, a heavy fan is installed in front of the experimental car. Final runs are performed on the same day with the same ambient temperature. Every run is conducted with the width open throttle (WOT), 3rd gear and locked lock-up clutch in a torque converter. Transmission and torque converter is switched to the manual operation by the CPU registers in the EEC V PCM.

The average Air to Fuel Ratio (AFR) is maintained around 0.84 lambda. It delivers the most boundaries of the knock occurrence. AFR changes in reach fuel areas have the minimal effect on the torque delivering of the engine so therefore no further changes in fuel Table are made. All boundary conditions are collected in Table 4.

Table 4. Environmental boundary conditions

Name	Value
Ambient temperature	15°C
Average AFR during pulls (WOT condition)	12.3 AFR
Fuel system status during pulls	OL
Gear	3. Manually locked by the CPU register
Lock up	Engaged. Manually locked by the CPU register
3rd gear ratio	1:1
Final gear ratio	3.73 Ford 8.8 LSD
IAT	20°C
Oil temperature during pulls	~100°C
Estimate rotating mass of the vehicle	100 kg
Rotating mass of the dynamometer	250 kg
Sum of the rotating mass	350 kg

All the values in Tables and graphs are presented in Newton-metre and horsepower due to the fact that the vast majority of calculations of the ECC V powertrain control module is also presented in this form. Output values from the PCM in PIDs do not present kilowatts. For easier and more accurate comparison between calculated values by the PCM and measured ones, horsepower was set as a main unit in the article.

3. Results

Figure 2 and Table 5 show the comparison of the results before and after the process of spark advance optimization. The most increase in the torque output can be observed in the low rpm areas. The biggest differences are presented at 2400 rpm for the power and at 2000 rpm for the value of torque. Most changes in the spark advance are achieved at 2400 rpm. After optimization, spark advance at 2400 rpm increased by 10.75 degrees to the total value of 21.5° referring to Table 6. Most significant points are bolded in red to emphasize the differences.

The highest absolute value of power is achieved at 3900–4000 rpm with the value of 93 horsepower (KM) which is equivalent to 69 (kW), while the peak of the torque occurs at 2800 rpm with the value of 190.84 Nm. Details for all rpm ranges are shown in Table 6.

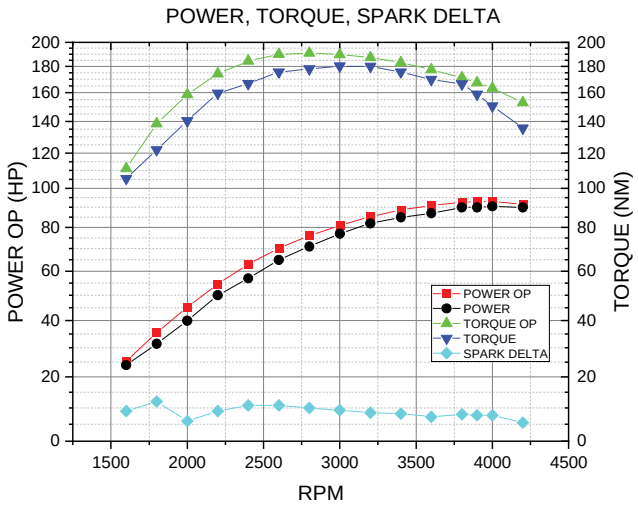

Fig. 2. Power, torque and spark delta before and after optimization

Table 5. Measurement data

n [rpm]	Power [HP] OP	Power [HP]	Delta [HP]	Torque [Nm] OP	Torque [Nm]	Delta [Nm]	SPARK° Delta
1600	25.3	24	1.3	111.03	105.32	5.71	9
1800	35.5	31.5	4	138.48	122.08	16.40	**12**
2000	45.2	40	5.2	158.69	140.43	**18.26**	6
2200	54.6	50	4.6	174.26	159.58	14.68	9
2400	63	57	**6**	184.32	166.67	17.65	**10.75**
2600	70.3	65	5.3	189.85	175.54	14.31	**10.75**
2800	76.1	71	5.1	**190.84**	178.04	12.80	10
3000	81	77	4	189.58	**180.22**	9.36	9.25
3200	85.3	82	3.3	187.17	179.93	7.24	8.50
3400	88.7	85	3.7	183.18	175.54	7.64	8.25
3600	91	87	4	177.49	169.69	7.80	7.25
3800	92.6	90	2.6	171.10	166.3	4.80	8
3900	**93**	90	3	167.44	158.86	8.58	7.75
4000	**93**	**90.5**	2.5	163.25	150.46	12.79	7.75
4200	91.5	90	1.5	152.97	135.64	17.33	5.50

Figure 3 shows the comparison between the calculated by the PCM NET torque and power values of the vehicle, before and after optimization. PCM calculated net values are represented by the estimated torque on the engine, minus implemented in the memory of the PCM, and Table of losses.

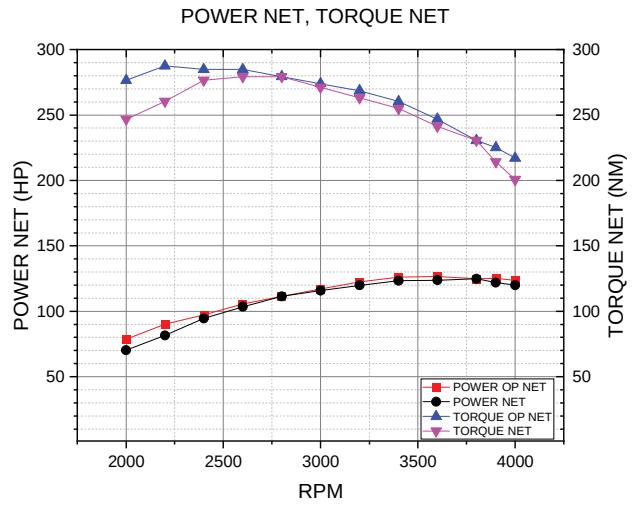

Fig. 3. Comparison between NET values before and after adjustments

Values of the NET torque should be higher than the dynamometer values according to the fact that the chassis dynamometer measures torque on the wheels, not directly engine torque. In the case of trying to measure the actual losses, by the chassis dynamometer, there is a demand to put the neutral gear, during the high wheel speed which can be dangerous for the automatic transmission, according to the lack of lubrication on the neutral gear. Specify values of the VE (Volumetric Efficiency) calculated by the PCM, air flow values (MAF) and the final spark advance, compared before and after the optimization, are shown in Table 6.

Referring to Table 6 and Figure 3 the highest value of the total spark advance is achieved at the highest rotation speed of the engine, independently of the process of optimization.

Table 6. Measurement data

n [rpm]	**SPARK° OP**	**SPARK°**	**Delta [°]**	**VE(%) OP**	**VE(%)**	**Delta of VE**	**MAF[g/s] OP**	**MAF[g/s]**	**Delta of MAF [g/s]**
2000	18.5	12.5	6	73.99	NaNd	NaNd	59.09	60.83	–1.74
2200	19.75	10.75	9	73.79	73.22	0.57	64.11	65.3	–1.19
2400	21	10.25	**10.75**	73.58	75.72	–2.14	70.12	70.82	–0.7
2600	21.5	10.75	**10.75**	73.9	76.05	–2.15	76.84	77.93	–1.09
2800	21.25	11.25	10	74.37	75.78	–1.41	83.56	84.4	–0.84
3000	21	11.75	9.25	74.92	75.28	–0.36	90.28	90.87	–0.59
3200	20.75	12.25	8.5	75.39	74.78	0.61	94.15	97.34	**–3.19**
3400	21	12.75	8.25	73.65	74.05	–0.4	98.27	100.07	–1.8
3600	21	13.75	7.25	71.44	71.9	–0.46	102.39	103.25	–0.86
3800	22.75	14.75	8	70.06	70.06	0	105.72	106.44	–0.72
4000	23.25	15.5	7.75	67.28	67.91	–0.63	104.39	107.01	–2.62
4200	23.75	17.25	6.5	59.99	63.91	**–3.92**	NaNd	107.21	NaNd
4400	24.75	19.25	5.5	NaNd	59.92	NaNd	NaNd	102.7	NaNd

Full graphs of the differences between spark advances angles are shown in Fig. 4.

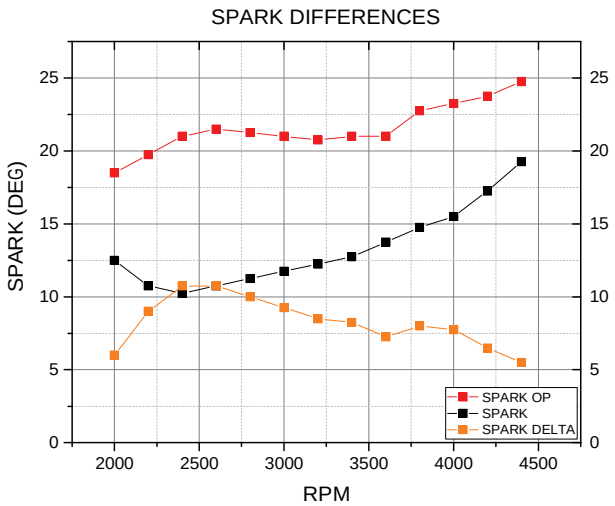

Fig. 4. WOT spark advance table values shared with a delta value

The final comparison between the PCM estimation and the chassis dynamometer values is presented in the shared Fig. 5. Values calculated by the PCM have shown a gain in torque output in the same manner as measured data by the dynamometer. However, values are different. Torque readings by the PCM cannot be used as a reference date in fa-

ther research. Torque values shown by the PCM are correct only for indicating significant changes in power output.

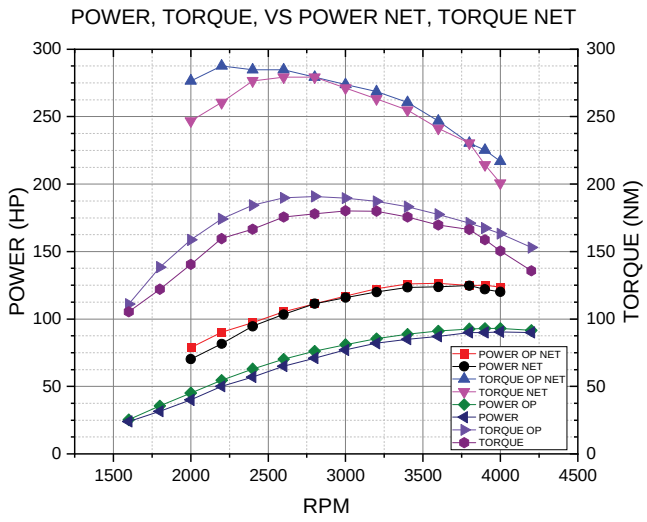

Fig. 5. Comparison between chassis dynamometer results and NET calculated values

There is a necessity of knowing that those values are based on mass air flow meter with conduct only changes in engine flows. Other physical phenomenon of the engine is not included in this type of calculation. As mentioned before NET values should be significantly higher according to the losses of the drivetrain.

4. Summary and conclusions

Optimization of the spark advance curve can significantly increase torque and power output from the engine, simultaneously reducing fuel consumption referring to the lowest indications of the air flow mass per second, from the MAF sensor. The highest gains can be observed in the area of the highest volumetric efficiency of the combustion engine which corresponds with the range of the highest torque output. Built-in functions of the Ford EEC V computer control unit give the possibilities for easy changes in main engine parameters like; fuel maps, spark advance maps, angles of injections maps etc. The flexibility of the PCM recalibration was proved by the results from the study. Changes in emissions from CARB to Europe OBD 2 (EURO 3 in this sample) were successfully achieved. No unintentional behavior of the engine was observed. No other parameters of the engine work significantly changed. The performance of the automatic transmission behavior was maintained. Highest improvements were achieved at the rate of 11.5% in power @2400 rpm and 13% in torque @2000 rpm. The most significant efficiency gain was observed at 3200 rpm with a value of 3.3%. The greatest spark advance change occurred at 2400 and 2600 rpm amounted to 10.75°.

Nomenclature

AFR	air fuel ratio
CFD	computational fluid dynamics
CNG	compressed natural gas
ECU	electronic control unit
EDIS	electronic distributor less ignition system
EEC	electronic engine control
EFI	electronic fuel injection
IAT	input air temperature
KAM	keep alive memory
LPG	liquefied petroleum gas
MAF	mass air flow
OHV	overhead valves
OL	open loop
PCM	powertrain control module
VE	volumetric efficiency
WOT	wide open throttle

Bibliography

[1] Ehsan M. Effect of spark advance on a gas run automotive spark ignition engine. J Chem Eng. 2010;1:42-49. https://doi.org/10.3329/jce.v24i0.5584

[2] El-Sharkawy MR, Abaskharon MBR, Abd-El-Tawwab AM, Ezzat Fawzy MH. Effect of static spark timing on the performance and emissions of a spark ignition engine using CNG. IOP Conf Ser Mater Sci Eng. 2019;518(3):12. https://doi.org/10.1088/1757-899X/518/3/032062

[3] General D. Internal FOR. Comparative study on the differences between the EU and US legislation on emissions in the automotive sector. Inst Eur Environ Policy. 2015;53(9): 1689-1699. https://doi.org/10.2861/503165

[4] Hristov R, Bogdanov K, Dimitrov R. Research the influence of spark plugs types on the performance of the engine operating on gaseous fuels. Mobility & Vehicle Mechanics. 2018;44(1):51-61. https://doi.org/10.24874/mvm.2018.44.01.05

[5] Ibrahim A, Bari S. A comparison between EGR and lean-burn strategies employed in a natural gas SI engine using a two-zone combustion model. Energy Convers Manage. 2009;50(12):3129-3139. https://doi.org/10.1016/j.enconman.2009.08.012

[6] Joshi A, Borse S. Study of the effect of spark advance, engine speed variation and number of spark plugs on engine performance using CFD software. Journal of Ocean, Mechanical and Aerospace. 2017;48(48):1-9. https://doi.org/10.36842/jomase.v48i1.170

[7] Lungu J, Siwale L, Luwaya E. Study and effect of ignition timing on the combustion characteristics of gasoline En 91 in a spark ignition engine. NAER-V1. 2021;104-2. https://doi.org/10.9734/bpi/naer/v1/7257D

[8] Marzec P. Tests of a SI engine powered by gaseous fuels blends of LPG + DME of various proportions with variable load. Combustion Engines. 2022;190(3):23-26. https://doi.org/10.19206/CE-144124

[9] Nawazish Mehdi S, Yousufuddin S. Effect of ignition timing, equivalence ratio, and compression ratio on the performance and emission characteristics of a variable compression ratio SI engine using ethanol-unleaded gasoline blends. International Journal of Engineering. 2008;21(1):97-106. https://www.ije.ir/article_71695_6566994fbcdb15e1ad6711b147c8c9a5.pdf

[10] Ramasamy D, Kadirgama K, Rahman M, Zainal Z. Analysis of compressed natural gas burn rate and flame propagation

on a sub-compact vehicle engine. International Journal of Automotive and Mechanical Engineering. 2015;11(1):2405-2416. https://doi.org/10.15282/ijame.11.2015.21.0202

[11] Tribbett EJ, Froehlich EM, Bayer L. Effects of ignition timing, equivalence ratio and compression ratio on RDH engine performance. 2002. https://api.semanticscholar.org/CorpusID:17643397

[12] Tunka L, Polcar A. Effect of various ignition timings on combustion process and performance of gasoline engine. Acta Univ Agric Silvic Mendelianae Brun. 2017;65(2):545-554. https://doi.org/10.11118/actaun201765020545

[13] Zareei J, Kakaee AH. Study and the effects of ignition timing on gasoline engine performance and emissions. Eur Transp Res Rev. 2013;5(2):109-116. https://doi.org/10.1007/s12544-013-0099-8

Adam Kamiński, MSc. – Faculty of Mechanical Engineering, Wroclaw University of Science and Technology, Poland.
e-mail: *adam.kaminski@pwr.edu.pl*

Maria Skrętowicz, DEng. – Faculty of Mechanical Engineering, Wroclaw University of Science and Technology, Poland.
e-mail: *maria.skretowicz@pwr.edu.pl*

Konrad Krakowian, DEng. – Faculty of Mechanical Engineering, Wroclaw University of Science and Technology, Poland.
e-mail: *konrad.krakowian@pwr.edu.pl*

Mateusz Kupski, Eng. – Faculty of Mechanical Engineering, Wroclaw University of Science and Technology, Poland.
e-mail: *mateusz.kupski@pwr.edu.pl*

Article citation info:
Gołębiowski W, Zając G, Sejkorová M, Wolak A. Assessment of oil change intervals in urban buses based on the selected physicochemical properties of used engine oils. Combustion Engines. 2024;196(1):15-23. https://doi.org/10.19206/CE-169807

Wojciech GOŁĘBIOWSKI
Grzegorz ZAJĄC
Marie SEJKOROVÁ
Artur WOLAK

Combustion Engines
Polish Scientific Society of Combustion Engines

Assessment of oil change intervals in urban buses based on the selected physicochemical properties of used engine oils

ARTICLE INFO

Received: 31 May 2023
Revised: 17 July 2023
Accepted: 19 July 2023
Available online: 14 August 2023

The paper presents the results of the analysis of selected physicochemical parameters of engine oils after their use. The oils were obtained both from urban buses belonging to the fleet of a municipal transport company in Lublin, Poland but also from the city of Pardubice in the Czech Republic. Five samples of 10W40 semi-synthetic oil and four samples of 5W30 synthetic oil were tested. Kinematic viscosity at 40°C and 100°C, oxidation, nitration, sulfonation, total acid number (TAN), total base number (TBN), remaining antiwear additives, water content and glycol content, were assessed using infrared spectroscopy (FTIR). The tests were performed on the basis of the ASTM E2412-10 standard. The article also presents the exceedance of the limit values results for the selected parameters. The results of the research can be used in optimizing the engine oil change interval so that the decision to replace the oil is justified both in economic and technical terms, taking into account the need to maintain the service life of the bus.

Key words: *degradation, engine oil, oil change, urban buses, FTIR*

1. Introduction

One of the biggest challenges that we are currently facing is climate change and the environmental problems which are associated with it. Public transport has a significantly more beneficial impact on nature and the environment than individual transport. The arguments for using public transport often focus on cost, accessibility, and environmental impact. To convince more people to change their communication habits, transport companies must offer high-quality transport services, increasing their availability and monitoring the costs associated with it.

Many processes are responsible for the proper maintenance of the vehicle, oil change being one of them [2]. During operation, engine oil ages and absorbs many contaminants. The oil aging process is affected by the process of its oxidation, nitration, contamination by fuel, and gases blown through during circulation in the engine, as well as polymerization under the influence of heat. All this leads to a deterioration in its quality. Finally, all this lead to the oil properties being insufficient, and the user's decision to continue to drive on it may start to cause engine problems. Therefore, it must be periodically replaced.

The engine oil change intervals (OCI) dictated by the vehicle manufacturers are based on a predetermined number of kilometers driven or a specified period of operation. This vehicle maintenance strategy is called preventive maintenance, and it aims to reduce the frequency and number of failures of a given device. The application of this strategy is based either on the experience of people employed in maintenance positions or on the recommendations of original equipment manufacturers (OEM). The problem with successfully implementing this type of strategy is achieving optimal (OCI) because vehicles operate in different environments, and due to their actual operating conditions, they may require different OCI. Whereas relying on the experience of people dealing with maintenance in the company creates problems for the company at a time when there is a high turnover among employees and various strategies for determining the optimal oil change date are mixed [1].

Predictive maintenance, also known as condition-based maintenance (CBM), is the second maintenance strategy option. This type of strategy is more expensive to implement than preventive maintenance due to the need to employ specialized staff with appropriate knowledge as well as to invest in appropriate measuring equipment. The CBM strategy is based on the registration and control of the obtained data, their thorough analysis using computer tools, as well as on the detection of trends of changes. Then, according to the CBM, the information obtained from the condition monitoring process is the basis for deciding the need for maintenance. The fact is that there are certain signals, symptoms or conditions before the equipment failure occurs. Therefore the motivation to use this type of strategy is to know in advance those symptoms that may indicate the occurrence of a specific failure [16, 17]. In general, maintenance decision-making in a CBM strategy is based on a real-time assessment of equipment conditions, which is ultimately expected to reduce costs by minimizing maintenance needs [14]. The oil condition monitoring process can provide in two ways: online and offline. The online process takes place when the equipment is in working condition (operational state), while the offline process takes place when the equipment is not working. To determine the optimal OCI and diagnose the lubricated system without disassembly, quick and precise analysis of the lubricant is extremely important. An effective oil analysis program often relies on offline oil analysis performed in laboratories where all properties of the oil are analyzed.

The operating conditions of a given device equipped with a combustion engine are important in the context of its maintenance, but looking through the prism of reliability and vehicle life, the properties of the oil with which it is lubricated are also of great importance [13]. The type of engine oil and its current condition affect not only the per-

formance parameters of the engine but also its wear and emissions [6]. Taking into account the different chemical compositions of engine oil and the irregular influence of external factors on the aging process, it is impossible to draw up a general schematic representation (model) of oil quality changes occurring during operation [5, 21]. Therefore, it is important to estimate the moment when the oil loses its functions and reaches the operational limit state.

Attempts to detect most changes in the operating parameters of oils during actual operation are difficult. A similar situation (during oil exploitation) takes place in the case of an attempt to indicate the moment when the oil reaches the limit values of its physicochemical properties. In the literature devoted to the problems of determining the limit values of lubricating oil parameters, we encounter attempts to determine acceptable changes in selected physicochemical properties of the oil, a parameter considered representative of the aging process, a package of parameters relating to the properties of the oil or the concentration of chemical agents. The most frequently chosen parameters to represent qualitative changes are kinematic viscosity (KV) at 40 and 100°C, oxidation, nitration and sulfonation, TAN and TBN, fuel content, soot content, susceptibility to foaming or content of elements [4, 11, 18, 20]. Therefore, to assess the condition of engine oil correctly, it is important to know the limit values of the tested parameters and the current values of the given coefficients. These pieces of information allow us to make the right decision – whether the used engine oil is still usable or not.

The research aimed to check whether the decision made by bus owners to change the oil, dictated by the specified service mileage of the vehicle recommended by the manufacturer, was optimal due to the number of exceedances of limit values. The paper presents the results of research on selected physicochemical properties of engine oils after a period of operation, which are important from the point of view of proper engine operation. The oils come from fleets of buses of various age structures and different operating conditions. Specific parameters were selected for the analysis and assessment of the operating properties of the tested oils because they characterize the oil aging process that takes place during operation, and are the basis for determining its suitability for further use [3, 7, 10, 12].

2. Materials and methods

The research material consisted of motor oils obtained during a standard oil change from two municipal transport companies, one from the city of Lublin, and the other, from the city of Pardubice in the Czech Republic. The oils come from 2 producers and differ in the SAE viscosity class: engine oils obtained from Pardubice have a viscosity class of 5W30, while oils obtained from Lublin have a viscosity class of 10W40. The key physicochemical properties of new engine oils are shown in Table 1.

Engine oils obtained from replacement were grouped by manufacturers, and then the given code names were applied: PU01-04 and OP01-05. 9 samples of used engine oils from 6 city buses of different manufacturers with various levels of mileage, were used in the research. During the sampling, the overall mileage of the bus (ODO) and the distance on oil interval were recorded. Buses of different age structures, and various technical solutions of diesel engines, were selected for the tests. The research material collected from the public transport company in Pardubice comes from one bus – Iveco Urbanway 12 and relates to four consecutive OCI. In the conducted research, the life of the oil, understood as the mileage of the bus recommended by the manufacturer, in which engine safety and work efficiency are ensured, was important. In the case of the PU 5W30 synthetic oil group, that period was set at 50,000 km, and in the case of OP 10W40 semi-synthetic oil at 60,000 km. Table 2 presents data on the buses used in the research.

Table 1. The key physicochemical properties of new engine oils

Parameter	Unit	Oil code	
		OP from Lublin, Poland	PU from Pardubice, Czech Republic
Viscosity class, SAE	–	10W40	5W30
Quality class, ACEA	–	E4, E7	E4, E6, E7
KV@100°C	mm^2/s	14.67	9.93
KV@40°C	mm^2/s	86.5	58.14
TBN	mg KOH/g	10.57	9.45
TAN	mg KOH/g	0	0.84
Oxidation	Abs/0.1 mm	0.13	0.23
Nitration	Abs/0.1 mm	0.04	0.10
Sulfonation	Abs/0.1 mm	0.2	0.23

The ERASPEC OIL apparatus manufactured by Eralytics was used in the research to analyze specific physicochemical parameters of engine oils after their use. The device is based on the Fourier Transform Infrared (FTIR) spectroscopic method, and it is in full compliance with ASTM, DIN, and JOAP methods. Analyzes were performed following ASTM E2412-10 infrared standard. The chemical structures of fresh and used engine oils are examined by comparing their FTIR spectra. The levels of individual bands for used oils were determined not directly from their spectra, but from differential spectra, i.e. spectra resulting from a mathematical operation: spectrum of used oil minus the spectrum of fresh oil. The parameters indicated in the introduction (i.e. KV@40°C and KV@100°C, oxidation, nitration, sulfonation,, TAN and TBN, remaining anti-wear additives (AW), water and glycol content) were chosen because they allow to show oil degradation as a result of bus operation. Triplicate tests were carried out for all oils, and then the result was averaged.

Changes in the parameters of the oils taken from the buses were compared to the parameters of fresh oils, which are listed in Table 1. Moreover, in order to determine the limit values, the values obtained for fresh oils were the reference point.. The literature analysis showed disparities in the determination of threshold values of indicators of the engine oil condition. The assessment of the current condition of the engine oil was made, based on the limit values adopted and presented in Table 3.

Table 2. Technical data and mileage of the tested buses

Oil group	Item	Bus model	Code of the sample	Bus ODO [km]	Distance on oil interval [km]	Engine/oil pan capacity [liter]
PU SAE 5W30	#1	Iveco Urbanway 12	PU01	51,394	51,394	Iveco Cursor 9/34
	#2	Iveco Urbanway 12	PU02	95,195	43,801	
	#3	Iveco Urbanway 12	PU03	146,496	51,301	
	#4	Iveco Urbanway 12	PU04	197,961	51,465	
OP SAE 10W40	#1	Autosan Sancity M12LF	OP01	170,178	60,500	Iveco Cursor 78 EEV/22
	#2	Merc.Benz Connecto 18	OP02	667,290	64,683	OM 470/35
	#3	Merc.Benz Connecto 18	OP03	678,258	64,162	
	#4	Merc.Benz Connecto 18	OP04	732,678	63,347	
	#5	Merc.Benz Connecto 12LF	OP05	1,038,973	61,131	OM 936/29

Table 3. Limit values of oil parameters adopted in the tests

Parameter	Unit	Limit values				
		based on the literature				Established in this study
		[8]	[10]	[15]	SAE J300-2015	
KV@100°C	mm^2/s	–	±15%	±15%	5W – min 9.3; max < 12.5 10W – min 12.5; max < 16.3	±15% 5W – min 8.4; max 11.4 10W – min 12.5; max 16.9
KV@40°C	mm^2/s	±15%	–	±15%	–	±15% (5W) – min 49.4; max 66.9 (10W) – min 73.5; max 99.5
TBN	mg KOH/g	< 30%	< 30%	< 30%	–	< 30% (5W) – max 7.4 (10W) – max 6.6
TAN	mg KOH/g	–	–	6 mg KOH/g	–	+2.5 mg KOH/g
oxidation	Abs/0.1 mm	> 1.0	> 0.15	> 0.4	–	> 0.4
nitration	Abs/0.1 mm	> 1.0	> 0.15	> 0.4	–	> 0.4
sulfonation	Abs/0.1 mm	> 1.0	> 0.20	> 0.4	–	> 0.4
Water content	wt%	> 0.3	> 0.2			> 0.2
Glycol content	wt%	> 0.3	> 0.08			> 0.3

To graphically present the distribution of the statistical feature of the results obtained for each of the analyzed variables, box charts for two oil groups were used. Measurements were made in triplicate. The obtained results were statistically analyzed using the Statistica 13 software package. The graphical form of the presentation of the results enabled the observation of the location, shape, and distribution of the empirical feature under examination. The charts include the following items: tested values (outliers and extremes); the median, and a box containing the quartile range (quartiles – 25th and 75th percentile).

3. Results and discussion

This section presents the most important results regarding the oil quality, degradation, and contaminant content parameters observed at the time of oil change after the specified period of oil life. In the end, a summary of exceedances of the limit values of individual oil parameters for the tested groups was introduced in Table 4.

When analyzing the test results (Fig. 1), it was observed that in three samples from the PU synthetic oil group, the limit value of the KV@40 parameter was exceeded. Exceeding the lower limit is visible, which can lead to a lack of protection of the friction mechanisms. In the case of the sample marked PU_03, a decrease of 30% was recorded, which is twice the limit value. Greases with the wrong viscosity for the application can cause, among other things, increased metal-to-metal contact, friction, wear, and increased oil loss in service [19]. Only in the case of oil change in the sample marked PU_02, the change compared to fresh oil was 12%, and the limit of the lower boundary of the value set at –15% was not exceeded. It is worth noting that in this particular sample, the oil was changed at 43,801 km, which is about 7,000 km earlier than in the other three. To maintain engine lubrication conditions at an appropriate level, this may be one of the arguments for the company to reduce the OIC to the level of 40,000 km. Analyzing the position of the box plot, the minimum of the non-outliers was 40.44 mm^2/s, the maximum of the non-outliers was 50.89 mm^2/s, and the median was 45.06 mm^2/s. No extreme values were recorded in this case. The data is not scattered, and the data plot looks symmetrical.

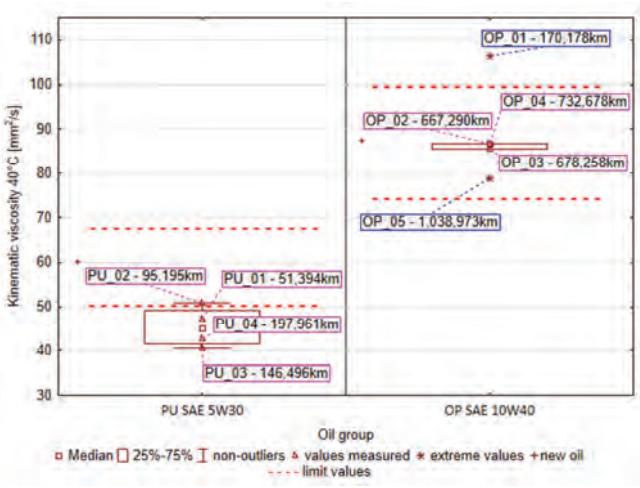

Fig. 1. Measurement of KV@40 in engine oil samples

In the case of the OP semi-synthetic oil group, only in one case, specifically in the OP_01 sample (bus after 170,178 km), the maximum viscosity value was exceeded, which may be the basis for excluding the oil from further use due to significant difficulties in oil distribution and, as a result, the possibility of insufficient lubrication of the moving parts of the mechanism. Compared to the viscosity determined for fresh oil, the viscosity of OP_01 increased by 23%. The remaining samples from this group, compared to the new oil, did not exceed 10% of the difference in values, and in three cases the changes did not even exceed 1.5% of the difference. A fact worth noting, in this case, is that a decrease of 8% compared to the new oil was recorded in the case of the bus with the highest operating mileage of 1,038,973 km, while the case of exceeding the maximum viscosity value was recorded in the vehicle with the lowest operating mileage in the entire tested oil group. Meanwhile, when analyzing the position of the box plot, the minimum of non-outliers was 85.47 mm^2/s, the maximum was 86.77 mm^2/s, and the median was 86.73 mm^2/s. Two extreme values were recorded, including one outside the limits set for this parameter. The data is scattered, and the shape of the graph, indicates a right-sided asymmetry.

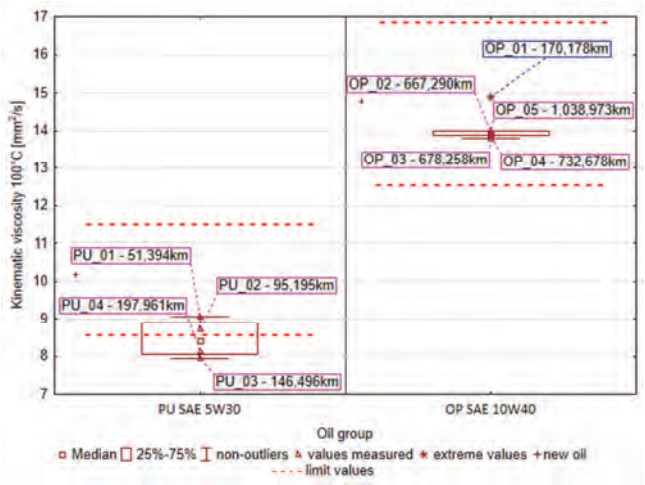

Fig. 2. Measurement of KV@100 in engine oil samples

The graph in Fig. 2 shows that the KV@100°C in a significant number of oil samples (7/9) was within the specified limits, which proves that the oils still met the criteria for a given parameter. Near the lower limit of the parameter, a sample marked as PU_02 was observed (a decrease of 12% compared to fresh oil). Looking at the results of the samples belonging to the OP semi-synthetic oil group, it was observed that all of them were within the prescribed limits. On the other hand, two samples of synthetic PU oil exceeded the lower limit value of the parameter, these were samples PU_03 after 51,301 km of operating mileage on oil (a decrease of 20% compared to fresh oil) and PU_04 after 51,465 km of mileage on oil (a decrease of 18%). From the point of view of viscosity classification according to SAE J300-2015, the measured viscosity for these samples, was fitted in the lower viscosity class (20). In addition, the analysis also showed a tendency to decrease the viscosity with the increase in the overall operating mileage of the tested bus. Oils operating at extremely high temperatures can begin to thermally crack. High temperatures can break/break oil molecules into smaller particles, resulting in a loss of fluidity. According to Macian et al. [9], fluctuations of this parameter are due to two reasons, firstly, due to variable thermal loads of the engine, with the process of base oil oxidation, and the second reason can be seen with the addition of a viscosity index improver to the oil recipe, which, together with the aging of the oil under the influence of high shear conditions and high temperatures encountered during normal engine operation cause a decrease in oil viscosity. According to the research results of Sejkorova et al. [12] KV@40 and KV@100°C of oils obtained from city buses did not exceed the tolerance of ±20% to the fresh oil.

Analyzing the position of the box plot for the PU synthetic oil group, the minimum of the non-outliers was 7.93 mm^2/s, the maximum of the non-outliers was 9.07 mm^2/s, and the median was 8.42 mm^2/s. No extreme values were recorded, the data is not dispersed, and the data graph looks symmetrical. Whereas, when analyzing the position of the box plot for the OP semi-synthetic oil group, the minimum of the non-outliers was 6.67 mm^2/s, the maximum of the non-outliers was 8.6 mm^2/s, and the median was 8.1 mm^2/s. One extreme value was recorded, the data is dispersed, and the shape of the data plot, again as in the first case, indicates a right-sided asymmetry.

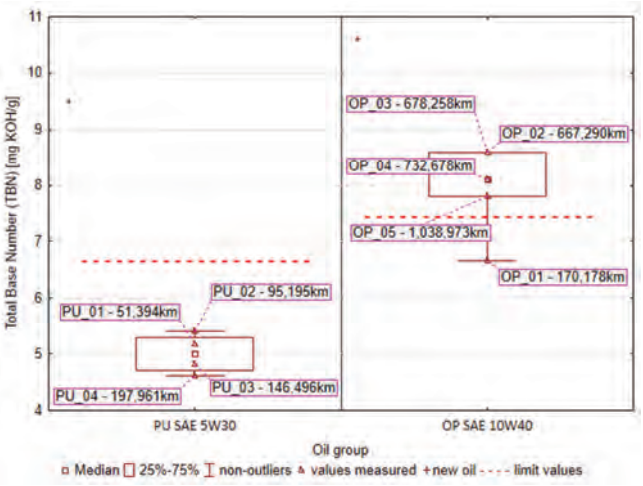

Fig. 3. Measurement of TBN in engine oil samples

TBN is the number of alkaline additives found in the oil to counteract the effects of acids entering the oil from combustion and other sources, and the TAN is a measure of this acidification. The results of the determination of the base number in the analyzed oils are shown in Fig. 3. All samples from the PU synthetic oil group exceeded the determined limit value set as a 30% decrease compared to the new oil. A trend of TBN loss was observed with the increasing mileage of the bus. All samples had similar TBN losses – with the average value being around 47%. The lowest decrease in TBN (at 43%) was observed for the PU_02 sample, which had an OCI 7,000 km less than the other three. This may be another argument for the company to reduce the OCI by 10,000 km. Similar observations regarding the size of changes were presented by Wolak [18],

where the average of changes in the case of passenger cars operated mainly in urban conditions was 50% compared to new oil. Macian et al. [9] analyzing OCI in city buses also noticed a 50% decrease in TBN.

Analyzing the results of TBN measurements in samples of used OP semi-synthetic oil, it was found that four out of five samples were within the specified limits and did not fall below the adopted minimum limit of 7.4 mg KOH/g in this case. In one OP_01 sample, a value lower than the established minimum was obtained, where its value was 6.67 mg KOH/g (decrease by 37% compared to new oil).

Analyzing the position of the box plot for the PU synthetic oil group, the minimum of the non-outliers was 4.6 mg KOH/g, the maximum of the non-outliers was 5.4 mg KOH/g, and the median was 5 mg KOH/g. No extreme values were recorded, the data is not dispersed, and the data graph looks symmetrical. Meanwhile, when analyzing the position of the box plot for the OP semi-synthetic oil group, the minimum of the non-outliers was 6.67 mg KOH/g, the maximum of the non-outliers was 8.6 mg KOH/g, and the median was 8.1 mg KOH/g. No extreme values were recorded, the data is scattered, and the shape of the data plot in this case, indicates a left-sided asymmetry.

During the combustion process, sulfur turns into sulfur dioxide, which in combination with water present in the exhaust gas becomes aggressive sulfuric acid. The higher the alkaline reserve, the longer it takes for acidic products to form in the oil.

The analysis of the TAN in the tested oils showed that in all the analyzed samples from both groups of oils, the limit value was not exceeded. It is worth noting that the higher TAN values were in the group of PU synthetic oil with a viscosity grade of 5W30. In this case, there is also a tendency to increase the TAN content with the increase in the vehicle's operational mileage. A similar conclusion was drawn by Chmielewski [4], where changes in selected physicochemical properties in the registered tests of engine oils from medium-duty trucks confirm the thesis about the correlation of the value of the observed parameter with the mileage of the vehicle. Two samples showed values very close to the limit value – PU_03 (2.25 mg KOH/g) and PU_04 (2.29 mg KOH/g). The results of determining the TAN in the analyzed oils are shown in Fig. 4.

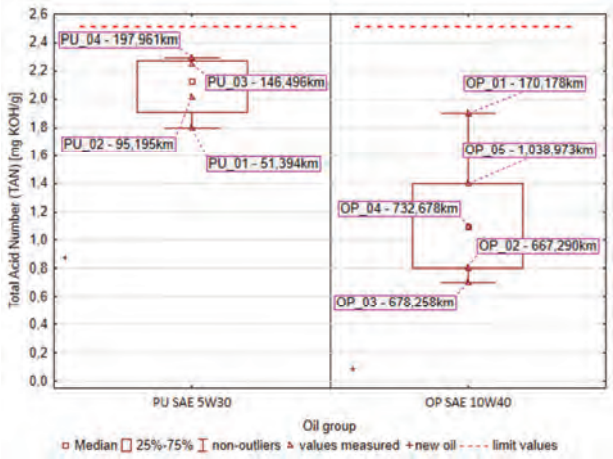

Fig. 4. Measurement of TAN in engine oil samples

Analyzing the position of the box plot for the PU synthetic oil group, the minimum of the non-outliers was 1.8 mg KOH/g, the maximum of the non-outliers was 2.29 mg KOH/g, and the median was 2.13 mg KOH/g. No extreme values were recorded, the data is not dispersed, and the shape of the data plot, in this case, indicates a left-sided asymmetry. Whereas, when analyzing the position of the box plot for the OP semi-synthetic oil group, the minimum of the non-outliers was 0.7 mg KOH/g, the maximum of the non-outliers was 1.9 mg KOH/g, and the median was 1.1 mg KOH/g. No extreme values were recorded, the data is scattered, and the shape of the data plot, in this case, indicates a right-sided asymmetry.

The degree of oxidation of the oil in the tested samples is shown in Fig. 5. Oxidation is a natural process that occurs during oil exploitation. A too-high degree of oxidation of the oil causes degradation of the oil, loss of its lubricating properties, and reduction of corrosion protection. None of the analyzed oils exceeded the established critical oxidation value of 0.4 Abs/0.1 mm. The highest degree of oxidation was recorded in the group of PU_03 oil (146,496 km of the total mileage of the bus), which was 0.32 Abs/0.1 mm. It is worth noting that the observed degree of oxidation in the case of PU_03 (0.32 Abs/0.1 mm) and PU_04 (0.31 Abs/0.1 mm) had an impact on exceeding the limit value of the viscosity parameter both at 40 and 100°C. The lowest value was observed in the OP oil group, in which the OP_05 sample (1,038,973 km of the total mileage of the bus), showed the value of this parameter at the level of 0.16 Abs/0.1 mm. Analyzing the results in terms of their percentage change, measuring fresh oil as a reference in the case of the OP semi-synthetic oil group, the average value was – 35%, while in the case of the PU synthetic oil group – 28%. The highest percentage change was 66% for sample OP_01. The percentage changes observed in the conducted studies are at lower levels than in the work of Macian et al. [9], where the observed changes reached the order of 120%, and in the case of CNG-powered buses even over 160%.

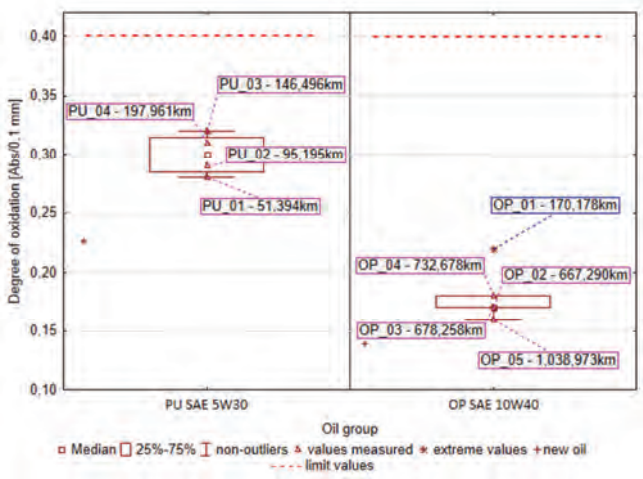

Fig. 5. Measurement of oxidation in engine oil samples

Analyzing the position of the box plot for the PU synthetic oil group, the minimum of the non-outliers was 0.28

Abs/0.1 mm, the maximum of the non-outliers was 0.32 Abs/0.1 mm, and the median was 0.3 Abs/0.1 mm. There are no extreme values recorded, the data is not dispersed, and the shape of the data graph looks symmetrical. Meanwhile, when analyzing the position of the box plot for the OP semi-synthetic oil group, the minimum of the non-outliers was 0.16 Abs/0.1 mm, the maximum of the non-outliers was 0.18 Abs/0.1 mm, and the median was 0.17 Abs/0.1 mm. One extreme value was recorded, the data is scattered, and the shape of the data plot, in this case, indicates a left-sided asymmetry.

As a result of the fuel combustion process in internal combustion engines, nitration products are formed. Excess oxygen is the main cause of most nitration products. Nitration is the process by which the oil reacts with nitrogen oxides (NO_x) to form deposits. The products of this process are oil sludge and other deposits formed on the metal parts of the engine, as a result of which the oil degrades, loses its lubricating properties, and reduces corrosion protection. The established limit value of the nitration degree of 0.4 Abs/0.1 mm was not exceeded in any of the analyzed samples. However, the highest value was observed in the PU synthetic oil group, in which the PU_04 sample showed the value of this parameter at the level of 0.143 Abs/0.1 mm. The lowest degree of nitration was observed in the OP oil group in the OP_03 oil sample (0.081 Abs/0.1 mm), which was taken from the bus after the oil exploitation mileage of 64,162 km. The oil nitration degree is shown in Fig. 6.

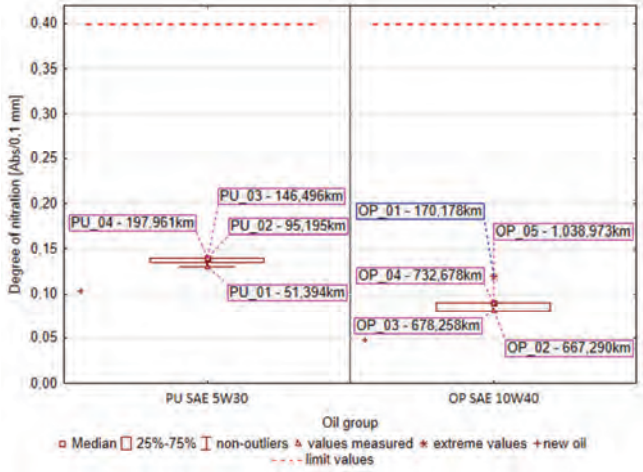

Fig. 6. Measurement of nitration in engine oil samples

The reaction of sulfur (mainly in the fuel) with oxygen results in a process called sulfonation. The products of this process are harmful deposits formed inside the engine, as well as sulfuric acid, which in turn is formed as a result of the reaction of sulfur oxides with water resulting from the combustion process. As with oxidation and nitration, excessive oil sulphonation leads to poor lubrication, deposits, sludge build-up, loss of corrosion protection, and it is an indication of an oil change. The established sulfonation threshold value was not exceeded in any of the tested samples, which proves that good-quality fuel was used in both cases. The highest value was recorded in the OP_01 semi-synthetic oil group, which amounted to 0.296 Abs/0.1 mm. However, the lowest value was also observed in the OP oil group, in which the OP_03 sample showed the value of this parameter at the level of 0.248 Abs/0.1 mm. The results of the degree of sulfonation are shown in Fig. 7.

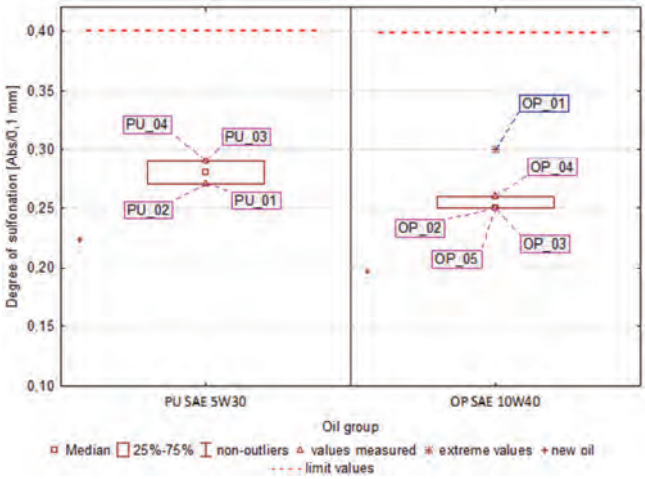

Fig. 7. Measurement of sulfonation in engine oil samples

Lubricants are refined with additives that improve the specific parameters of the oil or grease, and during operation, these additives are subject to wear. The degree of wear of individual additives, such as antioxidants or AW additives during operation, in conjunction with other tests, allows us to determine the intervals for replacing the lubricant in the friction node. Initially, phosphate AW additives break down and form a protective film by bonding to metal surfaces and through oxidative mechanisms. When analyzing the test results, it was observed that only three of them had more than 50% of the remaining content of AW additives – these were samples from the group of semi-synthetic oils OP_05, OP_03, and OP_02. Meanwhile, all samples from the PU synthetic oil group had less than 40% of AW additives during the oil change. The lowest values were observed in two cases OP_01 and OP_04 where these samples no longer had any of AW additives. The remaining content AW additives in the tested oils is presented in Fig. 8.

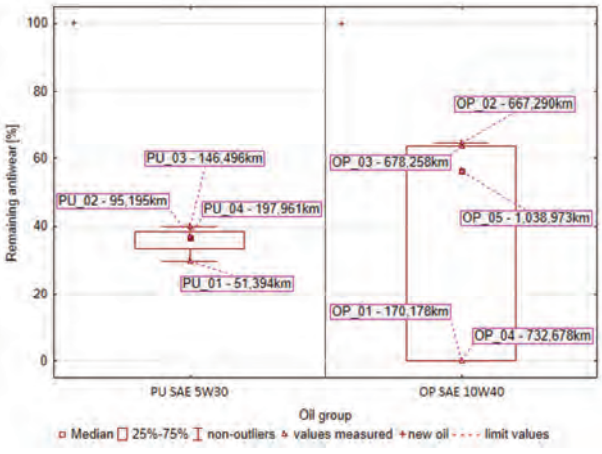

Fig. 8. The remaining content of AW additives in engine oil samples

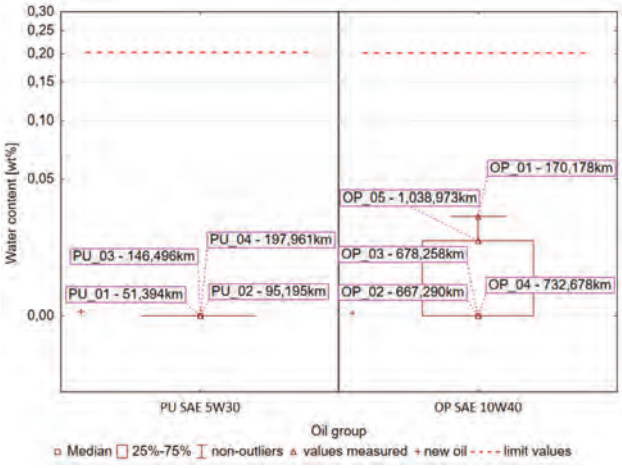

Fig. 9. Measurement of water content in engine oil samples

Figures 9 and 10 show the content of oil impurities in the form of water and glycol in the tested oils. Water is one of the most unfavorable contaminants in any type of service oil. This leads, among others, to oil degradation, and poor corrosion protection. Water in engine oil can cause, for example, condensation of some additives in the form of deposits or hydrolysis of detergents. The presence of too much water may indicate leaks in the cooling system. When observing the graph, no water content was observed in the tested oils, only a trace percentage of water was observed in the OP_01 (0.03 wt%) and OP_05 (0.02 wt%) samples. Referring to Raposo et al. [11], in 10 standard (12 m) city buses, similar percentages of water content oscillating around 0.1wt% were observed.

Figure 10 shows the glycol content in the tested oils. There should be no traces of glycol in the engine oil at all, its presence indicates a defect in the engine's tightness (crack of the head or wear of the head gasket). The presence of glycol leads to oil contamination, sludge and varnish build-up, and potential engine failure. In all tested cases, the limit value for this parameter was exceeded, which may indicate the poor condition of the tested engines.

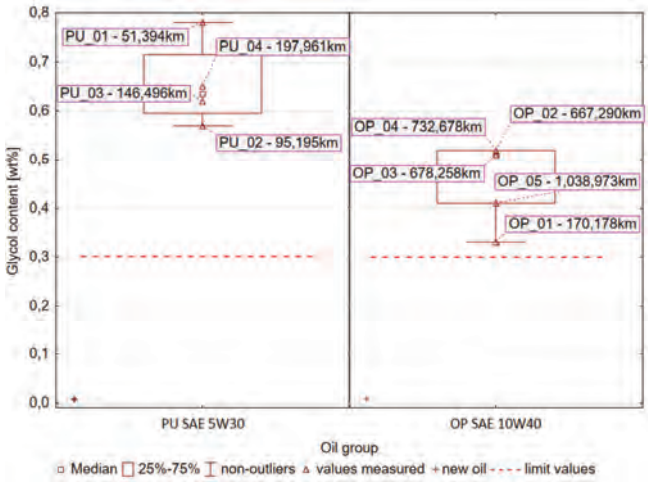

Fig. 10. Measurement of glycol content in engine oil samples

The test results of individual oil parameters for the tested groups are presented in Table 4. When analyzing all the tested samples and the number of exceedances of the limit values for the tested parameters, it was observed that in two cases there were two exceedances, in one case there were three exceedances, and in three cases as many as four exceedances were recorded. It should be emphasized that the OP semi-synthetic oil group fared better in the study, in which in three out of five cases only one exceedance of the

Table 4. The test results of individual oil parameters for the tested groups: summary

Engine oil	Code of the sample/Bus model	Bus ODO [km]	Distance on oil interval [km]	KV@40°C	KV@100°C	oxidation	nitration	sulfonation	TAN	TBN	remaining AW	water content	glycol content	Total
1	2	3	4	5	6	7	8	9	10	11	12	13	14	**15**
OP SAE 10W40	OP1/Autosan Sancity M12LF	170,178	60,500	X	√	√	√	Δ	Δ	X	X	√	X	**4/10**
	OP2/Merc.Benz Connecto 18	667,290	64,683	√	√	√	√	√	√	√	√	√	X	**1/10**
	OP3/Merc.Benz Connecto 18	678,258	64,162	√	√	√	√	√	√	√	√	√	X	**1/10**
	OP4/Merc.Benz Connecto 18	732,678	63,347	√	√	√	√	Δ	√	√	X	√	X	**2/10**
	OP5/Merc.Benz Connecto 12LF	1,038,973	61,131	√	√	√	√	√	√	Δ	√	√	X	**1/10**
Total				**1**	**0**	**0**	**0**	**0**	**0**	**1**	**2**	**0**	**5**	
1	2	3	4	5	6	7	8	9	10	11	12	13	14	15
PU SAE 5W30	PU1/Iveco Urbanway 12	51,394	51,394	X	√	√	√	√	√	X	√	√	X	**3/10**
	PU2/Iveco Urbanway 12	95,195	43,801	Δ	Δ	√	√	√	√	X	√	√	X	**2/10**
	PU3/Iveco Urbanway 12	146,496	51,301	X	X	Δ	√	Δ	√	X	√	√	X	**4/10**
	PU4/Iveco Urbanway 12	197,961	51,465	X	X	Δ	√	Δ	√	X	√	√	X	**4/10**
Total				**3**	**2**	**0**	**0**	**0**	**0**	**4**	**0**	**0**	**4**	
Legend: √ Normal Lubricant Δ To watch X Danger														

limit values for the tested parameters was recorded. The highest number of exceedances was recorded for the percentage of glycol in the oil, where it turned out that all the tested samples exceeded the limit value. Another parameter in which the limit values were exceeded was the total alkaline number, where all samples from the PU synthetic oil group did not fall within the set limits. In addition, only one sample from the same group did not exceed the limit value of oil viscosity at 40°C. There were no exceedances of limit values in such oil parameters as: TAN, oxidation, nitration and sulfonation, and water content.

4. Conclusions

When assessing the condition of used lubricating oils after actual operation, it is necessary to analyze as many parameters as possible. After determining the limit values of individual parameters based on fresh engine oil, the number of exceedances in the used oil samples needs to be checked. Oils no longer fulfill the functions assigned to them if any value reaches its limit, thus giving a diagnostic signal for its replacement. As a result of the conducted tests of selected physicochemical properties of two groups of used engine oils, the nature of their changes and the frequency of exceeding the previously established limit values were determined.

Exceedances were found in KV@40°C (44%) and 100°C (22%), the remaining content of AW additives (22%), TBN (56%) and glycol content (100%). The obtained results did not provide a clear answer to the question of whether the mileage since the last oil change – commonly used to determine the interval between oil changes – is the most reliable criterion. The fact is that, in more than 67% of the samples tested, more than one exceedance was detected. However, when we are guided by the size of these exceedances and the parameter that has been exceeded, the assessment no longer seems unambiguous.

In the case of the OP oil group, buses marked with the symbols OP_1 and OP_4, due to the zero content of AW additives, should be subjected to further in-depth observations, including elementary analysis, to analyze the potential excessive wear of the engine. It is also recommended to limit exceeding the OCI set by the manufacturer.

On the other hand, in the PU oil group, the case of a bus marked with the code PU_2 – where the oil was collected within 7,000 km shorter than the manufacturer's deadline, may constitute a recommendation for the vehicle maintenance program. Reducing the OCI in this case, indicates potential benefits to the condition of the engine and its components, which in turn can reduce maintenance costs as well as reduce downtime and repairs.

These types of tests require at least several oil change cycles, so they must be spread over time. Own experience and publications indicate that single replacement cycles do not reflect the actual state of oil quality in the context of its degradation. In consultation with the public transport company, a two-year research cycle was developed. This will allow the analysis of a minimum of two oil changes, which will allow for a more accurate determination of the condition of the oil.

The presented research should be treated as a pilot study, aimed at showing the problem related to determining the optimal OCI. The authors, are currently in the process of carrying out extended research with a larger number of vehicles and analyzed parameters, as well as an analysis of the specificity of bus operation, which will increase the chance for effective verification of oil change standards proposed by manufacturers.

Acknowledgements

The publication was funded by appropriations of the Faculty of Production Engineering University of Life Sciences in Lublin, within the framework of grant number TKA/MN-1/IMECH/22 to maintain the research potential.

Nomenclature

AW	anti-wear additives
CBM	condition-based maintenance
FTIR	Fourier transform infrared
KV	kinematic viscosity
OCI	oil change interval
ODO	odometer (overall mileage of vehicle)
TAN	total acid number
TBN	total base number

Bibliography

[1] Ahmad R, Kamaruddin S. An overview of time-based and condition-based maintenance in industrial application. Comput Ind Eng. 2012;63(1):135-149. https://doi.org/10.1016/j.cie.2012.02.002

[2] Caban J, Droździel P, Krzywonos L, Rybicka I, Šarkan B, Vrábel J. Statistical analyses of selected maintenance parameters of vehicles of road transport companies. Adv Sci Technol Res J. 2019;13(1):1-13. https://doi.org/10.12913/22998624/92106

[3] Chmielewski Z. Reliability of engine oil in operation (in Polish). Autobusy – Technika, Eksploatacja, Systemy Transportowe. 2017; 18(12):761-764.

[4] Chmielewski Z. Assessment of the kinetics of changes in selected physicochemical indicators of engine oil in operation. Combustion Engines. 2022;188(1):24-29. https://doi.org/10.19206/CE-141337

[5] Chmielewski Z, Stobiecki J, Górska M. The concept of evaluation of reliability of modern engine oils in operation. Autobusy – Technika, Eksploatacja, Systemy Transportowe. 2018;19(12):337-340. https://doi.org/10.24136/atest.2018.410

[6] Du Y, Wu T, Makis V. Parameter estimation and remaining useful life prediction of lubricating oil with HMM. Wear. 2017;376:1227-1233. https://doi.org/10.1016/j.wear.2016.11.047

[7] Gołębiowski W, Zając G, Sarkan B. Evaluation of the impact of tractor field works on changes in selected elements of engine oils. Agric Eng. 2022;26:1-12. https://doi.org/10.2478/agriceng-2022-0001

[8] Gołębiowski W, Zając G, Wolak A. Analysis of engine oils from farm tractors in the aspect of their change. Agric Eng. 2019;23(1):25-38. https://doi.org/10.1515/agriceng-2019-0003

[9] Kral Jr J, Konecny B, Kral J, Madac K, Fedorko G, Molnar V. Degradation and chemical change of longlife oils following intensive use in automobile engines. Measurement. 2014; 50:34-42. https://doi.org/10.1016/j.measurement.2013.12.034
[10] Macian V, Tormos B, Ruiz S, Miro G. Low viscosity engine oils: study of wear effects and oil key parameters in a heavy duty engine fleet test. Tribol Int. 2016;94:240-248. https://doi.org/10.1016/j.triboint.2015.08.028
[11] Raposo H, Farinha J, Fonseca I, Ferreira L. Condition monitoring with prediction based on diesel engine oil analysis: a case study for urban buses. Actuators. 2019;8(1):14. https://doi.org/10.3390/act8010014
[12] Raposo H, Farinha JT, Fonseca I, Galar D. Predicting condition based on oil analysis – a case study. Tribol Int. 2019; 135:65-74. https://doi.org/10.1016/j.triboint.2019.01.041
[13] Sejkorová M, Hurtová I, Glos J, Pokorný J. Definition of a motor oil change interval for high-volume diesel engines based on its current characteristics assessment. Acta Univ Agric Silvic Mendel Brun. 2017;65(2):481-490. https://doi.org/10.11118/actaun201765020481
[14] Sejkorová M, Hurtová I, Jilek P, Novák M, Voltr O. Study of the effect of physicochemical degradation and contamination of motor oils on their lubricity. Coatings. 2021;11(1):60. https://doi.org/10.3390/coatings11010060
[15] Semjonovs J, Springis G, Leitans A. Increasing of engine oil change interval by using additional oil filter in diesel engines. Eng Rur Develop. 2014;(13):247-252. http://www.tf.llu.lv/conference/proceedings2014/Papers/42_Semjonovs_J.pdf
[16] Shin JH, Jun HB. On condition based maintenance policy. J Comput Des Eng. 2015;2(2):19-27. https://doi.org/10.1016/j.jcde.2014.12.006
[17] Urzędowska W, Stępień Z. Selected issues concerning changes in the properties of engine lubricating oil in operation (in Polish). Nafta-Gaz. 2012;12:1102-1110.
[18] Vališ D, Zak L, Pokora O. Engine residual technical life estimation based on tribo data. Eksploat Niezawodn. 2014; 16(2):203-210. RIV/00216224:14310/14:00076267
[19] Vališ D, Žák L, Pokora O, Lánský P. Perspective analysis outcomes of selected tribodiagnostic data used as input for condition based maintenance. Reliab Eng Syst Saf. 2016; 145:231-242. https://doi.org/10.1016/j.ress.2015.07.026
[20] Wolak A. TBN performance study on a test fleet in real-world driving conditions using present-day engine oils. Measurement. 2018;114:322-331. https://doi.org/10.1016/j.measurement.2017.09.044
[21] Wolak A, Zając G. The kinetics of changes in kinematic viscosity of engine oils under similar operating conditions. Eksploat Niezawodn. 2017;19(2):260-267. https://doi.org/10.17531/ein.2017.2.14
[22] Zając G, Gołębiowski W, Szczepanik M, Wolak A, Sejkorová M. Analysis of changes in soot content in engine oils under operating conditions. Lubricants. 2023;11(2):89. https://doi.org/10.3390/lubricants11020089
[23] Zhu X, Zhong C, Zhe J. Lubricating oil conditioning sensors for online machine health monitoring – a review. Tribol Int. 2017;109:473-484. https://doi.org/10.1016/j.triboint.2017.01.015

Wojciech Gołębiowski, DEng. – Faculty of Production Engineering, University of Life Sciences in Lublin, Poland.
e-mail: *wojciech.golebiowski@up.lublin.pl*

Grzegorz Zając, DSc., DEng. – Faculty of Production Engineering, University of Life Sciences in Lublin, Poland.
e-mail: *grzegorz.zajac@up.lublin.pl*

doc. Marie Sejkorová, DEng. – Faculty of Transport Engineering, University of Pardubice, Czech Republic.
e-mail: *marie.sejkorova@upce.cz*

Artur Wolak, DSc., DEng. – Institute of Quality and Product Management Sciences, Cracow University of Economics, Poland.
e-mail: *artur.wolak@uek.krakow.pl*

Article citation info:
Sitnik LJ. Comparison of the cumulative energy demand of BEV's and FCEV's in their long-term operation. Combustion Engines. 2024;196(1):24-29. https://doi.org/10.19206/CE-168438

Lech Jerzy SITNIK

Combustion Engines
Polish Scientific Society of Combustion Engines

Comparison of the cumulative energy demand of BEV's and FCEV's in their long-term operation

ARTICLE INFO

Received: 6 April 2023
Revised: 9 June 2023
Accepted: 16 June 2023
Available online: 23 November 2023

The paper presents a method of using the theory of cumulative energy demand to assess this demand in long-term operation of vehicles with a mileage forecast of up to 350,000 km. Based on the results of operational "consumption" of energy and taking into account the energy "costs" of obtaining it, a comparison of the currently popular BEV's (Battery Electric Vehicles) and FCEV's (Fuel Cell Electric Vehicles) was presented. The question arises how much energy must be used to propel vehicles in their natural operation. After calculating using available data, the answer is – by operating FCEV's on average, two times more electricity is needed than by operating BEV's.

Key words: *energy, consumption, BEV's, FCEV's comparison*

1. Introduction

Discussions are underway and the first decisions regarding a significant reduction in carbon dioxide emissions have already been made. This also applies to transport. Today's proposals for transportation are either fully electric vehicles (BEV's) or hydrogen hybrid vehicles (FCEV's). Another direction perceived as future-oriented is the use of internal combustion engines powered by e-fuels (mainly ammonia (NH_3), methane (CH_4) or methanol (CH_3OH). This applies in particular to trucks. These vehicles consume significant amounts of fuel, but their number compared to passenger cars is small, and problems with developing new engines that can run on e-fuels are perceived as niche problems.

The issue of fuel consumption assessment is, of course very extensive and it is impossible to discuss it exhaustively here, however, some literature items on these issues seem to be very interesting.

The general way of treating an internal combustion engine in operation has been presented in [4]. A two-state model of transitions between engine states was developed, a risk function and a renewal (restitution) function were proposed. The possibility of assessing the credibility of the diagnosis for making operational decisions using the statistical decision theory was presented.

It has been found that electronic driver assistance systems help to reduce fuel consumption [7] by appropriately controlling the powertrain, and telling the driver how to steer the vehicle or which route to take. Examples of possibilities to reduce fuel consumption using an electronic controller are given. The support systems of two selected vehicle propulsion systems are described in detail. The article also includes examples of other driver assistance systems that can be used to reduce operational fuel consumption.

The paper [5] presents the results of analyzes of changes in fuel consumption depending on the intensity of everyday use of the vehicle, ambient temperature and cumulative mileage. The database included more than 600,000 kilometers of mileage and fuel purchase records, obtained from the data contained on the website http://fueleconomy.gov.

ICEV and HEV vehicles were compared. For ICEV vehicles, the variation within the same make and type was found to be 23% of the total variation, and 77% was between different vehicle brands and types. For hybrids, the figures are 19% and 81%, respectively. On-road fuel economy has been found to increase non-linearly as a function of mileage, with almost all of the increase occurring in the first few thousand miles. The trend for hybrid vehicles is very different from the trend for ICEVs.

Paper [13] presents a model of a fuel cell hybrid electric vehicle (FCHEV), its validation and a comparison of various control strategies for the Toyota Mirai (1st generation). The FCHEV model is created in the MATLAB® Simulink environment. The model was validated using operational data obtained from the open-source Argonne National Laboratory (ANL) database. According to the authors, the ECMS control strategy outperforms other strategies in all driving cycles by 0.4–15.6%.

The aim of the work [14] is to improve the energy efficiency of extended-range electric vehicles (EREV) and reduce the cumulative load on the batteries. The results show that the energy demand in the optimized operating mode under WLTP conditions increases by 4.49%, and the accumulated ampere-hours of the battery is reduced by 11.37%.

Fuel consumption in the WLTP tests was optimized, and the obtained data were verified with the results of controlled operation [2]. A fuel consumption map was created based on a large amount of ICEV data through fast data acquisition with the ISO-15765-4-CAN protocol. Next, a theoretical carbon dioxide (CO_2) map was generated. The obtained results were compared on the WLTC and the local route. Significant improvements in both consumption and CO_2 emissions were found. It was also found that the use of the hybrid system on local routes with a greater proportion of urban driving conditions resulted in a greater improvement despite a slight decrease in the overall efficiency of the electrical system.

This article [6] implements an artificial neural network (ANN) for fuel consumption modeling to predict total and

instantaneous fuel consumption while traveling based on parameters such as engine load (%), speed (rpm) and vehicle speed (km/h). Data used for modeling were collected at a frequency of 1 Hz using portable monitoring systems (PEMS). The performance of the artificial neural network was assessed using mean absolute error (MAE), and root mean square error (RMSE). The model was further evaluated based on operational data. Artificial neural networks were shown to perform slightly better than other machine learning techniques such as linear regression (LR) and random forest regression (RFR), with high R-square (R^2) and lower mean-square error.

The aim of the work [1] was to build a computational model of fuel consumption and CO_2 emissions, taking into account the technical specification, vehicle load and transport distance. The proposed model is evaluated on various examples for different types of vehicles. The model offers an effective tool for making operational decisions for transport systems by calculating fuel consumption and the resulting CO_2 emissions.

Although the presented works seem to be methodologically very interesting, it is difficult to find works covering the issue of long-term fuel consumption (for several years of vehicle operation), especially in relation to new energy carriers, such as for example hydrogen.

The problem of changing energy carriers is of course not new. The author, in the work entitled "Engine eco-fuels" published in 2004 [10], presented a drawing in which he presented the probable development of modern engine fuels.

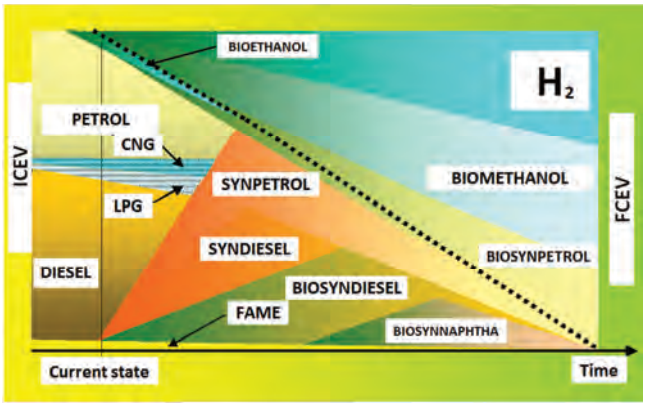

Fig. 1. Probable development of fuels for transport from the perspective of 2004 [10]

As the above (Fig. 1) shows, the main fuels should remain hydrogen (H_2), bio-methanol (biomethanol) and synthetic gasoline of biological origin (biosynpetrol). It seemed then that internal combustion engines would be replaced by fuel cells, while synthetic bio-gasoline would be the fuel for internal combustion engines operating in hybrid vehicle drives. Fuel cell vehicles were to be of two types; using hydrogen (FCEV) and biomethanol (DMFCEV) as fuel.

A return to electric vehicle drives was not envisaged at that time.

Today, the situation has changed fundamentally – precisely as a result of the introduction of BEV. Although, as you can see, it is difficult to predict the direction of further development of the automotive industry, but from today's point of view, it seems that in the future, two types of drive will be developed, i.e. electric drive (BEV) and hydrogen fuel cell drive (FCEV). Each of these options has known advantages and disadvantages. In electric vehicles, this is still a low energy density (batteries are still about 10× too heavy, and their charging time is about 30× too long). FCEV vehicles, similar in their assumptions but with an on-board source of converting hydrogen into electricity, are problematic in terms of storing hydrogen on board the vehicle (hydrogen technologies are mastered in large-scale stationary devices, the transition to small-scale and mobile devices is a new technological challenge) – hence the FCEV concept, which has been developed for over 30 years, has not yet conquered the car market.

However, the technological challenge is not limited to vehicle construction. The main problem is the issue of obtaining energy to drive vehicles from renewable resources. Without ensuring the possibility of using energy only from renewable resources, the implementation of new solutions in vehicles is pointless. Therefore, the question arises how much energy must be used to propel vehicles in their natural operation (less precisely defined as everyday) and how the BEV's and FCEV's compare in this aspect. This work is devoted to these issues.

The paper presents the theory of assessing cumulative energy demand and a method of using this theory to assess energy demand in long-term operation of vehicles with a mileage forecast of up to 350,000 km. Based on the results of operational "consumption" of energy and taking into account the energy "costs" of obtaining it, a energetically comparison of operating the currently popular BEV's and FCEV's was presented.

2. Use of the theory of cumulative energy/fuel consumption

Analyzed the energy consumption of BEV by the assumptions that E_i – i-th recharging, t_{di} – mileage to E_i, after i-th recharging it is as:

$$EE_i = \frac{100E_i}{t_{di} - t_{di-1}} \tag{1}$$

The term energy economy can be confusing. It is understood similarly to the classic fuel economy, which is based on the concept of fuel consumption. However, energy is not consumed but only changes its form, despite the fact that in the literature, the term energy consumption is used similarly to fuel consumption, so also energy economy seems possible for use.

The average energy economy (EEA) is

$$EEA_k = \frac{1}{k}\sum_{i=1}^{k} EE_i \tag{2}$$

CEC is given as:

$$CEC(t_{dk}) = \sum_{i=1}^{k} E_i \tag{3}$$

Using the BEV's database (spritmonitor.de [11], vehicle code 630364) as shown in Fig. 2. In this particular case, in the period from 2014.03.29 to 2017.08.13, the mileage of the car was in the range of 1,619 to 188,472 km, while the number of charges k = 103.

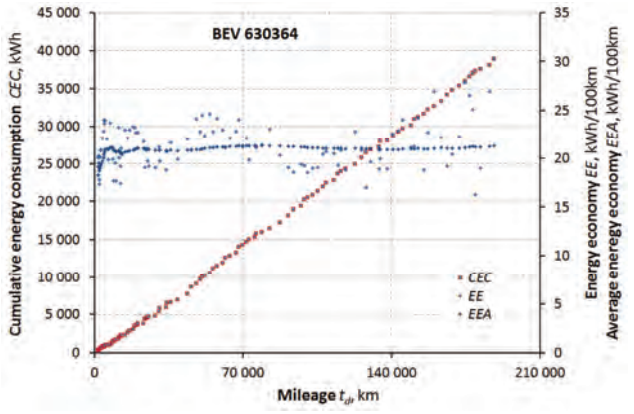

Fig. 2. Energy consumption of analyzed middle class BEV

EE in operation, changes between 16.26 and 30.25 kWh/100 km (about two times). At the same time the EEA changed from 18.25 to 21.31 kWh/100 km. On Fig. 2 is the CEC (in kWh) given, according to [9].

$$\mathrm{CEC(t)} = \mathrm{ct}^{a+1} \tag{4}$$

wherein: c, a – coefficients.

Most often, mileage "t_d" is proportional to the operation time "t" also ($t \rightarrow t_d$), therefore

$$\mathrm{CEC}(t_d) = \mathrm{ct}_d^{a+1} \tag{5}$$

The derivative of the CEC is the intensity of the cumulative energy consumption:

$$\mathrm{ICEC}(t_d) = \frac{\mathrm{dCEC}(t_d)}{\mathrm{dt}_d} = c(a+1)t_d^a \tag{6}$$

Specific cumulative energy consumption (SCEC) is given as

$$\mathrm{SCEC}(t_d) = \frac{\mathrm{CEC}(t_d)}{t_d} = \mathrm{ct}_d^a \tag{7}$$

The SCEC can be in kWh/km or in Ws/km. Coefficients „c" and „a" are to derived from the data from natural operation of vehicle. One of the good database is for example spritmonitor.de [11]. From this database were 9 BEVs randomly selected. On Fig. 3 are data for BEV 630364 as example presented.

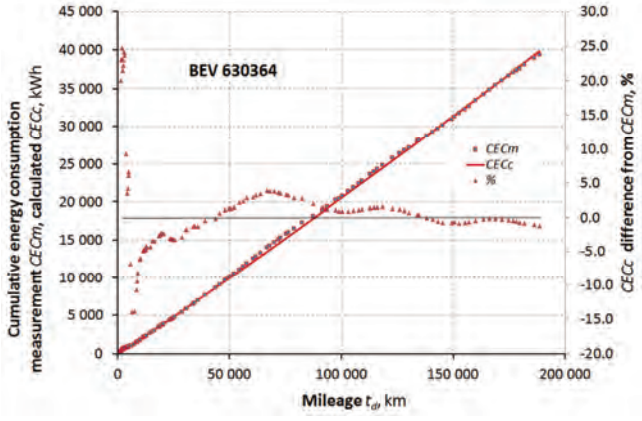

Fig. 3. Measured and model data and it's difference for cumulative energy consumption of BEV 630364

The difference DCEC (in %) results from the equation (8)

$$\mathrm{DCEC}(t_d) = 100\frac{\mathrm{CEC_c}(t_d) - \mathrm{CEC_m}(t_d)}{\mathrm{CEC_c}(t_d)} \tag{8}$$

For BEV 630364, the DCEC is on Fig. 3 showing. The adequacy data of the model (4) for all analyzed BEV's are collected in Table 1.

Table 1. Data of the analyzed BEVs

	BEV	R-Square	Rechargings	Coefficient *c*	Coefficient *a*
1	**658012**	0.99983	363	0.373468	-0.061132
2	**811970**	0.99860	31	0.829841	-0.124191
3	**651401**	0.99936	493	0.273221	-0.026875
4	**829324**	0.99989	104	0.193178	0.004073
5	**630364**	0.99811	103	0.123515	0.044163
6	**628759**	0.99966	812	0.302101	-0.029461
7	**804546**	0.99683	82	1.162061	-0.113322
8	**607293**	0.99863	744	0.205950	0.013584
9	**856153**	0.99973	38	0.176429	-0.012076

The high values of R-square are not an exception (see e.g. [9]). CEC as a function of mileage seems to be a straight line (Fig. 3), but this is not the case (because a#0).

By knowledge of „c" and „a" the further characteristics of CEC can be presented. These are the ICEC, SCEC. All these characteristics together form the energy footprint of the vehicle (for BEV 630364 – Fig. 4).

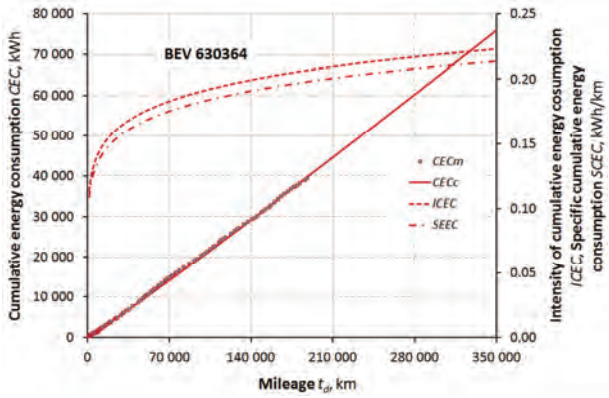

Fig. 4. Energy footprint of BEV 630364

For each of the nine analyzed BEVs the CEC are shown in Table 1 and Fig. 5.

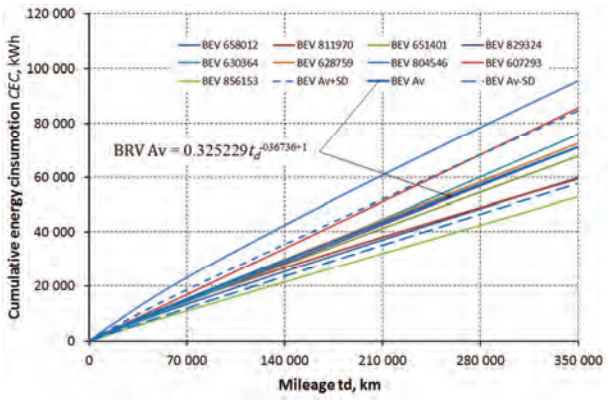

Fig. 5. Cumulative energy consumption of analyzed BEVs

Some CEC (e.g. BEV 804546 or BEV 856153) clearly differ from others. These data reflect the exploitation conditions e.g. BEV 804546 was almost 100% used on highway driving. Since it was decided that the comparison would be between BEV's and FCEV's cars, the cumulative energy consumption theory presented above was used to assess the cumulative energy (fuel) consumption of hydrogen by the FCEV's. An example of processing hydrogen consumption results is shown in Fig. 6. Figure 6 shows fuel economy (FE) calculated according to the same procedure as EE.

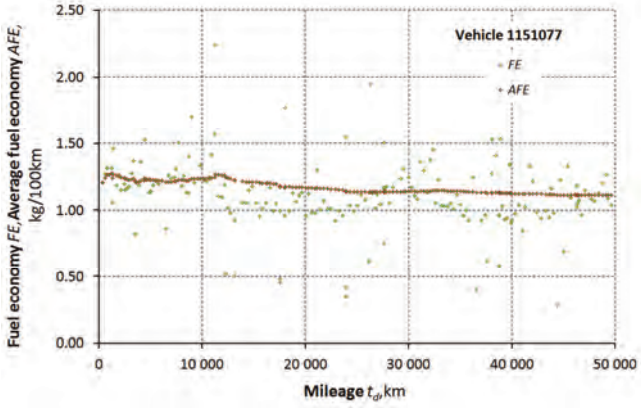

Fig. 6. Fuel economy (FE) and average fuel economy (AFE) for the vehicle 1151077

Fuel consumption footprint of FCEV 1151077 is presented on the Fig. 7.

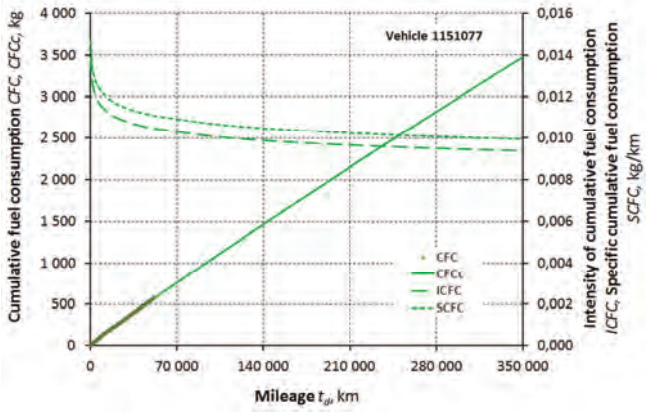

Fig. 7. Fuel consumption footprint of FCEV 1151077

The calculation results for the seven analyzed FCEVs are given in Table 2.

Table 2. The calculation results for footprint of analyzed FCEVs

	FCEV	R-Square	Refuelings	Coefficient *c*	Coefficient *a*
1	**1151077**	0.998687	197	0.020574	-0.056978
2	**1254191**	0.993665	40	0.016105	-0.044394
3	**1316958**	0.985653	8	0.005089	0.072905
4	**1195603**	0.996220	65	0.000080	0.460080
5	**1242674**	0.999922	5	0.006109	0.015091
6	**1349603**	0.999762	12	0.007836	-0.008227
7	**1394273**	0.999547	31	0.011271	-0.006655

Cumulative fuel consumption up to mileage of 350,000 km of analyzed FCEV's are presented here in the Fig. 8.

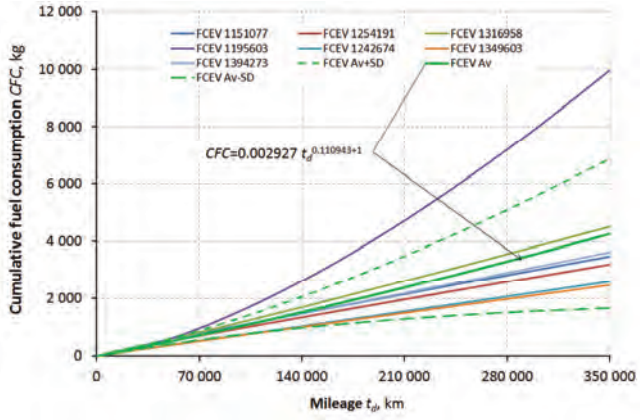

Fig. 8. Cumulative fuel consumption up to mileage of 350,000 km of analyzed FCEV's

As in the case of BEV's, there are significant deviations from the average value in the operation of hydrogen-powered FCEV's. These deviations increase as the mileage of the vehicles increases. Also in this case, these deviations are caused by very different operating conditions of individual cars. As stated earlier, obtaining electricity or fuel requires additional energy inputs related to, for example, transmission losses.

In the case of electricity generation, it is estimated that its supply to vehicle batteries is associated with approximately 20% losses. This means that when estimating the vehicle's demand for electric energy, it is to multiplying the CEC by 1.2.

Obtaining hydrogen involves the need to spend energy on electrolysis of water (if hydrogen is to be obtained from this resource), then purification of hydrogen, its compression (or liquefaction), transport to the gas station, and then pumping it to the tank of the vehicle. It is estimated that these activities require 40 kWh_e to 70 kWh_e of electricity for every 1kg of hydrogen.

In further considerations, it was assumed that in order to obtain 1 kWh of energy in a BEV battery, 1.2 kWh_e of electricity must be involved, while in order to obtain 1 kg of hydrogen for FCEV, a very favorable variant was adopted that "only" 40 kWh_e of electricity must be engaged. After the appropriate multiplication of the values of the cumulative electricity and cumulative fuel (hydrogen) consumption in the conditions of vehicle operation, were obtained for average values and standard deviations. The data is shown in Fig. 9.

The obtained results are quite "shocking". The demand for electricity for the operation of hydrogen-powered FCEV's is on average, about twice as high as for BEV's.

In addition, deviations from the average value of FCEV's electricity demand are more than four times higher than for BEV's. Of course, small numbers of vehicles were analyzed. As the number of analyzed vehicles increases, these deviations will, of course decrease. All this assuming the most favorable (currently) indicators. A general improvement in the situation is to be expected in the future.

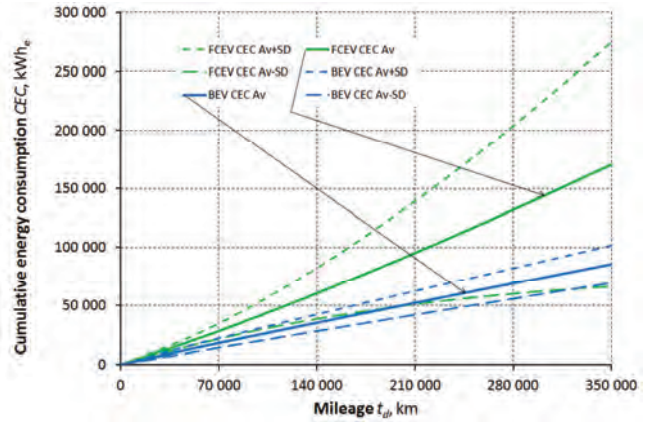

Fig. 9. Summarized cumulative electricity consumption of BEV's and FCEV's for their operation up to 350,000 km

Summary

The presented method for assessment of energy demand can be used for assessing of electricity demand for long term operation of vehicles.

The work concern comparison of BEV's and FCEV's. There are no published papers for direct discussion of this problem. The works (e.g. [3, 8, 12]) present part of problem but from the fully other point of view of assessing of energy consumption of vehicles in operation.

For analyzed here BEV's and FCEV's obtained was very good adequacy of the mathematical model of cumulative energy consumption. Correlation coefficients are very high e.g. R-square is higher than 0.99.

Mathematical models of cumulative energy consumption, intensity of this consumption and specific energy consumption, form together the vehicle's "energy footprint". Those footprint can be useful for further analyses.

It is noticed a large dispersion of courses of cumulative energy consumption (although the vehicles of the same type and brand in each group were analyzed). This dispersion increases with the mileage. As a result the discrepancies between the electricity demand in the vehicle group are large and increase with the mileage. In the analyzed case, discrepancies in electricity need are four times higher in case of FCEV's as in BEV's.

The average cumulative electricity consumption of FCEVs is twice BEV's (in analyzed examples with random data).

Acknowledgements

The author would like to thank the creators of the spritmonitor.de database for its creation and maintenance, as well as all those who present data from the use of vehicles there.

Nomenclature

a	coefficient
c	coefficient
e_i	i-th quantum of energy
$\bar{e}(t)$	average size of the quantum of energy
$n(t)$	energy quantum number
t	time
t_d	mileage
BEV	battery electric vehicle
EC	energy consumption
EE	energy economy
EEA	average energy economy
$CEC(t)$	cumulative energy consumption to the time t
$CEC(t_d)$	cumulative energy consumption to the mileage t_d
CFC	cumulative fuel consumption
$DCEC(t_d)$	difference calculated and measured energy consumption to the t_d
FCEV	fuel cell electric vehicle
$ICEC(t_d)$	intensity of the cumulative energy consumption
$SCEC(t_d)$	specific cumulative energy consumption

Bibliography

[1] Aksoy A, Küçükoğlu İ, Ene S, Öztürk N. Integrated emission and fuel consumption calculation model for green supply chain management. Procedia – Social and Behavioral Sciences. 2014;109:1106-1109. https://doi.org/10.1016/j.sbspro.2013.12.595

[2] Balcı Ö, Karagöz Y, Gezer O, Kale S, Köten H, Pusat S et al. Numerical and experimental investigation of fuel consumption and CO_2 emission performance for a parallel hybrid vehicle. Alexandria Eng J. 2021;60(4):3649-3667. https://doi.org/10.1016/j.aej.2021.02.025

[3] Braun A, Rid W. Energy consumption of an electric and an internal combustion passenger car. A comparative case study from real world data on the Erfurt circuit in Germany. Transp Res Procedia. 2017;27:468-475. https://doi.org/10.1016/j.trpro.2017.12.044

[4] Girtler J. Possibility of estimating the reliability of diesel engines by applying the theory of semi-Markov processes and making operational decisions by considering reliability of diagnosis on technical state of this sort of combustion engines. Combustion Engines. 2015;163(4):57-66. https://doi.org/10.19206/CE-116857

[5] Greene DL, Liu J, Khattak AJ, Wali B, Hopson JL, Goeltz R. How does on-road fuel economy vary with vehicle cumulative mileage and daily use? Transport Res D-Tr E. 2017;55:142-161. https://doi.org/10.1016/j.trd.2017.06.004

[6] Katreddi S, Thiruvengadam A. Trip based modeling of fuel consumption in modern heavy-duty vehicles using artificial intelligence. Energies. 2021;14(24):8592. https://doi.org/10.3390/en14248592

[7] Kropiwnicki J, Kortas P. Potentials for fuel consumption reduction by using electronic driver assistance systems. Combustion Engines. 2013;154(3):250-256.

[8] Li W, Stanula P, Egede P, Kara S, Herrmann C. Determining the main factors influencing the energy consumption of electric vehicles in the usage phase. Procedia CIRP. 2016; 48:352-357. https://doi.org/10.1016/j.procir.2016.03.014

[9] Sitnik LJ. Energy demand assessment for long term operation of vehicles. SAE Technical Paper 2020-01-2165. 2020. https://doi.org/10.4271/2020-01-2165

[10] Sitnik L. Engine eco fuels. Wroclaw Publishing House (in Polish). Wroclaw 2004.

[11] Spritmonitor. https://www.spritmonitor.de/

[12] Travesset-Baro O, Rosas-Casals M, Jover E. Transport energy consumption in mountainous roads. A comparative case study for internal combustion engines and electric vehicles in Andorra. Transport Res D-Tr E. 2015;34:16-26. https://doi.org/10.1016/j.trd.2014.09.006

[13] Usmanov U, Ruzimov S, Tonoli A, Mukhitdinov A. Modeling, simulation and control strategy optimization of fuel cell hybrid electric vehicle. Vehicles. 2023;5(2):464-481. https://doi.org/10.3390/vehicles5020026

[14] Xu Y, Zhang H, Yang Y, Zhang J, Yang F, Yan D et al. Optimization of energy management strategy for extended range electric vehicles using multi-island genetic algorithm. J Energy Storage. 2023;61:106802. https://doi.org/10.1016/j.est.2023.106802

Prof. Lech J. Sitnik, DSc., DEng. – Faculty of Mechanical Engineering, Wroclaw University of Science and Technology, Poland.
e-mail: *lech.sitnik@pwr.edu.pl*

Article citation info:
Zacharewicz M, Zadrąg R, Bogdanowicz A, Socik P, Wirkowski P, Hołownia J. Evaluation of the impact of the thermal state of a diesel engine on its efficiency. Combustion Engines. 2024;196(1):30-36. https://doi.org/10.19206/CE-170793

Marcin ZACHAREWICZ
Ryszard ZADRĄG
Artur BOGDANOWICZ
Paweł SOCIK
Paweł WIRKOWSKI
Jakub HOŁOWNIA

Combustion Engines
Polish Scientific Society of Combustion Engines

Evaluation of the impact of the thermal state of a diesel engine on its efficiency

ARTICLE INFO

Received: 31 May 2023
Revised: 7 August 2023
Accepted: 7 August 2023
Available online: 21 September 2023

The paper presents the results of model and empirical research on the influence of the thermal state of a diesel engine (oil temperature) on its indicated (thermal) efficiency. The paper contains a test plan, including a description of the test object, test equipment, and measurement points on a real object. In the following part, the results of tests carried out on a real object (laboratory single-cylinder engine) and the results of model tests obtained on the original engine model are presented. The results are presented both in tabular and graphical form. The obtained test results allowed to determine the relative value of the influence of the engine's thermal state on its efficiency for various operating conditions (load and rotational speed).

Key words: *marine diesel engine, engine efficiency, mathematical model*

1. Introduction

The issue of the influence of the thermal state of a diesel engine on its efficiency is important in the case of marine engines, both main propulsion and auxiliary engines driving marine generators. According to the operating guidelines, marine diesel engines of the main propulsion should be preheated [17, 18] to a temperature of about 323 to 333 K before starting them. This is done by heating the lubricating oil with electric heaters or with steam in the case of ships equipped with steam boilers. There are also solutions in which the oil is preheated in the main propulsion engines by means of water cooling the auxiliary engines.

The Polish Navy uses both wet and dry sump engines. For wet-sump engines, the oil heater is mounted in the engine crankcase. For engines with a dry sump (Zviezda type M 503 and M520), the heated oil is circulated by means of a pre-lubrication pump and a drain pump. There is no preheating requirement on auxiliary engines. Nevertheless, these engines, like the main engines, are installed in the ship's engine room and have an ambient temperature of about 293 K. In the case of the main engines, the heating process can be omitted in special situations, such as the ship's emergency exit to sea.

The idea of conducting research on the impact of the thermal state of a diesel engine on its efficiency is not new, but it has not been sufficiently explored in the case of powering marine reciprocating internal combustion engines.

Andrews et al. [1] showed that engine fuel consumption, for cars, has a linear dependence on ambient temperature. Over an urban drive cycle, the fuel consumption was shown to increase by 18% when the ambient temperature decreased from 304 K to 271 K. The work of Tobergte et al. [15, 17] highlighted a similar trend for three different variants of the engine (a 1200 cm^3 3-cylinder SI engine, a 1400 cm^3 4-cylinder SI engine, and an 1800 cm^3 SI engine) [11]. Kozak's research showed that the soot contamination of engine oil increases with its "mileage" [7, 8].

Burke et al. stated in their research work that an increase in the engine temperature from 323 K to 353 K reduces the engine friction by 44% because of 67% lower oil viscosity. Moreover, reduction in the emissions of nitrogen oxides (NO_x) and fuel consumption of 13.5% and 0.7% respectively have been achieved. The research investigated that hotter engine temperatures reduce ignition delay, making combustion occur earlier in the cycle, which has a positive effect on fuel consumption but a negative effect on NO_x emissions [4].

Genca and Radica in their research on the effect of heating a compression-ignition engine on its performance observed a decrease in fuel consumption and CO_2 production. The research was conducted in metropolitan and non-metropolitan conditions at low ambient temperatures [6].

Bielaczyc et al. [2] in their work point out that despite meeting the stringent standards imposed by the EU, toxic exhaust emissions, including NO_x, are still a major problem. According to the researchers, the main cause is the high viscosity of oil and friction of engine components. Therefore, they highlight the significance of the issue of conducting research on optimizing the performance of a cold-start vehicle both in terms of fuel consumption and toxic emissions.

Broatch A. et al. [3] evaluated the suitability of different biodiesel fuels, with and without additives, for cold starting DI (direct injection) diesel engines. The results have shown that the engine start-ability with pure biodiesel fuels can be deteriorated. The article also demonstrated that by using diesel/biodiesel blends the start-ability of the engine can be recovered with the additional benefit of reducing the opacity peak of the exhaust gases.

Tauzia et al. [14] show that the effects of coolant and oil temperature on engine behaviour are quite complex with several interactions :

- during the intake phase, the volumetric efficiency was modified. It affect for turbocharger (the energy available for the turbine being reduced when exhaust gas was at a lower temperature)
- turbocharger friction and heat transfer altered as well

– friction losses increased when oil or coolant temperature decreased
– the exhaust energy decreased.

Despite the requirement to heat the oil in the main engines before starting them, there are situations when the engine is started in the so-called cold state. Such a situation was recreated in the article, where empirical and model tests of the influence of the thermal state of the engine on its indicated efficiency (thermal efficiency) were carried out. In the empirical research, a stand of a single-cylinder engine driving an eddy current brake through a planetary gear was used. This stand was equipped with the equipment necessary for the tests, such as measurement of torque, crankshaft rotational speed, fuel and oil temperature, gravimetric measurement of fuel consumption, and the possibility of cylinder indication.

2. Study plan

In accordance with the research methodology, a test plan was developed, taking into account the test object, the measuring equipment used, and the measured energy parameters of the test object, i.e. in the case of the tested engine, its crankshaft rotational speed, engine torque load, oil temperature and indicated pressure. Parallel to the empirical research, model research was carried out using the author's model of a marine diesel engine with self-ignition [20, 21]. The study plan was presented in the form of an algorithm (Fig. 1).

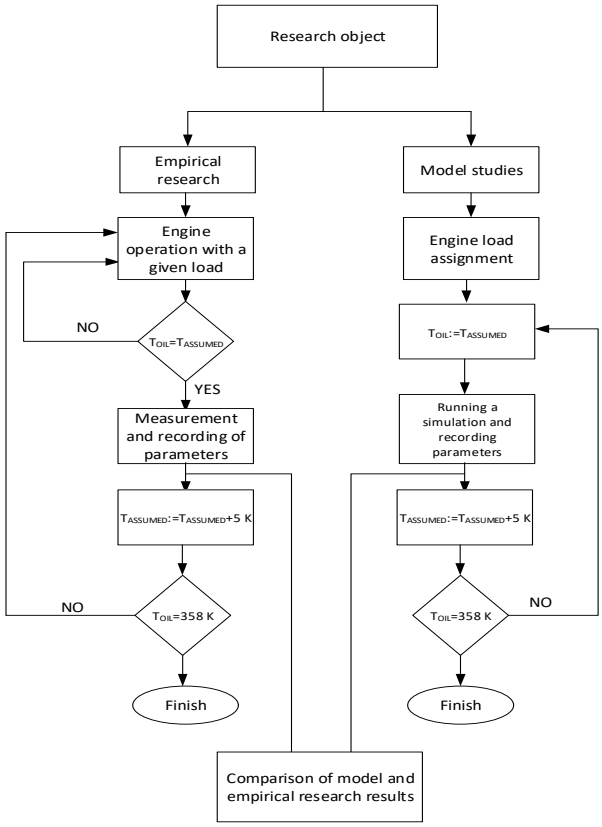

Fig. 1. An algorithm representing the study plan

Empirical and model tests were carried out for the same engine operating parameters (engine torque load and crankshaft rotational speed). In the case of the model, the thermal state of the engine itself was the input parameter (assumed the same as in the case of empirical tests). Both in the modelling and empirical studies, it was decided to measure to model) the course of the indicated pressure and the hourly fuel consumption. The courses of indicated pressure allowed to calculate the engine's indicated power. In addition, it was decided to calculate the engine power on the basis of its rotational speed and the torque registered on the eddy current brake.

It was decided to conduct tests for a fixed rotational speed of the crankshaft of 1000 and 1200 rpm, respectively, and for two load torque values using an eddy current brake (power generated by the engine of 5 and 6 kW respectively). It was assumed that the first measurement point would correspond to the oil temperature of 293 K, and each subsequent one would correspond to an increase in oil temperature by 5 K up to 353 K. During the tests, the following engine operating parameters were recorded:

– pressure indicated as a function of the angle of rotation of the crankshaft using a proprietary electronic indicator
– rotational speed of the crankshaft using a tachometric generator
– oil temperature with a PT100 type thermocouple
– hourly fuel consumption using a gravimeter
– torque on the basis of strain gauge readings installed on the eddy current brake.

The object of the research was a laboratory single-cylinder diesel engine installed at the stand at the Institute of Shipbuilding and Operation of the Polish Naval Academy. The basic engine data are grouped in Table 1, while the view of the laboratory stand is shown in Fig. 2 and Fig. 3 shows the control panel of the single-cylinder engine stand.

Table 1. Technical data of the engine used in the tests

Cylinder layout and number	horizontal, single cylinder
Piston stroke	160 mm
Cylinder diameter	135 mm
Cylinder displacement	2290 cm^3
Compression ratio	1:16
Maximum fuel consumption	215 g/kWh
Maximum torque at 1100 rpm	145 Nm
Maximum injection pressure	17 MPa
Maximum rated power	20 kW for 1500 rpm

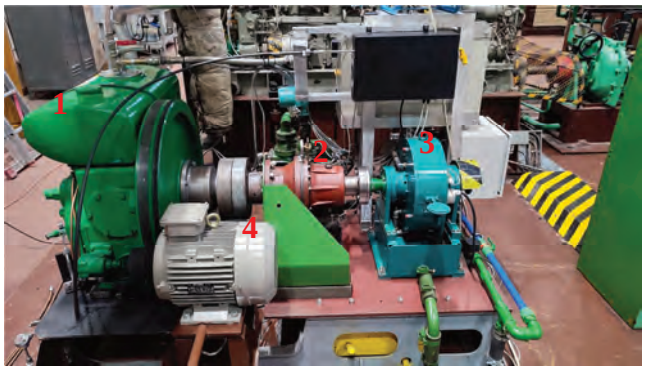

Fig. 2. Laboratory engine station: 1 – engine, 2 – planetary gear, 3 – brake, 4 – electric starter

The engine's fuel supply system consists of a fuel tank, a gravimetric system enabling measurement of fuel mass

flow, a filter, a piston injection pump, a high-pressure pipe, and an injector with a pintle tip. The injector is equipped with a single spring. The fuel is injected directly into the chamber located in the piston.

Fig. 3. Single-cylinder engine stand control panel: 1 – oil temperature, 2 – torque, 3 – engine power, 4 – rotation speed, 5 – mass of fuel in the tank

3. Empirical research

In accordance with the assumed test plan, all the mentioned parameters of engine operation were measured and recorded for given rotational speeds and loads. Measurements were recorded for oil temperatures ranging from 293 K to 353 K, respectively, with a resolution of 5 K. Engine operating parameters such as oil temperature, hourly fuel consumption, crankshaft rotational speed, and torque were recorded at a frequency of 1 Hz with a resolution of 12 bits. Indicated pressure was measured at a frequency of 10 kHz with a resolution of 12 bits. The measurement of the indicated pressure (for each measurement point) was repeated three times, and on its basis, the indicated engine power was calculated from dependence 1 [11–13, 16]:

$$N_i = V \cdot n \cdot p_i \cdot z \cdot i \tag{1}$$

where: V – engine cylinder capacity, n – average rotational speed of the crankshaft, z – number of ignitions per revolution of the crankshaft, p_i – indicated work, i – number of cylinders.

The indicated power calculated on the basis of eq. (1) was one of the input parameters to the mathematical model. In addition, the power was also calculated based on the measurement of the angular velocity of the crankshaft and the torque recorded by the sensors mounted on the eddy current brake based on the relationship:

$$N_c = \omega \cdot T \tag{2}$$

where:

$$\omega = 2 \cdot \pi \cdot n$$

Fuel consumption measurements to be calculated for the calculation of the enthalpy flux to the engine along with fuel from the relationship [20]:

$$\dot{H} = \dot{m} \cdot G_h \tag{3}$$

Having the values of the enthalpy flux supplied to the engine (eq. (3)) and the indicated power (eq. (1)), it was possible to calculate the indicated efficiency of the engine from the relation [9, 18, 19]:

$$\eta_i = \frac{N_i}{\dot{H}} \tag{4}$$

In addition, during the tests, the torque and rotational speed of the crankshaft measured on the brake made it possible to calculate the mechanical power of the engine-gearbox-brake system, and on this basis, to calculate the efficiency of the engine-gearbox-brake system based on the following relationship:

$$\eta_c = \frac{N}{\dot{H}} \tag{5}$$

In the case of the conducted tests, the fuel calorific value G_h was determined using a KL-11 type calorimeter, and the fuel mass flow was calculated using a gravimeter. On the other hand, the power value recorded on the eddy current brake takes into account all losses in the engine and in the planetary gear. Efficiency η_c can be described as the sum of indicated η_i, mechanical η_m, theoretical η_t, and transmission η_{tr} efficiency.

4. Model research

Parallel to the empirical research, model research was carried out. An original mathematical model implemented in a computer program was used for model research [21]. The program is based on thermodynamic relationships and allows to conduct research for virtually any compression-ignition engine.

Input parameters for the mathematical model include, but are not limited to:

- basic technical parameters of the engine, including cylinder stroke and diameter, number of cylinders, valve opening and closing angles, injection advance angle, combustion chamber volume, etc.
- rotational speed of the crankshaft
- indicated power
- physical and chemical parameters of the fuel
- supply air parameters such as pressure, temperature, humidity, density
- addition, filling efficiency and much more are taken into account.

In accordance with the adopted test plan, it was assumed that the simulated rotational speed of the engine crankshaft would be consistent with the setting of the real engine. The indicated power was assumed to be consistent with that obtained as a result of empirical tests. The calorific value of the fuel $G_h$was determined by Guzma formula [10]:

$$G_h = 340 \cdot C_m + 1017 \cdot H_m + \\ + 63 \cdot N_m + 191 \cdot S_m - 106 - 25 \cdot w_m \tag{6}$$

where: C_m – mass fraction of coal, H_m – mass fraction of hydrogen, N_m – mass fraction of nitrogen, S_m – mass fraction of sulfur, w_m – mass fraction of water

5. Research results

The results of both empirical and model tests were presented in the form of graphs of engine efficiency as a function of oil temperature. The efficiency of the real engine was calculated on the basis of dependence 4, while the efficiency of the modelled engine was calculated on the basis of dependence 5. In the case of empirical tests, the

value of indicated power was calculated on the basis of indicated pressure measurements, and the value of the enthalpy flux was calculated on the basis of the mass flow of the fuel supplying the engine (overflow included) and its calorific value (dependence 4). In the model tests, the value of the indicated power, obtained from dependence 1, was the input parameter to the model. Based on the equations of the mathematical model, the fuel mass flow and its calorific value were calculated (dependence 6). As a consequence, it allowed us to calculate the enthalpy flux $\dot{H}$. The efficiency of the modelled engine was calculated on the basis of dependence 5. The indicated power value adopted in the equation in some cases may slightly differ from the indicated power obtained as a result of empirical tests. This is due to the fact that in the mathematical model used, the fuel consumption is calculated (in successive iterations), and on its basis the course of the indicated pressure and, consequently, the indicated engine power is determined. The condition for completing the model calculations is obtaining the value of the indicated (calculated) power not differing by more than 2% in relation to the power constituting the input parameter. In the efficiency calculations, the indicated power calculated as a result of solving the model equations was used [5].

In the case of tests conducted for the rotational speed of the crankshaft of 1200 rpm, for technical reasons, the maximum oil temperature was decided to be 343 K.

Significant discrepancies between the given engine load and the indicated power result, among others, from the design of the test stand used. The tested engine is loaded with an eddy current brake. Optimal parameters of cooperation between the engine and the brake (adaptation of rotational speed) are ensured by the planetary gear, which is a source of significant mechanical losses. The carrie out preliminary tests showed that these losses are practically constant (independent of the rotational speed of the engine crankshaft and its load). They depend only on the temperature of the oil in the transmission, which during the tests was constant and amounted to 353 K. Therefore, they are treated as a constant error (all analyses referred to the indicated power).On the basis of the empirical and modelling data the courses of indicated engine efficiency as a function of oil temperature (for the rotational speed of the crankshaft of 1000 rpm) were developed. They are presented in Fig. 4

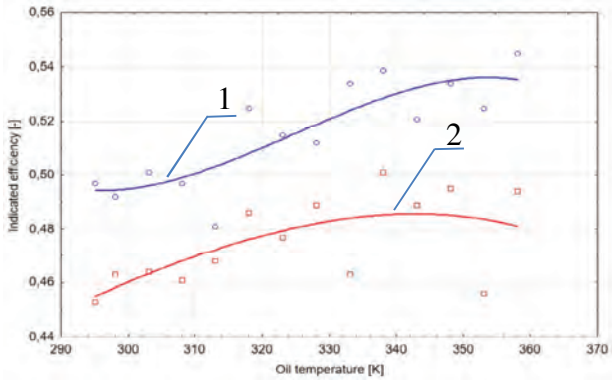

Fig 4. Courses of changes in engine efficiency as a function of oil temperature for an engine loaded with a power of 5 kW at a crankshaft speed of 1000 rpm: 1 – empirical research, 2 – model tests

– course for the engine load of 5 kW and Fig. 5 – course for the engine load of 6 kW. The waveforms obtained as a result of modeling for various loads are presented in Fig. 6, while the results of empirical tests are shown in Fig. 7.

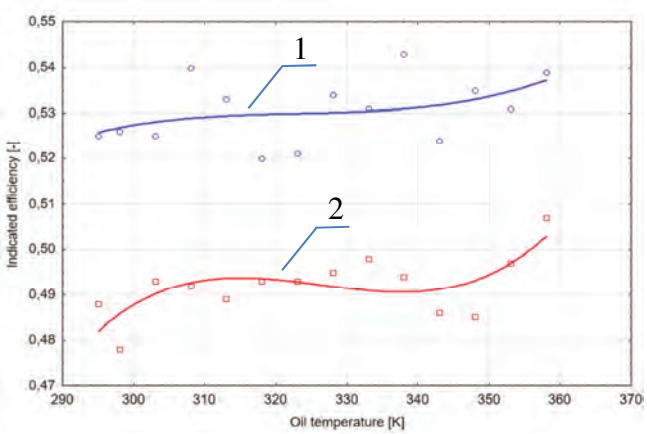

Fig 5. Courses of changes in engine efficiency as a function of oil temperature for an engine loaded with a power of 6 kW at a crankshaft speed of 1000 rpm: 1 – empirical research, 2 – model tests

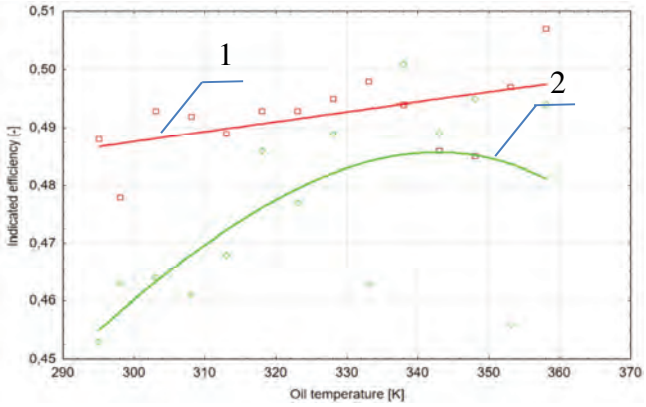

Fig. 6. Waveforms of changes in engine efficiency as a function of oil temperature obtained as a result of modelling an engine operating at 1000 rpm loaded with power: 1 – 6 kW, 2 – 5 kW

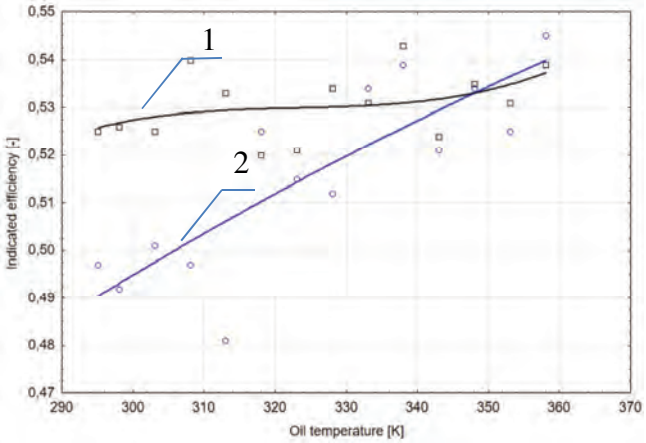

Fig. 7. Courses of changes in engine efficiency as a function of oil temperature obtained as a result of empirical tests for an engine with a rotational speed of 1000 rpm and loaded with the following power: 2 – 5 kW, 1 – 6 kW

On the basis of the empirical and modelling data, the courses of indicated engine efficiency as a function of oil

temperature (for the rotational speed of the crankshaft of 1200 rpm) were developed. They are presented in Fig.: 8 – course for the engine load with a torque of 5 kW and 9 – course for the engine load with a torque of 6 kW. The waveforms obtained as a result of modelling for various loads are presented in Fig. 10, while the results of empirical tests are shown in Fig. 11.

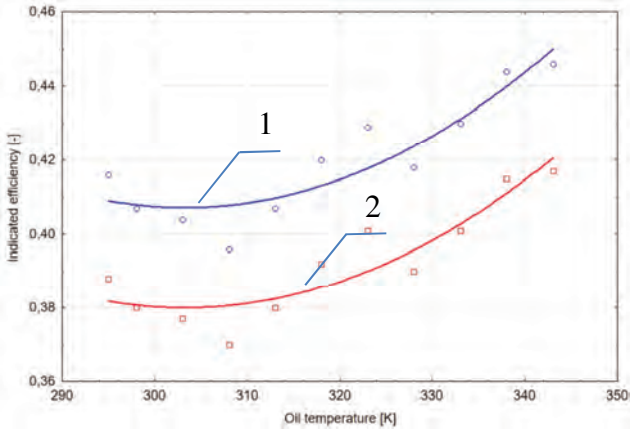

Fig. 8. Courses of engine efficiency changes as a function of oil temperature for an engine loaded with a power of 5 kW at a crankshaft speed of 1200 rpm: 1 – empirical tests, 2 – model tests

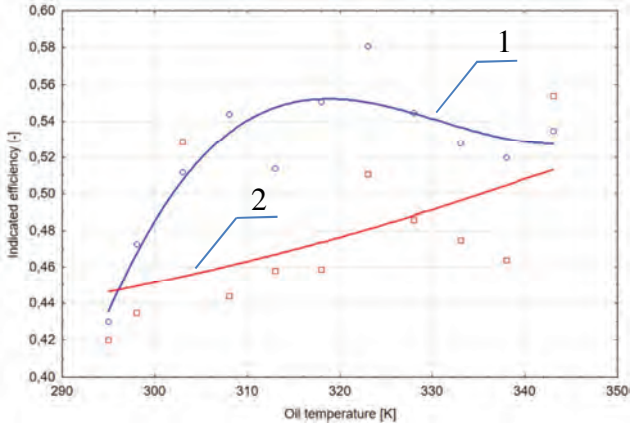

Fig. 9. Courses of changes in engine efficiency as a function of oil temperature for an engine loaded with a power of 6 kW at a crankshaft speed of 1200 rpm: 1 – empirical tests, 2 – model tests

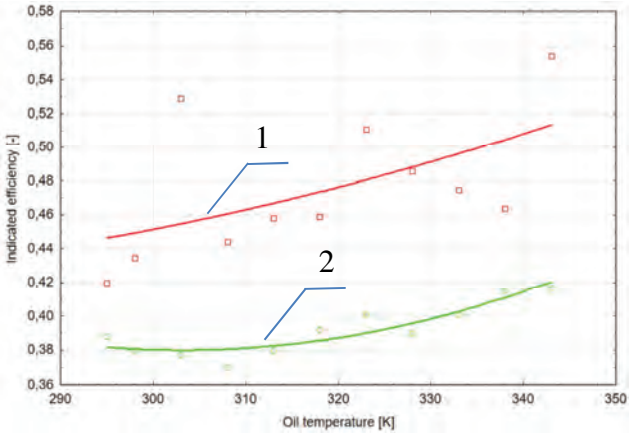

Fig. 10. Waveforms of changes in engine efficiency as a function of oil temperature obtained as a result of modelling an engine operating at 1200 rpm loaded with power: 1 – 6 kW, 2 – 5 kW

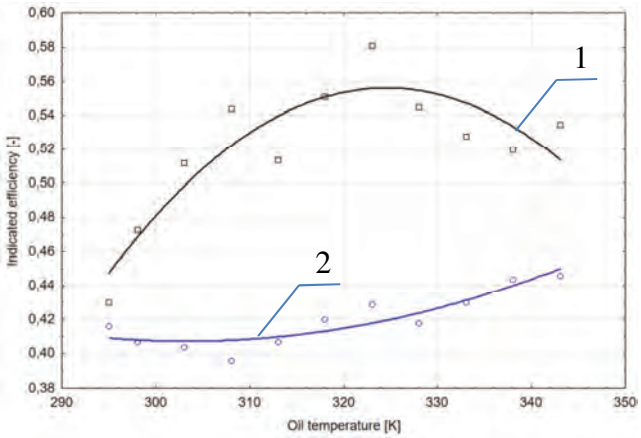

Fig. 11. Courses of changes in engine efficiency as a function of oil temperature obtained as a result of empirical tests for an engine with a rotational speed of 1200 rpm and loaded with the following power: 2 – 5 kW, 1 – 6 kW

The results obtained from the conducted tests show that the fluctuations in the indicated (thermal) efficiency are in line with the authors' expectations.

From the researchers' perspective, the relative changes in engine efficiency as a function of its thermal state (oil temperature) under different loads and crankshaft speeds are more significant than the specific shape of the efficiency curves. Additionally, it was observed that the relative increase in indicated efficiency for a warm engine compared to a "cold" engine is approximately 10%.

A comparative analysis of the results obtained from mathematical modelling and empirical studies clearly indicates that the indicated efficiency of the modelled engine is about 8% lower than that of the real engine. The nature of changes in efficiency as a function of oil temperature for model and empirical studies converges. The discrepancies between the model and empirical results are probably due to the simplifications adopted in the model regarding:

- the course of the combustion process
- heat exchange between the medium inside the cylinder and its walls
- calorific value of the fuel calculated based on dependence 6.

In addition, the discrepancies between the parameters obtained as a result of modelling and empirical research were significantly affected by the accuracy of the measuring equipment used. The approximately constant eight percent discrepancy between model and empirical tests may result, among others, from imperfections in the model, including the assumed material constants (heat conductivity coefficient) of the combustion chamber elements, incorrectly assumed engine cooling water temperature (temperature measurement cooling water on the real engine was carried out at the entrance to the radiator) and other causes that are difficult to clearly identify.

6. Summary

The results presented in the article, both from modelling and empirical research, indicate the significant influence of engine thermal parameters on its efficiency. In addition to the obvious observations that an increase in oil temperature is accompanied by an increase in indicated engine efficien-

cy, actual values of changes in indicated efficiency as a function of oil temperature were determined. The research was conducted for four operating conditions of the engine, namely rotational speeds of 1000 and 1200 rpm, and engine loads of 5 and 6 kW.

As a result of the research, it was found that an increase in oil temperature in the range of 295 K to 358 K is accompanied by an increase in the indexed efficiency of the engine by an average of about 10%. The course of the engine efficiency value as a function of oil temperature is not a linear function and depends on very many factors including engine operating parameters such as its load and crankshaft speed. In addition, the tests carried out showed the adequacy of the mathematical model developed by the authors at the level of 8%. The nature of the obtained waveforms (both model and empirical) indicates that the discrepancies are mainly due to systematic errors. In contrast, the contribution of random error is negligible. The probable source of systematic errors is the simplifications used in the model, and the limited accuracy of calculations implemented in multiple iterations. In turn, the likely source of random errors is the limited accuracy of the measurement apparatus used.

Nomenclature

C_m	mass fraction of coal
DI	direct injection
V	combustion chamber volume
G_h	calorific value
H_m	mass fraction of hydrogen
$\dot{H}$	enthalpy flux
i	number of cylinders
$\dot{m}$	mass flux
N_C	calculated power by break
N_i	Indicated power
N_m	mass fraction of nitrogen
n	rotation speed
p_i	indicated work
S_m	mass fraction of sulfur
SI	stratified injection
T	torque
w_m	mass fraction of water
z	number of ignitions per revolution of the crankshaft
μ_c	efficiency of the engine-gear-brake system
μ_i	indicated efficiency
μ_m	mechanical efficiency
μ_t	theoretical efficiency
μ_{tr}	transmission efficiency
ω	angular velocity

Bibliography

[1] Andrews G, Ounzain A, Li H, Bell M, Tate J, Ropkins K. The use of a water/lube oil heat exchanger and enhanced cooling water heating to increase water and lube oil heating rates in passenger cars for reduced fuel consumption and CO_2 emissions during cold start. SAE Technical Paper 2007-01-2067. 2007. https://doi.org/10.4271/2007-01-2067

[2] Bielaczyc P, Szczotka A, Woodburn J. An overview of cold start emissions from direct injection spark-ignition and compression ignition engines of light duty vehicles at low ambient temperatures. Combustion Engines. 2013;154(3): 96-103. https://doi.org/10.19206/CE-116992

[3] Broatch A, Tormos B, Olmeda P, Novella R. Impact of biodiesel fuel on cold starting of automotive direct injection diesel engines. Energy. 2014;73:653-660. https://doi.org/10.1016/j.energy.2014.06.062

[4] Burke RD, Brace CJ, Hawley JG, Pegg I. Review of the systems analysis of interactions between the thermal, lubricant, and combustion processes of diesel engines. P I Mech Eng D-J Aut. 2010;224(5):681-704. https://doi.org/10.1243/09544070JAUTO1301

[5] Engine technical documentation WOLA type SW-400.

[6] Gęca MJ, Radica G. Effect of compression ignition engine preheating on its performance under cold start conditions. Combustion Engines. 2022;188(1):67-74. https://doi.org/10.19206/CE-142346

[7] Kozak M. A comparison of thermogravimetric characteristics of fresh and used engine oils. Combustion Engines. 2019;178(3):289-292. https://doi.org/10.19206/CE-2019-350

[8] Kozak M, Siejka P. Soot contamination of engine oil – the case of a small turbocharged spark-ignition engine. Combustion Engines. 2020;182(3):28-32. https://doi.org/10.19206/CE-2020-305

[9] Piotrowski I, Witkowski K. Marine internal combustion engines. Trademar. Gdynia 1996.

[10] Pudlik W. Termodynamika. Publishing House of Gdańsk Univesity of Technology. Gdańsk 1998.

[11] Roberts A, Brooks R, Shipway P. Internal combustion engine cold-start efficiency: a review of the problem, causes and potential solutions. Energ Convers Manage. 2014;82: 327-350. https://doi.org/10.1016/j.enconman.2014.03.002

[12] Rychter T, Teodorczyk A. Theory of piston engines. WKŁ. Warsaw 2006.

[13] Spencer C. Internal combustion engine pronciples – with vehicle applications. Vince Press. NY 2018.

[14] Tauzia X, Maiboom A, Karaky H, Chesse P. Experimental analysis of the influence of coolant and oil temperature on combustion and emissions in an automotive diesel engine. Int J Engine Res, 2019;20(2):1-14. https://doi.org/10.1177/1468087417749391

[15] Tobergte M. Private communication (email): AW. The importance of advanced test processes to reduce emissions and fuel consumption – Frank Will. In: ICSAT conference, 16th August 2011.

[16] Wajand JA, Wajand JT. Medium and high-speed internal combustion piston engines. WNT. Warsaw 2005.

[17] Will F, Boretti A. A new method to warm up lubricating oil to improve the fuel efficiency during cold start. SAE Technical Paper 2011-01-0318. 2011. https://doi.org/10.4271/2011-01-0318

[18] Wontka L. Mechanical losses as a diagnostic parameter of the technical condition of a marine diesel engine. Polish Naval Academy. Doctoral Thesis. Gdynia 2017.

[19] Wontka L. Methods for determining mechanical losses of marine diesel engines. Scientific Journal of Polish Naval Academy. 2018;214(3):25-38. https://doi.org/10.2478/sjpna-2018-0017
[20] Zacharewicz M. A method of diagnosing the working spaces of a marine engine on the basis of gas-dynamic parameters in the turbocharger supply duct. Doctoral Thesis. Gdynia 2009.
[21] Zacharewicz M. Possibilities of parametric assessment of the technical condition of a marine diesel engine with low diagnostic susceptibility (book in Polish). Akademia Marynarki Wojennej. Gdynia 2019.

Marcin Zacharewicz, DSc. DEng. – Faculty of Mechanical and Electrical Engineering, Polish Naval Academy, Poland.
e-mail: *m.zacharewicz@amw.gdynia.pl*

Paweł Socik, MEng. – Faculty of Mechanical and Electrical Engineering, Polish Naval Academy, Poland.
e-mail: *p.socik@amw.gdynia.pl*

Ryszard Zadrąg, DSc., DEng. – Faculty of Mechanical and Electrical Engineering, Polish Naval Academy, Poland.
e-mail: *r.zadrag@amw.gdynia.pl*

Paweł Wirkowski, DEng. – Faculty of Mechanical and Electrical Engineering, Polish Naval Academy, Poland.
e-mail: *p.wirkowski@amw.gdynia.pl*

Artur Bogdanowicz, DEng. – Faculty of Mechanical and Electrical Engineering, Polish Naval Academy, Poland.
e-mail: *a.bogdanowicz@amw.gdynia.pl*

Jakub Hołownia, Eng. – student of Faculty of Mechanical and Electrical Engineering, Polish Naval Academy, Poland.
e-mail: *pjakub20001210@gmail.com*

Article citation info:
Puzdrowska P. Adoption of the F-statistic of Fisher-Snedecor distribution to analyze importance of impact of modifications of injector opening pressure of a compression ignition engine on specific enthalpy value of exhaust gas flow. Combustion Engines. 2024;196(1): 37-45. https://doi.org/10.19206/CE-168520

Patrycja PUZDROWSKA

Combustion Engines
Polish Scientific Society of Combustion Engines

Adoption of the F-statistic of Fisher-Snedecor distribution to analyze importance of impact of modifications of injector opening pressure of a compression ignition engine on specific enthalpy value of exhaust gas flow

ARTICLE INFO

Received: 15 May 2023
Revised: 17 June 2023
Accepted: 19 June 2023
Available online: 5 July 2023

This article analyzes the effect of modifications of injector opening pressure on the operating values of a compression ignition engine, including the temperature of the exhaust gas. A program of experimental investigation is described, considering the available test stand and measurement capabilities. The structure of the test stand on which the experimental measurements were conducted is presented. The method of introducing real modifications of injector opening pressure to the existing test engine was characterized. It was proposed to use F statistic of Fisher-Snedecor (F-S) distribution to evaluate the importance of the impact of modifications of injector opening pressure on the specific enthalpy of the flue gas flow. Qualitative and statistical studies of the results achieved from the measurements were carried out. The specific enthalpy of the exhaust gas for a single cycle of the compression ignition engine, determined from the course of rapidly variable flue gas temperature, was analyzed. The results of these studies are presented and the usable adoption of this type of assessment in parametric diagnosing of compression ignition engines is discussed.

Key words: *diagnosis, injector opening pressure, F statistic of the Fisher-Snedecor distribution, compression ignition engine, exhaust gas temperature*

1. Introduction

The opening pressure of the injector p_{inj} is a parameter that significantly affects the combustion process and heat release in a compression ignition engine [2]. It affects the operational parameters of the engine, and also emissions of harmful and toxic ingredients of exhaust gas. The necessity of parametric assessment based on rapidly variable flue gas temperatures is due to the limited controllability of marine engines (there are no indicator valves) with the concomitant requirement to measure exhaust gas temperatures [9–11, 20–22]. The thermal and flow processes occurring in such engines are comparable to the ones in the single-cylinder research engine. Therefore, it was proposed to make diagnostic deductions about the functional state of the fuel supply system of a compression ignition engine based on observations of rapidly varying flue gas temperature in the exhaust duct. For this purpose, F statistic of F-S distribution was used, which makes it allowed to assess whether the opening pressure of the injector p_{inj} significantly affects the specific enthalpy of the exhaust gas flow h_{exh} averaged for a single engine cycle, identified on the basis of the quickly varying temperature of the flue gas of a compression ignition engine.

2. The impact of injector opening pressure modifications on exhaust gas temperature

One of the major quantities influencing the quality of combustion of fuel in a compression ignition engine and the composition of the exhaust gas is the opening pressure of the injector p_{inj}. Too low pressure p_{inj} results in disturbances in the combustion process, for example, in the form of increased maxima in the combustion process: pressure and temperature [17]. On the other hand, too high p_{inj} causes, for example, "hard" engine operation, resulting in excessive dynamic forces of the piston-crank mechanism. Measurement of the rapidly fluctuating temperature of the flue gas can allow to detection of the state of fractional fitness or operational unfitness of the engine, resulting from an increased or decreased value of p_{inj}.

2.1. Defectiveness of the injection system of a compression ignition engine

Compression ignition engines, which are the main propulsion system of ships as well as their electric power plants, generate operating costs that account for more than 70% of the cost of maintaining the overall power plant on a ship, mainly due to the high prices of fuels and lubricating oils [29]. There is a strong relationship between engine reliability and ship safety. Taking into account these two aspects – shipping safety and ship operating costs – diagnostic methods and devices are being developed mainly with the reliability of ship engines in mind. However, keeping in mind that it has a very complicated structural construction, it is necessary to carry out its logical decomposition into functional systems, components and elements to determine the depth of the diagnosis to be made. A schematic representation of the division of the structural design of a marine engine into appropriate levels, according to the increasing detail (depth) of the classification of the technical condition carried out – Fig. 1. The last element of the subject of diagnosis is considered indivisible [17].

Statistics show that marine engines are the most unreliable machines on a ship [29, 30]. Among the most common damages, those affecting low-speed engines account for 38% of the total number of damages, while medium-speed engines account for 15.7% of all accidents considered.

Analyzing the failure of marine engines, regardless of their purpose, essential functional systems should be considered: the fuel supply system (almost 50% of all damages) and working medium exchange system (24.7%). For the fuel supply system, injectors (41%) and injection pumps (38%) are the components usually fail [29].

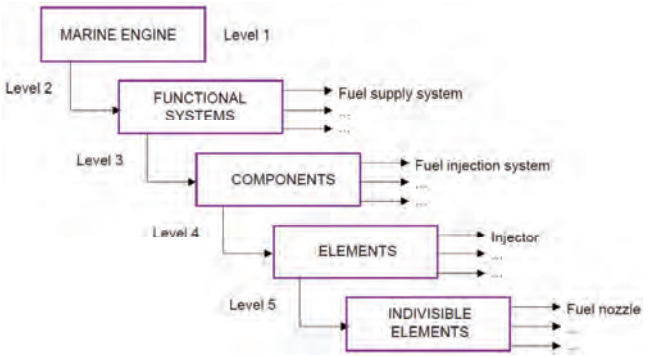

Fig. 1. Schematic of the decomposition of a marine compression ignition engine

Authors prove in their statistical studies that injectors are the most unreliable elements in all components of the fuel supply system of marine engines. Bruski, in his doctoral dissertation, presented the results of statistical studies collected at the Naval Academy's Institute of Ship Construction and Operation for medium-speed engines operated on Navy ships [4]. The author indicates that malfunctions were occurring with the highest incidence in the following functional systems: fuel supply (72%), valve train (19%), and air supply (9%). While 54% of injector breakdowns occurred in the fuel supply system, they represented 38.9% of all malfunctions of marine engines in operation.

The problem of the reliability of structural elements that are part of the functional systems of a marine piston engine was also studied by a scientific team from Vietnam consisting of Ta et al. [28]. The authors of the publication point to the main and auxiliary engines as the components of a marine ship's engine room and electric power plant that are most often damaged, while generating the highest costs from insurance and repairs. Of the authors' analysis of 558 failures of the main marine propulsion units (main and auxiliary engines, reduction gears, utilization boilers, propeller shafts and others), 41.6% involved main engines and 21.5% involved auxiliary compression ignition engines. The authors described the injection system is the one of all marine engine components that are wearing out most rapidly – every additional 500 hours of engine running doubles the probability of failure of this system's components.

The issue of reliability of marine IC engines was also dealt with by Czajgucki [5]. On the basis of the data collected on their damage statistics, he showed that the injectors are the component of the engines studied that is most often damaged (more than 60% of all the components analyzed by the author), primarily due to the low quality of the marine fuel used. The proportions of damages to each of the elements included in the systems of CEGIELSKI-SULZER type 6RD68 engines with a power of 5.5 MW are shown in Fig. 2. The graph was created on the basis of the courses of the reliability functions of injectors, injection pumps, starting valves, piston rings, cylinder liners, pistons and heads of 6RD68 engines supplied with residual marine fuel, which have worked 1500 hours.

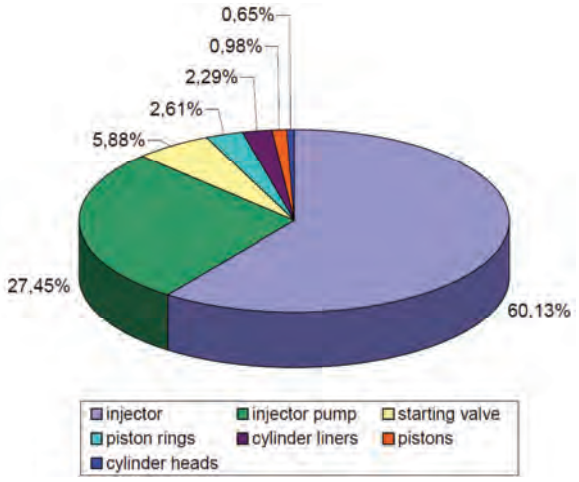

Fig. 2. Percentages of damage to individual structural elements of CEGIELSKI SULZER engines type 6RD68 with a power of 5.5 MW

The most common damage to injectors is primarily due to the extreme adverse conditions of high fuel pressures and, in the case of the nozzle itself, additionally high and variable temperatures of the working medium in the combustion chamber [4, 8, 13, 27]. As a consequence, the injector leaks, the opening pressure drops relative to the reference pressure, and the precision pair is excessively degraded [30]. The most common nozzle failures include the complete or fractional loss of clearance of the nozzle holes, deformation of the shape and change in geometric dimensions ("recalibration") of these holes as a result of erosive and thermal wear, leakage of the seating of the pin, or stuck pin in the guideway.

The following factors affect the technical condition of the injector:

- erosive and corrosive effects of various types of impurities contained in the fuel, e.g. particulate matter, water, vanadium, sulfur – in the case of non-sulfurized fuels or so-called "cat fines" – for low-sulfur residual fuels
- the propensity of low-quality fuel to form carbon build-ups and lakes
- overheating of the injector due to disruption of its cooling process.

In newly produced low-sulfur residual fuels, impurities in the form of hard, lightweight and difficult to remove aluminum and silicon oxide particles – so-called "cat fines" – are often present. These can lead to serious damage to components of the engine's functional systems, as a result of the abrasive effects present in the unpurified fuel in the form of catalytic fines. It is a byproduct of the catalytic hydrocracking process [15, 16]. The fuel atomizer itself can also suffer this type of mechanical damage, as can be seen in Fig. 3 [1].

In the case of the injector spring, due to operation at high temperatures and pressures, over time wear occurs due to the loss of its own elasticity. The result can then be a reduced injector opening pressure, causing combustion interference [17].

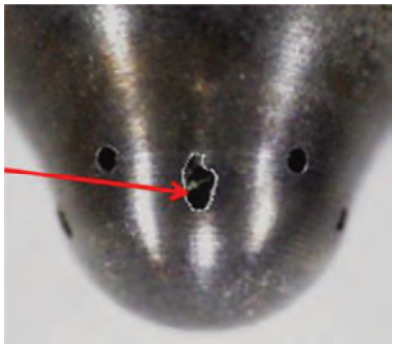

Fig. 3. Destroyed marine engine fuel nozzle due to destructive effects of catalytic fines [1]

Modifications of the opening pressure of the injector p_{inj} usually occur as a result of changes in the spring's own elasticity (adjusted by shims under the spring), and also as a result of leaks in the injection pump [3, 7, 14, 26, 29].

It should also be kept in mind that when the working process of an engine is disturbed, its heat loads increase, so any malfunctions that aggravate the engine and/or its associated systems can result in heat overload. The engine systems affecting the increase in heat loads are considered to be, in order: the fuel supply system, the supply air system, the piston-ring-cylinder liner set, the cylinder liner lubrication system and the cooling system [29].

Analyzing the results of reliability studies on the functional systems of marine engines, it was decided to subject to experiment and statistical and merit analysis those failures that occur most frequently. In selecting the changes to be made to the structural design to reflect the states of operational unfitness allowed in an engine in use in real conditions, i.e. on a ship. The technical capabilities of the compression ignition research engine were also taken into account. Thus, the following damage was taken into account for the applied experimental plan:

- loss of air inlet duct clearance (reduced inlet air pressure), the analysis of which was presented in the paper [25]
- leakage of the combustion chamber (reduced compression ratio), discussed in the article [24]
- injector spring relaxation (reduced injector opening pressure), the results of which are presented in this paper.

2.2. Temperature of exhaust gas

There is a relationship between flue gas temperature and injector opening pressure, according to simulation and investigation studies conducted in this area. In the article [23], the author shows the analytical data from a numerical simulation of the working of a compression ignition engine. A laboratory Farymann Diesel type D10 engine was successfully implemented in the DIESEL-RK application. Chosen malfunction of its operational fuel supply system – cut down opening pressure of the injector p_{inj} – was implemented. One of the values of adequate diagnostic values was exhaust gas temperature T_{exh}. The variability runs of changes in the temperature of the flue gas T_{exh}, major discrepancies in the values of this value occur in area of maximum – Fig. 4. Cut down injector opening pressure p_{inj} from 12 MPa to 10 MPa caused an increment of exhaust gas temperature by about 10 K at the maximum value of T_{exh}. Discrepancy in amounts of flue gas temperatures T_{exh} for the two reviewed states is also visible for remaining part of the engine cycle, however it is lower.

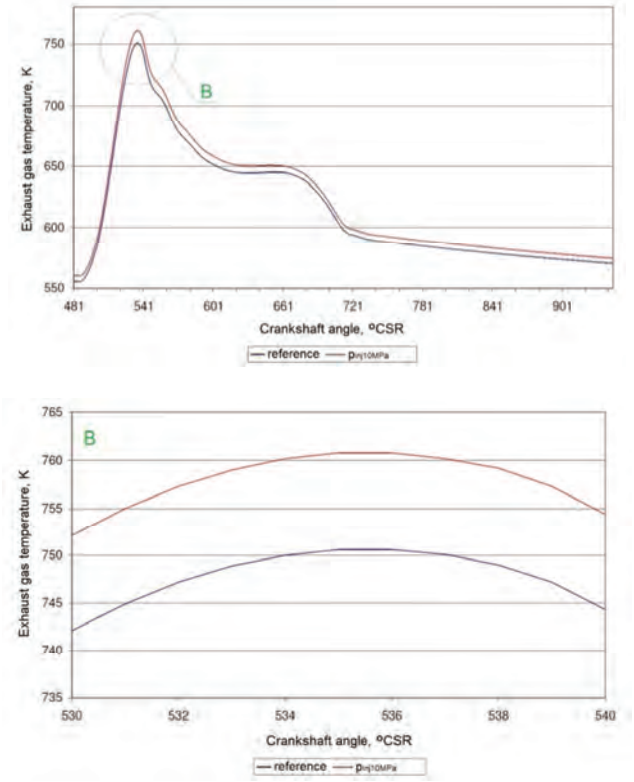

Fig. 4. Runs of changes in the temperature of the exhaust gas T_{exh} value for the crankshaft rotation angle, for portion of the engine operating cycle and for the region of existence of the peak value of the flue gas temperature, obtained by numerical simulation in the DIESEL-RK program for two values of injector opening pressure p_{inj} [23]

Experimental studies on, for among other things, the impact of injector opening pressure on exhaust gas temperature were carried out by the authors of the paper [19]. In these investigations, 2-butanol was added volumetrically to the diesel fuel and injector atomization pressures were modified. A single-cylinder, four-stroke and direct injection diesel engine was subjected to experimental tests on a direct current dynamometer. A 2-butanol-diesel fuel mixture was prepared by volumetrically adding 3% (B3 in Fig. 4), 5% (B5), 8% (B8) and 10% (B10) 2-butanol to regular diesel fuel (B0). The injection pressure of the injectors was set as 180 bar, 200 bar (originally), and 220 bar. The outputs of the experiment illustrate the comparison with standard engine operating conditions. Figure 5 shows the changes in flue gas temperature as a function of injection pressure for 2-butanol diesel mixtures. Exhaust gas temperature dropped for all additive fractions of 2-butanol versus pure diesel. The lower viscosity, density and cetane number result in worse in cylinder combustion and lower final combustion pressure and temperature, also flue gas temperature. Exhaust gas temperature dropped at 200 bar injection pressure, but not as much as at 180 bar. But the largest decrease is observed at 220 bar. Note, however, that increasing the injection pressure reduces the diameter of the fuel particles and upgrades the fuel's ability to diffuse into the combus-

tion chamber. Greater diesel and 2-butanol mixtures spraying capacity immediately consume more energy from air in combustion chamber for evaporation, thereby cooling the cylinder and lowering the temperature of the final combustion and flue gas. However, regardless of the composition of the fuel tested, the impact of fuel injection pressure on exhaust gas temperature is noticeable.

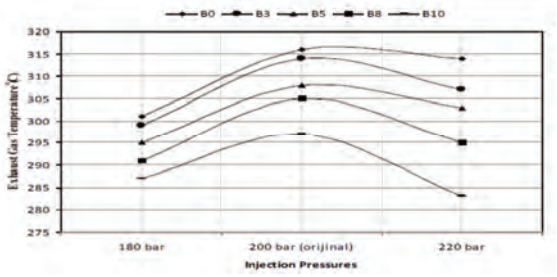

Fig. 5. The impact of injection pressure on exhaust gas temperature [19]

Studies by other authors have investigated the performance evaluation of a low heat rejection (LHR) combustion chamber engine with an air gap insulated piston and an air gap insulated liner when operating on clean diesel fuel with varying injector opening pressures [12]. Operating values (brake thermal efficiency, exhaust gas temperature, coolant load, volumetric efficiency, sound level) and exhaust emissions (particulate matter and nitrogen oxide emissions) were specified at different values of the engine's mean brake effective pressure (BMEP). The authors prove that the engine with the LHR combustion chamber upgraded performance at 80% of full-load operation and continued to increase with increasing injector opening pressure. In Table 1, we can see that the flue gas temperature (EGT) dropped slightly with increasing injector opening pressure in diesel operation. This was due to upgraded fuel-air ratios with better atomization characteristics.

Table 1. Variation of performance parameters with injector opening pressure with Diesel operation; BTE – brake thermal efficiency, BSFC – brake specific fuel consumption, EGT – exhaust gas temperature, VE – volumeric efficiency [12]

Parameter/unit	Conventional engine			Engine with LHR combustion chamber		
	190	230	270	190	230	270
Peak BTE [%]	28	29	30	29	30	30.5
BSFC [kg/kW·h]	0.34	0.33	0.32	0.35	0.34	0.33
EGT [°C]	425	410	395	475	450	425
Coolant load [kW]	4.0	4.2	4.4	4.5	4.2	3.8
VE [%]	85	86	87	79	80	81
Sound levels [dB]	85	80	75	90	85	80

3. Investigation on experimental compression ignition engine in the conditions of actually implemented modifications of the injector opening pressure

Identifying of the impact of dropped injector opening pressure on engine running is allowed through investigational research. Incidence imitation of the state of fractional serviceability by actually implemented modifications of p_{inj} makes it possible to register chosen control values under these requirements. Exhaust gas temperature gives a diagnostic measures and enables a determination of the impact of the modified injector opening pressure on the specific enthalpy of the flue gas. Nevertheless, it is necessary to be mindful of suitable statistical and mathematical treatments tools in order to maximize the diagnostic reporting of flue gas temperature.

3.1. Overview of laboratory bench and applied testing equipment

Measurements were conducted on a laboratory bench test of a four stroke, a single cylinder engine Farymann Diesel engine type D10 (Fig. 6), situated in the Laboratory of Marine Power Plants, Faculty of Mechanical Engineering and Ship Technology, Gdansk University of Technology. Main data specifications of the engine are these:

- power nominal value 5.9 kW
- rotational speed nominal value 1500 min^{-1}
- torque nominal value 38 N·m
- diameter of cylinder 90 mm
- piston stroke 120 mm
- compression ratio 22:1
- volume of cylinder stroke 765 cm^3.

The design solution of the Farymann Diesel type D10 research engine makes it allowed to minimize the delay of self-ignition of fuel, approximating the combustion process to the process of isochoric heat input in the preliminary combustion chamber and the process of isobaric heat input in gas volume space over the piston (major combustion chamber) with a significant greater displacement. Both chambers are joined by a narrow flow (turbulent) duct, which, for one thing, offers ideal environment for studying the fuel combustion procedure in the pre-chamber (dynamics of pressure changes, thermal emission and self-ignition capability of the feed fuel), and, for another, reduces the mechanical and thermal load in the major combustion chamber coupled straight to the piston-crank mechanism. In addition, in the pre-chamber, although a straight (reliable) spigot injector is used, very good conditions for complete combustion of the fuel are achieved. Also, the engine is at a lower susceptibility to burning fuels with low autoignition ability. Disappointingly, this comes at the cost of a large reduction in the effectiveness of the implemented operating process, primarily because of the hydraulic losses of the return flow of the working medium through the chamber connecting channel, and also higher heat losses raised by the coolant from the walls of the expanded combustion chamber.

During the tests, the following engine control values were recorded:

- exhaust gas pressure and temperature
- current of generator (motor) load
- voltage at generator armature terminals
- piston top dead center signal
- outlet valve opening signaling.

It is presented in Table 2 with a synthesis of the tested control values measured and the sensing equipment which was used in the tests.

A DT-9805 type multifunction recording and measuring module was used to record the fast variables: temperature and flue gas pressure, and the top dead center piston signal. Matlab software was used to save the measured data. The test results presented are the mean of 90 successive measurements registered at the same engine working conditions defined by engine load, speed of the crankshaft and environmental values. Throughout the experiments, the engine burned MGO-type marine fuel. During the entire test, the crankshaft rotational speed was kept constant at 1442-1444 rpm. The sampling frequency was about 7000 Hz.

3.2. Experimental investigations agenda

Within the study conducted by the present article's author, the main objective was determining the informability of the diagnostic value, which is the rapidly varying flue gas temperature of a compression-ignition engine, as a function of actual modifications of chosen values of its structural design. A randomized static and complete experimental scheme was used [18]. Presented in the current article is a portion of results of a broader program of conducted studies: the impact assessment of the injector opening pressure on the specific enthalpy of the test engine's flue gas. According to this, it is therefore feasible to apply the results of laboratory tests to full-size marine engines for diagnosis inference.

Laboratory tests were conducted on a Farymann Diesel type D10 engine. The object of the study of thermal-fluid processes was determined through the structural elements that limit the working space of the cylinder, as well as the injection system. In the conducted investigations and analyses, the processes taking place in the in-cylinder volume have not been dealt with, but only the rapidly varying flue gas temperature signal registered in the flue gas duct. Diagnostic measures were determined from the registered rapidly varying flue gas temperature report signal, but this article only discusses the specific enthalpy of the average flow of flue gas in a single cycle of a compression-ignition engine – h_{exh}.

Table 2. The values of the Farymann D10 a single cylinder compression ignition engine measured on the laboratory bench

Item	Value	Measuring device	Unit	Measurement range
1.	Exhaust gas temperature – T_{exh}	Type K welded thermocouple with 0.5 mm outer diameter connector, manufactured from inconell	°C	0–1000
2.	Exhaust gas pressure in the exhaust duct – p_{exh}	Optical pressure sensor – Optrand C12296	V	0–689475.73 Pa (0–100 psi), sensitivity $6.01 \cdot 10^{-8}$ V/Pa (41.43 mV/psi)
3.	Engine speed (angular position – CA) – n Top dead center – TDC	Induction engine speed sensor and TDC sensor	min^{-1}	0–3000
4.	Current of generator (motor) load – I_{gen}	Electric current meter	A	0–15
5.	Voltage at generator armature terminals – U_{gen}	Voltmeter	V	0–250
6.	Outlet valve opening signaling	Gap type opto-isolator with a comparator LM393	V mm	0–5 10 (gap)

a) b)

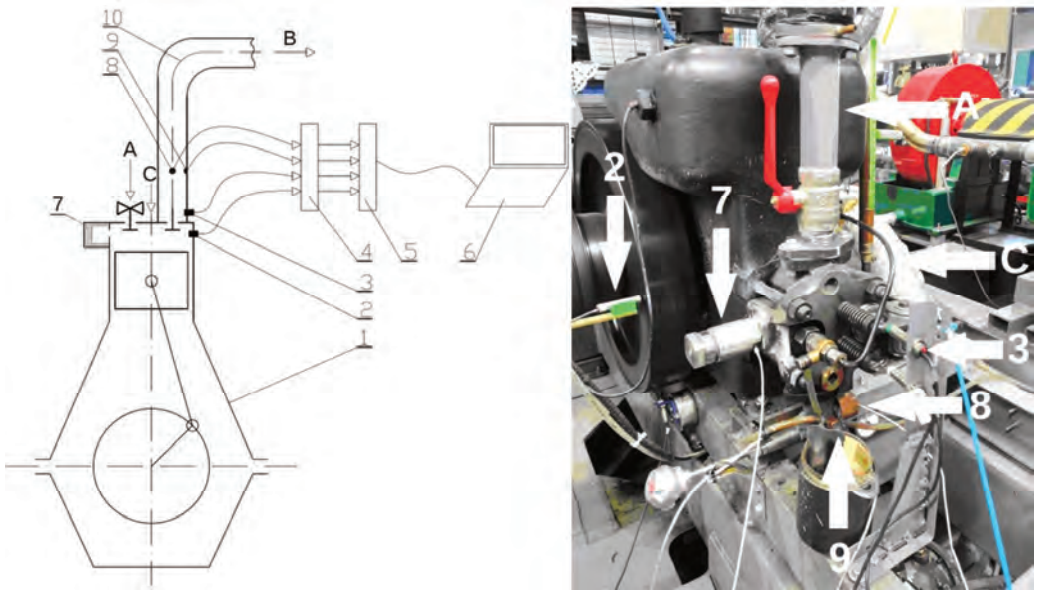

Fig. 6. a) Schematic of the bench with detectors installation points indicated as: 1 – Farymann D10 engine, 2 – TDC and engine speed sensor, 3 – outlet valve opening sensor, 4 – A/C converter, 5 – data recorder, 6 – analysis software, 7 – element that enlarges the capacity of the combustion chamber, 8 – pressure sensor, 9 – thermocouple in the water jacket, 10 – exhaust gas duct, A – intake air, B – exhaust gas, C – fuel line

b) Visual image of laboratory bench with indicated locations of sensors for registered values: 2 – TDC and engine speed sensor, 3 – outlet valve opening sensor, 7 – element that enlarges the capacity of the combustion chamber, 8 – pressure sensor, 9 – thermocouple in the water jacket, C – fuel line

In steady states, three characteristics of a compression ignition engine's operation are allowed. In the conducted studies, the regulator characteristics were applied, with a variable speed within the scope of astatic operation of the controller. During the experimental investigation conducted on a Farymann Diesel type D10 engine, measurements were carried out for 3 operating points according to the regulator characteristics – Table 5.

In this stage of investigation and mathematical processing and statistical analysis, modifications were made to the structure's parameter of injector spring tension through appropriate selection of shims. In this way, its relaxation lowering the opening pressure of the injector was simulated. In the engine under test, was installed an injector with shims with a thickness of δ_{inj} equal to 2.3 mm in sum, causing a fuel injector opening pressure of about 12 MPa (the value for the reference condition). During the test for condition 3, shims with a total thickness of 1.8 mm were mounted in the injector, resulting in a reduction of the injector opening pressure to 10 MPa, which simulated a failure of the fuel injection system involving too early injection of fuel into the combustion chamber – Fig. 7.

Fig. 7. Preview of injector parts which were used in the tests, among them exchangeable (adjustable) shims under the injector spring

During a diagnosis study of an engine under steady-state conditions, diagnostic values are determined from among its output values. Those are selected that respond more strongly to changes in the values of structural quantities than to changes in the values of input quantities, forcing an ongoing work process. Comparing the susceptibilities of multiple control values, in various units, requires taking the relative values of input, output and structural values for this study [17]. The null hypothesis used in the study assumes no influence of the input parameter on the output parameter. The impact of an input parameter is important if the calculated value of the applied statistic is equal to or greater than the critical value, given in the tables for the adopted significance level α and the number of freedom degrees $f = n - 1$. The conditions for the application of one-sided parametric tests were met, so an F statistic with an F-S distribution was adopted [6, 18]. It was assumed that the results of measurements of all control quantities can be modeled as random variables with a specified expectation value and variance and normal distribution, the variances of the random variables are equal or close in value, and the parametric tests used have a one-sided critical area. The chance of an error of first kind, involving an assumed significance level α, and the possibility of an error of second kind, with a value of $\beta = 1 - \alpha$, were taken into account.

Table 3 shows the matrix of an operational testing program, in this case a randomized static plan, enabling to assess the significance of the effect of the opening pressure of the injector p_{inj} realized within a certain range of variation, on the determined output factor, which is the specific enthalpy of the flue gas flow in the range of one duty cycle – h_{exh}.

Table 3. Matrix of experimental investigation program – static randomized complete plan

Input factor level	The number of experience		
	1	...	4
p_{inj1}	h_{exh11}	...	h_{exh41}
p_{inj2}	h_{exh12}	...	h_{exh42}

In addition, once a factor is considered significant ($F_{cal} > F_{cr}$), it is allowed to compare the difference $\Delta F = F_{cal} - F_{cr}$ for particular diagnosis measures. That enables an assessment of precisely whose diagnostic measures are more highly affected by the input parameter (for example, structures) – the greater the ΔF, the greater the impact there will be.

3.3. Statistical analysis results for variable injector opening pressure p_{inj}

Outgoing factor amounts, being the specific enthalpy of the flue gas per each cycle of engine operation, for three engine steady-state power conditions, are shown in Tables 4a–c. The points P_1, P_2 and P_3 defined by values are due to the adopted performance steering characteristics of the engine.

In order to determine the value of the F_{obl} statistic, the following null hypothesis was set:

H_0: the value of the injector opening pressure has no impact on the value of the specific enthalpy of the exhaust gas flow mean within a single engine cycle ($S_{II2} = S_{I2}$).

Based on the numerical data summarized in Tables 4a–c and the adopted importance level $\alpha = 0.05$ and based on the right-hand critical zone scenario, the specific enthalpy of the flue gas flow in a single engine cycle was calculated for every test point (P_i), with the number of degrees of freedom for the numerator and denominator ($f_1 = 1$ and $f_2 = 6$). Then the critical value of the $F_{cr} = F(0.05;1;6) = 5.9874$ statistic was read from the statistical tables [17], and the values of F_{cal} were determined, the values of which are shown in Table 5. When evaluating the influence of the mean within a single cycle of the specific enthalpy of the exhaust gas stream h_{exh}, it (specific enthalpy) has a significant impact ($F_{cal} > F_{cr}$) only at point 3 of the engine's control characteristics.

Based on the results of the statistical analysis – Table 4 and 5, and the prepared characteristics of the variation of the specific enthalpy of the exhaust gas flow h_{exh} – Fig. 8, in the considered range of set load variation and the value of injector opening pressure, it can be concluded that the statistical a single-factor analysis unambiguously showed that the injector opening pressure has no important impact on the specific enthalpy of the exhaust gas stream in load states 1 and 2 according to the engine's control characteristics, while in state 3 the effect of this diagnostic parameter was significant ($\Delta F = 9.06$). Therefore, it was considered that the two-factor analysis would not take into account the injector opening pressure as a factor affecting the specific enthalpy of the flue gas stream within a single engine cycle. From the characteristics shown in Fig. 8, it can be deduced that lowering the injector opening pressure results in a decrease in the specific enthalpy value of the exhaust gas. This decrease is greater if the engine load is higher.

Table 4a. The value of the mean within a single cycle specific enthalpy of the exhaust gas h_{exh} for variable values of injector opening pressure p_{inj} at a point P_1

Input parameter	Value, MPa	Load point 1 (432 W; 5.1 A; 72 V)				
		Number of experience				
		1	2	3	4	y_i
p_{inj1}	12	12.1299	12.1986	12.2763	12.2176	12.2056
p_{inj2}	10	12.2516	12.2652	12.0890	11.8609	12.1167

Table 4b. The value of the mean within a single cycle specific enthalpy of the exhaust gas h_{exh} for variable values of injector opening pressure p_{inj} at a point P_2

Input parameter	Value, MPa	Load point 2 (768 W; 6.8 A; 96 V)				
		Number of experience				
		1	2	3	4	y_i
p_{inj1}	12	13.8992	13.6571	13.4404	13.3947	13.5979
p_{inj2}	10	13.3819	13.3464	13.2356	13.2772	13.3103

Table 4c. The value of the mean within a single cycle specific enthalpy of the exhaust gas h_{exh} for variable values of injector opening pressure p_{inj} at a point P_3

Input parameter	Value, MPa	Load point 3 (1200 W; 8.5 A; 120 V)				
		Number of experience				
		1	2	3	4	y_i
p_{inj1}	12	15.4712	15.4883	15.3075	15.3299	15.3992
p_{inj2}	10	15.0728	15.1370	14.8994	14.6505	14.9399

Table 5. The value of statistics F_{cal} and ($\Delta F = F_{cal} - F_{cr}$) for cut down injector opening pressure p_{inj} and its impact on h_{exh}

Point according to regulator characteristics	F_{cal} and ($\Delta F = F_{cal} - F_{cr}$) for h_{exh} [kJ/kg]
P_1 (432 W; 5.1 A; 72 V)	0.81 (–5.18)
P_2 (768 W; 6.8 A; 96 V)	5.72 (–0.27)
P_3 (1200 W; 8.5 A; 120 V)	15.05 (9.06)

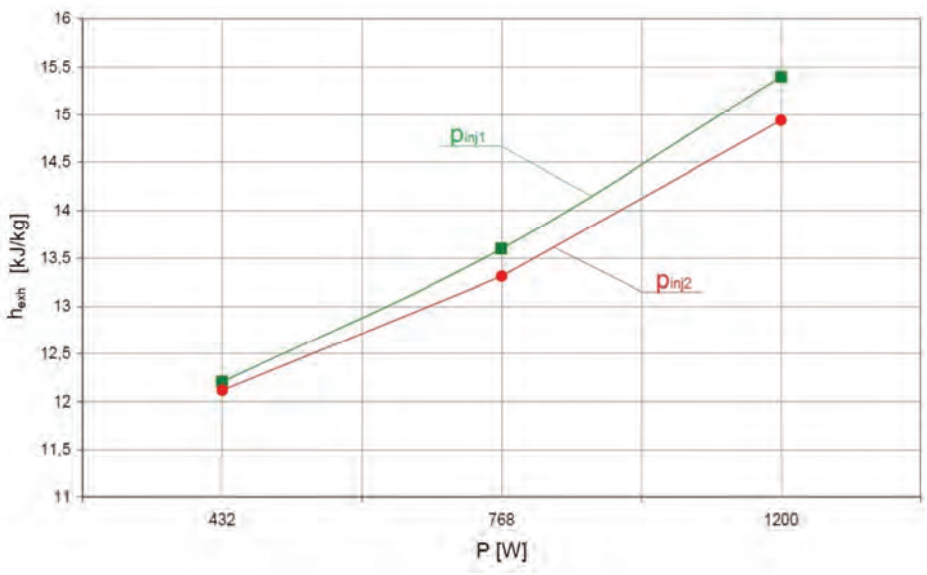

Fig. 8. Effect of the injector opening pressure on the value of the mean within a single cycle of the exhaust gas enthalpy $h_{śr}$ for compression ignition engine loads according to the regulator characteristics

4. Comments and final conclusions

The opening pressure of the injector p_{inj} is significant amount characterizing the operation of a compression ignition engine. It is a parameter that often accompanies damage to the injection system. Thus, it should be alarming to the engine user if it increases or decreases, indicating appearance of a status of partial utility or malfunction. Measurement of the quickly varying exhaust gas temperature

makes it allowed to determine the impact of a modification in the input p_{inj} on a diagnostic measure such as h_{exh} only for a loaded engine (above 20% of the engine's nominal load). Then it is allowed, thanks to the use of a statistical instrument such as F statistic of F-S distribution, to determine the significant effect of p_{inj} on h_{exh} in the studied scope of engine load changes. The applied investigation and analytical method was considered effective for assessing impact of importance of modifications of input factor – structure (p_{inj}) on output value (h_{exh}). It is also allowed to determine other diagnostic measures on basis of rapidly changing exhaust gas temperature and determine impact of p_{inj} on it, thanks to use of F statistics. At the same time, this input value was eliminated in two-factor analysis, analyzing simultaneous impact of injector opening pressure and engine load on the specific enthalpy of the flue gas of a compression ignition engine.

Nomenclature

BTE	brake thermal efficiency
BSFC	brake specific fuel consumption
EGT	exhaust gas temperature
f	number of degrees of freedom for the numerator and denominator
F	statistic of Fisher-Snedecor distribution
H	hypothesis
I_{gen}	current of generator (motor) load
n	rotational speed value
p_{inj}	injection pressure
T_{exh}	temperature of exhaust gas
U_{gen}	voltage at generator armature terminals
VE	volumetric efficiency

Bibliography

[1] Aabo K, Åström G, Daniels A. Marine diesel engines, catalytic fines and a new standard to ensure safe operation: separation performance standard. Alfa Laval, BP Marine, Sweden 2005.

[2] Babiak M, Merkisz J, Waligórski M, Kniaziewicz T. Analysis of marine combustion engine processes with vibroacoustic methods for environment protection strategy. Combustion Engines. 2013;153(2):28-39. https://doi.org/10.19206/CE-116999

[3] Bielawski P. Problems of reciprocating machine valve diagnostics (in Polish). Pomiary Automatyka Robotyka. 2013; 12(2013): 82-89.https://doi.org/10.14313/PAR_202/82

[4] Bruski S. Application of methods of frequency analysis of torsional vibrations of the propeller shaft to identify the technical condition of fuel injectors of a medium-speed marine engine in operation. PhD dissertation. Politechnika Gdańska. Gdańsk 2005 (in Polish).

[5] Czajgucki JZ. Reliability of marine diesel power plants. Maritime Publishing House. Gdansk 1984 (in Polish).

[6] Dally, J.W. Statistical Analysis of Experimental Data. Sharpe W. (eds). Springer Handbook of Experimental Solid Mechanics. Springer Handbooks. Springer, Boston 2008. https://doi.org/10.1007/978-0-387-30877-7_11

[7] Girtler J. Energetic aspect of diesel engine operation. Combustion Engines. 2009;37(2):84-92. https://doi.org/10.19206/CE-117183

[8] Grochowalska J. Analysis of the macrostructure of the fuel spray atomized with marine engine injector. Combustion Engines. 2019;179(4):80-85. https://doi.org/10.19206/CE-2019-413

[9] International Association of Classification Societies. Requirements Concerning Machinery Installations. M35: Alarms, remote indications and safeguards for main reciprocating I.C. engines installed in unattended machinery spaces. 2016.

[10] International Association of Classification Societies. Requirements Concerning Machinery Installations. M36: Alarms and safeguards for auxiliary reciprocating I.C. engines driving generators in unattended machinery spaces. 2016.

[11] International Association of Classification Societies. Requirements Concerning Machinery Installations. M73: Turbochargers. 2016.

[12] Janardhan N, Murali Krishna MVS, Ushasri P. Influence of injector opening pressure on performance and exhaust emissions in DI diesel engine with air gap insulated piston and air gap insulated liner with diesel operation. International Journal for Advance Research in Engineering and Technology. 2014; 2(4):107-115.

[13] Kapusta ŁJ, Pielecha I, Wisłocki K, Teodorczyk A. Autoignition and combustion of n-hexane spray in subcritical and supercritical environments. J Therm Anal Calorim. 2016;123:819-828. https://doi.org/10.1007/s10973-015-4927-z

[14] Klyus O, Rajewski P, Lebedevas S, Olszowski S. Determination of fuel atomization quality in compression ignition engines using acoustic emission signal. Combustion Engines. 2022;191(4):83-91. https://doi.org/10.19206/CE-149370

[15] Korczewski Z. Methodology of testing marine fuels in real working conditions of a self-ignition engine. Publishing House of the Gdańsk University of Technology. Gdansk 2022 (in Polish).

[16] Korczewski Z. Methodology for determining the elemental composition, as well as energy and ignition properties of the low-sulfur marine fuels. Combustion Engines. 2021;186(3): 96-102. https://doi.org/10.19206/CE-141573

[17] Korczewski Z. Operational diagnostics of marine internal combustion engines – piston and turbine. Selected Issues. Publishing House of the Gdańsk University of Technology. Gdańsk 2017 (in Polish).

[18] Korzyński M. Experiment methodology. Planning, implementation and statistical processing of the results of technological experiments. WNT Publishing House. Warsaw 2017 (in Polish).

[19] Özdalyan B, Özer S. The effects of using 2-butanol-diesel fuel mixture on a compression ignition engine at different injector spraying pressures. Technology. 2011;14(1):23-31.

[20] Polish Register of Shipping. Recipes. Publication Vol. 5/P. Requirements for turbochargers. Chapter 2. Required Documentation. Gdańsk 2016 (in Polish).

[21] Polish Register of Shipping. Recipes. Publication Vol. 28/P. Tests of internal combustion engines. Chapter 1. Type test of internal combustion engines. Chapter 2. Delivery and acceptance tests of internal combustion engines (especially the paragraph 2.2.2). Gdansk2019 (in Polish).

[22] Polish Register of Shipping. Rules for the Classification and Construction of Sea-going Ships. Part VI: Machinery Installations and Refrigerating Plants. Gdansk 2022 (in Polish).
[23] Puzdrowska P. Evaluation of the influence of the opening pressure of a marine Diesel engine injector on the results of numerical simulation of the working cycle and their comparison with the results of the laboratory experiment. Combustion Engines. 2023;193(2):9-14. https://doi.org/10.19206/CE-155873
[24] Puzdrowska P. Application of the F-statistic of the Fisher-Snedecor distribution to analyze the significance of the effect of changes in the compression ratio of a diesel engine on the value of the specific enthalpy of the exhaust gas flow. Combustion Engines. 2021;186(3):80-88. https://doi.org/10.19206/CE-141346
[25] Puzdrowska P. Evaluation of the significance of the effect of the active cross-sectional area of the inlet air channel on the specific enthalpy of the exhaust gas of a diesel engine using statistics F of the Fisher-Snedecor distribution. Combustion Engines. 2020;182(3):10-15. https://doi.org/10.19206/CE-2020-302
[26] Stobnicki P. Research analysis of fuel injection in terms of ecological properties of a self-ignition engine. PhD dissertation. Poznań 2013 (in Polish).
[27] Sun Y, Guan Z, Hooman K. Cavitation in diesel fuel injector nozzles and its influence on atomization and spray. Chemical Engineering and Technology. 2019;42:6-29. https://doi.org/10.1002/ceat.201800323
[28] Ta TV, Thien DM, Cang VT. Marine propulsion system reliability assessment by fault tree analysis. International Journal of Mechanical Engineering and Applications. Special Issue: Transportation Engineering Technology, Part III. 2017;5(4-1):1-7. https://doi.org/10.11648/j.ijmea.s.2017050401.11
[29] Witkowski K. Research the possibility of obtaining diagnostic information about the ships engine fuel injection system condition based on the analysis of characteristics of heat release. Journal of KONES. 2019;26(3):249-256. https://doi.org/10.2478/kones-2019-0080
[30] Witkowski K. The increase of operational safety of ships by improving diagnostic methods for marine diesel engine, Transnav the International Journal on Marine Navigation and Safety of Sea Transportation. 2017;11(2):317-321. https://doi.org/10.12716/1001.11.02.15

Patrycja Puzdrowska, MEng. – Faculty of Mechanical Engineering and Ship Technology, Gdansk University of Technology, Poland.
e-mail: *patpuzdr@pg.edu.pl*

Article citation info:
Daszkiewicz P, Kołodziejek D. Comparison and analysis of modern combustion powertrain systems of rail vehicles. Combustion Engines. 2024,196(1):46-53. https://doi.org/10.19206/CE-171385

Pawel DASZKIEWICZ
Daniel KOŁODZIEJEK

Combustion Engines
Polish Scientific Society of Combustion Engines

Comparison and analysis of modern combustion powertrain systems of rail vehicles

ARTICLE INFO

Received: 25 May 2023
Revised: 17 August 2023
Accepted: 18 August 2023
Available online: 28 October 2023

The article presents the currently used technologies and solutions for rail vehicle drive systems that can be used in the future. The most popular systems used in locomotives and multiple units are described. In addition, modern solutions such as bi-mode locomotives and hybrid vehicles are shown. The article also discusses the possibility of using ultracapacitors, batteries, or fuel cells in order to increase the efficiency of the powertrain of a rail vehicle. The selection of the appropriate solution depends on the intended use of the vehicle and the assumed traction characteristics and requires a thorough analysis including, among others, modeling of the drive system and its management.

Key words: *rail vehicles, combustion engines, powertrains, hybrid, energy storage*

1. Introduction

Rail transport is one of the important branches of development in the context of the transport of both goods and people. The land connection between Europe and Asia, as well as the convenience of traveling by rail on short and medium-length routes, make the development of rail vehicles an area in which a lot of work is carried out. Still, a large part of the rolling stock owned by Polish carriers are vehicles powered by systems that include internal combustion engines. Figure 1 shows the share of diesel locomotives in all locomotives operated in Poland over the years (2003–2018). It changed over time, but remained constantly at the level of over 50%.

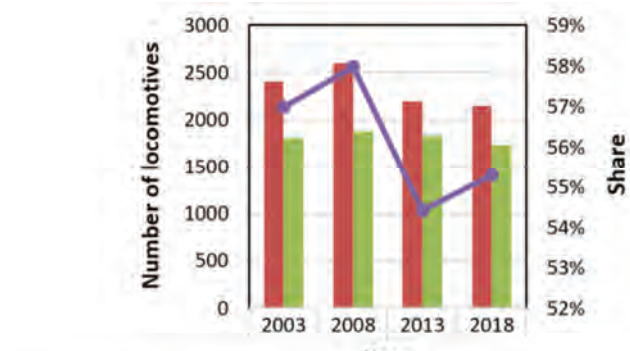

	2003	2008	2013	2018
Diesel locomotives	2405	2602	2194	2149
Electric locomotives	1816	1886	1838	1738
Share of diesel locomotives in all locomotives used in Poland	57%	58%	54%	55%

Fig. 1. The structure of the rolling stock in Poland in 2003-2018 [10]

The structure of the rolling stock is closely related to the available infrastructure. Figure 2 shows the distribution of electrified and non-electrified lines on the map of Poland. Lines with different characteristics are adjacent to each other, and non-electrified lines constitute a large part of the Polish railway network, which in 2021 consisted of 19.3 thousand km [3]. Electrified lines have a length of 12.1 thousand km. It should be noted, however, that it is the non-electrified lines that allow the development of transport on a local scale and allow people to move from smaller towns to agglomerations, e.g. to their work or schools.

Fig. 2. Map of Polish electrified (yellow line) and non-electrified (green line) railway lines as of 18.03.2023 [8]

One of the most important factors influencing the development of internal combustion engines in rail vehicles are the successively introduced exhaust emission standards. The latest document on this issue in the context of the NRMM category, which also includes rail vehicles, is the "Regulation of the European Parliament and of the Council (EU) 2016/1628 of September 14, 2016. The regulation introduces subsequent stages determining the maximum

emission values of toxic compounds. The dynamics of changes in the maximum emission values of toxic compounds for stages IIIA, IIIB, and V are presented in Fig. 3. Over the years, more restrictive values have been introduced for the emission of hydrocarbons, nitrogen oxides, and particulate matter.

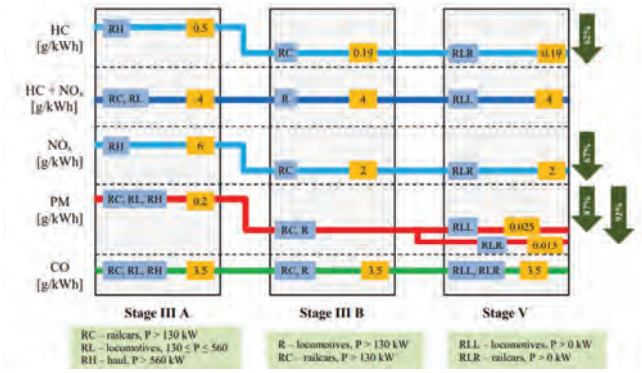

Fig. 3. Change of the permissible maximum emission values of harmful substances for Stage IIIA, IIIB, and V [17]

Rail vehicles, due to the nature of the use of internal combustion engines and the desire to work in stationary conditions, are tested in the NRSC test, and the result is the value of specific emission in g/kWh. The procedure for locomotives and DMUs is in accordance with ISO 8178, type F. In this case, the test determines three operating points covering the entire range of possible loads and engine speeds, to which weighting factors are assigned, determining the impact on the final value of specific emission (Table 1). It should be noted, however, that idling is of the greatest importance, as much as 0.6.

Table 1. ISO 8178, type F exhaust emission measurement test cycle [5]

Mode number	1	2	3	4	5	6	7	8	9	10	11
Torque [%]	100	75	50	25	10	100	75	50	25	10	0
Speed	Rated speed					Intermediate speed					Low idle
Locomotives											
Type F	0.25	–	–	–	–	–	–	0.15	–	–	0.60

2. Diesel locomotives

Diesel locomotives had their heyday in Poland in the times of the People's Republic of Poland. A small degree of electrification was conducive to the development of diesel rolling stock. At that time locomotives popular in Poland, such as: SM42, ST44, SM30, ST43, and SM48 were produced. Characteristic for diesel locomotives is the power transmission system based on an electric gear, where the power on the crankshaft is converted into electricity using the main generator. A diagram showing the construction of a vehicle with such architecture is shown in Fig. 4. Fuel is supplied to the internal combustion engine, then mechanical energy is supplied to the main generator via the shaft. The electric energy is sent through the control element to the electric motor, which drives the wheels of the locomotive wheelset through the transmission. At the same time, some of the electricity on the shaft coming out of the internal combustion engine is used to drive an auxiliary generator that provides electricity to power the batteries, lights, HVAC, compressors, etc.

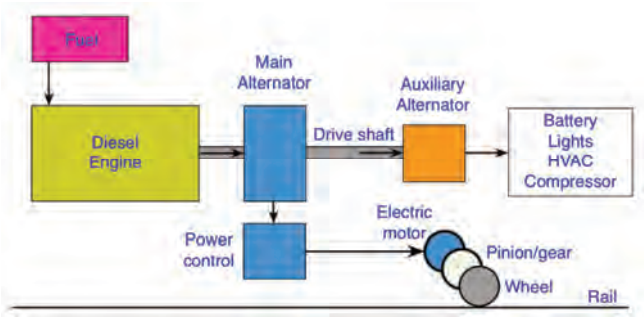

Fig. 4. Diesel locomotive powertrain architecture scheme [24]

New generation engines that meet Stage V requirements must be equipped with an extensive off-engine exhaust aftertreatment system. Due to the degree of its complexity and the amount of space occupied, manufacturers try to create systems that can be adapted to specific customer needs. An example is the modular system offered by MAN (Fig. 5). It has been designed to meet Stage V requirements. The main advantages include the ability to configure the system to match the shape of the system to the designed vehicle and versatility, as one system can be combined with a wide range of engines that are used in different types of non-road vehicles (e.g. forestry, mining or water vehicles). When designing a vehicle or making a retrofit, the possibility of free configuration of the system allows designers to better use the available space, as well as to build the system in a way that facilitates maintenance or repair work. The modular system also allows for easier replacement in the event of damage, thanks to which the time a vehicle is out of service is significantly reduced.

Fig. 5. MAN Modular Exhaust aftertreatment System [16]

3. Diesel multiple units

Due to the need to connect the drive system and passenger space, diesel multiple units are an area of intensive construction work. The development of the drive system in a way that interferes with the areas intended for passengers as little as possible resulted in the separation of two basic types of drive system solutions [6]. These are:

– mounting the engine under the vehicle frame and mechanical connection of the engine with the drive trolley
– using a separate engine compartment with a generator (electric transmission).

Depending on the adopted solution, internal combustion engines with power ranging from 300 to 500 kW are used

for the DMUs. More compact in-line engines (usually six-cylinder) are used, mounted under the floor, or larger engines, even V12, when they are installed in the engine compartment. In connection with the trends in rail vehicles, there is a tendency to build modules that can then be universally used in various vehicles on a plug & play basis. One of the signs of this approach is the creation of Powerpack solutions that integrate the combustion engine with the transmission and other elements of the drive system. An example of such a solution is PowerPack Series 1800 from MTU (technical data shown in Table 2). An important feature of this module is the ability to choose one of three types of gears [23]. The manufacturer allows the ordering party to choose:

– six-speed mechanical transmission with retarder and optional reverse gear
– electric transmission with a permanent magnet synchronous generator or an asynchronous generator
– two-stage hydraulic transmission.

The choice of transmission allows the use of such a module regardless of the adopted vehicle architecture, which is an advantage for both the module manufacturer (reduced technology development costs), the rolling stock manufacturer (possibility of using one solution in many vehicles), and the final recipient (simplified service).

Different versions of the solution are available to meet Stage V requirements. Their power ratings range from 315 to 375 kW at 1800 rpm. The ratio of the cylinder diameter to its stroke is 128/166 mm. The engine has 6 cylinders with a displacement of 2.14 dm^3 each, which translates into a displacement of 12.8 dm^3. The Stage V aftertreatment system consists of: DOC, DPF, and SCR. MTU's PowerPack is shown in Fig. 6.

Table 2. MTU PowerPack Series 1800 technical data [23]

Configuration	6H
Rated power	315–375 kW
Rated speed	1800 rpm
Bore/stroke	128 mm/166 mm
Displacement	2.14 dm^3
Displacement, total	12.8 dm^3
Emission qualification	EU Stage V
Exhaust aftertreatment system	DOC, DPF, SCR

Fig. 6. MTU PowerPack 6H 1800 [23]

4. Hybrid and bi-mode solutions

Due to the development of drive systems used in vehicles in general, modern hybrid drives have also been used in rail vehicles. Their main task is to increase the efficiency of the system, reduce energy consumption and emissions of harmful substances. This trend is common for all types of non-road machinery. The author of the article [9] states that the development of powertrains faces two major challenges: increasing working parameters and decreased fuel consumption. These two design assumptions are often contradictory to each other and make development more complex. That's why introducing more efficient electrified or hybrid solutions becomes more and more popular. The basic elements of such systems include in the case of locomotives:

– internal combustion engine as the main source of propulsion
– main generator with traction rectifiers
– traction motors cooperating with axial gears
– high-performance battery
– DC/AC power converter and auxiliary converters
– drive control and diagnostics.

It is also worth noting the basic difference between bi-mode and hybrid solutions used in rail vehicles. Due to the presence of electrical systems in the classic solutions of drive systems, these terms are not always interpreted unambiguously, and are often used interchangeably, despite the differences that are easy to identify. It should be noted that a characteristic feature of the hybrid drive is the desire to optimize the operation of the system and achieve the synergy effect. For this purpose, the various drive sources form a single, more complex system. However, they require energy storage. Bi-mode solutions isolate the individual drive sources used, and so, for example, in the case of locomotives, sometimes they work as a diesel locomotive, and sometimes as an electric one (the systems do not interact with each other). Examples of such solutions can be Pesa Gama Dual Power (111DE) or Siemens Vectron Dual Power. Arrangement of devices on the 111DE locomotive is shown in Fig. 7. As the authors of the publication [19] indicate, such a vehicle can be used both in freight and passenger traffic. The advantage is the possibility of smooth travel on electrified and non-electrified lines. Thanks to this, bi-mode solutions fit into the assumptions of intermodal transport. However, they do not allow to manage the flow of energy in the drive because they do not have an element capable of accumulating to the necessary extend.

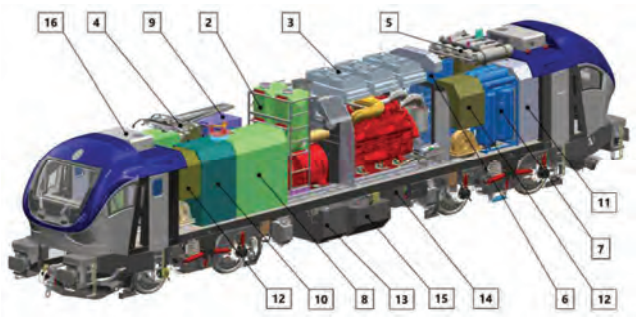

Fig. 7. Arrangement of devices on the 111DE locomotive [19]: 1 – power generator, 2 – set of SCR catalysts, 3 – set of engine coolers, 4 – pantograph, 5 – main air tanks, 6 – compressor module, 7 – panel module, 8 – traction inverter cabinet, 9– cooling column with braking resistor, 10 – high-voltage cabinet 11 – ETCS cabinet, 12 – low voltage cabinet with traction motor fan, 13 – line choke, 14– battery box, 15 – fuel tank, 16 – air conditioner

Due to the characteristics of the drive system and the specificity of the tasks performed, it seems to be particularly advantageous to use hybrid solutions in the DMUs. It is possible to install a parallel hybrid system which shows particular advantages in the conditions of frequent stops and starts, which are an inherent element of regional and agglomeration traffic. In addition, it is possible to use the recuperation of kinetic energy during braking in order to increase the efficiency of the entire system and save energy. A popular system solution in the DMUs is the use of a hybrid PowerPack. An example of such a device may be the 1800 Series from MTU. The module consists of an internal combustion engine, a gearbox with an electric motor (parallel hybrid), a set of batteries, a cooling system, and an exhaust system. The Hybrid PowerPack 6H 1800 is shown in Fig. 8, while an example of the installation on a rail vehicle is shown in Fig. 9. It should be noted that the design assumes the use of only a mechanical transmission, excluding the use of a system with an electric transmission. The PowerPack must, therefore be mounted under the floor of the vehicle, whereby the batteries can be attached to the roof or under the floor due to the electrical connection. Mounting on the roof allows for a larger area of the low floor and saves space for the installation of other devices that should be placed under the vehicle frame. In addition, it is easier to solve the issue of cooling the batteries, which is also of great importance.

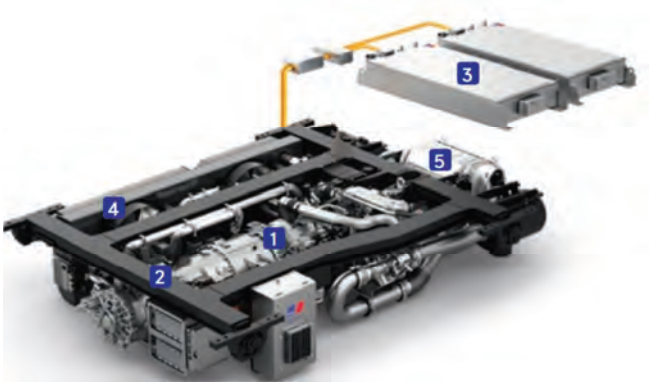

Fig. 8.MTU Hybrid PowerPack 6H 1800 structure [23]: 1 – engine, 2 – power transmission, 3 – battery system, 4 – cooling system, 5 – exhaust system

Fig. 9. MTU Hybrid PowerPack 6H 1800 installation [23]

The parameters of the device are presented in Table 3. Depending on the selected version, the combustion engine power is 315 or 375 kW at a rotational speed of 1800 rpm. The ratio of the bore to stroke is 128 to 166 mm. The engine has a 6-cylinder with an in-line configuration, and each cylinder has a displacement of 2.14 dm^3, which translates into a displacement of 12.8 dm^3. It is adapted to meet the requirements of Stage V. Thanks to the use of a hybrid system, the PowerPack has the possibility of energy recuperation, boost mode, and the ability to drive only using the 142 kW electric motor. MTU combines its hybrid PowerPack solutions with battery modules with a capacity of 34.4 kW. The number of modules can be selected individually for each designed vehicle. The exhaust system is equipped with DOC, DPF, and SCR to meet Stage 5 requirements. The operation of the system is supervised by an intelligent automation system used to optimize its operation. Technical data of the PowerPack are shown in Table 3.

Table 3. MTU Hybrid PowerPack 6H 1800 technical data [23]

Combustion engine types	
6H 1800 R76	315 kW
6H 1800 R86	375 kW
Speed	1800 rpm
Bore/stroke	128 mm/166 mm
Cylinder configuration	6/in line
Displacement	2.14 dm^3
Displacement, total	12.8 dm^3
Emission qualification	Stage V
Standard equipment	
E-Drive	For recuperating, boosting and pure electric drive; 142 kW
Energy storage	Li-Ion batteries incl. battery management system and conditioning system. Underfloor or roof installation. 34.4 kWh per battery module
Transmission	Mechanical gearbox with integrated reversing function/Mechanical gearbox without integrated reversing function
Cooling system	Integrated in PowerPack, electrically driven
Exhaust gas aftertreatment system	EU Stage V, aftertreatment combi system with DOC, DPF and SCR; reducing agent injection with suppling and dosing unit
IDM (Intelligent Drive Manager)	Smart automation system to optimize the operation of the Hybrid PowerPack based on GPS and track data
On-board power supply	3P~AC, 400 V/50 Hz; up to 70 kVA

The choice of a bi-mode or hybrid solution should be preceded by a broad recognition of needs, a series of simulations and comparisons. Power demand should be determined based on traction characteristics and potential gains and losses. Both financial and energy terms should be determined. Due to the above, the creation of an appropriate drive system is a difficult process that requires experience, but also multi-criteria optimization. Modeling the fuel consumption and energy flow is a demanding study. Article [15] shows the mathematical model demonstarting the synergy of HEV. It also shows different types of energy management systems. For example, they can be based on:

heuristic hypotheses, statistical optimisation, stochastic-dynamic programming, algorithms of the equivalent fuel consumption strategy, and particle swarm optimisation. Variety of available approaches is another challenge as modeling every type makes it necessary to perform many characteristics and assumptions. Preparing models for different architectures requires a lot of resources for the research and development phase, increasing the price of the vehicle design. Moreover, the negative influence of a vehicle life cycle can be reduced using new types of oxygenated fuels, reducing emissions of PM and NO_x [11, 12].

One of the important aspects of hybrid drives is the energy storage system. Its selection should be preceded by a thorough analysis of its usefulness in a given vehicle on the basis of its traction characteristics, but also the nature of work or route profiles. Choosing the right solution is not easy, and it can help, for example, by optimization, which helps to quantitatively select the best solution in given conditions and under certain boundary conditions. When selecting an energy storage element in a hybrid system, its operational parameters should be considered, such as:

– mass
– efficiency
– energy density
– power density
– lifetime.

However, it is also worth considering aspects related to the production and recycling of the energy storage system. In order to evaluate the solutions, the following can be compared:

– energy consumption of production and recycling
– production and recycling emissions
– resources needed for production
– recyclable.

One of the most popular technology decades ago, and at the same time the simplest ways to store energy is the use of flywheels and thus the storage of mechanical (kinetic) energy. In this way, energy can be easily stored, provided that it is used in a short time. However, this technology is mainly used in bus projects.

Currently, the most popular way to store energy is the use of batteries, i.e. the use of electrochemical energy. Primarily, lithium-ion batteries are used, which are currently popular in all areas of life.

Saft company offers a battery system of various capacities, which consists of blocks of cells connected in sets of 108, 180 or 360 cells. Thanks to this, the capacities of 7.5, 12.5, and 25 kWh are achieved, respectively. Technical data of a single cell are shown in Table 4.

Li-ion batteries disadvantage is safety and average power density. In addition, there are significant fluctuations between their capacity depending on the temperature. This presents scientists with the challenge of developing a technology that will allow the creation of electrochemical batteries with a higher power and energy density, and at the same time ensure safe and durable use. A partial answer to these needs is the development of solid electrolyte battery technology. Replacing the electrolyte in a liquid state with a solid substance allows for several advantages. The level of safety is increased because there is no risk of fire or explosion. The energy density is higher compared to lithium-ion batteries [25]. This technology also creates the possibility of using cathodes from new materials due to the greater potential of anodes with a solid electrolyte. For this reason, that technology is considered to be the future of energy storage development in vehicle drives. Solid electrolytes can be divided into: polymeric, inorganic, and composite materials. However, before it can be disseminated on a large scale, scientists need to solve the problems arising from the use of solid electrolytes related to the electrochemical properties of the electrolyte. Comparison of Li-Ion and solid state battery schemes is shown in Fig. 10. Moreover nanocomposites and hybrids are used for Li-Ion batteries to achieve new, improved characteristics [13].

Table 4. Saft LP 28MTi Li-ion power cell technical data [20]

Nominal characteristics at +25°C	
Nominal voltage [V]	2.25
Energy [Wh]	63
Gravimetric energy [Wh/kg]	78
Mechanical characteristics	
Width [mm]	148
Heigth [mm]	101.7
Depth [mm]	26.5
Weight [g]	810
Cell typical operating conditions at +25°C	
Typical cut off voltage [V]	1.6
Charging method	Constant current Constant voltage
Charging voltage [V]	2.7 ±0.05
Maximum continuous charge/discharge current [A]	280
Maximum pulse charge/discharge current 30 s [A]	450
Cycling performances	20 000 cycles (80% DOD) 1.6 mil cycles (3% DOD)

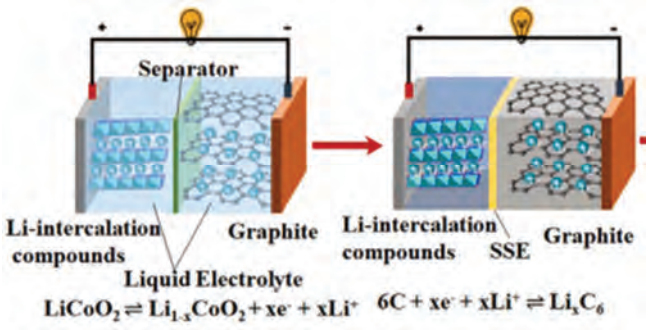

Fig. 10. Comparative diagram of Li-ion battery (left) and solid-state battery (right) [25]

Another concept is to use electricity directly through the use of ultracapacitors. No chemical reaction takes place in them, which allows for durability. In addition, they allow for quick loading and unloading. The development possibilities of increasing the capacitance of capacitors are limited only by the possibility of obtaining larger surfaces of their electrodes and reducing the distance between them. Supercapacitors can be divided into [14]:

– Pseudocapacitors or Redox Capacitors
– Electric double layer capacitors (EDLCs)
– Hybrid capacitors.

The most important quantity characterizing supercapacitors is specific capacitance, which defines the capacitance

per unit mass. The value depends on the material used, but the creation method also has an impact.

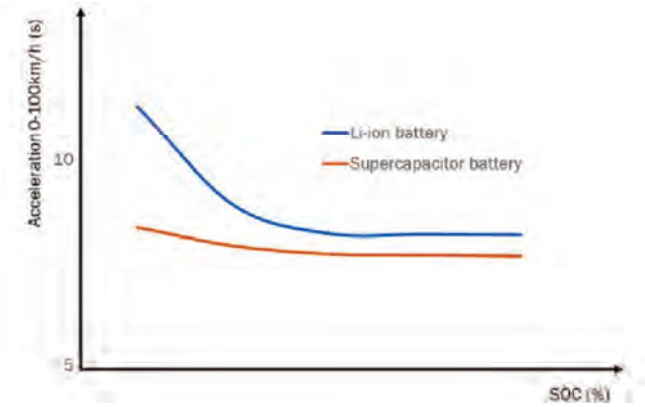

Fig. 11. HEV acceleration 0–100 km/h [7]

When it comes to technology performance, supercapacitors show great stability in the power output compared to the li-ion battery. Figure 11 shows the comparison of acceleration of a vehicle powered by these power sources. Decreasing SOC has a significant influence on electrochemical battery power and therefore acceleration time increases. It can be assumed that that supercapacitor can be used in a wider range of SOC without compromising the vehicles performance.

Figure 12 shows a comparison of the energy density and power density of various energy storage devices. Supercapacitors and li-ion batteries have a similar range of energy density but the power density is higher in supercapacitors. Fuel cells have high energy densities and low power densities. however, they are becoming more and more popular due to the possibility of creating zero-emission energy using hydrogen. It's one of the possible ways to achieve climate neutrality

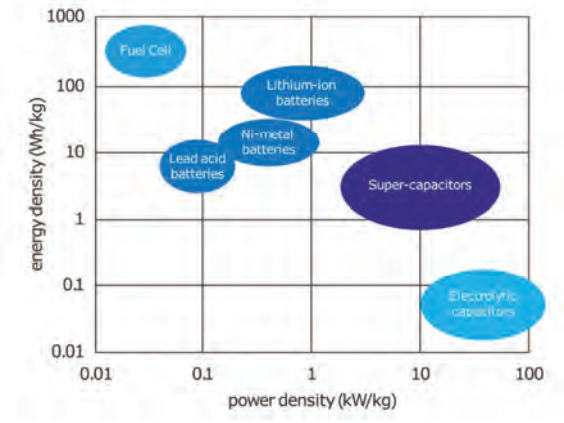

Fig. 12. Ragone plot of energy density vs power density of various energy storage devices including supercapacitors [26]

Hydrogen fuel cells have a number of advantages, the most important of which are a simple principle of operation negligible emission of harmful substances, and relatively large values of efficiency [4]. The electrical efficiency of a typical cell is in the range of 40–60%, and the total efficiency can reach 80–90% during electricity generation. Key factor that needs to be considered is the production of hydrogen. There's a variety of different methods and "brown" and "green" hydrogen can be separated [21]. Green methods are sustainable and these can be:

– Electrolysis of water using renewable power
– Steam methane reforming with carbon capture and storage techniques
– Gasification of biomass and biogas to produce syngas
– Fermentation of biowastes to produce H_2, CO, CO_2.

Brown methods, on the other hand are considered to be unsustainable and these can be:

– Steam methane reforming
– Coal gasification
– Oil partial oxidation.

Apart from hydrogen production, also its storage is a widely developed issue. The most popular architecture uses 35 MPa compressed hydrogen [2]. This technology offers good storage capacity at a low cost for regional passenger transport. Unfortunately, there's no technology in sight enabling to reach higher energy densities required for ensuring the constant high-power demand of a mainline locomotive.

In the cells, only a chemical reaction of hydrogen with oxygen takes place:

$$2H_2 + O_2 = 2H_2O \quad (1)$$

The first rail vehicle using hydrogen fuel cells is the Coradia iLint manufactured by Alstom.

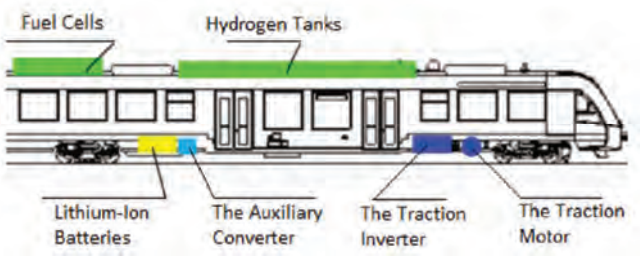

Fig. 13. Scheme of the Coradia iLint powertrain [22]

The construction of the vehicle is relatively simple (Fig. 13). Two compressed hydrogen (35 MPa) tanks and PEM fuel cells [18] are located on the roof of the vehicle. A lithium-ion battery that can store excess energy generated by the fuel cell has been placed under the floor of the vehicle. An auxiliary generator has been installed next to it, which provides power for devices such as sliding doors, HVAC, etc. Traction converters and traction motors are located near the drive trolleys. The presented vehicle does not have a combustion engine, but it is possible to use hybrid vehicles combining combustion and hydrogen drive as an intermediate link on the way to complete zero-emissions. Such a vehicle could support non-electrified traction. Authors of [21] state that hydrogen powered vehicles should be considered when long-term technical, environmental and/or economic factors make electrification a poor option. Table 5 shows technical data of a Ballard's FCmove™-XD fuel cell (Fig. 14). System power reaches 100 kW with a wide range of operating current and voltage.

Table 5. Ballard FCmoveXD fuel cell technical data [1]

Net system power [kW]	100 (±2)	
Operating system current [A]	20–360	
Operating system voltage [V]	280–560	
Dimension L × W × H [mm]	Roof Top	1714 × 812 × 360 (excluding air filter)
	Engine Bay	1240 × 572 × 702 (excluding air filter)
Dry weight [kg]	275	
Environmental protection	IP67	
Start-up temperature [°C]	–25	
Environmental operating temperature [°C]	(–30)–(+50)	
Short-term storage temperature [°C]	(–40)–(+80)	
Peak efficiency [%]	57	
Idle power [kW]	9	
Nominal radiator coolant outlet temperature [°C]	70	

Fig. 14 Ballard FCmoveXD fuel cell [1]

5. Conclusions

Rail vehicles powered by powertrains containing internal combustion engines remain an important part of transport in Poland. The level of electrification of the networks means that they will be used for many years to come. Design changes related to the development of drive systems for diesel locomotives and DMUs include mainly the development of exhaust gas aftertreatment systems. New possibilities are provided by the hybridization of systems and the creation of bi-mode vehicles. Bi-mode locomotives can be used for intermodal transport. Diesel multiple units can be equipped with hybrid powerpacks. Creating a hybrid vehicle requires the installation of an energy storage system. It can be a li-ion battery, a supercapacitor, or a fuel cell. Each of these methods is being developed. Work is being carried out on batteries with solid state electrolyte and materials for supercapacitors, which will ensure their high capacity. Fuel cells also have been dynamically developing for years, thanks to which they can successfully power vehicles, including rail vehicles such as shown the Coradia iLint translation.

Comparison of the weight and dimensions of a fuel cell and an MTU 6R 1300 engine shows that power per unit mass and per unit volume are similar (Table 6). That comparison shows that a modern fuel cell can be competitive when it comes to replacing combustion engines on non-electrified lines. Another technical problem is the storage of hydrogen used to power the fuel cell. Mounting hydrogen tanks takes a valuable place that is very much needed during designing a rail vehicle. Many devices used in vehicles are necessary for securing high level of passengers comfort but also to provide safety in rail transport. Because of that, it's not an easy task to find more space to mount hydrogen tanks. This can lead to a small range of a vehicle.

Table 6. Comparison of Ballard FCmoveXD fuel cell and MTU 63 1300 C diesel engine [1, 23]

	FCmove-XD	MTU 6R 1300 C 20	MTU 6R 1300 C 60
Weight	275 kg	1140 kg	1140 kg
Power	100 kW	320 kW	390 kW
Volume	0.5 dm^3	1.7 dm^3	1.7 dm^3
Power to volume ratio	200 kW/dm^3	188 kW/dm^3	230 kW/dm^3
Power to mass ratio	0.36 kW/kg	0.28 kW/kg	0.34 kW/kg

There's no possibility to choose one powertrain architecture that suits all of the vehicles and their scope of work. Exact analysis is needed including modelling of the powertrain and its management. This leads to a variety of solutions offered by rolling stock producers.

Nomenclature

AC alternating current
DC direct current
DMU diesel multiple unit
DOC diesel oxidation catalyst
DPF diesel particle filter
HVAC heating, ventilation, air conditioning
ISO Organization for Standardization
NO_x oxide
NRMM non-road mobile machinery
NRSC non-road steady cycle
PEM proton exchange membrane
PM particulate matter
SCR selective catalytic reduction
SOC state of charge

Bibliography

[1] Ballard FCmove HD+ data sheet, Ballard. https://www.ballard.com (accessed on 05.2023).

[2] Böhm M, Fernández Del Rey A, Pagenkopf J, Varela M, Herwartz-Polster S, Nieto Calderon B. Review and comparison of worldwide hydrogen activities in the rail sector with special focus on on-board storage and refueling technologies. Int J Hydrogen Energy. 2022;47(89):38003-38017. https://doi.org/10.1016/j.ijhydene.2022.08.279

[3] Concise Statistical Yearbook of Poland 2022. Warsaw 2022.

[4] Daszkiewicz P, Kurc B, Pigłowska M, Andrzejewski M. Fuel cells based on natural polysaccharides for rail vehicle application. Energies. 2021;14:1144. https://doi.org/10.3390/en14041144

[5] DieselNet. Engine & emission technology online – since 1997. https://dieselnet.com (accessed on 05.2023).

[6] Far M. Study of new solutions for drive and control systems for light rail vehicles (in Polish). Poznań 2021.

[7] Guo L, Hu P, Wei H. Development of supercapacitor hybrid electric vehicle. Journal of Energy Storage. 2023; 65:107269. https://doi.org/10.1016/j.est.2023.107269

[8] Interactive Map of Railway Lines – http://mapa.plk-sa.pl (accessed on 05.2023).

[9] Kalociński T. Modern trends in development of alternative powertrain systems for non-road machinery. Combustion Engines. 2022;188(1):42-54. https://doi.org/10.19206/CE-141358

[10] Kamińska M, Kołodziejek D, Szymlet N, Fuć P, Grzeszczyk R. Measurement of rail vehicles exhaust emissions. Combustion Engines. 2022;189(2):10-17. https://doi.org/10.19206/CE-142526

[11] Kozak M, Merkisz J, Bielaczyc P, Szczotka A. The influence of oxygenated diesel fuels on a diesel vehicle PM/NO_x emission trade-off. SAE Technical Paper 2009-01-2696. 2009. https://doi.org/10.4271/2009-01-2696

[12] Kozak M, Merkisz J. Oxygenated diesel fuels and their effect on PM emissions. Applied Sciences. 2022;12:7709. https://doi.org/10.3390/app12157709

[13] Kurc B, Pigłowska M, Rymaniak Ł, Fuć P. Modern nanocomposites and hybrids as electrode materials used in energy carriers. Nanomaterials. 2021;11:538. https://doi.org/10.3390/nano11020538

[14] Lamba P, Singh P, Singh P, Singh P, Bharti, Kumar A et al. Recent advancements in supercapacitors based on different electrode materials: classifications, synthesis methods and comparative performance. Journal of Energy Storage. 2022;48:103871. https://doi.org/10.1016/j.est.2021.103871

[15] Lisowski M, Gołębiewski W, Prajwowski K, Danilecki K, Radwan M. Modeling the fuel consumption by a HEV vehicle – a case study. Combustion Engines. 2023;193(2):71-83. https://doi.org/10.19206/CE-157112

[16] MAN Truck & Bus. https://www.mantruckandbus.com (accessed on 05.2023).

[17] Merkisz J, Pielecha I, Andrzejewski M, Daszkiewicz P, Stawecki W. Legal conditions in the aspect of pollutant emissions from exhaust systems of rail vehicles engines. Journal of KONES. 2018;25(1):257-264. https://doi.org/10.5604/01.3001.0012.2475

[18] Pielecha I, Dimitrov R, Mihaylov V. Energy flow analysis based on a simulated drive of a hybrid locomotive powered by fuel cells. Rail Vehicles/Pojazdy Szynowe. 2022;(1-2):68-76. https://doi.org/10.53502/RAIL-152703

[19] Pietrzkiewicz H, Domagała R, Michalak P. Application of locomotive dual mode type 111DE for intermodal transport. Research and Technical Papers of Polish Association for Transportation Engineers in Cracow. Series: Proceedings. 2021;2(123):305-314.

[20] Saft LP 28MTi Rechargeable LTO PHEV-2 cell data sheet, Saft, 22024-1019-2, 2019.

[21] Shirres D, Baxter J. The future for hydrogen trains in the UK. 2019. https://www.imeche.org/policy-and-press/reports/detail/the-future-for-hydrogen-trains-in-the-uk (accessed on 06.2023)

[22] Siwiec J. Application of hydrogen fuel cells in railway transport. Railway Reports. 2021;190:53-57. https://doi.org/10.36137/1906P

[23] Sustainable power that matters. https://www.mtu-solutions.com (accessed on 05.2023).

[24] The Railway Technical Website. http://www.railway-technical.com/_Media/diesel-loco-block-diagram_m_med_hr.png (accessed on 05.2023).

[25] Xia S, Wu X, Zhang Z, Cui Y, Liu W. Practical challenges and future perspectives of all-solid-state lithium-metal batteries. Chem. 2019;5(4):753-785. https://doi.org/10.1016/j.chempr.2018.11.013

[26] Zurich Instruments. https://www.zhinst.com/europe/en/blogs/using-mfia-impedance-analyzer-characterize-esr-super-capacitor (accessed on 05.2023).

Paweł Daszkiewicz, DEng. – Faculty of Civil and Transport Engineering, Poznan University of Technology, Poland.
e-mail: *pawel.daszkiewicz@put.poznan.pl*

Daniel Kołodziejek, MEng. – Institute of Railway Transportation, Poznan, Poland.
e-mail: *daniel.kolodziejek@itstech.pl*

Article citation info:
Bober B, Andrych-Zalewska M, Boguś P. Influence of exhaust manifold modification on engine power. Combustion Engines. 2024;196(1):54-65. https://doi.org/10.19206/CE-171389

Bartosz BOBER
Monika ANDRYCH-ZALEWSKA
Piotr BOGUŚ

Combustion Engines
Polish Scientific Society of Combustion Engines

Influence of exhaust manifold modification on engine power

ARTICLE INFO

Received: 20 April 2023
Revised: 5 June 2023
Accepted: 19 August 2023
Available online: 7 September 2023

The article deals with the subject of the impact of an exhaust system on the power of the internal combustion engine. In particular the article shows the possibility of increasing the power of the gasoline drive unit, interfering only with an exhaust system. The purpose of the tests carried out is to compare the results of measurements from the chassis dynamometer before and after the modification, and additionally to perform simulations for the key parts of the system in terms of shaping the power and torque curves. The analysis includes a simulation model of the exhaust gas flow through the serial manifold and also the sport manifold, especially the pressure distribution and the course of the velocity vectors at the characteristic points of the element. Before obtaining the final results of power measurements on the sport units, the roughness of the steel from which the collectors were made was also measured. The final stage is the measurement of power on the new exhaust system. The obtained results of power measurements and simulations were presented in the form of a summary, which focused on the impact of individual fluid mechanics phenomena on the formation of power and torque curves and detailed the advantage of the new exhaust system in comparison with the factory system in terms of increasing the performance of the tested vehicle.

Key words: *exhaust manifold, engines, CFD*

1. Introductions

The constructions of internal combustion engines commonly used in the automotive industry consist of many interdependent systems that affect the final use of the vehicle. Taking into account the internal combustion engine, through power transmission systems, braking systems, suspension systems, steering systems, or exhaust systems discussed in more detail in this work. So many systems involved in the conversion of thermal energy into mechanical energy contribute to the formation of a significant number of potential energy loss centers and thus give an opportunity for optimization of individual systems in order to increase the performance of the entire vehicle [7].

The impact of the exhaust system on the engine's operating indicators is an aspect that, along with the development of the automotive industry, has become particularly important in terms of optimizing vehicle performance. This significantly complicated the stage of designing the exhaust systems, because it has a decisive impact on the efficiency of exhaust gas removal, which ultimately translates into the nature of the torque curve as a function of engine speed. Initially, this condition was somewhat inconsistent with maintaining normative noise levels (acoustic silencers effectively inhibited the flow of exhaust gases, which led to their less effective removal and thus to a reduction in the power generated by the engine). Over some time, the interest started to focus on finding a compromise between noise suppression and maximizing vehicle performance, which was, among other, the reason for the creation of various silencer designs. In a situation where, however, we focus on increasing the performance itself, expanding and separating dampers should be used. This solution ensures free expansion of the gas (reducing the energy of the sound wave) and thus by separating the flue gas column by a bundle of parallel pipes with small cross-sections will help to avoid too much throttling of the flow (very advantageous in terms of increasing power). As a result of such a solution, we will not disturb the effective exhaust gas flow and ensure sufficient damping [12, 13].

However, the sound pressure generated in the exhaust system can be used to maximize engine performance. After opening the exhaust valve, the exhaust gases coming out of the combustion chamber will generate the so-called "reflection" of pressure pulses. The returning vacuum wave flowing into the cylinder while a piston approaches the bottom dead center (intake valve opening) will purge the chamber of exhaust gas and accelerate the intake cycle at the same time. The choice of the co-opening stage of the valve will result in more effective filling of the cylinder and almost complete exhaust gas removal. However, this may result in some unburned mixture entering the exhaust pipe, which will certainly increase fuel consumption. This phenomenon is commonly used in sports cars, where they are additionally equipped with structurally matched camshafts, which are to ensure the extension of the valve co-opening interval and thus increase the probability that the negative vacuum wave will ensure more effective cylinder filling [12–14].

2. Literature review

Exhaust manifolds collect exhaust gases from the engine cylinders and release them into the atmosphere through the exhaust system. Engine efficiency and combustion characteristics depend on the method of exhaust gas removal from the cylinder. The design of the exhaust manifold for an internal combustion engine depends on many parameters, such as. exhaust back pressure, exhaust velocity, etc. [11] The exhaust manifold affects emission efficiency and fuel economy, which is why its proper sizing is so important.

The authors of the publication [18] designed the original and modified X-shaped system model using Catia software and then analyzed them using CFD software in terms of

flow velocities and temperature distribution in the exhaust gas models. The best modification was determined.

The subject of manifold modifications was also addressed in the publication [4], where the exhaust manifold was redesigned by determining the thermal stresses and deflections occurring under various working conditions with different materials and temperatures. The article aimed to ensure the suitability of the design for a specific material from the point of view of reliability and usability. Existing multiple defects include cracks that typically occur due to prolonged exposure to temperature extremes, casting defects, and repeated thermal cycling. Weld areas and curved profiles are critical failure areas. A methodology has been developed to ensure the best adaptation of the structure and material to the given working conditions. The different behavior of cast iron was analyzed. By redesigning the curved profiles, the impact of fumes on the welds can be reduced. Creo 3.0 software was used to prepare the CAD model of the 4–1 exhaust manifold.

In the investigations [3], the operation of the exhaust manifold of a four-stroke four-cylinder gasoline engine when using three types of fuel (gasoline, methane and methanol) was analyzed to estimate the characteristics of flow and back pressure. Modeling is done in Fluent 18.0, followed by analysis and meshing in ANSYS. Velocity, pressure and temperature profiles were run at an engine speed of 1000 rpm. It was found that methanol provided the highest exit temperature and back pressure, while methane provided the lowest exit pressure. Back pressure decreased while using gasoline. Methane resulted in the best exhaust manifold performance.

The design geometry of the exhaust manifold plays an important role in the smooth combustion and emission reduction of a gasoline engine. In the publication [24], by analyzing and comparing the exhaust back pressures and their speeds of different types of manifold models selected for different engine operating load conditions, the best model 5 exhaust manifold was found and its use in a multipurpose cylinder engine was for engine emission control and environmental protection recommended. The analysis is carried out with a virtual manifold model. The modeling and analysis of the exhaust manifold is done with the software CATIA v5 and ANSYS.

The article [21] discusses the challenges associated with the transformation of the existing multi-cylinder diesel breather system into an innovative monolithic collector model. Reaction gases after cleaning car engines are increasingly used for the benefit of environmental quality, especially in a large metropolitan area of the country, using exhaust systems to eliminate their main pollutants. A well-conditioned exhaust system increases engine performance. The efficiency of the collector has a significant impact on the performance of the engine. With the accelerated development of modern technologies and numerical methods, computer simulation has become a valuable method for research and development of fluid flow systems. Industrial CFD software was used to analyze the exhaust manifold system. In order to expand the basic understanding of diverse processes, extensive knowledge about the distribution of flow and heat transfer properties was gained. Calculations were performed to examine the parametric effect of operating conditions and mathematics on manifold exposure. Suggestions were made to improve the complex plan and execution.

The aim of the work [15] is to analyze the operation of the engine exhaust manifold. This is because the engine's exhaust manifold is a key factor in engine performance. In this work, the distributor design is created with CAD software and analyzed with ANSYS. This CFD analysis and thermal analysis were also performed to verify the performance of the redesigned exhaust manifold. The purpose of the CFD simulations carried out is to investigate the behavior of the volumetric exhaust gas efficiency.

The article [11] presents the latest research [5, 8–10, 22, 23, 25] on exhaust manifold design, evaluation of its operation with experimental methods, and collection and discussion of numerical methods (CFD), different geometry types of exhaust manifolds and their impact on performance.

3. Research methodology

3.1. Research object

The object of research in the conducted experiment is a vehicle with a factory exhaust system, except for the end silencer, which was custom-made to the dimensions of factory exhaust pipes. The material from which the silencer was made is stainless steel 304. Due to the small impact of the final silencer itself on the power of the tested engine, we assume that the exhaust system before modification is fully serial. The vehicle was also modified in the form of replacing the engine with a unit with a larger capacity than the factory one. All transmission systems such as gearbox, propeller shaft, axle shafts and differential have remained unchanged. The factory exhaust manifold is shown in Fig. 1 and 2.

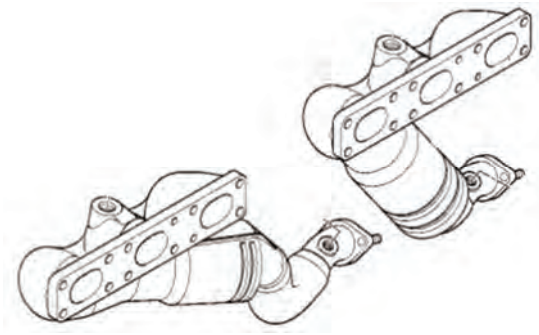

Fig. 1. Factory exhaust manifolds [19]

Fig. 2. Factory manifolds mounted on the engine

Table 1. Parameters of the tested vehicle

Stroke capacity [cm^3]	2979
Power* [HP]	231
Torque* [Nm]	300
Acceleration* 0–100 [km/h]	6.9
Yearbook	2003
Course [km]	290 000
Fuel consumption in the combined cycle* [l/100 km]	9.6
Fuel consumption in city driving* [l/100km]	13.4
Fuel consumption on the road* [l/100km]	7.3
*Parameters such as: power, torque, acceleration and fuel consumption are catalogue parameters presented by the manufacturer and due to the mileage of the vehicle they may differ from the actual measurement results from the dynamometer.	

3.2. Chassis dynamometer test bed

The power measurement was carried out on the MAHA LPS 3000 chassis dynamometer test bed at the Wroclaw University of Technology. The LPS 3000 consists of:

- communicating desktop with PC, monitor and mouse
- remote control
- roller set.

The dynamometer is equipped with a rotational speed sensor, an oil temperature sensor, an exhaust gas temperature sensor, a fan, and a junction box. The range of rotations that can be measured is: 0–10,000 rpm, with a measurement accuracy of 2%. Load simulation is carried out using an eddy current brake. The LPS 3000 test bad allows you to measure the power of petrol, gas and diesel engines. The use of an appropriate roller set and electronic system allows for measurements of 4-wheel drive vehicles. More detailed specifications of the research setup have been compiled in Table 2 [16].

Before the measurement, the tire pressure level in the vehicle was checked; all driving assistance systems (two-stage DSC system), and air conditioning were turned off and the maximum airflow was turned on to switch the cooling system into a circuit that included an additional fan. The view of the vehicle on the measuring stand is shown in Fig. 3.

Fig. 3. View of the test stand

Table 2. MAHA LPS 3000 specifications

	R50	R100/1	R100/2	R200/1	R200/2
Roller Set					
Length [mm]	1420	3345	4140	4550	2260
Width [mm]	1100	1100	1100	1100	1100
Height [mm]	505	520	520	570	800
Weight incl. packing	550 kg	1400 kg	1700 kg	2500 kg	2800 kg
Axle load	1.5 t	2.5 t	2.5 t	15 t	15 t
Roller length	220 mm	750 mm	750 mm	900 mm	900mm
Track min.		800 mm	800 mm	820 mm	950 mm
Track max.		2300 mm	2300 mm	2620 mm	2750 mm
Smallest testable wheel	12″	12″	12″	12″	12″
Roller diameter	318 mm	318 mm	318 mm	318 mm	318 mm
Roller axle separation	560 mm	540 mm	540 mm	565 mm	565 mm
Lifting Bar					
Pneumatic	min. 5 bar max. 8 bar	min. 5 bar max. 8 bar	min. 5 bar max. 8 bar		
Hydraulic				up to max. 40 bar	up to max. 40 bar
Electrical Data					
Eddy current brake	260 kW	260 kW	2 × 260 kW	2 × 260 kW	2 × 260 kW
Power supply	230 V/ 50 Hz	230 V/ 50 Hz	230 V/ 50 Hz	400 V/ 50 Hz	400 V/ 50 Hz
Fuse	16 A slow	16 A slow	35 A slow	35 A slow	63 A slow
Display Range					
Test speed	max. 300 km/h	max. 260 km/h	max. 260 km/h	max. 200 km/h	max. 200 km/h
Wheel power	max. 260 kW	max. 260 kW	max. 520 kW	max. 400 kW	max. 600 kW
Traction	max. 6 kN	max. 6 kN	max. 12 kN	max. 15 kN	max. 25 kN
Measurement accuracy	± 2%	± 2%	± 2%	± 2%	± 2%

4. Flow simulation

4.1. Serial collector

Due to the complexity of the calculations and the difficulty in measuring the entire system, the flow analysis will only include calculations for both collectors (before and after the modification). The model of the serial collector was made in the Autodesk Inventor environment (Fig. 4). The collector model has been simplified so that it contains only the nephralgic points of the structure. Autodesk Inventor is a high advanced software 3D to make projects of mechanical elements. The design was made in Inventor. The finished model was exported in the STEP format to the Ansys program, where exhaust gas flow simulations were performed.

Fig. 4. Model of serial collector (designed in Autodesk Inventor)

By comparing the prepared model with the actual geometry of the collector, it becomes evident that a catalyst is positioned just after the channel that connects all the outputs. However, owing to the complexity of calculations and the aim to solely highlight the impact of collector geometry on computational analysis, the catalyst was omitted. Moreover, the extension of the output channel was undertaken to stabilize simulation results upon exiting the connector. This research was grounded in a comparative analysis of two collector geometries, with the goal of elucidating the effects of geometric disparities on flow resistances, subsequently leading to losses in exhaust evacuation efficiency. In line with these premises and to simplify the factory collector model's design (excluding the catalyst's influence from the analysis), a section right after the convergence of the three channels was represented as a straight pipe. This decision stemmed from the area's limited influence on final analysis outcomes; primary flow losses occur where the pipes assume curvilinear shapes. The first step in the analysis was to determine the consistency of the model geometry. The program correctly read the converted format, so the next step was to generate the mesh. The purpose of the following analysis was to establish, in a comparative manner, the superiority of employing a sports collector over a factory collector. The CFD simulation was also rooted in a comparative study design, leading to the adoption of mesh size and quantity at consistent levels, which were justified by the substantial influence of mesh resolution on the study outcomes.

Consequently, mesh refinement was implemented in potentially significant regions for analysis (high accuracy meshing was applied to areas directly adjacent to pipe walls, where the flow of exhaust gases undergoes rapid changes in direction and velocity). These regions were categorized into a boundary layer and a central layer. Introducing excessive variability in mesh refinement would raise concerns about inaccuracies in results due to disparities between precise and less precise outcomes. This, in turn, could lead to a misconstrued interpretation of flow behavior, challenges in achieving a stable numerical equilibrium state, prolonging the simulation process, or even impeding its completion. Moreover, countermeasures were taken to mitigate turbulence and to preclude the program from autonomously interpolating unstable mesh regions.

In accordance with the aforementioned premises and the comparative nature of the entire study, boundary conditions were established.

The parameterization was carried out automatically, and in order to increase the accuracy on the boundary layer, the "Inflation" function was used (parameters are shown in Table 3), which allows you to create a zone of directional compaction on the selected volume [1, 2, 7, 17]. The compaction value was defined by determining the height of the first layer, which was 0.0001 m, the rest of the value was left unchanged. The grid of the collector model is shown in Fig. 5. The determination of ultimate parameters was preceded by iteratively conducting simulations for different values. The selection rationale was grounded in the program's relatively modest computational demand and the satisfactory precision of research findings.

Table 3. Assumed parameter values in the "Inflation" function

Scope	
Scoping method	Geometry selection
Geometry	1 body
Definition	
Suppressed	No
Boundary scoping method	Geometry selection
Boundary	13 faces
Inflation option	First layer thickness
First layer height	0.001 m
Maximum layers	5
Growth rate	1.2
Inflation algorithm	Pre

Fig. 5. Grid of the serial collector model

The next stage of the simulation is to determine the boundary conditions that will simplistically represent the tested flow. The nature of the flue gases leaving the combustion chamber and the geometry of the collector affect the lack of identity between the parameters of individual gas molecules, so the computational model assumes the presence of turbulent flow [1]. The material from which the serial collector was made is not known, and the simulation itself concerns the influence of geometry at the given input parameters, therefore the material of the model is steel, while the substance that will imitate the fuel combustion product is air. The next stage of determining the boundary conditions was to determine the places of inlet and outlet of the gas stream by assigning an appropriate function to the previously named walls. The purpose of the following analysis was to establish, in a comparative manner, the superiority of employing a sports collector over a factory collector. As a result, computations were carried out under uniform conditions. The selection of the inlet gas velocity was set at 200 m/s, and its value does not reflect the actual gas emanating from the engine chamber. Nevertheless, the order of magnitude closely approximates the existing conditions in internal combustion engines. The calculations were carried out for the number of iterations equal to 200.

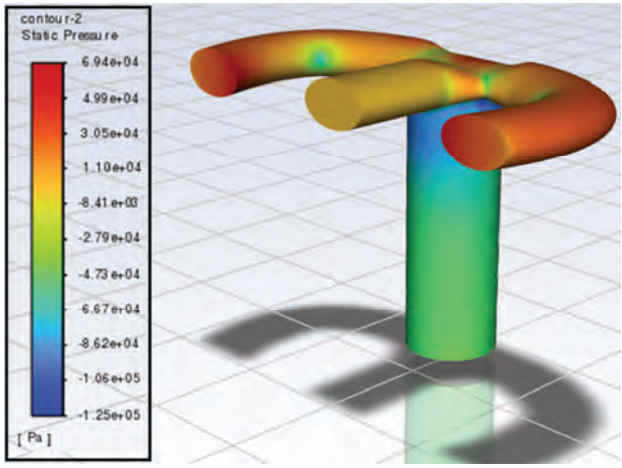

Fig. 6. Pressure distribution on the manifold walls

The simulation result, shown above, presents the distribution of pressure exerted on the manifold walls by the flowing gas stream. The geometry of the collector contributes to a significant variation in the level of pressure values achieved. Considering the model as divided into two parts, we can specify the area in which the pipe channels led from the engine block allow the flow of exhaust gases in the horizontal plane and the area in which, after connecting the individual pipes, the flow takes place in the vertical plane. In the first area, the pressure inside the system builds up, the exhaust gases coming out of the exhaust valve, in the case of cylinders one and three or four and six, are forced by the geometry of the manifold to change the flow direction by 90 degrees. Despite the gentle rounding of the channels, these areas are the zones of the greatest gas pressure on the walls of the considered element and thus will be potential centers for generating the largest energy losses in the flow. Observing the second part of the conventional division of the collector model, where the flue gas again is forced to change the flow direction by the value of a right angle, and the individual channels merge into one pipe, one can notice a huge difference in the pressure inside. This is the area where the flow resistance will be lower, and such a high pressure drop will probably increase the efficiency of mixing streams from individual channels. The results of the simulation of pressure distribution on the walls of a standard collector are shown in Fig. 6.

4.2. Sports collector

The model of the sports manifold was also made in Autodesk Inventor, and then converted in the STEP format to Ansys 2022. In the case of the new system, the catalyst was a separate element, which is located further down, while the exhaust channel, as in the previous manifold, was extended. The collector model is shown in Fig. 7.

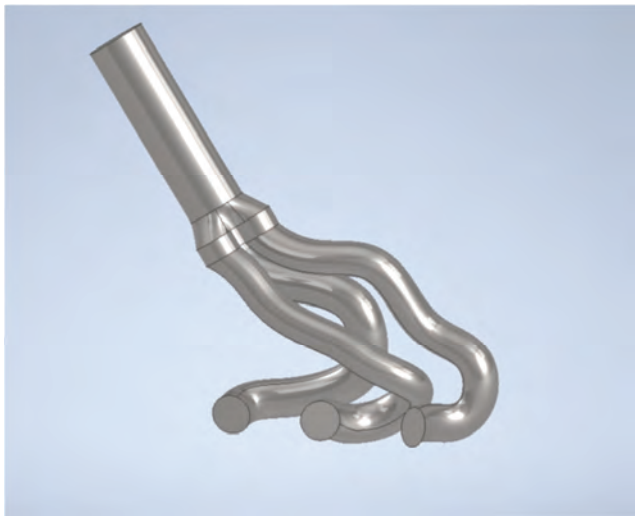

Fig. 7. Sport collector model (Autodesk Inventor)

The stage of creating the model mesh was the same as in the case of the serial collector, for the same values of the boundary layer density. The boundary conditions in this case also took into account the turbulent nature of the gas flow, the material was steel, while the inlet velocity was Vi = 200 m/s and was carried out by the adopted gas, i.e. air. The calculations were also carried out for the number of iterations of 200. The mesh model is shown in Fig. 8.

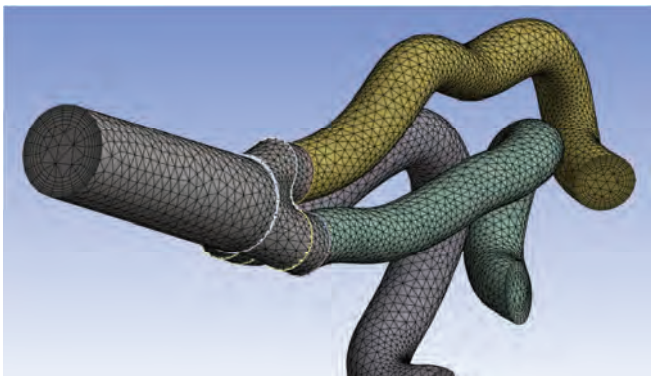

Fig. 8. Grid of the sports collector model

Figure 9 shows the local extremes in the pressure course on the considered geometry. It can be seen that the highest values occur right at the flue gas inlet to the collector, which is probably due to the shape of the pipe, which with its numerous bends is not conducive to free flue gas outflow. The main centers of maximum pressure are located on the outer walls of the bent pipe, where the flow of fluid as it exits the engine, in the direction normal to the outlet port, is reflected from the inside of the manifold, causing a sudden change in flow direction. Such a scenario results in a high pressure of the dynamically flowing exhaust gases on the pipe wall and thus generates an increase in flow resistance. The focus of the maximum pressure in the model will probably also be the place of maximum resistance in the outflow of exhaust gases from the engine.

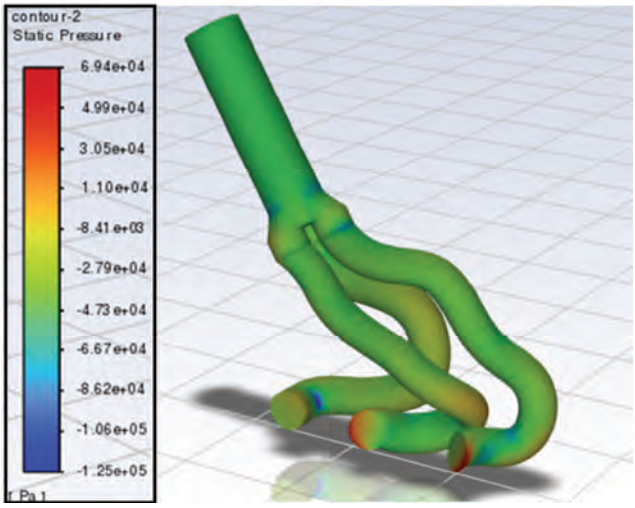

Fig. 9. Distribution of pressures on the collector walls and flow velocity in the sports collector

5. Roughness analysis

In order to check and compare the surface of steel from which the individual systems are made, the roughness measurement of material samples from the factory manifold and the sports manifold was carried out. The examination was performed using the PHENOM X-PRO scanning microscope for 500–2000x magnification. Before the measurement, the samples of individual steels were thoroughly cleaned and degreased and then mounted on the appropriate test table. In order to increase the reliability of the test, the roughness was measured in three different areas and for five different reference lines in each area.

The carried out roughness measurements show a measurable degree of unevenness for both tested steels. The increased amount of unevenness of the inner surface of the steel pipe will directly translate into an increase in the resistance to movement of the flowing gas in the area of the boundary layer. It should be noted that the first steel sample was cut from a previously used factory manifold, so any contamination and wear from a previous use will affect the roughness.

The values of the R_a and R_z roughness parameters are given in μm and are a kind of averaged roughness value. R_a differs from R_z in the method of measuring and calculating the parameter value. Taking into account the profile as the function y on mean line distance x R_a parameter is define as

$$R_a = \frac{1}{l}\int_A^B |y|dz \approx \frac{1}{n}\sum_{i=1}^{n}|y_i| \quad (1)$$

and describes arithmetic mean of absolute values of deviation between observed profile and mean line on the elementary interval in l length (in practice this is calculated as the sum absolute values of successive values of profile y_i in l length). In turn R_z parameter is define as

$$R_z = \frac{1}{5}\left(\sum_{i=1}^{5}|y_{pi}| + \sum_{i=1}^{5}|y_{vi}|\right) \quad (2)$$

and describes arithmetic mean of absolute values of five highest altitudes and five lowest valleys heights of observed roughness profile on the elementary interval in l length.

The higher the value of the parameter, the greater the roughness (larger scratches and surface irregularities). If $R_a > 12.5$, the surface is considered to have high roughness, R_a between 10 and 1.25 is medium roughness, and $R_a < 1.25$ is low roughness (high surface smoothness). The mirror-look steel surface is R_a less than 0.2 [6].

The test result effectively details the advantage of the steel used for the production of the sports manifold, where, according to the R_a parameter, the average roughness of the second steel is lower by 3.26 μm, while in relation to the R_z parameter, this difference will be as much as 11 μm. Differences in roughness values for individual coefficients result from the nature of their determination. To determine the degree of unevenness according to the R_a parameter, the values of deviations on the section specified by Polish standards are read, while to determine the degree of roughness R_z, the five largest elevations and five largest holes on the surface should be measured. A clear difference in the R_z values indicates a high amplitude of surface irregularities for the steel used for the serial collector.

The measurement results for the standard collector are shown in Fig. 10, 11 and in Table 4. The measurement results for the modified collector are shown in Fig. 12, 13 and in Table 5.

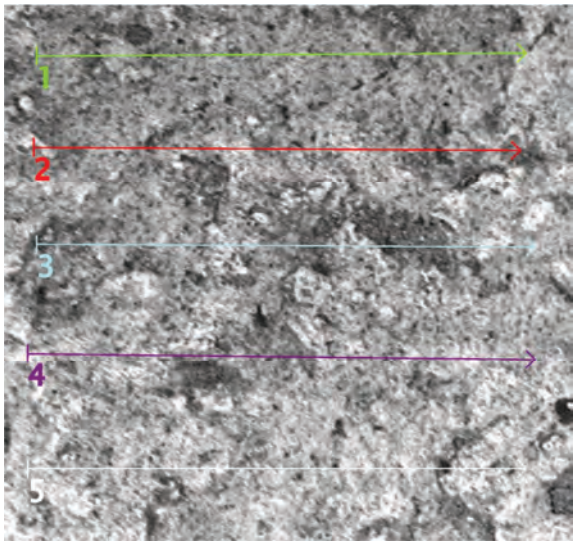

Fig. 10. Surface of a steel sample from a serial collector (2D)

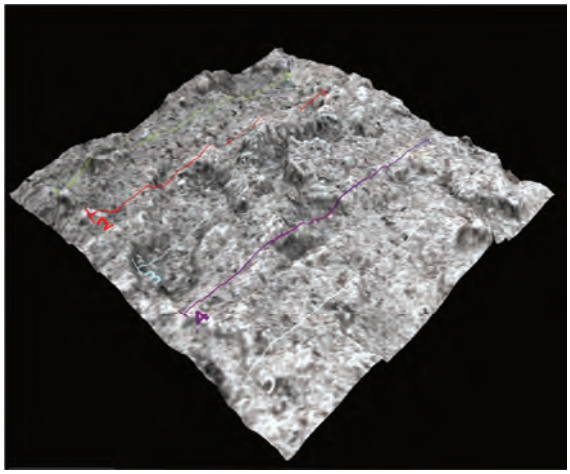

Fig. 11. Surface of a steel sample from a serial collector (3D)

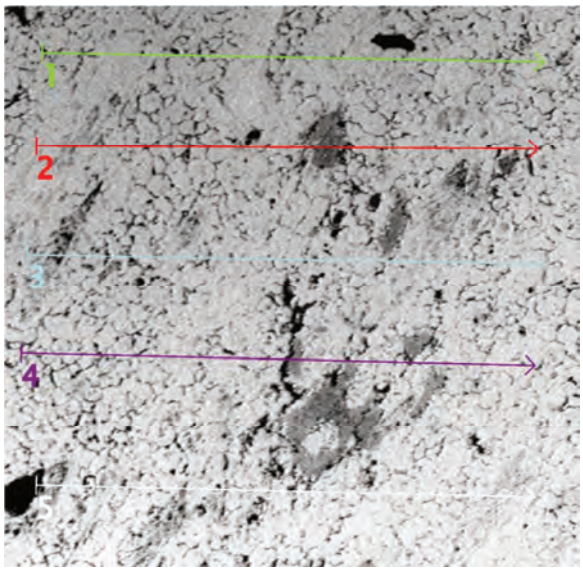

Fig. 12. Surface of a steel sample from a sports collector (2D)

Table 4. Roughness measurement results (series collector)

Area no	Measurement no	R_z [µm]	R_a [µm]
I	1	23.96	14.50
	2	24.63	12.00
	3	33.18	15.67
	4	16.25	8.21
	5	20.85	9.25
II	1	21.73	10.37
	2	24.27	7.76
	3	26.55	11.26
	4	18.77	8.43
	5	16.23	9.81
II	1	20.20	7.40
	2	23.95	18.24
	3	14.72	5.47
	4	11.29	5.00
	5	9.96	4.32
Mean value [µm]		20.44	9.85

An unique proof of the influence of roughness on flow resistance will be an analysis in which two identical pipes are put together, for which the boundary conditions of the flow will be the same, but will differ in the roughness of the inner surface. Figures 15 and 16 show the simulation results for pipes with a diameter of 49.4 mm and a length of 500 mm. The grid parameterization was carried out for the values used in the previous simulation of the collectors. The material used is steel with the average R_z value of both cases, determined based on the conducted microscopic measurements. The calculations were made for the input velocity Vi = 200 m/s and the number of iterations equal to 1000. The pressure distribution for a pipe with a roughness of R_z = 20.44 µm is shown in Fig. 14. The pressure differences for this case are shown in Fig. 15. The pressure distribution for a pipe with roughness R_z = 9.44 µm are shown in Fig. 16. Pressure differences for this case are shown in Fig. 17.

Table 5. Roughness measurement results (sports collector)

Area no	Measurment no	R_z [µm]	R_a [µm]
I	1	12.73	7.65
	2	14.99	7.99
	3	7.93	4.23
	4	6.51	4.45
	5	6.32	4.58
II	1	9.69	4.07
	2	6.32	5.68
	3	8.58	4.90
	4	6.70	2.86
	5	6.53	6.71
II	1	11.45	3.63
	2	14.18	15.08
	3	7.41	9.13
	4	11.35	9.71
	5	10.94	8.17
Mean value [µm]		9.44	6.59

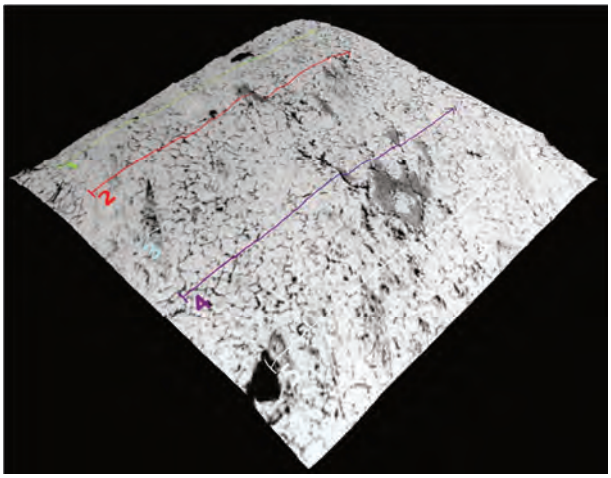

Fig. 13. Surface of a steel sample from a sports collector (3D)

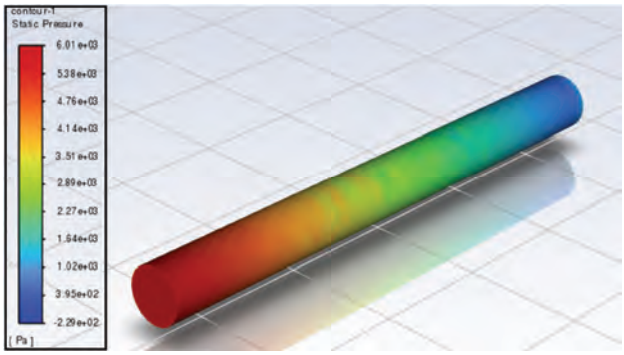

Fig. 14. Pressure distribution in a pipe with roughness R_z = 20.44 µm

Area-Weighted Average Static Pressure	[Pa]
(inlet)	5709.2167
(outlet)	476.26152
Net	3092.7391

Fig. 15. Differential pressure at the inlet and outlet (R_z = 20.44 μm)

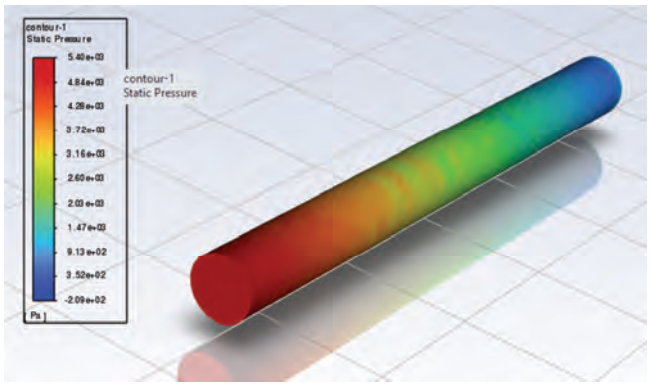

Fig. 16. Pressure distribution in a pipe with roughness R_z = 9.44 μm

Area-Weighted Average Static Pressure	[Pa]
(inlet)	5099.9846
(outlet)	471.78094
Net	2785.8828

Fig. 17. Differential pressure at the inlet and outlet (R_z = 9.44 μm)

Comparing the calculation results for both pipes, we can observe the pressure difference at the inlet and outlet of the pipe. In the case of a pipe with a greater roughness, the pressure drop between the beginning and the end of the pipe is 5233 Pa, while in the case of the second pipe this value is 4628 Pa. The summary shows the influence of surface irregularities on flow resistance, which in the analysis, where the only lack of identity between the parameters is roughness, will be manifested in the pressure drop along the length of the pipe.

6. Modification of the exhaust system

Compared with the standard equipment, the system was almost completely modified, starting with the replacement of collectors (Fig. 18), and the replacement of catalysts (Fig. 19), which, in combination with the previously mentioned collectors, are to guarantee the increases declared by the manufacturer. Going further in the system, the pipes are joined in the shape of the letter "X" (Fig. 20), which is to ensure effective pressure equalization between the two columns of flowing flue gases. At the very end of the system there is a final silencer, which has not changed. The selected design solutions resulted in the removal of two middle silencers, which will certainly increase the noise level but should also be used to reduce flow resistance. The view of the entire exhaust system is shown in Fig. 21.

Fig. 18. Sports collectors used in the tested object [20]

Fig. 19. Sports catalysts used in the test object [20]

Fig. 20. X-pipe connector

Fig. 21. The entire exhaust system after modification

7. Measurement results

7.1. Testing on a dynamometer before modifications

The first measurement was carried out on gasoline fuel. The measurement results show the curve of engine power, wheel power, torque and power losses. The left vertical axis shows the engine power value. The torque value is on the right vertical axis.

The horizontal axis shows the scale of the engine rotational speed. As you can see in the graph, there are two curves corresponding to the power curve – no. 1 (engine power) and no. 2 (wheel power), the former shows the power generated by the engine, while the second shows the power that the vehicle has in terms of ratio to the wheels, i.e. it takes into account the losses generated by the drive train. The measurement of losses is possible thanks to the dynamometer algorithm, which, after measuring the power on the wheels, is able to take into account the losses generated by the transmission system and convert them into the final result of the power on the engine. In practice, the reading of losses consists in pressing the clutch pedal, after accelerating the engine to the maximum value, which results in disconnecting the gearbox from the shaft of the drive unit. The result will be a reading of the operating characteristics of all drivetrain elements between the engine and the wheels of the vehicle. The loss curve is also shown on the chart (curve no. 3). The measurement results are shown in Fig. 22.

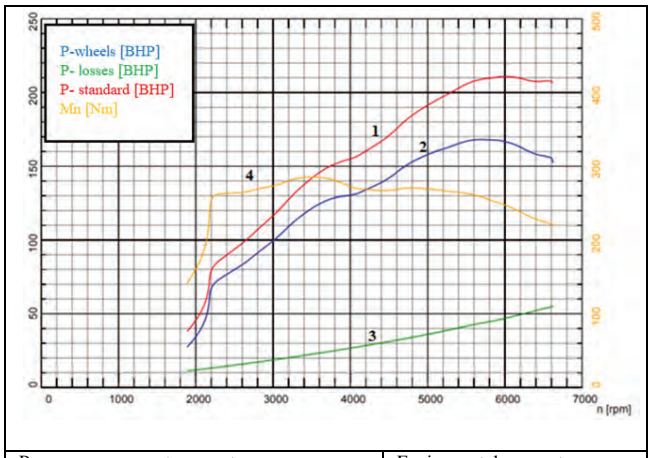

Power measurement parameters		Enviromental parameters	
1 Power according to standards	210.7 BHP/155.0 kW	Ambient temperature	24.0 °C
1 Power on engine	213.5 BHP/15.0 kW	temp. intake air	13.2 °C
2 Power on wheels	166.9 BHP/122.8 kW	Air humidity	55.0 %
3 Power loss	46.5 BHP/34.2 kW	Atmospheric pressure	1014.4 hPa
Maximum power at	5965 rpm/174.3 km/h	Steam pressure	16.4 hPa
4 Torque	285.2 Nm	Oil temperature	–
Maximum torque at	3525 rpm/103.0 km/h	Fuel temperature	–
Max. achieved rotational speed	6620 rpm/193.2 km/h		
[1)] Correlation by DIN 70020			
Correlation coefficient Q_v = 0%			

Fig. 22. Power characteristics of the engine with the factory exhaust system

The maximum power of the engine was 210.7 HP, which differs from the declared catalogue value of 231 HP by just over 20 HP, which translates into an approximately 8.7% decrease in power. This difference is probably due to the mileage of the vehicle, which is over 290,000 km. Before the measurement, the engine itself was partially regenerated – valve seals were replaced and the variable valve timing system (Vanos) was regenerated, while the sealing piston rings were left, which may be one of the reasons for the decrease in power. Torque peaks at 285.2 Nm at an engine speed of 3525 rpm and stays close to this value over a wide rev range, resulting in high engine flexibility between 2100 and 5000 rpm. Maintaining this rpm range will result in the most effective acceleration of the vehicle and the most efficient hill climbing. The maximum value of the torque declared by the manufacturer is 300 Nm, which in relation to the value generated by the tested vehicle gives a decrease of 5%. Comparing this value to the decrease in power, which is the product of torque and engine speed, with its highest value in the upper range of revolutions (i.e. 5965 rpm), it can be concluded that the losses caused by the vehicle mileage increase with the increase in engine speed. The engine operating at high load (high-speed range) due to the high pressure generated in the cylinder, creates favorable conditions for generating high losses caused by poor sealing of the combustion chamber, which in a way may be a good justification for earlier predictions of the reasons for power drops.

7.2. Testing on the dynamometer after modification

After modifications, the maximum engine power reached 231.9 HP for an engine speed of 5740 rpm. The torque curve, after exceeding 2050 rpm, remains close to the maximum level, while it reaches its peak at a rotational speed of 3475 rpm, for which it takes the value of 317.3 Nm. The torque characteristic illustrates the flexibility of the engine in which range it will most effectively accelerate and climb hills, this range starts at 2050 rpm and ends at 5000 rpm. After reaching this value, the curve assumes lower and lower torque values as the engine speed increases. The measurement results are shown in Fig. 23.

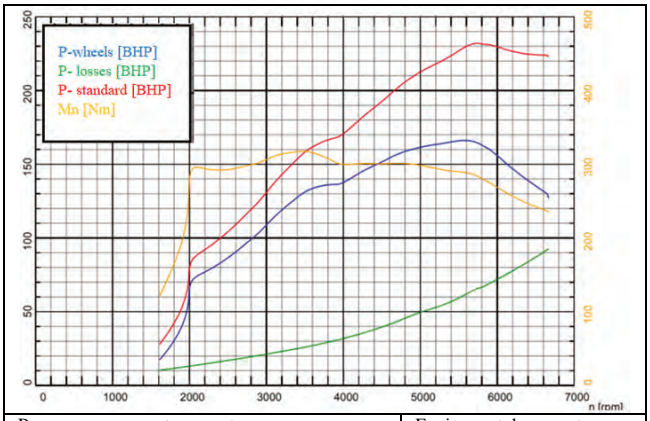

Power measurement parameters		Enviromental parameters	
Power according to standards	231.9 BHP/170.5 kW	Ambient temperature	22.7 °C
Power on engine	230.0 BHP/169.1 kW	temp. intake air	14.7 °C
Power on wheels	164.3 BHP/120.9 kW	Air humidity	28.2 %
Power loss	65.6 BHP/48.3 kW	Atmospheric pressure	995.6 hPa
Maximum power at	5740 rpm/199.7 km/h	Steam pressure	7.8 hPa
Torque	317.3 Nm	Oil temperature	–
Maximum torque at	3475 rpm/120.9 km/h	Fuel temperature	–
Max. achieved rotational speed	6665 rpm/231 km/h		
[1)] Correlation by DIN 70020			
Correlation coefficient Q_v = 0%			

Fig. 23. Engine power characteristics after modifications

7.3. Comparison of dyno measurements bed

Figure 24 shows a summary of the measurement results, before and after the modification, comparing both runs, an increase in the maximum values of engine power and torque can be seen. The power curve after the modification is almost uniform until it reaches around 3500 rpm. After exceeding this value, the power begins to take higher values for the same rotational speed as before replacing the exhaust system. Referring to the maximum values in both measurements – the power increased by 21.2 HP, which gives an increase of 10% of the power before the modification. Comparing the courses of the torque curves, it can be seen that above the value of 2250 rpm, the measurement made after the modification reaches higher torque values over all the graph. And the maximum value increased by 32 Nm and this way ensured an increase of 11%.

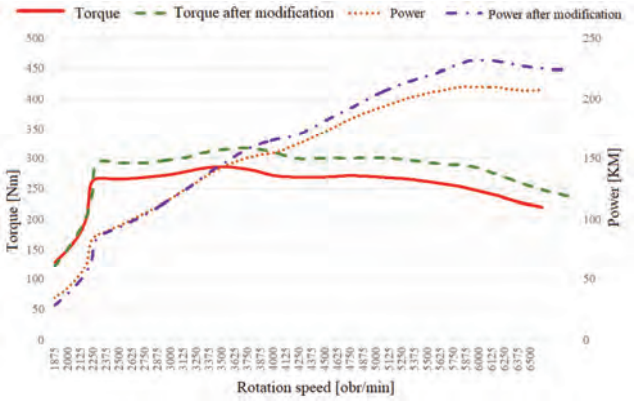

Fig. 24. Comparison of the results of both measurements

8. Conclusions

Comparing the computational models of both collectors, the first observation that comes to mind is the difference in pressure distribution. Exhaust gases flowing through the serial collector generate a very non uniform pressure distribution inside the ducts, while the sports collector outside individual zones is characterized by a stable level of gas pressure on the walls throughout its volume. Such a state of flow parameters will certainly be more advantageous, taking into account for example the uniformity of wear of individual fragments of the tested element. The analysis did not take into account the temperature distribution in individual sections, but local pressure increases can certainly increase the thermal impact, which may result in dangerous heating of the collector. High temperature on the uninsulated manifold can adversely affect the performance of the drive unit due to the lack of additional heat dissipation from the engine compartment. On the other side considering the effect of this phenomena, some benefits can be find in high temperature of the flue gases entering the catalyst, which will increase the efficiency of the reactor in the catalysis process. In the case of a sports manifold, the flowing exhaust gases will not influence on temperature inside the engine compartment, and the structure itself will be less strained due to the even distribution of forces in individual channels. The other expected benefit of the method of routing the pipes in the modified system, apart from the uniform distribution of stresses, will be the distance to which the channels coming out of the engine block are led out. This solution is rationally justified by the distribution of the energy of the escaping gas over a larger surface and the resulting discharge of excessive temperature outside the engine chamber. Considering condition of the surface of both collectors and its impact on the free flow of gas (referring to the roughness analysis), it can be concluded that the low roughness of the modified system and the stable pressure distribution will have a more beneficial effect on reducing the resistance to movement of the flowing exhaust gases, and thus their more effective discharge.

The measurement power after the modification successfully confirmed the hypothesis of the possibility of increasing engine performance by interfering with the exhaust system only. The comparison of both characteristics in one coordinate system shows the impact of modifications on the increments of operational parameters. A very satisfactory effect is the translation of the torque curve along the Y axis, what gives the possibility of having higher acceleration of the vehicle in the same engine speed range as before the modification. This modification is clearly felt during drive, especially when the gearbox is overvoltage in third gear, the vehicle has a very efficient acceleration ability in this respect. Analyzing the course of the power curve, it can be seen that after the modification it is almost the same, but after exceeding the barrier of about 3500 rpm, it takes on higher values. The increase in power can also be defined on the basis of the maximum engine speed achieved, for which the vehicle speed increased by 38.6 km/h. Changes in the achieved maximum parameters of the engine are most consistent with the increases declared by the manufacturer, probably in the case of a unit with a lower mileage and less wear of individual components, the impact of the modification would be even more effective, which would additionally confirm the effectiveness of the exhaust system used.

The comparison of individual construction solutions and the physical benefits resulting from them in relation to the unit measurement of output parameters is a very risky move. The study shows the change in the power and torque curve under the influence of modifications to the design of one engine with specific initial parameters. And it is difficult to systematize the reason of individual increases in a more universal nature. But based on the knowledge of people experienced in this field who had the opportunity to observe the impact of individual modifications on the formation of torque and power curves, one can attempt to correlate certain phenomena. One of them is the use of collectors with a higher flow capacity, which could increase the torque.

According to the opinion of experienced mechanic engineers, the result of such a change is having higher torque at an earlier stage of engine speed. The above statement is justified by the results of the tests, observing the course of the torque. It reaches values close to the maximum at 2200 rpm already, whereas before the modification such values could be observed for a rotational speed of about 3500 rpm. Potential correlations can also be found in the use of sports catalytic converters. Their metallic filling (providing less resistance) and a smaller number of channels guarantee better exhaust gas flows in comparison with classic catalyt-

ic reactors with ceramic filling, which concerning the engine's output parameters, are supposed to increase the maximum power. The measurement after the modification clearly indicates the possibility increasing the power by as much as 21 HP. But this merit should not be attributed only to this solution. The system was completed by one manufacturer who had previously calculated the efficiency of his set and probably the power increase would not have reached such values without interfering with the construction of the collector. The remaining parts of the system, despite occurrence of favorable physical phenomena during the exhaust gas flow, will have a rather marginal impact on the formation of the engine output parameters and can be classified as a complement to the effectively constructed system. Fragments of this type are used in the tested object: X-pipe type connector and pipes with relatively low roughness, made of 304 stainless steel. The effect of the modification, apart from increasing engine parameters, are also other usable aspects, such as increased noise emission. The vehicle was tested with unprofessional measuring equipment in the form of a mobile application, where the result before the replacement was 100 dB, and after the modification it reached the value of 112 dB. The reason for the increase in noise emissions was undoubtedly the removal of the center mufflers, which could also be a potential obstacle to maximizing the vehicle's performance.

Acknowledgements

The article was written in cooperation with Autocomp Management Sp. z o.o. from Szczecin, Research and Development Center – producer of simulators on the military and civilian market from Poland.

Nomenclature

BHP	brake horsepower
CFD	computational fluid dynamics
DSC	dynamic stability control
Ra	roughness average
Rz	mean roughness depth

Bibliography

[1] ANSYS. ANSYS-Fluent-Tutorial-Guide_r170.pdf.
[2] ANSYS. ANSYS Meshing User's Guide_r130.pdf. ANSYS 2013.
[3] Allawi MKA, Oudah MH, Mejbel M. Analysis of exhaust manifold of spark-ignition engine by using computational fluid dynamics (CFD). Journal of Mechanical Engineering Research and Developments. 2019;42(5). https://doi.org/10.26480/jmerd.05.2019.211.215
[4] Chandak A. Investigation and design modification in exhaust manifold. SSRN Electronic Journal. 2020:6. https://doi.org/10.2139/ssrn.3524751
[5] Cho K-S, Son K-B, Kim U-K. Design of exhaust manifold for pulse converters considering fatigue strength due to vibration. Journal of the Korean Society of Marine Engineering. 2013; 37(7):694-700. https://doi.org/10.5916/jkosme.2013.37.7.694
[6] Detailed drawing and dimensioning – auxiliary materials. Gdynia Maritime University. http://wm.umg.edu.pl/cwiczenia/grafika/oznaczanie_chropowatosci_materaily_pomocnicze.pdf
[7] FLUENT User's Guide. ANSYS 2013.
[8] Hessamedin N, Davood DG, Mofid G, Ghasem J, Mojtaba K. A parametric design of compact exhaust manifold junction in heavy duty diesel engine using computational fluid dynamics codes. Thermal Science. 2011;15(4):1023-1033. https://doi.org/10.2298/TSCI100417041N
[9] Han-Chi H, Hong-Wu H, Yi-Jie B. Optimization of intake and exhaust system for FSAE car based on orthogonal array testing. International Journal of Engineering and Technology. 2012;2(3). https://www.semanticscholar.org/paper/Optimization-of-Intake-and-Exhaust-System-for-FSAE-Han-chi-Hong-wu/7279378088fff0ad35490a4c904214449f67e65b
[10] Hasan JM, Mohammad WS, Mohamed TA, Alawee WH. CFD simulation for manifold with tapered longitudinal section. International Journal of Emerging Technology and Advanced Engineering. 2014;4(2):28-35. www.ijetae.com
[11] Kanawade N, Siras O. A literature review on exhaust manifold design. International Journal of Scientific Research Engineering & Technology. 2016;5(5). www.ijsret.org
[12] Kordziński C. Exhaust systems of high-speed internal combustion engines. WKL. Warsaw 1964.
[13] Kowalewski A. Exhaust systems. Construction, tasks, requirements; update date: 2016.10.21.
[14] Kordziński C. Increasing engine performance for cars and motorcycles. WKL. Warsaw 1964.
[15] Krishnara JC, Rajesh Ruban S, Subramani N. Analysis of exhaust manifold to improve the engine performance. International Journal of Engineering & Technology. 2018;7(2.8): 539-542. https://doi.org/10.14419/ijet.v7i2.8.10517
[16] LPS 3000 – chassis dynamometer. Original instructions for use BA052301-pl.
[17] Mączyński J. Fluid mechanics. National Scientific Publishing House. Warsaw 1966.
[18] Muchhetti M, Suman DS, Abhiman B, Madhukar S. Design and analysis of X shaped exhaust system operation using different types of profiles on high capacity vehicle. International Journal of Scientific Research in Science, Engineering and Technology. 2021;8(4):19-27. https://doi.org/10.32628/IJSRSET218411
[19] Parts catalog of original parts BMW. www.realoem.com/bmw (accessed on 17.04.2023).
[20] Schmiedmann online store. www.schmiedmann.com (accessed on 17.04.2023).
[21] Thangapandian P. Design and analysis of exhaust manifold for multicylinder diesel engine with monolith catalytic converter using CFD. International Journal of Applied Science and Engineering. 2022;19(1):1-9. https://doi.org/10.6703/IJASE.202203_19(1).003
[22] Umesh KS, Pravin VK, Rajagopal K. CFD analysis of exhaust manifold of multi-cylinder SI engine to determine optimal geometry for reducing emissions. International Journal of Automobile Engineering Research and Development. 2023;3(4):45-56. http://www.tjprc.org/publishpapers/--1380373503-5.%20CFD%20Analysis.full.pdf

[23] Usan M, Weck O, Whitney D. Exhaust system manifold development enhancement through multi-attribute system design optimization. AIAA 2005-2066. 46th AIAA/ASME/ASCE/AHS/ASC Structures, Structural Dynamics and Materials Conference. April 2005. https://doi.org/10.2514/6.2005-2066

[24] Venkatesan SP, Ganesan S, Devaraj R, Hemanandh J. Design and analysis of exhaust manifold of the spark ignition engine for emission reduction. International Journal of Ambient Energy. 2020;41(6):659-664. https://doi.org/10.1080/01430750.2018.1484811

[25] Zhang X, Luo Y, Wang J. Coupled thermo-fluid-solid analysis of engine exhaust manifold considering welding residual stresses. Transactions of JWRI, 2012:75-77. https://doi.org/10.18910/23075

Bartosz Bober, Eng. – Faculty of Mechanical Engineering, Wroclaw University of Science and Technology, Poland.
e-mail: *bartoszbober383@gmail.com*

Monika Andrych Zalewska, DEng. – Faculty of Mechanical Engineering, Wroclaw University of Science and Technology, Poland.
e-mail: *monika.andrych@pwr.edu.pl*

Piotr Boguś, DSc., DEng. – Head of Department of Physics and Biophysics of Medical University of Gdańsk, Poland.
e-mail: *piotr.bogus@gumed.edu.pl*

Article citation info:
Cieślik W, Mielcarzewicz D, Rawecki M. Reverse engineering as a modern methods of test bed modernization. Combustion Engines. 2024;196(1):66-72. https://doi.org/10.19206/CE-171521

Wojciech CIEŚLIK
Dawid MIELCARZEWICZ
Michal RAWECKI

Combustion Engines
Polish Scientific Society of Combustion Engines

Reverse engineering as a modern methods of test bed modernization

ARTICLE INFO

Received: 25 July 2023
Revised: 3 August 2023
Accepted: 23 August 2023
Available online: 25 August 2023

The main purpose of the work is to demonstrate the individual stages involved in the reverse engineering process by using a dynamometer equipped with a single-cylinder research engine AVL 5804 as an example. The project entails theoretical and practical aspects of measurements using 3D scanners. The Scantech KSCAN Magic hand-held optical scanner was used to obtain measurements of the geometry of the dynamometer. The CAD model was created in the Autodesk Inventor program, and its accuracy was verified by comparing it to the scan and generating a scale of deviations along with a color-coded representation of their size in the GOM Inspect program. The work was summarized with an example of upgrading the current stand based on a previously made design, which significantly shortened the process of modifying the intake system.

Key words: *modification of test benches, 3D laser scanning, research engine, intake system development, CAD modeling*

1. Introduction

The rapidly changing automotive market is forcing designers to integrate new technologies into vehicle construction. One of the primary reasons for this shift is the climate crisis caused by the harmful compounds emitted by internal combustion engines, mainly carbon dioxide. The concentration of CO_2 in the atmosphere is on the rise [10, 11], and it leads to an increase in the greenhouse effect. To address this issue, efforts have been made to enhance the efficiency of internal combustion engines. These include transitioning from multi-point injection to direct injection [7, 12], using variable valve timing systems [14, 21], engine rightsizing [9, 28], using exhaust after-treatment systems [18, 24], using exhaust gas recirculation [16, 27]. The current most developed direction of the powertrain evolution is the hybridization or electrification of drive systems [1, 4, 15, 17]. Previously mentioned trends are focused on lowering the fuel consumption of internal combustion engines and reducing CO_2 emissions. As a result of these innovations, the driving pattern of the vehicle is changing. To meet the challenges dictated by the automotive market, it is necessary to conduct tests on engine dynamometers as well as tests under actual RDE road conditions. Engine dynamometers ensure repeatable conditions during testing.

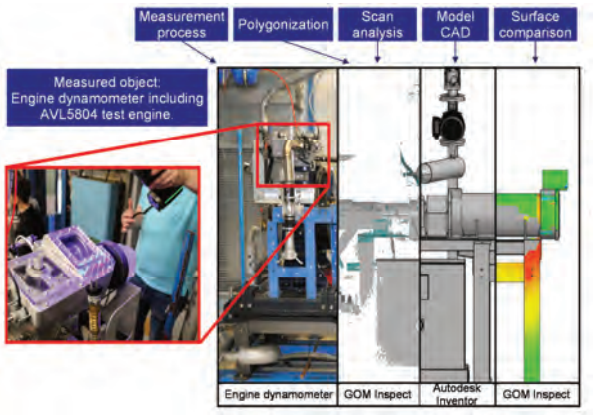

Fig. 1. Steps for obtaining a 3D model during scanning of a test bench

To accurately simulate operating conditions, test benches should be adjusted to current solutions, which require constant updates. Modifications of existing constructions create the need for careful planning of all related operations, which is why the CAD model can be useful. Through reverse engineering, it is possible to digitally recreate an existing object based on its physical form. While previous reverse engineering solutions have been focused on smaller-sized objects, it is now feasible to replicate significantly larger objects using laser scanners. The article presents the scanning process used to acquire a 3D model of an entire test bench (Fig. 1).

2. Object of study

The studying object is a dynamometer test bench with a single-cylinder research engine AVL 5804. This engine is located in the Institute of Combustion Engines and Powertrains at Poznan University of Technology. The dynamometer is used to simulate operating conditions for research purposes. The bench allows researchers to monitor the combustion process during engine operation.

The engine unit has a piston diameter of 85 mm and a stroke of 90 mm. Over the past few years, the research carried out at this test bench has focused on:

- using the ionization voltage signal to diagnose the combustion process of a spark ignition engine fueled with natural gas [8]
- assessing the impact of different CNG fueling methods on the stability of engine operation with a prechamber [26]
- research of new solutions for engine ignition systems and combustion of lean air-gas mixtures with the use of two-stage combustion systems [19, 20]
- investigating the potential of cold-flame-combustion while working with high Exhaust Gas Recirculation (EGR) rates [6].

The AVL 5804 engine was updated several times. Initially, it was a self-ignition engine with direct injection into the combustion chamber with a rotary distributor pump. Now engine has a common rail injection system with a spark TJI ignition which enables it to work with gas and

liquid fuels. Additionally, a variable valve timing system VVT-iE, which uses an electric motor to rotate the camshaft, has been added to the engine [3]. The engine head was modified to adjust for the variable camshaft phasing. In this case reverse engineering has been used. Optical scanning and computer tomography were used to create a project of the new cylinder head with VVT-iE. The external geometry of the engine head was measured using 3D scanning, while the internal structure data was acquired through tomography.

The reverse engineering process for the AVL 5804 engine head has been completed successfully. The knowledge acquired and documented during earlier tests will be used in the next process of reverse engineering, this time for the whole dynamometer bench. The dynamometer model was combined with the previously obtained cylinder head model to provide a complete model of the external dimensions of the research bench.

3. Measurement method

3.1. Selection of the measurement method

During creating a model of a dynamometer bench, it is crucial to know its external dimensions. For this purpose, it is necessary to select one of several measurement methods (Fig. 2). The dynamometer has complex geometry and is situated in a laboratory that restricts freedom of movement around it, therefore the non-contact optic method was opted for. There are various optical methods available, which can be divided into two types: passive and active methods [5, 23]. Passive scanners operate under natural light and therefore do not require an additional light source. Active scanners, on the other hand, need to be provided with an additional light source.

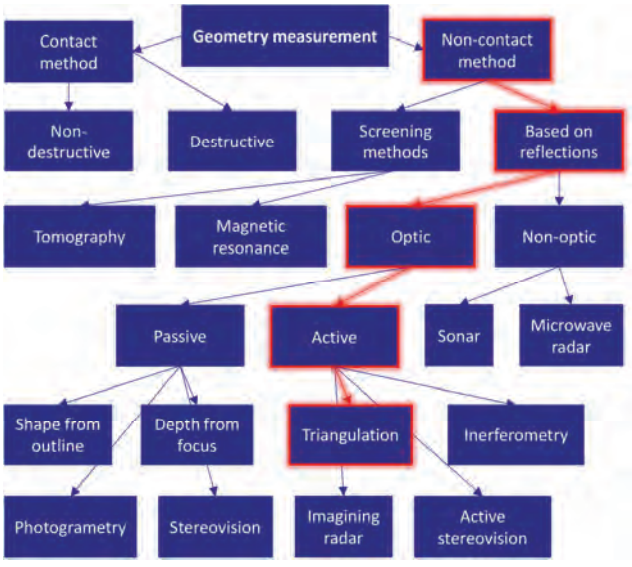

Fig. 2. Division of measurement methods along with an indication of the method used in the research (based on [5])

Passive methods include:
- photogrammetry
- shape from the outline
- depth from focus
- stereovision.

Active methods include:
- triangulation
- interferometry
- imaging radar
- active stereovision.

Due to the dynamometer's large size, limited space, and length of scanning process, only two methods were considered, photogrammetry and triangulation scanning.

Photogrammetry scanning works by processing multiple images of the surveyed object and accurately representing the geometric relationships between them [22]. Since the dynamometer bench is over two meters long, using photogrammetry would require taking numerous photos, which would be time-consuming. Moreover, there is not enough space in the laboratory to take pictures from every angle.

On the other hand, triangulation is a technique that uses the position and angles between a light source and recording devices to obtain geometry data (Fig. 3). A beam of light is sent at a suitable angle to the element under examination. The recorder captures the light reflected and distorted on the surface, sends the information back to the control unit, and the computer calculates the position of the surface [13]. Laser scanning has several advantages, including measurement speed (up to 1350000 measurements per second), high measuring accuracy (reaching up to 0.01 mm), and the ability to take measurements in confined spaces.

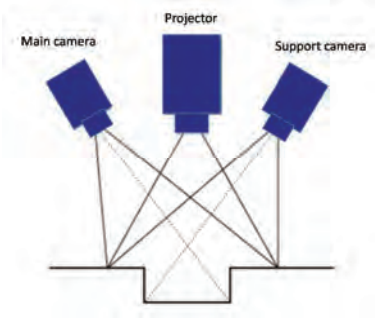

Fig. 3. The principle of triangulation [13]

For the reverse engineering of the dynamometer bench, a laser triangulation method was selected. This scanning process is presented in the following sections of the publication.

3.2. Scanning process

In order to carry out the research, a handheld scanner called Scantech KSCAN Magic was used (Fig. 4). The scanner is constructed with two cameras and a source of vision-safe blue laser. On the back of the scanner is located a control panel that enables the user to adjust the operating mode while scanning. Additionally, an LED bar on the housing indicates the correct positioning of the scanner in relation to the object. When the LED light is green, the scanner is at the correct distance. If the distance between the scanner and the object is too large or too small, the light turns red.

The scanner also offers a photogrammetry function. While working in photogrammetry mode, the Scantech KSCAN Magic collects coded points based on photos, and

then in reference to these coded points acquires geometric data using either blue laser light or infrared light. The scanner has four modes of operation (Fig. 5):

– fast: uses eleven blue laser crosses
– accurate: seven parallel blue laser lines
– deep holes: one blue laser beam
– large area: infrared light.

Fig. 4. Scantech KSCAN Magic construction [23]

The scanner uses a total of forty-one laser lines and takes measurements with an accuracy of 0.015 mm. The measuring speed of the scanner reaches 1350 points per second. Each mode of operation has its advantages and disadvantages, making scanning adjustable for different types of surfaces. For example, the eleven crossed blue laser lines are ideal for quickly measuring a big area, making it suitable for scanning large flat surfaces. Seven parallel laser lines are a perfect mode for scanning surfaces with different types of irregularities. A single line allows for scanning deep and difficult-to-reach pockets and holes. The infrared laser measurement is used for scanning large areas. The scanner also has a photogrammetry function for collecting reference points, which are used to decrease measurement error. During measurements, the scanner needs to be connected to a computer with suitable software.

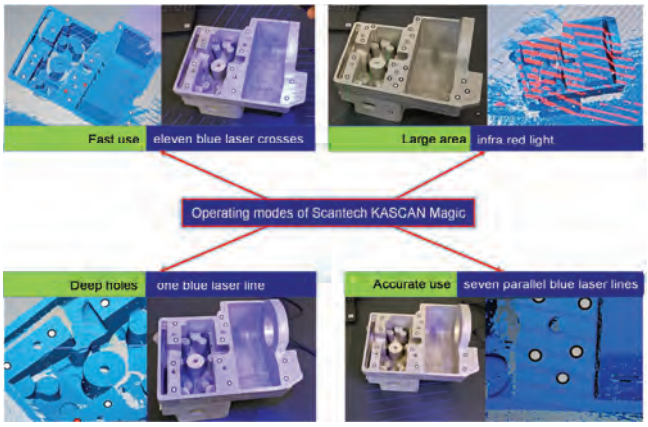

Fig. 5. Scantech KSCAN Magic modes

Before scanning, it is necessary to calibrate the scanner. To achieve this calibration plate must be scanned. The scanner measures the plates from different distances and angles. The computer monitor displays the actual position and positions where the scanner must be placed (Fig. 6).

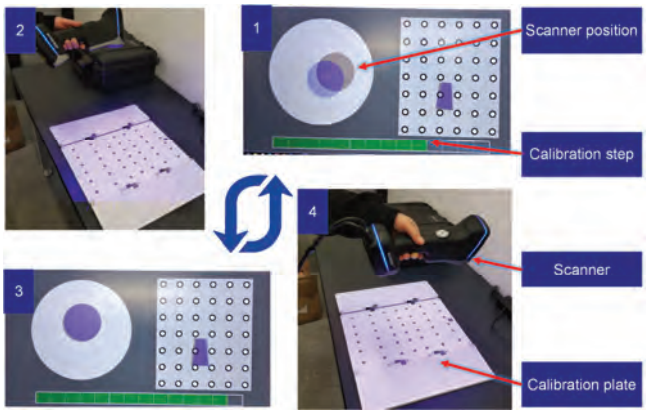

Fig. 6. Calibration process: 1 – the software indicates the angle and position in which to place the scanner, 2 – operator sets up the scanner, 3 – software indicates another angle and position to set up the scanner, 4 – operator repositions the scanner; the steps shown in the figure are per formed repetitively until the end of calibration process

The calibration process of the Scantech KSCAN Magic involves fourteen steps that must be followed. During the process, the scanner should be positioned towards the calibration plate at the angle and distance indicated by the software. A progress bar at the bottom of the screen shows the progress of the calibration. Once completed, the software will display a calibration deviation, which is usually in the range of 0.0048 mm to 0.0075 mm for the Scantech KSCAN Magic (Fig. 7).

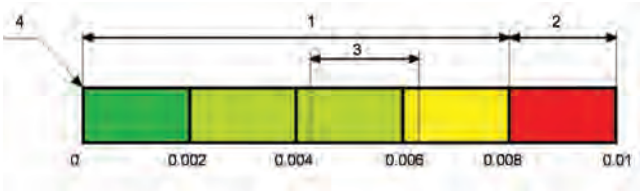

Fig. 7. Calibration deviations: 1 – acceptable deviation, 2 – unacceptable deviation, 3 – most frequent deviation, 4 – impossible to achieve deviation

Before measurement with the Scantech KSCAN Magic, it is important to properly set up the test bench. Since the scanner does not physically touch the measured component, it requires reference points to function accurately. In the measured area of the scanner must be placed at least three reference points. The reference points should be placed both on and around the object. Thanks to them scanner tracks the position of the component in space. The size of used reference points depends on the size of the object and the measurement area of the scanner. For example, points with an inner circle diameter of 1.5 mm are typically used for measuring areas of 320 mm × 320 mm, while larger areas require points with a diameter of 3 mm or 6 mm. However, using too many reference points can reduce measurement accuracy by approximating the geometry data at each point.

The next step is to scan the reference points so that the scanner would be able to accurately place data in three-dimensional space (Fig. 8).

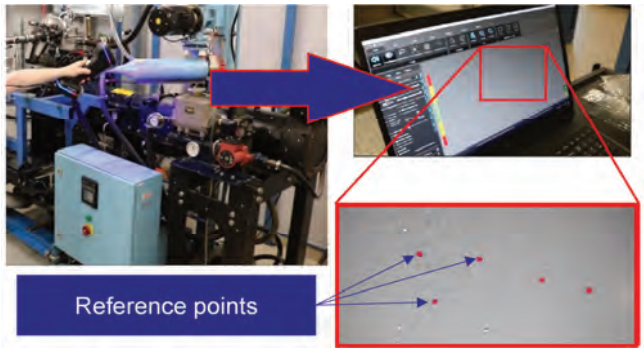

Fig. 8. Acquisition of reference points

After registering reference points, the scanner proceeds to acquire the geometry data. During the measurement process a fast triangulation mode with eleven crossed blue laser lines was used (Fig. 9). While measuring the scanner should move smoothly and steadily, gradually filling the point cloud with more data. The real-time preview allows the operator to see where data has not been collected properly and to return to those areas to gather more data. The final scan result was the acquisition of accurate data on the following systems:

– AVL 5804 engine
– shaft housing
– cooling system
– frame
– brake.

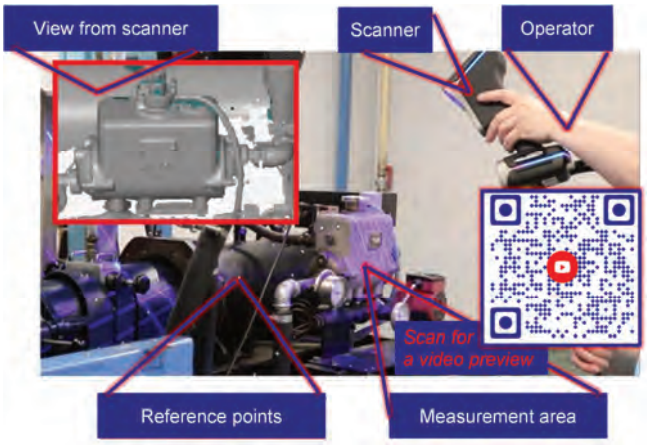

Fig. 9. Scanning process with eleven crosses blue line laser mode – to view a video of the scanning process use the QR code [25]

3.3. Model

After scanning and quality control of the acquired points cloud, the next step was polygonization. This process involves converting the cloud of points into a mesh [2] using specialized software and algorithms. During polygonization operator can only control a few parameters (Fig. 10) which are:

– optimization of the triangle mesh (max edges length)
– triangle mesh compaction (number of points)
– triangle mesh smoothing level (surface tolerance).

The measurement data file before the polygonization process was 895,100 KB (0.85 GB) in size and required considerable computing power for its analysis. The mesh thinning process performed reduced the file to a size of 177,771 KB, which is less than 20% of the original file size. This procedure makes it possible to work on the model on a computer with minimal hardware requirements for design software such as GOM Inspect or Autodesk Inventor. Such a large reduction in file volume was realized by increasing surface tolerances, reducing the number of measurement points by 80% and extending edge lengths. Depending on the design demand, the above treatments are justified or omitted.

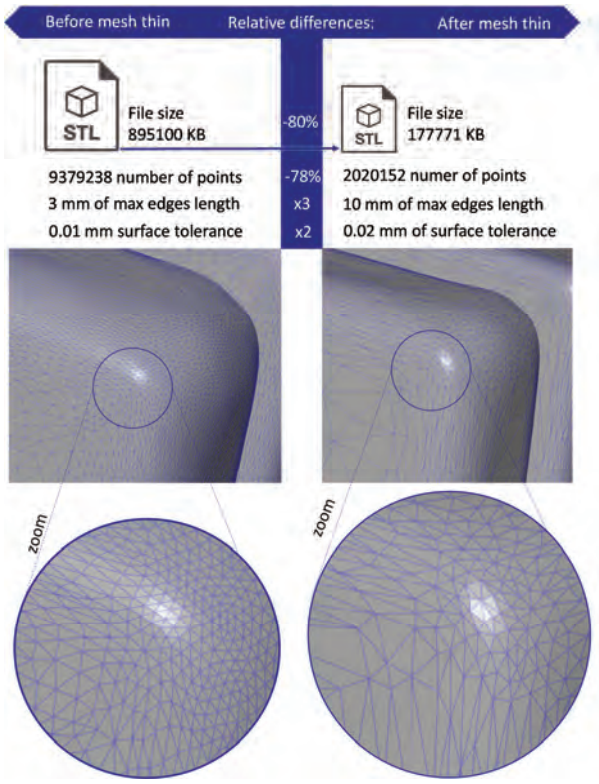

Fig. 10. Mesh before and after thin

The mesh file serves as a geometrical representation of external geometry, allowing reverse engineering to be made. The CAD model was created using Autodesk Inventor software, and the dimensions of the dynamometer bench were measured using the GOM Inspect program (Fig. 11).

This CAD model contains both internal engine structure and external information about the entire dynamometer bench. To obtain the external geometry of the bench, 3D scanning measurements were utilized, while 2D documentation was used to get knowledge about the engine's internal structure (Fig. 12).

The documentation did not contain any information regarding the modified engine head. Therefore, the previously created model of the cylinder head for the GasOn project at Poznań University of Technology was used to complete the CAD model of the bench. The first created component of the unit was the AVL 5804 engine, which includes a working crank-piston system. Next, the frame and brake were made. After the cooling system was reproduced.

Following that, a model of the control room was added to the 3D design. The dimensions of the control room were determined through traditional contact methods (Fig. 13).

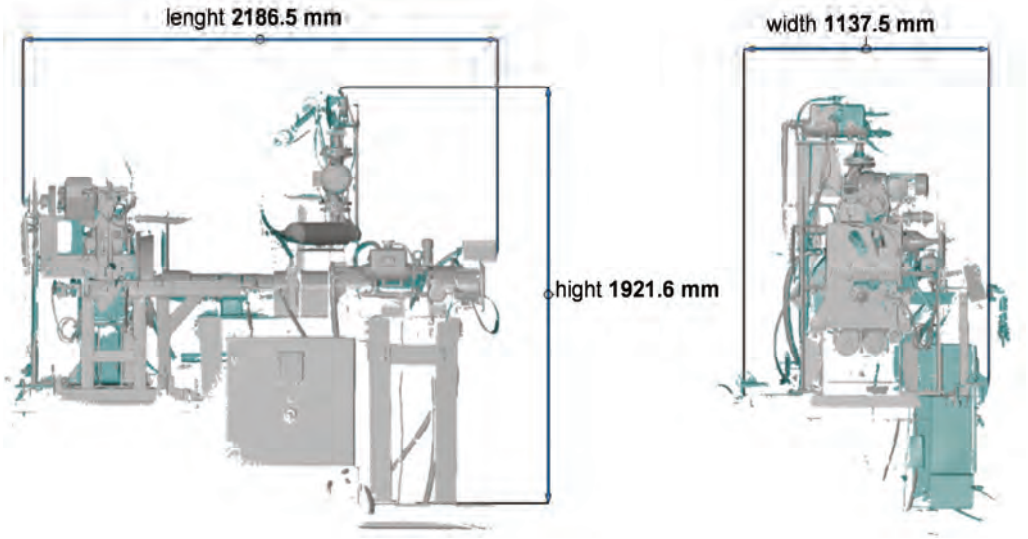

Fig. 11. External dimensions of dynamometer

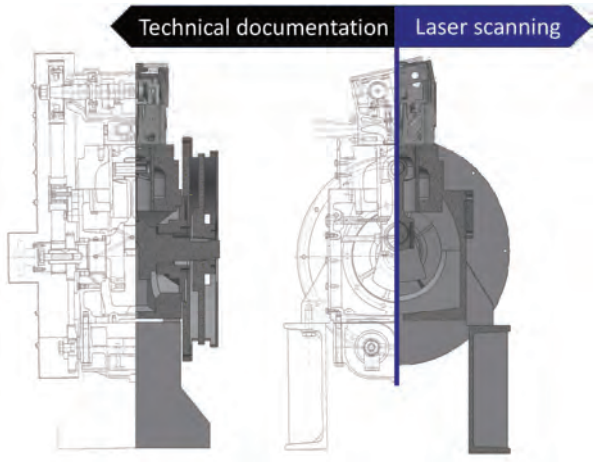

Fig. 12. Comparison of the completed CAD model with available manufacturer's technical documentation

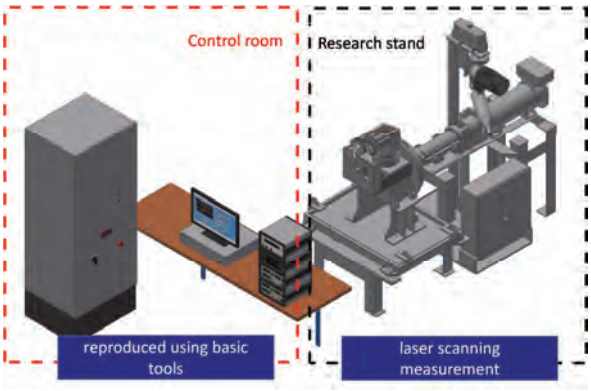

Fig. 13. View of the complete model of the engine dynamometer with the control room (control room made with basic measurement methods)

The performance section of the bench consists of four components: the engine, the frame, the brake and the oil cooling system. Each assembly was modeled separately before being combined together (Fig. 14). The oil and coolant pipes were not included in the model since there was insufficient data on their geometry collected during the scanning process.

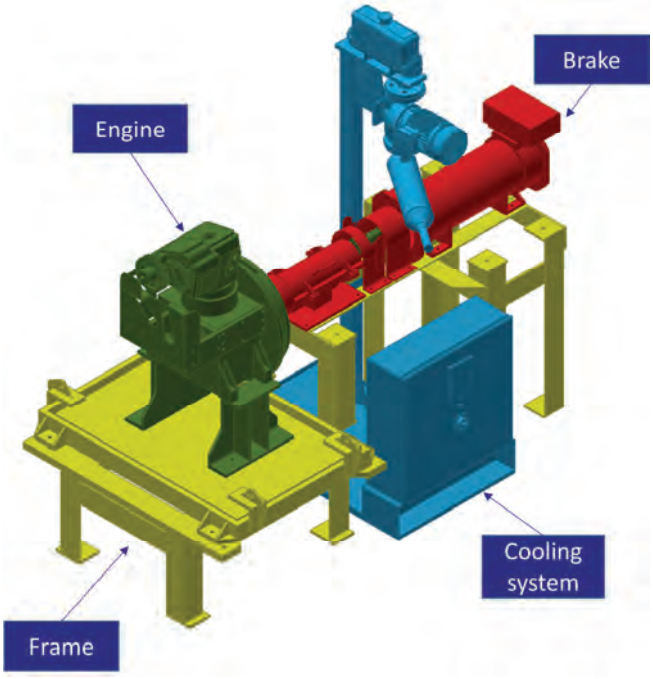

Fig. 14. Dynamometer bench CAD model with color-signed systems: green – engine, yellow – frame, blue – cooling system, red – brake

4. Model analysis

The final product of the reverse engineering process is a CAD model of the studied object. The model can be used to create technical documentation or relevant analysis, for example strength analysis. The GOM Inspect program allows for comparison between the model and scan by opening both files in a single project. The files must be aligned in a common coordinate system. A color deviation map is then generated on the scan surface (Fig. 15).

The deviation scale includes the maximum and minimum deviation. The maximum deviation, located on the oil cooler system, is +12.60 mm, while the minimum deviation is placed on the base of the engine frame and it is –12.93 mm. The extreme deviation values occur where oil lines are placed, that were not included in the CAD model due to insufficient data.

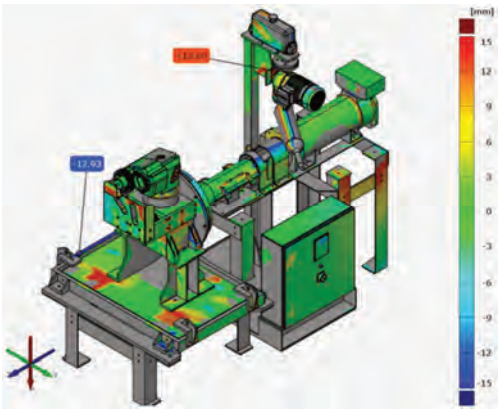

Fig. 15. Surface comparison with colored deviation map; maximum and minimum deviation

The GOM Inspect program can display a histogram of the deviation, allowing users to determine how much of the object falls within a given range of deviation. The standard deviation for the measured deviations is approximately ±6 mm. In the measurements presented here, this result was obtained for 66% of the scan area (Fig. 16).

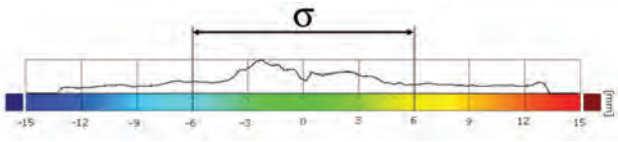

Fig. 16. Deviation histogram

5. Modification of the intake system

A CAD model proved to be helpful during modifying the inlet system of the AVL 5804 engine. This modification aims to adapt the intake system to burn gas mixtures using both direct and indirect injection. The 3D design allows the intake system to be made using 3D bending technology, thus ensuring continuous flow without interference from uneven welding (Fig. 17).

6. Conclusion and directions for further work

The presented method used for reproducing a test bench as a CAD model simplifies future upgrades of the studied object. The advantage of this method is that it acquires a large amount of data in a short time, thanks to 3D scanning. The complicated geometry of the dynamometer and the limited space around it cause measurement problems that cannot be resolved without a handheld 3D scanner. However, the disadvantage of this method is that the internal structure of the test bench cannot be reproduced as a CAD model without technical documentation or additional measurements using an appropriate method such as computer tomography.

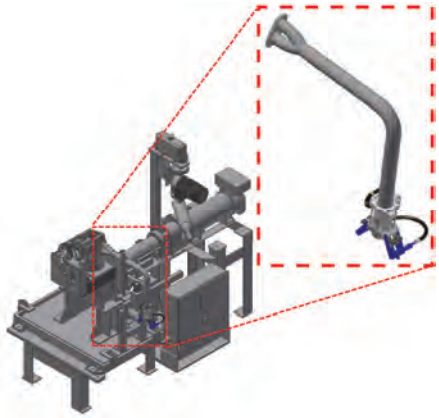

Fig 17. New intake system

The final product of the reverse engineering process is a CAD model of the whole test bench. Due to time limits and low demand, part of the scan was done in a cursory manner. However, this did not negatively affect the obtained 3D model. An adequate definition of the area of interest reduces measurement time and model size. Future research work and modifications necessary to carry it out will use the presented test bed model. The current model does not take into account the electrical connections and the cooling system, intake and exhaust pipes, which will probably be completed in future works.

Acknowledgments

This work was supported by the Reversesolutions company, which provided the equipment and software that made it possible to perform the reverse engineering process described.

Nomenclature

CAD	Computer Aided Design
CAE	Computer Aided Engineering
CI	compression ignition
CNG	compressed natural gas
DI	direct injection
FEM	finite element method
LPG	liquified petroleum gas
SI	spark ignition
STEP	standard for the exchange of product data
STL	standard triangulation language
VVT-iE	variable valve timing-inteligent by electric motor

Bibliography

[1] Almeida S, Kruczan R. Effects of drivetrain hybridization on fuel economy, performance and costs of a fuel cell hybrid electric vehicle. Int J Hydrogen Energ. 2021;46(79):39404-39414. https://doi.org/10.1016/j.ijhydene.2021.09.144

[2] Araujo BR, Lopes DS, Jepp P, Jorge JA, Wyvill BM. A survey on implicit surface polygonization. ACM Comput Surv. 2015;47(4):1-39. https://doi.org/10.1145/2732197

[3] Cieślik W, Szwajca F, Wisłocki K. Reverse engineering of research engine cylinder-head. Combustion Engines. 2022; 189(2):73-82. https://doi.org/10.19206/CE-143481

[4] Cieslik W, Szwajca F, Zawartowski J, Pietrzak K, Rosolski S, Szkarlat K et al. Capabilities of nearly zero energy building (nZEB) electricity generation to charge electric vehicle

(EV) operating in real driving conditions (RDC). Energies. 2021;14(22):7591. https://doi.org/10.3390/en14227591
[5] Curless B, Seitz S. Course on 3D photography. http://www.cs.cmu.edu (accessed on 03.2023).
[6] Czajka J, Wisłocki K, Pielecha I, Borowski P. Examination of the influence of multi-injection strategy on thermodynamic indexes of engine cycle and on the emission of toxic compounds. Combustion Engines. 2014;157(2):45-59. https://doi.org/10.19206/CE-116944
[7] Duan Y, Sun B, Li Q, Wu X, Hu T, Luo Q. Combustion characteristics of a turbocharged direct-injection hydrogen engine. Energ Convers Manage. 2023;291:117267. https://doi.org/10.1016/j.enconman.2023.117267
[8] Fiedkiewicz Ł, Pielecha I, Wisłocki K. Use of the gas ionization signal for combustion process diagnostics in the cylinder of a spark ignition engine. Combustion Engines. 2017;171(4):196-200. https://doi.org/10.19206/CE-2017-433
[9] Finding the right engine size for your application. https://www.volvopenta.com/ (accessed on 03.2023).
[10] Fontaras G, Zacharof N-G, Ciuffo B. Fuel consumption and CO_2 emissions from passenger cars in Europe – laboratory versus real-world emissions. Prog Energ Combust. 2017;60:97-131. https://doi.org/10.1016/j.pecs.2016.12.004
[11] Gong C, Si X, Liu F. Comparative analysis on combustion and emissions between CO_2 and EGR dilution GDI engine at half-load, stoichiometric and lean-burn conditions. Fuel. 2022;309:122216. https://doi.org/10.1016/j.fuel.2021.122216
[12] Gong C, Yu J, Liu F. Influence of direct-injection ratio on combustion and emissions of a stoichiometric spark-ignition dual-injection gasoline engine at different throttle percentages and injection timings of direct-injection. Fuel. 2023;346:128262. https://doi.org/10.1016/j.fuel.2023.128262
[13] Karczewski M, Koliński K, Walentynowicz J. Failure analysis of combustion engines elements with scanner 3D (in Polish). Zeszyty Naukowe Akademii Marynarki Wojennej. 2011;1(184):59-66.
[14] Liu F, Liu B, Zhang J, Wan P, Li B. Study on a novel variable valve timing and lift mechanism for a Miller cycle diesel engine. Energies. 2022;15:8521. https://doi.org/10.3390/en15228521
[15] Mariani V, Rizzo G, Tiano FA, Glielmo L. A model predictive control scheme for regenerative braking in vehicles with hybridized architectures via aftermarket kits. Control Eng Pract. 2022;123:105142. https://doi.org/10.1016/j.conengprac.2022.105142
[16] Meng H, Ji C, Shen J, Yang J, Xin G, Chang K et al. Analysis of combustion characteristics under cooled EGR in the hydrogen-fueled Wankel rotary engine. Energy. 2023;263(B):125815. https://doi.org/10.1016/j.energy.2022.125815
[17] Nassif G, Almeida S. Impact of powertrain hybridization on the performance and costs of a fuel cell electric vehicle. Int J Hydrogen Energ. 2020;45(41):21722-21737. https://doi.org/10.1016/j.ijhydene.2020.05.138
[18] Pei Z, Liu K, Luo W, Yang J, Li Y. Experimental study on the effect of aftertreatment system on the energy flow pattern and emission reduction of a natural gas engine under world harmonized transient cycle. Energy. 2023;263(B):125729. https://doi.org/10.1016/j.energy.2022.125729
[19] Pielecha I, Cieslik W, Wislocki K. Optimization of two-stage combustion system fueled by lean-burn compressed natural gas mixtures for light-duty vehicle engines. SAE Int J Engines. 2020;13(4):503-519. https://doi.org/10.4271/03-13-04-0033
[20] Pielecha I, Wislocki K, Cieslik W, Borowski P, Bueschke W, Skowron M. Analysis of a dual-fuel combustion engine fueled with diesel fuel and CNG in transient operating conditions. SAE Technical Paper 2016-01-2305. 2016. https://doi.org/10.4271/2016-01-2305
[21] Rehman A, Tanveer A. GA-based motor drive control of planetary gears of a variable valve system of an internal combustion engine. Engineering Proceedings. 2023;32(1):11. https://doi.org/10.3390/engproc2023032011
[22] Remondino F. Heritage recording and 3D modeling with photogrammetry and 3D scanning. Remote Sens. 2011;3:1104-1138. https://doi.org/10.3390/rs3061104
[23] Reverse engineering. https://reversesolutions.pl/ (accessed on 03.2023).
[24] Ritzmann J, Lins G, Onder C. Optimization method for the energy and emissions management of a hybrid electric vehicle with an exhaust aftertreatment system. IFAC-PapersOnLine. 2020;53(2):13797-13804. https://doi.org/10.1016/j.ifacol.2020.12.888
[25] Scanning the AVL 5804 engine dynamometer. https://youtu.be/UT3n2IZL5ck (accessed on 07.2023).
[26] Szwajca F, Wisłocki K. Thermodynamic cycles variability of TJI gas engine with different mixture preparation systems. Combustion Engines. 2020;181(2):46-52. https://doi.org/10.19206/CE-2020-207
[27] Wei Y, Zhu Z, Liao Y, Liu S, Shi Z, Zeng Z et al. Numerical investigations on the effects of EGR routes on the combustion characteristics and efficiency of a heavy-duty SI methanol engine. Fuel Process Technol. 2023;250:107861. https://doi.org/10.1016/j.fuproc.2023.107861
[28] Wurms R, Budack R, Grigo M, Mendl G, Heiduk T, Knirsch S. Der neue Audi 2.0l mit innovativem Rightsizing – ein weiterer Meilenstein der TFSI-Technologie. Vienna Motor Symposium. 2015. https://www.greencarcongress.com/2015/05/20150514-gen3b.html (accessed on 03.2023).

Wojciech Cieślik, DEng. – Faculty of Civil and Transport Engineering, Poznan University of Technology, Poland.
e-mail: *wojciech.cieslik@put.poznan.pl*

Dawid Mielcarzewicz, Eng. – Faculty of Civil and Transport Engineering, Poznan University of Technology, Poland.
e-mail: *dawid.mielcarzewicz@student.put.poznan.pl*

Michał Rawecki, MEng. – Reversesolutions sp. z o.o., Measurement and 3D Scanning, Poland.
e-mail: *m.rawecki@reversesolutions.pl*

Article citation info:
Matla J, Kaźmierczak A, Haller P, Trocki M. Hydrogen as a fuel for spark ignition combustion engines – state of knowledge and concept. Combustion Engines. 2024;196(1):73-79. https://doi.org/10.19206/CE-171541

Jędrzej MATLA
Andrzej KAŹMIERCZAK
Piotr HALLER
Marcin TROCKI

Combustion Engines
Polish Scientific Society of Combustion Engines

Hydrogen as a fuel for spark ignition combustion engines – state of knowledge and concept

ARTICLE INFO

Received: 31 May 2023
Revised: 8 August 2023
Accepted: 24 August 2023
Available online: 6 September 2023

Accelerating the process of the transport and energy sectors increases the interest in fuels derived from renewable sources. The predicted three-fold increase in hydrogen production by 2050, driven by its falling production costs, justifies the direction of research aimed at its popularisation as a fuel for internal combustion engines (H2ICE). The presented article provides an overview of the state of knowledge on hydrogen combustion systems, which are currently the most attractive development path, mainly due to the well-developed production technology and relatively low recycling cost compared with fuel cells. The paper contains a comprehensive analysis of currently available solutions covering issues related to the production, storage, and transmission of hydrogen, with particular emphasis on the Polish market, which is one of the largest in Europe in terms of its production. The authors also propose their own concept of a hydrogen combustion system for application in an internal combustion engine. The presented solution is based on the idea of prechamber introduction in order to improve combustion process parameters and hence overall engine efficiency.

Key words: *H2ICE, alternative fuels, hydrogen combustion, hydrogen knock, polish hydrogen market*

1. Introduction

1.1. General

As an alternative fuel source for vehicles, hydrogen has many advantages, the most important of which is the elimination of carbon, which is a key aspect in the decarbonization of the transport sector. Due to its high gravimetric energy density (143 MJ/kg) hydrogen is classified as a high-energy fuel and is therefore an alternative to battery technologies [28]. The biggest disadvantage in the use of hydrogen to drive motor vehicles is its low volumetric energy density, which requires the use of relatively large tanks. Currently, mainly because of the geopolitical situation, a very important factor is the possibility of producing hydrogen anywhere in the world, which of course requires the selection of the appropriate technology, but allows for a given region to become energy independent [31].

1.2. Historical background

The emergence of the concept of the hydrogen economy dates back to the 1970s and originally referred to the replacement of fossil fuels in transport with hydrogen fuel [8]. At that time, the main stimulus for development was the fuel crisis, which largely contributed to the development of research directions in the field of alternative fuels. The decline in the popularity of alternative sources of vehicle propulsion coincided with the stabilization of the oil market in the 1980s, but the topic returned in the next decade thanks to the popularization of activities for climate protection. During the so-called second wave of hydrogenation of the economy, solutions aimed at the popularization of hydrogen as a fuel have been superseded to a large extent by electric vehicles, which to this day constitute an increasing percentage of vehicles on the market. Currently, we are dealing with the third wave of hydrogenation of the economy, mainly because of the extension of this concept to sectors such as metallurgy, agriculture, and the chemical industry. A clear stimulus for the development of the hydrogen economy in Europe was the announcement by the EU of the Hydrogen Strategy in 2020 and the entry into force of the Directive of the European Parliament and of the Council of EU on the promotion of the use of energy from renewable sources (the so-called RED II directive) in 2018. Their main goal is to achieve climate neutrality by the EU by 2050 (European Green Deal). In order to achieve this, it is necessary to increase the share of renewable energy sources in the electricity production process and replace fossil fuels commonly used in transport with alternative fuels such as hydrogen.

2. Polish hydrogen market

2.1. Poland in comparison to other EU Member States

The development of hydrogen technologies in the world was also reflected in Poland, as a result of which, in 2021, the Polish Hydrogen Strategy was announced, defining specific goals for building a hydrogen economy in the next decades. Analyzers show that in the next dozen or so years, hydrogen, in particular green, may become the basis for the functioning of the industry in Poland [10]. Currently, Poland is one of the largest hydrogen producers in Europe. Four countries account for more than half of hydrogen consumption in Europe: Germany (22%), the Netherlands (14%), Poland (9%) and Belgium (7%). Hydrogen production in Poland is dominated by production for companies own needs, mainly for the chemical sector. Its largest producers are Grupa Azoty (approx. 400 thousand tonnes per year, of which includes 600 tonnes of merchant), PKN Orlen and LOTOS Group (approx. 145 thousand tonnes per year each) [13].

Table 1. Polish companies with experience in selected branches of the hydrogen market [25]

Economic activity	Name of company	Range of operation
Production	Jastrzębska Spółka Węglowa (JSW)	Hydrogen separation from coal gas
	Lotos, Polskie Sieci Elektroenergetyczne (PSE)	Hydrogen separation from coal gas
	Sescom	Sale of PV powered electrolysers
	Grupa Azoty	Production of merchant grey hydrogen
	Polenergia	Production and utilization of green hydrogen; cogeneration adoption to hydrogen combustion
	RB Consulting	Electrolysers distribution
	Zespół Elektrowni Pątnów Adamów Konin (ZE PAK)	Application of biomass powered electrolysers
	PKN Orlen	Application of RES powered electrolysers
	Tauron Wytwarzanie	Production of SNG; Hydrogen production from RES powered electrolysers; CO_2 capture systems
	Wałbrzyskie Zakłady Koksownicze „Victoria”	Hydrogen separation from coal gas
	Stalprodukt	Methane steam reforming
Storage	PGNiG	Hydrogen pumping into distribution networks; underground storage
	Stako (Worthington Industries Group)	Pressure vessels
Application	Lotos Group	Hydrogen refuelling stations
	PKP Cargo	Hydrogen application in rail vehicles
	H. Cegielski	Hydrogen powered locomotive prototype
	PKN Orlen	Hydrogen refuelling stations
	PGNiG	Hydrogen refuelling stations
	EC Grupa (Energocontrol Sp. Z o.o.)	Fuel cells development
	APS Energia (with Gdańsk Technical University)	Hydrogen emergency power supply system
	Remontowa Holding	Conceptual design of hydrogen powered marine units
	Solaris	Hydrogen powered buses production
	Polenergia (with Siemens)	Hydrogen combustion in gas turbines
Pipeline transfer	PGNiG	Hydrogen blending in pipelines
Instruments	Intergaz	Gas meters
	cGAS controls	Pressure tanks
	Emag Serwis	Sensors
	Frankoterm	Cryostatic devices

Poland, as one of the largest hydrogen producers in Europe, has highly developed technologies for its production and use mainly in the field of chemical and energy industries. With this state of matter in mind, it is justified to think that in the near future the development of hydrogen technologies will also be reflected in road transport.

2.2. Predictions in numbers

The annual demand for hydrogen in Poland in 2040 is expected to exceed 100 TWh, of which 20 GW will come from electrolysers. The total installed RES capacity at that time is to be 60 GW. It is planned to produce hydrogen as part of three main paths: the use of surplus RES (energy storage), the operation of a separate part of RES in an off-grid system integrated with electrolysers, and distributed production for local needs, e.g. vehicles refueling [10].

3. Hydrogen production methods

3.1. Colors of hydrogen

Currently, approximately 96% of the hydrogen produced in the world is estimated to come from the processing of fossil fuels, mainly as a result of the steam reforming of natural gas, which is currently considered the most economical hydrogen production technology [19]. In the near future, this share will be reduced in favour of electrolysers powered by renewable energy sources, which should significantly contribute to reducing the carbon footprint and lowering the prices of green hydrogen production. Depending on the primary energy sources used in the production of hydrogen, different colours are used in order to describe it [17, 30] as it is shown in the Fig. 1.

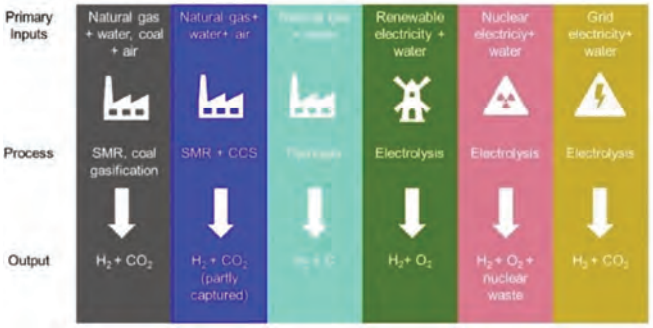

Fig. 1. Hydrogen production technologies in relation with colours [1]

3.2. Methane steam reforming

Natural gas steam reforming is the most widely used hydrogen production process today. The reforming process takes place at high temperatures, ranging from 1023–1223 K, in the presence of a nickel catalyst. The reactions take place in oven tubes filled with the catalyst. Water vapor is added to the methane. As a result of this process, a gas mixture containing mainly carbon monoxide and hydrogen, known as the synthesis gas, is obtained. The efficiency of the process is estimated at 75%, but its disadvantage is the generation of large amounts of CO_2, up to 12 kg per 1 kg of hydrogen (gray). The syngas created in the steam reforming process is used for the Fischer-Tropsch synthesis toward the production of the so-called synthetic hydrocarbons. The undoubted advantage of syngas is the absence of nitrogen. One of the ways to reduce CO_2 emissions is CCU and CCS technologies, which enable the reduction of CO_2 emissions by up to 95%. We are then talking about blue hydrogen [49].

3.3. Methane pyrolysis

Another method of hydrogen production, which is a subject of investigation, is natural gas pyrolysis. The process involves splitting of methane into solid carbon and gaseous hydrogen. To make the reaction possible and achieve relatively high conversion rates, process temperature should be maintained at a level of 1773 K [6]. Since the solid carbon obtained from the reaction is easy to handle and is considered as unharmful to the environment, the main problem is the high cost of reactors and their complexity. However, the gases obtained in the process require additional treatment to remove impurities (Fig. 2). Methane pyrolysis is a relatively low energy-consuming process, and if this energy comes from renewable resources, hydrogen could be produced on an industrial scale without almost any CO_2 emissions. Hydrogen obtained in this method is described as turquoise.

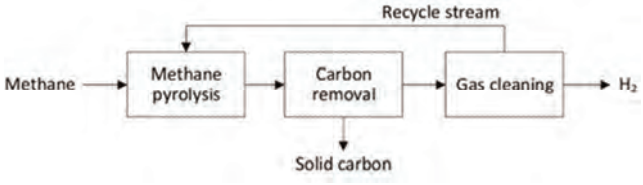

Fig. 2. Schematic diagram of methane pyrolysis process [17]

3.4. Coal gasification

Coal gasification is the oldest method of producing hydrogen. It was used when natural gas was not yet available. The coal is heated and mixed, in the presence of a catalyst, with steam, which gives us synthesis gas. Hydrogen and other chemicals are extracted from this gas or burned to generate electricity. There have been many scientific studies focused on reducing emissions of pollutants such as nitrogen and sulfur oxides, mercury and carbon oxides [16, 23].

3.5. Biomass

Hydrogen can also be produced from biomass derived from plant and animal wastes, using pyrolysis and gasification processes. When biomass is used to produce gas fuel, no carbon dioxide is emitted into the environment. Unfortunately, the unit price of hydrogen obtained using biomass is much higher than that of hydrogen derived from fossil fuels [5]. The biological processes of producing hydrogen from biomass are fermentation, anaerobic fermentation, and metabolic processes; however, they are considered as inefficient compared to traditional hydrogen production techniques [15, 33].

3.6. Electrolysis

In the future, the most supported method of producing hydrogen in the European Union will be the production of hydrogen by electrolysis of water using electricity from renewable energy sources. Unfortunately, currently the production of hydrogen with the use of electricity reaches approx. 4% of the total production. Moreover, most of this hydrogen is a by-product of chlorine production in the brine electrolysis technology called white hydrogen (formed as a by-product of further chemical reactions). If the hydrogen is produced by electrolysis of water, and the electricity used comes from renewable sources, this hydrogen is called green. Green hydrogen is emission-free and has the greatest potential to reduce greenhouse gas emissions. During the electrolysis of water, the chemical bond between the hydrogen and oxygen is broken in the solution to form hydrogen and oxygen gas. Currently, the overall efficiency is around 50–60% depending on the use of cell technology. About 9 liters of water and about 50 kWh of electricity are needed to produce 1 kg of hydrogen [4]. Recently, research in this area has focused mainly on reducing the cost of hydrogen production through the use of carbon-based materials electrodes [21].

Currently, the potential for red hydrogen production in newly developed fourth-generation nuclear reactors using high-temperature electrolysis of water vapor on cells with solid oxidants is being discussed [35].

4. Hydrogen storage

Hydrogen as a fuel has many storage options. It can be stored in the form of a compressed gas, a liquid, or in the form of metal hydrides, chemically bonded or on the surface of materials, e.g. carbon materials with a large surface, such as graphite or carbine nanotubes [12, 48]. Currently, gaseous compressed hydrogen is mentioned as the most promising and also the most effective technology for its storage, mainly because of the relatively simple method of carrying out this process [26]. Hydrogen compressed in this way tends to volatilize, but there are ways to counteract this phenomenon by using appropriate tanks to minimize storage losses.

Depending on the application, these tanks can be divided into small tanks for short-term storage (e.g. car tanks) with 99% efficiency and high discharge rate, and large-size industrial tanks ensuring long-term protection of hydrogen reserves [43].

In the view of materials used, the tanks for short-term hydrogen gas storage can be divided into:

- metal tanks – cylinders made of steel or aluminum, used to store hydrogen at a pressure of up to 20 MPa, used mainly for laboratory purposes
- reinforced tanks – made of aluminum, reinforced with glass or carbon fiber with a maximum working pressure up to approx. 30 MPa
- composite tanks – built based on glass or carbon fiber with a metal insert with a storage pressure of up to approx. 40 MPa, they are twice lighter than in the case of metal tanks
- carbon fiber tanks covered with a polymer layer – withstanding pressures up to approx. 70 MPa, commonly used in hydrogen powered vehicles (FCHV) [7].

Due to the high permeability of hydrogen in the tanks, polymer coatings are used to limit the volatilization of hydrogen [2].

The pressures required for hydrogen road transport tanks are in range of 35–50 MPa. On the other hand, in the case of applications in hydrogen powered vehicles, mainly because of ensuring the appropriate range, the hydrogen pressure in the tank is 70 MPa. Research is currently underway to reduce the size of the tanks, mainly by increasing the maximum storage pressure. Currently, at a pressure of 70 MPa, compressed hydrogen has approximately 15% of

the volumetric energy density of gasoline (Fig. 3), which entails the need to use larger tanks.

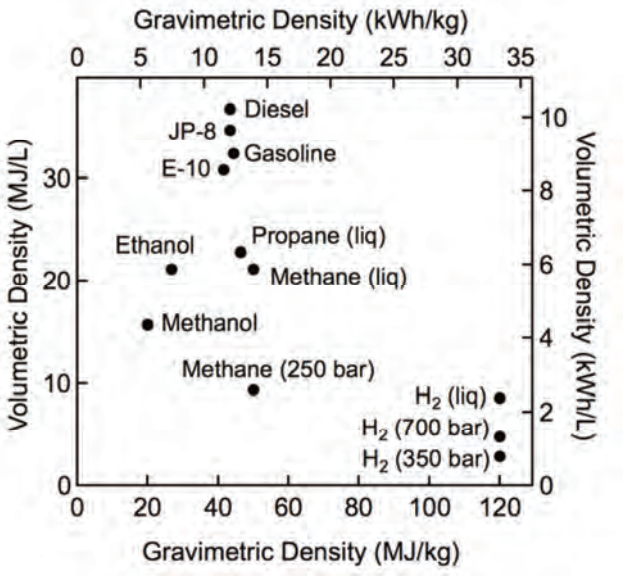

Fig. 3. Comparison of specific energy and energy density for selected fuels based on their LHV [44]

For long-term storage of hydrogen on an industrial scale, geological storage is indicated as the best solution [42]. There is a method of storing hydrogen in underground storage facilities created as a result of the exploitation of oil or gas deposits. Currently, work is underway in Poland to store hydrogen in salt caverns, which are already used as natural gas storage facilities [41]. Their use minimizes the risk of hydrogen contamination while allowing its safe storage. This solution is used in the USA and UK, and recently also in Germany. The pressure level in the underground tanks is between 2 and 18 MPa.

An alternative to hydrogen storage is condensation, which allows it to increase its volumetric energy density by more than three times, thus reducing the size of the tanks. However, this process is burdened with higher compression energy, which in the case of condensation amounts to 30–40% of the energy contained in the fuel, compared to 15–20% in the case of gas compression. In addition, this type of storage requires the temperature to be kept at 20 K, which increases the cost of hydrogen storage, therefore condensation is considered as a technology for short-term storage [47].

5. Hydrogen combustion engines – H2ICE

5.1. Hydrogen vehicles

Hydrogen fuelling of internal combustion engines is an idea known and implemented for many years, however, due to legal regulations limiting the possibility of using fossil fuels in transport, there is a noticeable increase in interest in the development of hydrogen propulsion technology. In recent years, there has been an increase in the market share of fuel cell vehicles (Fig. 4), characterized by higher efficiency than H2ICE, which are no less attractive alternatives due to well-developed production technologies and high production potential.

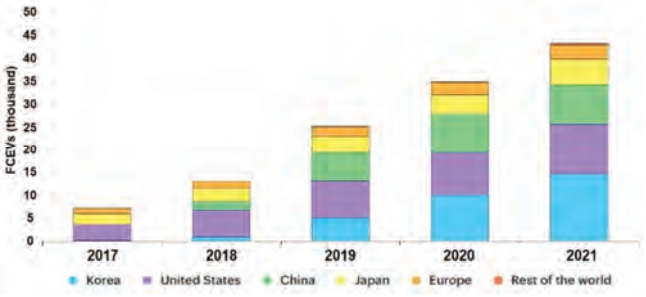

Fig. 4. Fuel cell vehicle stock by region, 2017–2020 [20]

The process of introducing hydrogen as fuel to internal combustion engines on a large scale is carried out gradually, starting from large generating units, engines for propulsion of floating units and traction units [14, 29]. In recent months, there has also been an increase in interest in this technology among manufacturers of heavy duty vehicles.

Due to the form of hydrogen supply to the combustion chamber, two main methods can be distinguished: gaseous and liquid hydrogen injection. While hydrogen in the liquid state is characterized by a higher energy density than in the gaseous state, it requires maintaining the temperature at the level of 20 K, which generates a high cost of such an installation. Depending on the location of the injector, these systems are divided into direct and indirect injection (Fig. 5).

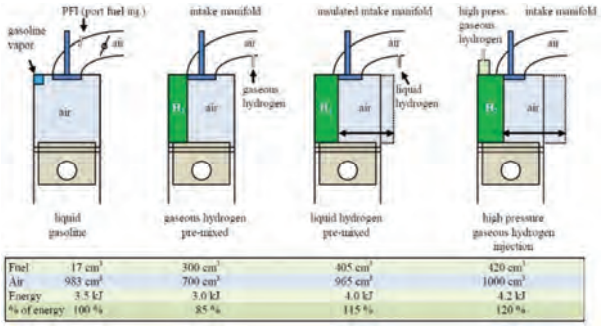

Fig. 5. Hydrogen injection systems [32]

5.2. Hydrogen combustion

The process of hydrogen combustion in an internal combustion engine generates some problems and the main reason for that is the so-called dual nature of hydrogen knock. With respect to definition, knocking is assumed to be incorrect combustion of an air-fuel mixture resulting in the generation of uncontrolled pressure waves acting against the main combustion source leading to a decrease in overall engine efficiency [18]. Practice shows that despite the high autoignition temperature and compression resistance of hydrogen resulting from the high octane number (RON > 130) it is very likely to achieve knocking phenomena [37]. The reason for such state seems to be the low ignition energy of hydrogen and the fact that the octane number is not an appropriate parameter in order to describe the properties of gaseous fuel. As research shows a much better indicator of describing the probability of a heavy run of the engine while combusting hydrogen, the so-called methane number proposed by Ryan et al. [34]. It is a parameter that describes the percentage content of methane in the reference mixture of hydrogen and methane. Since me-

thane is assumed to have the highest index, hydrogen is considered to be the most vulnerable to knock occurrence with MN = 0 (Table 2).

Table 2. Methane number of selected gaseous fuels [24]

Fuel	Hydrogen	Coal gas	Propane	Natural gas	Methane
MN	0	24–30	34	75–95	100

Dual nature of hydrogen knock is an outcome of two main mechanisms of its occurrence. The first one called heavy knock is described as air-fuel mixture autoignition at the end of compression stroke as a result of elevated temperature and pressure in combustion chamber. It occurrence being a highly undesirable phenomena leads to engine thermal load increase and excessive wear of crank system bearings. The other mechanism of incorrect hydrogen combustion described in literature as light knock results from unstable combustion of ignited air-fuel mixture initiated by the controlled source of combustion and it is assumed to be less harmful to engine durability and performance than heavy knock, however, still being undesirable [40]. Hydrogen knock occurrence is also affected by other engine parameters such as compression ratio, which has a direct impact on its operation is shown in the Figure 6. The intensity of knock is a parameter used to describe it is pressure pulsation intensity and in case of light knock is assumed to fit in the range of 20–100 kPa.

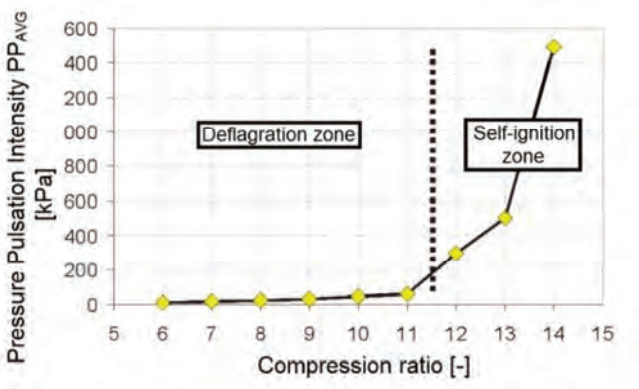

Fig. 6. Compression ratio influence on pressure pulsation intensity [38]

There are many ways to hamper knock occurrence in H2ICE among which the most effective ones are lean engine operation with SCC [22], modification of engine operation cycle (ex. Miller cycle with split injection) [45], water anti-detonant direct injection [9] into combustion chamber or dilution of hydrogen rich gases with exhaust gas recirculation [39]. Research shows that in case of hydrogen fueled engines modifications in combustion chamber geometry might result in better control of combustion process [46].

6. Hydrogen combustion system concept

Basing on conducted literature review authors of following paper are proposing their own idea of hydrogen combustion system for application in an internal combustion engines. The main idea of system is introduction of prechamber into engine cylinder head since its main task is to increase control of air-fuel mixture formation. The system main function is to impede risk of light knock occurrence by stabilization of pre-ignited flame propagation, thus allowing for higher compression ratio implementation. System design presented in the Fig. 7 consist of two injectors allowing for formation of mixtures with different equivalence ratios in main chamber and prechamber independently and resulting in stratified charge combustion.

Presence of active prechamber enables formation of ultra-lean mixture in region of ignition which should allow for decrease in flame propagation rate so charge in main chamber will ignite in more ordered matter. Author's considerations are based on research conducted with use of gas-powered engines equipped with prechambers giving promising results [3, 36]. System being the subject of following chapter is under constant development and it is also considered to apply direct hydrogen injection in the future as it exhibits acceptable results [11].

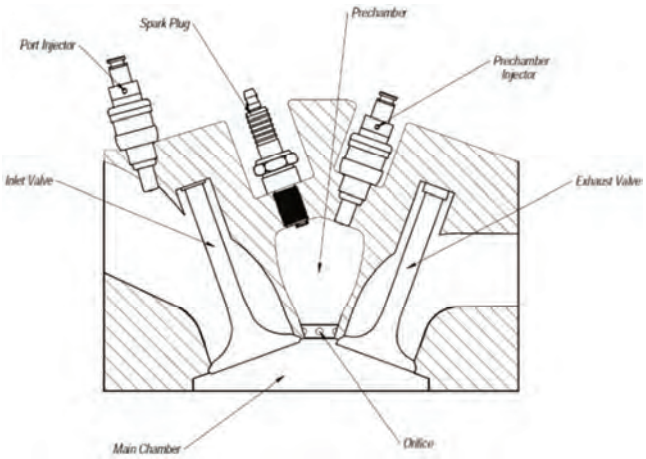

Fig. 7. Scheme of system proposed by the authors [27]

7. Conclusions

Conducted analyzes indicate that in the near future, the dominant method of obtaining hydrogen will be electrolysis, in which electricity will be obtained from renewable sources such as wind, sun or water; however, the current pace of development of renewable energy does not offer any opportunity to meet the demand for hydrogen in the future; therefore, it is necessary to introduce appropriate legislative changes regarding the production, transmission, and storage of hydrogen and to create financing opportunities.

According to the research, it is expected in the near future to observe increased interest in solutions that will allow for the use of hydrogen as a fuel for combustion engines, especially regarding to Polish market, thus it is justified to conduct research in this field.

The effectiveness and profitability of hydrogen storage are strictly related to the need to ensure the permeability of the tank at the lowest possible level while ensuring its high energy efficiency at the same time. Therefore, the dominant trend for hydrogen storage in vehicles is gaseous form with increased pressure.

In the near future, storage of large volumes of hydrogen for industrial purposes will be dominated by underground caverns obtained from rock salt deposits.

Direct hydrogen combustion in an internal combustion engine brings a lower energy expenditure than the combustion of hydrocarbon fuels; however, the authors perceive the possibility of improving the efficiency of this process by increasing the resistance to hydrogen knock precisely in the way of separating the combustion process into its initiation in the prechamber and main combustion in the main chamber.

Nomenclature

CCU	carbon capture and utilization
CCS	carbon capture and storage
EU	European Union
FCHV	fuel cell hydrogen vehicle
H2ICE	hydrogen fueled internal combustion engine
MN	methane number
LHV	lower heating value
RES	renewable energy sources
RON	research octane number
SCC	stratified charge combustion

Bibliography

[1] Ajanovic A, Sayer M, Haas R. The economics and the environmental benignity of different colors of hydrogen. Int J Hydrogen Energ. 2022;47(57):24136-24154. https://doi.org/10.1016/j.ijhydene.2022.02.094

[2] Almeida Neto GR, Gonçalves Beatrice CA, Leiva DR, Pessan LA. Polymer-based composite containing nanostructured $LaNi_5$ for hydrogen storage: improved air stability and processability. Int J Hydrogen Energ. 2020;45(27):14017-14027. https://doi.org/10.1016/j.ijhydene.2020.03.069

[3] Alvarez CEC, Couto GE, Roso VR, Thiriet AB, Valle RM. A review of prechamber ignition systems as lean combustion technology for SI engines. Appl Therm Eng. 2018;128:107-120. https://doi.org/10.1016/j.applthermaleng.2017.08.118

[4] Anwar S, Khan F, Zhang Y, Djire A. Recent development in electrocatalysts for hydrogen production through water electrolysis. Int J Hydrogen Energ. 2021;46(63):32284-32317. https://doi.org/10.1016/j.ijhydene.2021.06.191

[5] Arnaiz del Pozo C, Cloete S, Jiménez Álvaro Á. Carbon-negative hydrogen: Exploring the techno-economic potential of biomass co-gasification with CO_2 capture. Energ Convers Manage. 2021;247:114712. https://doi.org/10.1016/j.enconman.2021.114712

[6] Ashik UPM, Wan Daud WMA, Abbas HF. Production of greenhouse gas free hydrogen by thermocatalytic decomposition of methane – a review. Renew Sust Energ Rev. 2015;44:221-256. https://doi.org/10.1016/J.RSER.2014.12.025

[7] Benitez A, Wulf C, de Palmenaer A, Lengersdorf M, Röding T, Grube T et al. Ecological assessment of fuel cell electric vehicles with special focus on type IV carbon fiber hydrogen tank. J Clean Prod. 2021;278:123277. https://doi.org/10.1016/j.jclepro.2020.123277

[8] Bockris JOM. The origin of ideas on a Hydrogen Economy and its solution to the decay of the environment. Int J Hydrogen Energ. 2002;27(7-8):731-740. https://doi.org/10.1016/S0360-3199(01)00154-9

[9] Boretti A. Stoichiometric H_2ICEs with water injection. Int J Hydrogen Energ. 2011;36(7):4469-4473. https://doi.org/10.1016/j.ijhydene.2010.11.117

[10] Brodacki D, Gajowiecki J, Hajduk R, Kacejko P, Kowalski S, Mataczyńska E et al. Green hydrogen from RES in Poland Use of wind energy and PV. Wrocław 2021. http://psew.pl/en/wp-content/uploads/sites/2/2021/12/Report-Green-hydrogen-from-RES-75MB.pdf

[11] Brzeżański M, Rodak Ł. Investigation of a new concept of hydrogen supply for a spark-ignition engine. Combustion Engines. 2019;178(3):140-143. https://doi.org/10.19206/CE-2019-324

[12] Cheng G, Dou K, Yuan G. Hydrogen separation of porous carbon nanotubes: A density functional theory study. Diam Relat Mater. 2022;125:108986. https://doi.org/10.1016/j.diamond.2022.108986

[13] Gawlik L, Mokrzycki E. Analysis of the Polish hydrogen strategy in the context of the EU's strategic documents on hydrogen. Energies. 2021;14(19):6382. https://doi.org/10.3390/en14196382

[14] Gis M, Gis W. The current state and prospects for hydrogenisation of motor transport in Northwestern Europe and Poland. Combustion Engines. 2021;190(3):61-71. https://doi.org/10.19206/CE-144560

[15] Guo J-X, Tan X, Zhu K, Gu B. Integrated management of mixed biomass for hydrogen production from gasification. Chem Eng Res Des. 2022;179:41-55. https://doi.org/10.1016/j.cherd.2022.01.012

[16] He S, Gao L, Dong R, Li S. A novel hydrogen production system based on the three-step coal gasification technology thermally coupled with the chemical looping combustion process. Int J Hydrogen Energ. 2022;47(11):7100-7112. https://doi.org/10.1016/j.ijhydene.2021.12.050

[17] Hermesmann M, Müller TE. Green, Turquoise, Blue, or Grey? Environmentally friendly Hydrogen Production in Transforming Energy Systems. Prog Energ Combust. 2022;90:100996. https://doi.org/10.1016/j.pecs.2022.100996

[18] Heywood JB. Internal combustion engines fundamental. McGraw-Hill Inc. New York 1988. https://www.accessengineeringlibrary.com/content/book/9781260116106

[19] Howarth RW, Jacobson MZ. How green is blue hydrogen? Energy Sci Eng. 2021;9(10):1676-1687. https://doi.org/10.1002/ese3.956

[20] IEA. Fuel cell electric vehicle stock by region, 2017-2020. https://www.iea.org/data-and-statistics/charts/fuel-cell-electric-vehicle-stock-by-region-2017-2020

[21] Kordek-Khalil K, Walendzik I, Rutkowski P. Low-overpotential full water splitting with metal-free self-supported electrodes obtained by amination of oxidised carbon cloth. Sustainable Energy Technologies and Assessments. 2022;53(B):102569. https://doi.org/10.1016/j.seta.2022.102569

[22] Lee S, Kim G, Bae C. Lean combustion of stratified hydrogen in a constant volume chamber. Fuel. 2021;301:121045. https://doi.org/10.1016/j.fuel.2021.121045

[23] Li J, Fan S, Zhang X, Chen Z, Qiao Y, Yuan Z et al. Investigation on co-combustion of coal gasification fine ash and raw coal blends: Thermal conversion, gas pollutant emission and kinetic analyses. Energy. 2022;246:123368. https://doi.org/10.1016/j.energy.2022.123368

[24] Luo Q, Sun B. Inducing factors and frequency of combustion knock in hydrogen internal combustion engines. Int J Hydrogen Energ. 2016;41(36):16296-16305. https://doi.org/10.1016/j.ijhydene.2016.05.257

[25] Maj M, Szpor A. Hydrogen economy in Poland. Observations based on the research framework of the Technological System of Innovation. Polski Instytut Ekonomiczny. Warszawa 2020.
[26] Markidis S. Hydrogen storage and compression. Vol. 11. Methane and Hydrogen for Energy Storage. 2016. https://doi.org/10.1049/PBPO101E_ch1
[27] Matla J. Possible applications of prechambers in hydrogen internal combustion engines. Combustion Engines. 2022; 191(4):77-82. https://doi.org/10.19206/CE-148170
[28] Mazloomi K, Gomes C. Hydrogen as an energy carrier: Prospects and challenges. Renew Sust Energ Rev. 2012; 16(5):3024-3033. https://doi.org/10.1016/j.rser.2012.02.028
[29] Menes M. Program initiatives of public authorities in the field of hydrogenation of the economy in a global perspective, as of the end of 2020. Combustion Engines. 2022; 189(2):18-29. https://doi.org/10.19206/CE-142170
[30] Newborough M, Cooley G. Developments in the global hydrogen market: The spectrum of hydrogen colours. Fuel Cells Bulletin. 2020;11:16-22. https://doi.org/10.1016/S1464-2859(20)30546-0
[31] Noussan M, Raimondi PP, Scita R, Hafner M. The role of green and blue hydrogen in the energy transition – a technological and geopolitical perspective. Sustainability. 2020; 13(1):298. https://doi.org/10.3390/su13010298
[32] Pielecha I, Engelmann D, Czerwinski J, Merkisz J. Use of hydrogen fuel in drive systems of rail vehicles. Rail Vehicles/Pojazdy Szynowe. 2022;1-2:10-19. https://doi.org/10.53502/RAIL-147725
[33] Rosa L, Mazzotti M. Potential for hydrogen production from sustainable biomass with carbon capture and storage. Renew Sust Energ Rev. 2022;157:112123. https://doi.org/10.1016/j.rser.2022.112123
[34] Ryan TW, Callahan TJ, King SR. Engine knock rating of natural gases – methane number. J Eng Gas Turbines Power. 1993;115(4):769-776. https://doi.org/10.1115/1.2906773
[35] Şahin S, Şahin HM. Generation-IV reactors and nuclear hydrogen production. Int J Hydrogen Energ. 2021;46(57): 28936-28948. https://doi.org/10.1016/j.ijhydene.2020.12.182
[36] Santos NDSA, Alvarez CEC, Roso VR, Baeta JGC, Valle RM. Combustion analysis of a SI engine with stratified and homogeneous pre-chamber ignition system using ethanol and hydrogen. Appl Therm Eng. 2019;160:113985. https://doi.org/10.1016/j.applthermaleng.2019.113985
[37] Swain MR, Filoso PA, Swain MN. Ignition of lean hydrogen-air mixtures. Int J Hydrogen Energ. 2005;30(13-14): 1447-1455. https://doi.org/10.1016/j.ijhydene.2004.10.017
[38] Szwaja S. A study of combustion pressure pulsations in a hydrogen-powered internal combustion piston engine (in Polish). Częstochowa University of Technology Publishing House. Częstochowa 2010.
[39] Szwaja S. Dilution of fresh charge for reducing combustion knock in the internal combustion engine fueled with hydrogen rich gases. Int J Hydrogen Energ. 2019;44(34):19017-19025. https://doi.org/10.1016/j.ijhydene.2018.10.134
[40] Szwaja S, Naber JD. Dual nature of hydrogen combustion knock. Int J Hydrogen Energ. 2013;38(28):12489-12496. https://doi.org/10.1016/j.ijhydene.2013.07.036
[41] Tarkowski R, Uliasz-Misiak B. Towards underground hydrogen storage: A review of barriers. Renew Sust Energ Rev. 2022;162:112451. https://doi.org/10.1016/j.rser.2022.112451
[42] Thiyagarajan SR, Emadi H, Hussain A, Patange P, Watson M. A comprehensive review of the mechanisms and efficiency of underground hydrogen storage. Journal of Energy Storage. 2022;51:104490. https://doi.org/10.1016/j.est.2022.104490
[43] Transport. Transport 4.0 Development of electromobility and hydromobility in the world and in Poland. Part II Infrastructure ▪ Financing ▪ Arp Initiatives. Warszawa: 2021.
[44] US Department of Energy (DOE). Comparison of specific energy (energy per mass or gravimetric density) and energy density (energy per volume or volumetric density) for several fuels based on lower heating values. https://www.energy.gov/eere/fuelcells/hydrogen-storage
[45] Wei H, Shao A, Hua J, Zhou L, Feng D. Effects of applying a Miller cycle with split injection on engine performance and knock resistance in a downsized gasoline engine. Fuel. 2018;214:98-107. https://doi.org/10.1016/j.fuel.2017.11.006
[46] Xu H, Gao J, Yao A, Yao C. The relief of energy convergence of shock waves by using the concave combustion chamber under severe knock. Energ Convers Manage. 2018; 162:293-306. https://doi.org/10.1016/j.enconman.2018.02.024
[47] Xu X, Xu H, Zheng J, Chen L, Wang J. A high-efficiency liquid hydrogen storage system cooledby a fuel-cell-driven refrigerator for hydrogen combustion heat recovery. Energ Convers Manage. 2020;226:113496. https://doi.org/10.1016/j.enconman.2020.113496
[48] Yang F, Wang J, Zhang Y, Wu Z, Zhang Z, Zhao F et al. Recent progress on the development of high entropy alloys (HEAs) for solid hydrogen storage: a review. Int J Hydrogen Energ. 2022;47(21):11236-11249. https://doi.org/10.1016/j.ijhydene.2022.01.141
[49] Yu M, Wang K, Vredenburg H. Insights into low-carbon hydrogen production methods: Green, blue and aqua hydrogen. Int J Hydrogen Energ. 2021;46(41):21261-21273. https://doi.org/10.1016/j.ijhydene.2021.04.016

Jędrzej Matla, MEng. – PhD student, Wrocław University of Science and Technology, Poland.
e-mail: *jedrzej.matla@pwr.edu.pl*

Prof. Andrzej R. Kaźmierczak, DSc., DEng. – Faculty of Mechanical Engineering, Wrocław University of Science and Technology, Poland.
e-mail: *andrzej.kazmierczak@pwr.edu.pl*

Piotr Haller, MEng. – Faculty of Mechanical Engineering, Wrocław University of Science and Technology, Poland.
e-mail: *piotr.haller@pwr.edu.pl*

Marcin Trocki, MEng. – Research and Development Centre, AC S.A. Białystok, Poland.
e-mail: *marcin.trocki@ac.com.pl*

Article citation info:
Szczepański E, Jachimowski R, Rudyk T. Simulation studies of fleet vehicle selection in terms of pollutant emissions. Combustion Engines. 2024;196(1):80-88. https://doi.org/10.19206/CE-169802

Emilian SZCZEPAŃSKI
Roland JACHIMOWSKI
Tomasz RUDYK

Combustion Engines
Polish Scientific Society of Combustion Engines

Simulation studies of fleet vehicle selection in terms of pollutant emissions

ARTICLE INFO

Received: 2 June 2023
Revised: 11 July 2023
Accepted: 19 July 2023
Available online: 10 August 2023

This article presents the vehicle selection problem in the vehicle fleet of a retail and service company. In practical solutions, fleet managers focus on minimizing TCO (total cost of ownership) while ignoring the impact of the fleet on the environment. Therefore, a literature review of current solutions in fleet selection and their determinants is presented. Considering the latest trends and regulations, an optimization model for vehicle selection was developed, considering the issues of emissions and external costs. The developed model was implemented in a simulation environment, and a sensitivity analysis of the solutions obtained was carried out. The research made it possible to indicate the impact of the pollutant emission factor on the fleet structure.

Key words: *fleet management, pollutant emission, optimization model, simulation studies, FlexSim*

1. Introduction

Car fleet management is a set of processes to ensure mobility within a given enterprise. They include planning and organizing the transport of people and materials, optimizing the use of rolling stock, managing safety, and ensuring economic efficiency as part of the total cost of vehicle ownership (TCO) [4, 24, 29].

The selection of vehicles for the fleet is an essential aspect of the enterprise functioning, especially for those with high mobility needs and, thus, a large fleet in terms of quantity. Fleet managers in this aspect are mainly guided by TCO, including the costs of financing vehicles, materials, fuel, service, and insurance. Other factors influencing the choice of the vehicle include engine capacity, body style, and equipment. Practical experience shows that environmental impact and safety issues are marginalized or ignored during vehicle selection. These aspects are taken into account only through the economic calculation related to vehicle equipment and fuel consumption [2, 8, 23].

Due to the great emphasis on sustainable transport systems development, which is often overlooked in the actual decisions of fleet managers, this article examines the impact of the selection of vehicles for the fleet in terms of emissions of pollutants (exhaust gases) into the environment. This is an important issue due to the share of fleet vehicles in the total number of vehicles on the road (in Poland 74% are fleet vehicles [27]. Thus, even a slight unit reduction in the negative impact of the fleet functioning on a national scale will bring significant benefits. In addition, this aspect is important due to the impact on the indirect participants of transport processes, their health, and life comfort. It is also significant from the point of view of the company's image, which is increasingly influenced by care for the environment.

Therefore, the purpose of this article is to conduct research showing the impact of the selection of the vehicle fleet according to the main criterion, which is the TCO on pollutant emissions, as well as a comparison of this approach with the approach that takes into account the external costs of exhaust emissions. The article in the following parts has been organized as follows: section 2 is a literature review of vehicle fleet management in terms of TCO and pollutant emissions, section 3 is a description of the research method used in this article, section 4 is a mathematical formalization of the fleet selection problem, and a simulation model, section 5 is a calculation example. The article ends with section 6, i.e., conclusions from the conducted considerations and directions for further work.

2. Literature review

The research undertaken in this article focuses on the area of environmentally friendly transport solutions. The background for the work is research in the aspect of criteria for the selection of vehicles for the fleet, TCO, pollutant emissions, and vehicle fleet management.

Undoubtedly, costs play a vital role in the transport system functioning [11, 13]. The most popular metric is the Total Cost of Ownership [3, 18]. The research conducted in [18] indicates the dominant character of this indicator. They also show that the issues of ecology in terms of exhaust emissions are often overlooked, and the use of alternative fuels is analyzed mainly in terms of TCO. In Polish conditions, based on surveys conducted with fleet managers, a fleet manager who plans to replace the fleet is guided by costs in the first place [3]. In the first place is the monthly cost of the vehicle. A very common approach to cost analysis is to consider only the amount of the rental installment or the cost of leasing or purchasing the vehicle. Thanks to the TCO analysis, and as it results from the research carried out in [3], it is essential in the process of comparing the total costs of different vehicles to take into account operating costs, and mainly fuel. Safety issues are marginalized, and only 10% of fleet managers set the selection criterion focusing on ensuring safety. Only 2% of fleet managers pay attention to ecological issues. TCO is the primary criterion for selecting vehicles to carry out tasks, fleet operational management, and rolling stock renewal planning. Paper [14] presents studies in which TCO is an indicator that allows the selection of vehicles in a short-term rental – in a car rental company. The considerations were mainly based on economic aspects. The TCO criterion also allows fleet managers to consciously plan fleet replacement (FRP –

fleet replacement problem). This aspect was considered in the work [17], where, considering the preferences of fleet users, guidelines for selecting specific vehicles were proposed. The selection of vehicles based on TCO but considering the vehicle loss ratio and its impact on costs was considered in [23]. Another approach to selecting vehicles for the fleet is a detailed analysis of the operational characteristics of the vehicles. Such an approach was presented in [10].

Regarding heavy goods vehicles, the authors of the report [7] considered the total cost of ownership. They performed a spatial and temporal analysis of different vehicles for six powertrain technologies, including diesel, hybrid electric, plug-in hybrid electric, compressed natural gas, battery, and electric fuel cell. More and more often, in terms of TCO, a comparison of the use of vehicles with different drive technologies is considered. As the authors of the paper [24] indicate, eLCV vehicles (electric light commercial vehicles), even though they have a higher TCO/km than conventional vehicles, are a significant competition to conventional vehicles, taking into account financial and regulatory incentives and the possibility of charging them at the company base. The authors [29] analyzed the use of eLCV from the economic and environmental point of view. The research presented included an analysis of trends in the EU and the impact of vehicle electrification on CO_2 emissions reduction, showing that it is possible to reduce emissions by 30% by 2030 with LCV. They also addressed the issue of total cost of ownership (TCO) compared to conventional vehicles. A similar case was discussed in works [2, 4, 25]. From the point of view of environmental impact, interesting studies are presented in article [8], discussing the issue of noise emission from eLCV.

The works presented above consider the aspect of using environmentally friendly vehicles. However, their selection is mainly based on assessing TCO or CO_2 emissions. More detailed studies on exhaust emissions are not directly related to the selection of vehicles for the tasks in the company's fleet. These studies include analyzes of exhaust gas emissions in transport systems on a macro scale, e.g., in works [5, 12, 22].

An important basis for these studies are the pollution emission models. In this respect, measurements are carried out in real conditions to determine the actual level of exhaust gas emissions depending on various road conditions and traffic areas [1, 20]. However, these studies are expensive, and a detailed analysis of a wide range of vehicles, various drives, and environmental conditions would be ineffective in decision-making models and practical use by fleet managers. Hence, it is possible to use predictive models for pollutant emissions based on averaged indicators. Detailed characteristics and possibilities of their use are presented in a review article [15].

A rather difficult issue is assessing the impact and the possibility of using zero-emission vehicles. Such research regarding selecting zero-emission vehicles to carry out tasks was presented in works [9, 21].

Many factors, as well as an extensive structure of processes within the vehicle fleet management framework, require appropriate methods and tools. For this purpose, optimization and simulation tools are used to support decision-making processes. They are based on mathematical models of the task assignment problem in terms of single and multi-criteria, as well as algorithms that allow to determine solutions. The work [6] presents the integration of forecasting, simulation, and optimization techniques in the performance and revenue management system in a short-term rental company – Europcar. Such approaches, often called hybrid ones, allow to consider the problem of fleet selection in a multi-faceted and comprehensive way and to study the impact of the fleet structure on its effectiveness. Similar works considering the hybrid approach in the application of decision support in fleet management were presented for example in [19, 30].

Summing up the literature analysis, it should be stated that in both scientific and industry publications, the problem of selecting vehicles, considering alternative technologies that reduce pollutant emissions is increasingly discussed. In these studies, however, the main emphasis is placed on economic efficiency or possibly CO_2 emissions. Therefore, this article proposes a method that assesses the impact of the selected fleet structure and the driver to carry out tasks on exhaust emissions in terms of other harmful substances.

3. Research methodology

This article's research subject is the problem of vehicle fleet selection regarding the harmful substances emission. The works will be carried out according to the diagram presented in Fig. 1. It should be emphasized that the research is of an iterative nature, i.e., in the course of the work, both the mathematical model and its implementation were modified to represent the real problem best. The results presented in the article are the result of numerous calculations and synthetically present a solution to the problem of fleet selection, taking into account the issue of harmful substance emissions.

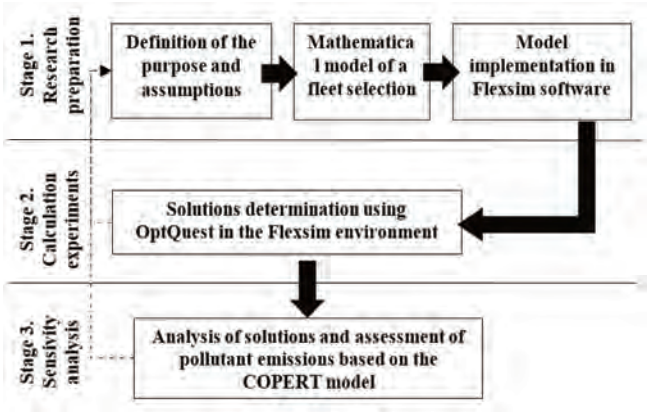

Fig. 1. Methodology of the research on the impact of the vehicle fleet selection on pollutant emissions

Stage 1. Research preparation. This stage consists of three elements. The first element is to define the research's purpose and make assumptions for the calculations. Another element is the development of a mathematical model containing the characteristics of the input data, decision variables, constraints imposed on the solution, and the criterion function. The last element is the implementation of the

developed mathematical model in the Flexsim environment and the mapping of the process of carrying out tasks by the vehicle fleet. These elements in the application for the fleet selection problem are presented in Chapter 4.

Stage 2. Computational experiments. At this stage, based on the developed model, its implementation, and adopted assumptions, solutions to the fleet selection problem are determined, i.e., the values of decision variables that meet the task constraints are defined. This is achieved using the OptQuest module in the Flexsim environment. Searching the solution space in the OptQuest module is achieved using a metaheuristic algorithm. Thus, a set of solutions is returned. Computational experiments were carried out considering single and multi-criteria optimization. The results of the calculations are presented in Chapter 5.2.

Step 3. Sensitivity analysis. The last stage of the research is the analysis of the sensitivity of the solutions to changes in the input data, as well as the assessment of the emission of harmful substances. The input data and vehicle traffic conditions, including the average speed and average distance, as well as the number of serviced areas, were changed for the best solutions identified during optimization. Additional assessment indicators were determined in the field of ownership costs and exhaust gas emissions using the COPERT model [16]. The analysis of solutions is presented in Chapter 5.3.

4. Mathematical and simulation model

4.1. Assumptions

As already indicated, vehicle fleet management is a complicated decision-making process. At the same time, it is possible to use mathematical and simulation modeling tools to map existing problems and support managers in making decisions. The aim is to conduct research showing the impact of the selection of the vehicle fleet according to the main criterion, which is the TCO, on pollutant emissions, as well as comparing this approach with the approach that considers the external costs of exhaust emissions. For research, the following assumptions were made:

- the mathematical model of fleet management is developed using the set theory
- the simulation model is developed in the Flexsim environment
- the mapped decision problem concerns a commercial enterprise and is built for the needs of managing a fleet of passenger vehicles in terms of the selection of resources for the implementation of the tasks
- the solution of the formulated task includes the determination of decision variables for the interpretation of the vehicle number and the driver number assigned to the service of a given area
- the analysis period is the number of days in which the solution to the fleet selection problem is considered
- the analysis period should correspond to the time horizon of vehicle financing or depreciation
- the selection of the driver-vehicle set for serving the area does not change during the analysis period, and this is based on the assumption that the vehicle is regarded as an individual working tool and an additional benefit for the employee
- the number of services in the area is the expected value of the sum of random variables defining the occurrence of the service. The occurrence of service, and the intensity, is described by a certain probability distribution
- the distance during the service of a given area is also a random variable, and its value is described by a certain probability distribution
- the vehicle fleet may be heterogeneous in terms of make, model, or vehicle characteristics
- the model includes driver training in the field of eco-driving
- own financing of the vehicle was adopted
- the optimization criteria were the average income from completed tasks and external costs resulting from CO_2 emissions per task
- only exhaust emissions resulting from vehicle use are considered in the model. Other emissions are omitted. In addition, noise emissions or, for example, particulate matter from the braking system are not taken into account
- solving the optimization task in terms of various criteria results in a set of solutions subject to further analysis, including the use of emission factors from the COPERT model.

The developed model considers the randomness of two model parameters, i.e., the occurrence of service and the distance covered during its implementation. This approach is aimed at mapping the variability in the tasks performed and the different characteristics of service areas. For example, in urban areas, there may be a lot of tasks, and the distance covered during their implementation may be small.

4.2. Mathematical formulation of the vehicle fleet selection problem in terms of pollutant emissions

The developed model considers elements such as drivers, vehicles, service areas, and their characteristics. In addition, it was necessary to define decision variables, criterion functions, and constraints to formulate optimization tasks. This is presented in the next part of the article. For the formalization of the model, a time horizon (analysis period) was adopted, defined as a set T which elements are the numbers of individual days $\mathbf{T} = \{t: t = 1,2,\ldots,T\}$ where value T depends on the length of the analysis period, e.g., for a period of one year, it will be 365. The set of vehicles in the model was formulated as $\mathbf{NV} = \{nv: nv = 1,2,\ldots,NV\}$, a set of drivers as $\mathbf{ND} = \{nd: nd = 1,2,\ldots,ND\}$ and a set of service areas $\mathbf{NA} = \{na: na = 1,2,\ldots,NA\}$. The elements of the above sets have the interpretation of the numbers of vehicles, drivers, and service areas, respectively, and take values from the set of natural numbers. The decision variables in the vehicle fleet selection problem have binary values: y1(nv,na) and have the interpretation of the vehicle assignment to the service area and interpretation of the driver assignment to the service area. Decision variables have value 1 when the vehicle nv and driver nd are assigned to service area na. Two criteria functions were formulated. Function F1 (equation 1) has an interpretation of the company's income from the tasks performed. Function F2 (equation 2) has an interpretation of CO_2 emission as a result of the tasks implementation.

$$F1 = \frac{\sum_{na \epsilon \mathbf{NA}} [INC(na) - CC(na) - CE(na) - CD(na)]}{\sum_{na \epsilon \mathbf{NA}} \sum_{t \epsilon \mathbf{T}} s(na,t)} \rightarrow \max \quad (1)$$

$$F2 = \frac{CCO_2 \cdot \sum_{na \epsilon \mathbf{NA}} \left[\sum_{nv \epsilon \mathbf{NV}} \left[\begin{bmatrix} y1(nv,na) \cdot \\ \cdot \sum_{t \epsilon \mathbf{T}} \begin{bmatrix} s(na,t) \cdot dist(na,t) \cdot \\ fu(nv) \cdot \\ \cdot \sum_{nd \epsilon \mathbf{ND}} \begin{bmatrix} dr(nd) \cdot \\ y2(nd,na) \end{bmatrix} \\ \cdot ECO_2(nv) \end{bmatrix} \end{bmatrix} \right] \right]}{\sum_{na \epsilon \mathbf{NA}} \sum_{t \epsilon \mathbf{T}} s(na,t)} \rightarrow \min \quad (2)$$

$$\forall na \, \epsilon NA \quad INC(na) = zp(na) \cdot \sum_{t \epsilon \mathbf{T}} s(na,t) \quad (3)$$

$$\forall na \, \epsilon NA \quad CC(na) = \sum_{nv \epsilon \mathbf{NV}} \begin{bmatrix} y1(nv,na) \cdot T \cdot \\ \cdot (cp(nv) + ci(nv)) \end{bmatrix} \quad (4)$$

$$\forall na \, \epsilon NA \quad CE(na) = \sum_{nv \epsilon \mathbf{NV}} \left[\left[\begin{bmatrix} y1(nv,na) \cdot \\ \sum_{t \epsilon \mathbf{T}} [s(na,t) \cdot dist(na,t)] \cdot \\ \left(\begin{matrix} cr(nv) + \\ cf(nv) \cdot fu(nv) \cdot \\ \sum_{nd \epsilon \mathbf{ND}} [dr(nd) \cdot y2(nd,na)] \end{matrix} \right) \end{bmatrix} \right] \right] \quad (5)$$

$$\forall na \, \epsilon NA \quad CD(na) = \sum_{nd \epsilon \mathbf{ND}} \begin{bmatrix} y2(nd,na) \cdot \\ [T \cdot cd(nd) + cs(nd)] \end{bmatrix} \quad (6)$$

$$\forall na \, \epsilon NA \quad \sum_{nd \epsilon \mathbf{ND}} y1(nv,na) = 1 \quad \wedge \quad \sum_{nd \epsilon \mathbf{ND}} y2(nd,na) = 1 \quad (7)$$

The F1 function is determined on the basis of the difference in the company's income INC(na) – equation 3, fixed costs of vehicles CC(na) – equation 4, running costs CE(na) – equation 5, as well as the driver costs CD(na) – equation 6. Company income INC(na) is the product of the average income from a single service in the area – zp(na) and the number of services in the area s(na,t). Value s(na,t) = 1 means service of area na in moment t, 0 when there is no such a service. Area service in moment t is performed with the probability described by the selected distribution. Vehicle fixed costs CC(na) results from the involvement of vehicle nv, analysis period T and unit costs of vehicle depreciation cp(nv) and the insurance costs ci(nv). Vehicle running costs CE(na) depends on the total travel distance of a vehicle nv, which results from the number of services s(na,t) and a distance dist(na,t) in a given area. Distance covered during the service in an area na in moment t is a random variable described by a certain probability distribution. These costs are the product of the distance and the service costs per unit of distance – cr(nv), as well as the unit costs of fuel cf(nv) and the amount of fuel consumed per unit of distance fu(nv). Fuel consumption can be reduced with driver training dr(nd). The correction factor dr(nd) may have values of less than 1 when the driver applies eco-driving principles. Still, it may also be greater than 1 when the driver incorrectly uses the vehicle. The last component of function F1 is the driver cost CD(na), which consists of the product of the length of the analysis period and the unit cost of employing the driver cd(nd), as well as the training costs cs(nd). The F2 criterion function has an interpretation of the CO_2 emission costs and thus is calculated based on the total distance and fuel consumption as well as the unit $ECO_2(nv)$ emission and the external cost of the unit CO_2 emission. In the defined problem, there is one constraint described by the formula (7) and has the interpretation of assigning exactly one vehicle and exactly one driver to service a given area.

4.3. Simulation model in the Flexsim environment

The *next* step was to implement the developed model in the Flexsim environment. This environment was chosen because of its high functionality and the ability to use the simulation-optimization approach to conduct research. It is possible to map the structure of the transport system of a given company using the basic elements of the mass service theory in the simulation model. Thus, it is possible to study the impact of various assumptions and changes in given assumptions on the obtained results. To map the transport system, the following were used:

- the source, responsible for generating tasks in the area with the intensity determined by the selected probability distribution
- the processor corresponding to the process of servicing the area by a given set (driver–vehicle) and counting the distance traveled
- the queue corresponding to the counter of completed tasks and the collection of results against specific optimization criteria, as well as other evaluation indicators
- the source-queue system, responsible for counting the analysis time and returning the results of the criterion function.

A diagram for two areas is shown in Fig. 2. To test more service areas, it is necessary to duplicate such a system. To solve the problem of fleet selection, the built-in OptQuest module was used, which is parameterized in accordance with the developed mathematical model and the adopted assumptions.

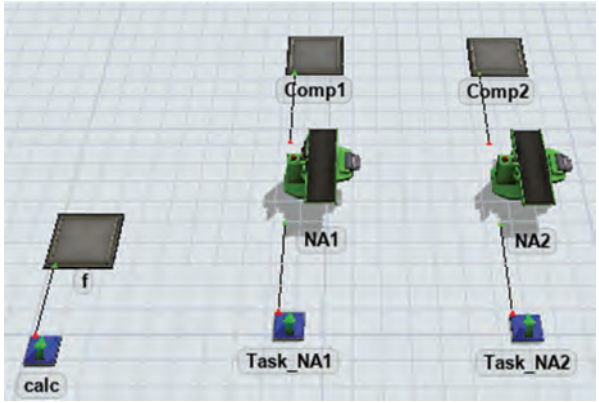

Fig. 2. A block of simulation elements representing the implementation of tasks in the company's transport system

5. Calculation example

5.1. Input data

The calculation example was prepared for a certain fragment of a real transport system of a trading company. The following input assumptions were adopted for the analyses:

- the research was performed on a representative part of the company's fleet to present a method to select resources for tasks
- analysis period T = 1095 days
- number of service areas NA = 5
- number of vehicles NV = 5
- number of drivers NA = 5
- the cost of CO_2 emissions was estimated based on research [6], and as a result, it was adopted as CCO_2 = EUR 0.33/kg
- intensity and distance were described by the Poisson distribution (X∼Poiss(λ)) and the values λs(na,t) for the call intensity and λdist(na,t) for the distance were adopted, respectively, when s(na,t) = 1
- the OptQuest module using metaheuristic methods was used, and the number of iterations of the algorithm was 250 for each scenario.

The data characterizing the vehicles comes from analyzing car dealers' market offers and ADAC reports. The fuel consumption data came from vehicle manufacturers but was further verified against actual fuel consumption based on the company's operating history. The cars were selected from the segment of popular C-class cars (compact, middle class – lower). Due to the nature of the research, the brand and model were considered irrelevant. The lease period was assumed to be 5 years, and the monthly instalment was converted to 1 day. Data for vehicles are presented in Table 1. Characterizing the vehicles descriptively, it should be noted that the vehicle nv = 1 is a diesel vehicle with the Euro 5 combustion standard, characterized by low financing costs, but high service costs (due to age), it is the current vehicle used in the enterprise. Other vehicles are new vehicles. Vehicle nv = 2 is a spark-ignition vehicle with Euro 6 combustion standard, nv = 3 is a compression-ignition vehicle with Euro 6 combustion standard, nv = 4 is a gasoline-free hybrid vehicle with Euro 6 combustion standard, nv = 5 is an electric vehicle. 4 categories of drivers were identified, where nd = 1 drivers are characterized by average driving experience and a neutral impact on fuel consumption, nd = 2 drivers are less experienced drivers with a lower unit bone but higher fuel consumption, nd = 3 drivers are medium experienced drivers with eco-driving training, drivers nd = 4 are drivers with little experience, but with eco-driving training. The cost of the training is around EUR 250. Fuel savings are set at 25% from baseline. Data for drivers is presented in Table 2.

Table 1. Vehicles characteristics

Vehicles (nv)						
nv	unit	nv = 1	nv = 2	nv = 3	nv = 4	nv = 5
cp(nv)	EUR/day	6.7	12.6	14.0	14.5	30.1
ci(nv)	EUR/day	0.201	0.380	0.420	0.440	0.903
cr(nv)	EUR/km	0.078	0.020	0.28	0.17	0.11
cf(nv)	EUR/l	1.08	1.23	1.08	1.23	0.44
fu(nv)	l/km	0.048	0.060	0.045	0.047	0.155
ECO_2(nv)	g/l	2.68	2.35	2.68	2.35	0

Table 2. Drivers characteristics

Drivers (nd)					
data	unit	nd = 1	nd = 2	nd = 3	nd = 4
cd(nd)	EUR/day	55	37	55	37
cs(nd)	EUR	0	0	250	250
dr(nd)	–	1	1.4	0.75	1.05

The areas have the characteristics of mixed areas (urban and rural routes) with different intensities, distances, and revenues. Data for areas are presented in Table 3.

Table 3. Service areas characteristics

Service area (na)						
data	unit	na = 1	na = 2	na = 3	na = 4	na = 5
cp(na)	EUR/task	150	200	250	300	350
λs(na,t)	– (days)	1.2	1.2	1.5	2	2.5
λdist(na,t)	– (km)	60	100	100	120	150

5.2. Experiment results

As a result of the calculations carried out using the experimenter module (OptQuest) in the Flexsim environment, solutions to the problem of selecting vehicles and drivers for tasks in service areas were determined. The obtained solutions are presented in Table 4 according to:

- Single-criteria optimization with respect to F1 (3 best solutions S1.1, S1.2, S1.3) – Fig. 3
- Single-criteria optimization with respect to F2 (3 best solutions S2.1, S2.2, S2.3) – Fig. 4
- Multi-criteria optimization (3 solutions selected from the Pareto front S3.1, S3.2, S3.3) – Fig. 5.

Table 4. Summary of solutions to the problem of selecting vehicles and drivers (decision variables and values of the criterion function)

ScenarioID	S1.1	S1.2	S1.3	S2.1	S2.2	S2.3	S3.1	S3.2	S3.3
y1(1)	1	1	1	5	5	5	4	1	5
y2(1)	4	2	4	4	4	3	4	4	4
y1(2)	1	1	1	5	5	5	5	1	1
y2(2)	4	4	2	4	1	4	4	1	4
y1(3)	1	1	1	5	5	5	5	5	1
y2(3)	4	4	4	4	4	3	4	4	4
y1(4)	1	1	1	5	5	5	5	5	5
y2(4)	4	4	4	4	4	3	4	2	4
y1(5)	1	1	1	5	5	5	4	1	1
y2(5)	4	4	4	4	3	4	4	4	4
F1 (EUR/task)	161.6	161.4	161.3	111.9	111.6	111.1	125.6	137.8	144.4
F2 (EUR/task) [F2·10^{-3}]	4.7	4.9	5.0	0.0	0.0	0.0	1.6	2.7	3.1

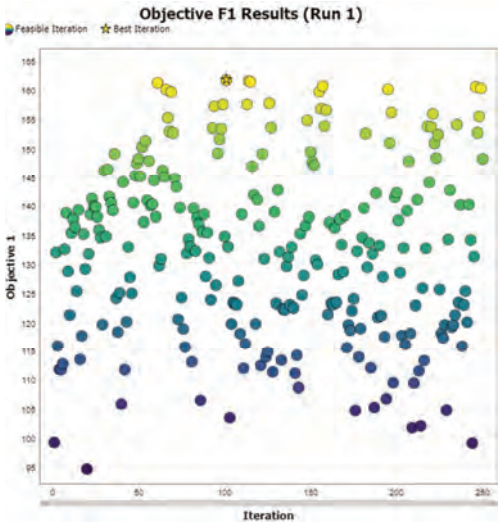

Fig. 3. The space of solutions with respect to the function F1

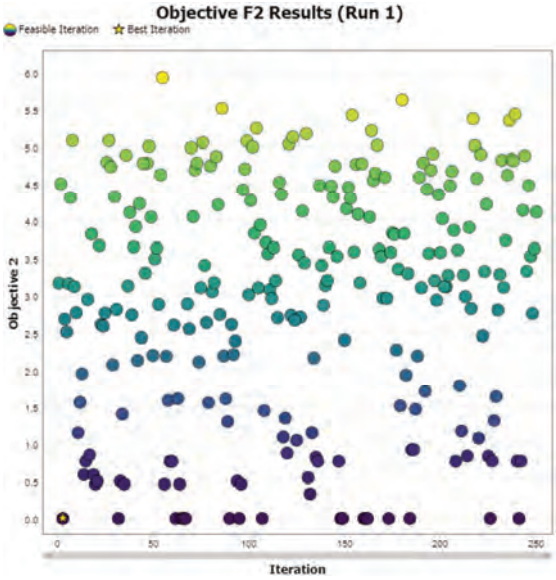

Fig. 4. The space of solutions with respect to the function F2

The graph in Fig. 3 shows the solution space of the formulated decision problem against the F1 criterion. The Y axis is the value of the criterion in EUR/task, while the X axis is the number of iterations of the algorithm. The best solutions are marked in yellow (maximized criterion), and the best solution is marked with an asterisk. Similarly, the space for the F2 function is shown in Fig. 4. In this case, however, the best solutions are marked in black (minimized criterion). On the other hand, Fig. 5 shows the solution space in multi-criteria optimization. The Y-axis shows the F2 (minimized) criterion, and the X-axis shows the F1 (maximized) criterion. Non-dominated solutions, i.e., Pareto optimal, are marked with asterisks. The indicated graphs of the F2 function are in the conversion of 10^{-3}. Analyzing the results presented, the great diversity of the solution space and the relationship between the criterion functions should be pointed out. The increase in corporate income for the assumptions made is associated with higher external costs of CO_2 emissions.

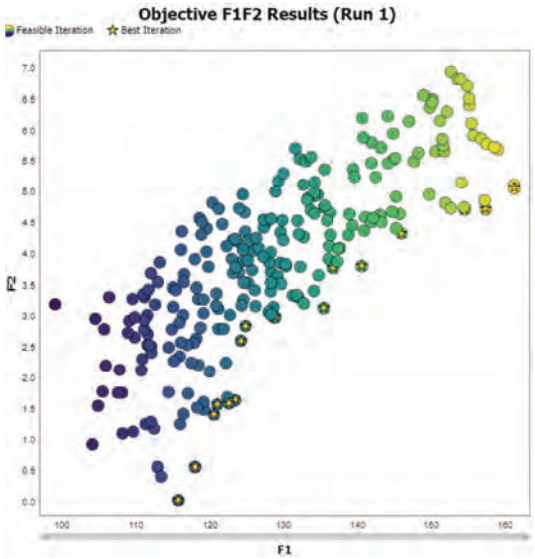

Fig. 5. Pareto solution in multicriteria optimization

5.3. Sensitivity analysis

For further analysis of the obtained solutions, additional measures were introduced, i.e., functions F1.1 and F2.1 presenting income and costs in units [EUR/km], and therefore it is a modification of formulas (1) and (2):

$$F1.1 = \frac{\sum_{na \epsilon \mathbf{NA}} [INC(na) - CC(na) - CE(na) - CD(na)]}{\sum_{na \epsilon \mathbf{NA}} [s(na,t) \cdot dist(na,t)]} \quad (8)$$

$$F2 = \frac{CCO_2 \cdot \sum_{na \epsilon \mathbf{NA}} \left[\sum_{nv \epsilon \mathbf{NV}} \left[y1(nv,na) \cdot \sum_{t \epsilon \mathbf{T}} \left[s(na,t) \cdot dist(na,t) \cdot fu(nv) \cdot \sum_{nd \epsilon \mathbf{ND}} [dr(nd) \cdot y2(nd,na)] \cdot ECO_2(nv) \right] \right] \right]}{\sum_{na \epsilon \mathbf{NA}} [s(na,t) \cdot dist(na,t)]} \quad (9)$$

Moreover, additional measures were introduced to determine the emission of a given type of harmful substance expressed in [kg], i.e.:

$$CO = \frac{efCO}{1000} \cdot \sum_{na \epsilon \mathbf{NA}} \sum_{t \epsilon \mathbf{T}} [s(na,t) \cdot dist(na,t)] \quad (10)$$

$$NO_x = \frac{efNO_x}{1000} \cdot \sum_{na \epsilon \mathbf{NA}} \sum_{t \epsilon \mathbf{T}} [s(na,t) \cdot dist(na,t)] \quad (11)$$

$$NMVOC = \frac{efNMVOC}{1000} \cdot \sum_{na \epsilon \mathbf{NA}} \sum_{t \epsilon \mathbf{T}} [s(na,t) \cdot dist(na,t)] \quad (12)$$

$$PM = \frac{efPM}{1000} \cdot \sum_{na \epsilon \mathbf{NA}} \sum_{t \epsilon \mathbf{T}} [s(na,t) \cdot dist(na,t)] \quad (13)$$

The values of efCO, efNO$_x$, efNMOVC, efPM were adopted on the basis of the COPERTV model [16][16] and are presented in Table 5. Since emissions are related to the mileage of a vehicle with a specific technology, calculations were made in accordance with the fuel consumption over that distance.

For the obtained solutions presented in section 5.2, the results of additional assessment measures were obtained. They are presented in Table 6.

Table 5. Specific emissions of harmful substances based on the COPERTV model

COPERT model emission factors						
Harmful substance	unit	nv = 1	nv = 2	nv = 3	nv = 4	nv = 5
efCO	(g/km)	0.62	0.04	0.049	0.043	0
efNO$_x$	(g/km)	0.065	0.008	0.008	0.001	0
efNMVOC	(g/km)	0.061	0.55	0.17	0.013	0
efPM	(g/km)	0.0014	0.0021	0.0015	0.000142	0

Table 6. Evaluation of the obtained solutions using additional measures

Scenario	S1.1	S1.2	S1.3	S2.1	S2.2	S2.3	S3.1	S3.2	S3.3
CO	227.82	239.58	247.83	0.00	0.00	0.00	5.40	135.04	149.52
NO$_x$	23.88	25.12	25.98	0.00	0.00	0.00	0.13	14.16	15.68
NMVOC	22.41	23.57	24.38	0.00	0.00	0.00	1.63	13.29	14.71
PM	0.51	0.54	0.56	0.00	0.00	0.00	0.02	0.30	0.34
F1.1	7.61	7.59	7.59	5.22	5.07	5.05	5.91	6.51	6.62
F2.1	0.22	0.24	0.24	0.00	0.00	0.00	0.08	0.13	0.13

By adopting the developed criteria, the assumptions were modified, and the designated solutions for the selection of vehicles and drivers for the tasks were re-evaluated. The characteristics of the area where the tasks are carried out have changed. It was assumed that an urban area would affect the change in fuel consumption. The adjusted values are presented in Table 7. It was assumed that hybrid and electric vehicles in urban areas consume less fuel than outside the city, contrary to conventional internal combustion engines. The results of the assessment for the changed assumptions are presented in Table 8.

Table 7. Change in fuel/energy consumption in the sensitivity analysis of the solution

Vehicles (nv)						
data	unit	nv = 1	nv = 2	nv = 3	nv = 4	nv = 5
fu(nv)	l/km or kWh/km	0.062	0.08	0.06	0.042	0.145

To sum up, the considerations carried out should be pointed out that the best solutions from the company's point of view are based on the current fleet and a trained driver. This results from low vehicle financing costs and relatively low fuel consumption, which compensates for higher service costs. Nevertheless, it should also be pointed out that this is definitely the worst solution in terms of pollutant emissions. However, by choosing between scenarios S1.1 and S3.3, giving up 12% of income, it is possible to reduce the external cost of CO_2 emissions by over 41%. The obvious result, guided by ecological considerations, are the S2.1–S2.3 variants, which use electric vehicles, and, thus, in simple terms, do not emit exhaust gases into the atmosphere. However, the cost of financing these vehicles exceeds, for example, in variant S1.1 several times, and thus any savings in operating costs cannot compensate for this in such a period.

Table 8. Results analysis of the sensitivity of the solution to changes in fuel/energy consumption

Scenario	S1.1	S1.2	S1.3	S2.1	S2.2	S2.3	S3.1	S3.2	S3.3
CO	294.27	309.46	320.11	0.00	0.00	0.00	4.83	174.43	193.13
NO_x	30.85	32.44	33.56	0.00	0.00	0.00	0.11	18.29	20.25
NMVOC	28.95	30.45	31.49	0.00	0.00	0.00	1.46	17.16	19.00
PM	0.66	0.70	0.72	0.00	0.00	0.00	0.02	0.39	0.44
F1	159.90	159.68	159.49	112.34	112.10	111.66	126.22	137.09	143.42
F2	6.11	6.34	6.49	0.00	0.00	0.00	1.44	3.51	4.03
F1.1	7.53	7.51	7.51	5.25	5.10	5.08	5.94	6.48	6.58
F2.1	0.29	0.31	0.31	0.00	0.00	0.00	0.07	0.17	0.17

Performing a sensitivity analysis highlights the differences in pollutant emissions. Undoubtedly, older vehicles generate more pollution and, therefore, even higher external costs. Changing the traffic area, and thus fuel or energy consumption, reduced the cost differences between the variants in favor of new vehicles and electric vehicles. Nevertheless, in the adopted analysis period, this impact is too small to be decisive for changing the approach and selecting other vehicles for the fleet. For conventional vehicles, revenue has declined in urban areas; income increases slightly with electric and hybrid vehicles. However, this indicates a certain regularity that the characteristics of the area of operation of the vehicle-driver combination play an important role in the selection of means of transportation. In urban areas, hybrid vehicles perform best, followed by electric vehicles, while combustion vehicles perform best in rural areas. However, from a purely economic calculus point of view, internal combustion vehicles dominate regardless of the work area. It should be noted that in most variants, the drivers were inexperienced but trained in the principles of eco-driving employees. Lower employment costs outweigh training costs.

Conclusions

The purpose of this article was to conduct research showing the impact of the selection of the car fleet according to the main criterion, which is the TCO for pollutant emissions, as well as a comparison of this approach with the approach that considers the external costs of exhaust emissions. The article proposes a research method based on the developed mathematical model and the use of the Flexsim environment with the OptQuest optimization module. The method was used to conduct experiments on a fragment of the transport system of a selected company. It should be pointed out that the proposed method is easy and quick to apply and can be used by fleet managers in practice. It takes into account the marginalized problem of pollutant emissions in their daily work.

The computational experiments were performed on a small computational example. It should be noted that for a larger scale and more diverse fleet, as well as the tasks carried out, the pollutant emissions will be much higher. Thus, the ecological criterion should be an important indicator in the selection of vehicles. In addition, based on the obtained results, certain regularities are visible, which at the same time are barriers to the development of a sustainable transport system and the increase in the share of environmentally friendly vehicles (EFV). They mainly concern the costs of financing such vehicles in the enterprise. Lower fuel consumption or lower service costs cannot compensate for the vehicle's high price. Thus, in Polish conditions, where the approach to minimizing costs and maximizing profits dominates, the possible choice of EFV vehicles will be dictated by other criteria, such as image benefits. This is also influenced by the country's transport policy. The introduction of additional tax reliefs, preferences for users of such vehicles, or higher subsidies for their purchase could increase the popularity of such vehicles.

The directions for further research can also be indicated based on the sensitivity analysis results. It should be noted that the COPERT (Tier 2) methodology adopted considers constant emission values for different motor vehicle technologies. Therefore, to indicate the impact of changing the characteristics of the service areas, this was related to fuel consumption. However, to more accurately predict the impact of changing the area, it would be necessary to use a detailed COPERT methodology (Tier 3), taking into account the type of traffic area and HOT and COLD emissions. More detailed studies, however, require precise data on the speed profile or atmospheric conditions. Therefore, this is the direction of research that could indicate to what extent the advantage of EFV vehicles in terms of emissions is greater than vehicles with a conventional drive, depending on the area. Another area for further research is the introduction of a limitation in the model regarding the maximum costs or limiting the possibility of using vehicles of

a given type. This would better represent the actual decision problem. Additional modifications should also consider many more factors influencing the income effect. It should be pointed out here, for example, the possibility of charging the vehicle at the base (lower energy costs), possible surcharges and discounts, variable operating costs, and finally, reliability and safety. For example, in the case of inexperienced drivers (with lower employment costs), the risk of an accident may increase, and thus the possibility of more damage. As a result, fewer orders will be completed, costs will increase, and the company's revenues will decrease. Another modification to be explored in future studies is the possibility of changing the assignment of a driver to a vehicle within an owned fleet during the analysis period.

Summing up, research in the field of car fleet management in terms of pollutant emissions will be continued because, as indicated based on the literature review and the author's experience, this problem is marginalized in practical applications and, at the same time, is very important from the point of view of the development of a sustainable transport system. At the same time, it should be noted that despite the simplified nature of the decision-making model, based on the research results, it can be indicated that in the current conditions, companies will continue to favor cheaper vehicles to reduce operating costs and maximize income, and thus use vehicles that cause more environmental pollution.

Acknowledgments

This research was funded by the National Science Centre, Poland (project no. 2022/04/Y/ST8/00134). Project title: Energy optimal urban logistics as a service (E-Laas). Project implemented as part of the call ERA-NET Cofund Urban Accessibility and Connectivity (EN-UAC China Call) organized by JPI Urban Europe and the National Natural Science Foundation of China (NSFC) funded from the European Union's Horizon 2020 research and innovation programme under grant agreement No 875022.

Nomenclature

CCO_2	cost of CO_2 emissions
eLCV	electric light commercial vehicles
EFV	environmentally friendly vehicles
F1	interpretation of the company's income from the tasks performed
F2	interpretation of CO_2 emission
FRP	fleet replacement problem
NA	service areas
ND	set of drivers
NV	vehicles in the model
T	numbers of individual days
TCO	total cost of ownership

Bibliography

[1] Andrych-Zalewska M, Chłopek Z, Merkisz J, Pielecha J. Analysis of the operation states of internal combustion engine in the Real Driving Emissions test. Archives of Transport. 2022;61(1):71-88. https://doi.org/10.5604/01.3001.0015.8162

[2] Arroyo JL, Felipe Á, Ortuño MT, Tirado G. Effectiveness of carbon pricing policies for promoting urban freight electrification: analysis of last mile delivery in Madrid. Cent Eur J Oper Res. 2020;28(4):1417-1440. https://doi.org/10.1007/s10100-019-00627-y

[3] Carfleet. Keralla Research Institute, commissioned by Carefleet S.A. 3Q2021; 2021 (in Polish). https://carefleet.pl/storage/2021/09/Raport-285-proc.-firm-z-sektora-MSP-korzysta-z-wynajmu-dlugoterminowego.pdf

[4] Giordano A, Fischbeck P, Matthews HS. Environmental and economic comparison of diesel and battery electric delivery vans to inform city logistics fleet replacement strategies. Transport Res D-TR E. 2018;64:216-229. https://doi.org/10.1016/j.trd.2017.10.003

[5] Gołębiowski P, Żak J, Jacyna-Gołda I. Approach to the proecological distribution of the traffic flow on the transport network from the point of view of carbon dioxide. Sustainability. 2020;12(17):6936. https://doi.org/10.3390/su12176936

[6] Guillen J, Ruiz P, Dellepiane U, Maccarrone L, Maccioni R, Pinzuti A et al. Europcar integrates forecasting, simulation, and optimization techniques in a capacity and revenue management system. Informs J App Analytics. 2019;49(1):40-51. https://doi.org/10.1287/inte.2018.0970

[7] Hunter C, Penev M, Reznicek E, Lustbader J, Birky A, Zhang C. Spatial and temporal analysis of the total cost of ownership for Class 8 Tractors and Class 4 Parcel Delivery Trucks. 2021.08. NREL/TP-5400-71796, 1821615, MainId: 6232. https://www.osti.gov/servlets/purl/1821615/

[8] Ibarra D, Ramírez-Mendoza R, López E. Noise emission from alternative fuel vehicles: Study case. Appl Acoust. 2017;118:58-65. https://doi.org/10.1016/j.apacoust.2016.11.010

[9] Izdebski M, Jacyna M. An efficient hybrid algorithm for energy expenditure estimation for electric vehicles in urban service enterprises. Energies. 2021;14(7):2004. https://doi.org/10.3390/en14072004

[10] Izdebski M, Jacyna-Gołda I, Nivette M, Szczepański E. Selection of a fleet of vehicles for tasks based on the statistical characteristics of their operational parameters. Eksploat Niezawodn. 2022;24(3):407-418. https://doi.org/10.17531/ein.2022.3.2

[11] Jachimowski R, Szczepański E, Kłodawski M, Markowska K, Dąbrowski J. Selection of a container storage strategy at the rail-road intermodal terminal as a function of minimization of the energy expenditure of transshipment devices and CO_2 emissions. Rocz Ochr Sr. 2018;20(2):965-988.

[12] Jacyna M, Merkisz J. Proecological approach to modelling traffic organization in national transport system. Archives of Transport. 2014;30(2):31-41. https://doi.org/10.5604/08669546.1146975

[13] Kwasiborska A, Stelmach A. Analysis of airport traffic in the context of environmental throughput. Transport Prob. 2014;9(1):129-140.

[14] Mazur B, Wasiak M. TCO-Total Cost of Ownership as a tool supporting the selection of a car fleet for car rental companies (in Polish). Prace Naukowe PW Transport. 2018; 123:95-109.

[15] Mądziel M. Vehicle emission models and traffic simulators: a review. Energies. 2023;16(9):3941. https://doi.org/10.3390/en16093941
[16] Ntziachristos L, Samaras Z. Methodology for the calculation of exhaust emissions – SNAPs 070100-070500. European Environment Agency; October 2021:147. https://www.eea.europa.eu/publications/emep-eea-guidebook-2019/part-b-sectoral-guidance-chapters/1-energy/1-a-combustion/1-a-3-b-i/at_download/file
[17] Ogonowski K. The comparison of various financial forms of car fleet replacement. OWPW. Warsaw 2020.
[18] Oliveira LKD, Bertoncini BV, Nascimento CDOL, Rocha LB, Batista LAMDL, Cellin LV. Factors affecting the choice of urban freight vehicles: issues related to Brazilian Companies. Sustainability. 2019;11(24):7010. https://doi.org/10.3390/su11247010
[19] Pérez J, Maldonado S, López-Ospina H. A fleet management model for the Santiago Fire Department. Fire Safety J. 2016;82:1-11. https://doi.org/10.1016/j.firesaf.2016.02.008
[20] Pielecha J, Skobiej K. Evaluation of ecological extremes of vehicles in road emission tests. Archives of Transport. 2020; 56(4):33-46. https://doi.org/10.5604/01.3001.0014.5516
[21] Pyza D, Gołda P, Sendek-Matysiak E. Use of hydrogen in public transport systems. J Clean Prod. 2022;335:130247. https://doi.org/10.1016/j.jclepro.2021.130247
[22] Pyza D, Jacyna-Gołda I, Gołda P, Gołębiowski P. Alternative fuels and their impact on reducing pollution of the natural environment. Rocz Ochr Sr. 2018;20:819-836.
[23] Rudyk T, Szczepański E, Jacyna M. Safety factor in the sustainable fleet management model. Archives of Transport. 2019;49(1):103-114. https://doi.org/10.5604/01.3001.0013.2780
[24] Scorrano M, Danielis R, Giansoldati M. Electric light commercial vehicles for a cleaner urban goods distribution. Are they cost competitive? Res Transp Econ. 2021;85:101022. https://doi.org/10.1016/j.retrec.2020.101022
[25] Sendek-Matysiak E, Pyza D, Łosiewicz Z, Lewicki W. Total cost of ownership of light commercial electrical vehicles in city logistics. Energies. 2022;15(22):8392. https://doi.org/10.3390/en15228392
[26] Statistics Poland (GUS). Development of the methodology and estimation of the external costs of air pollution emitted from road transport at national level. Szczecin: Statistics Poland; 2018;82. https://stat.gov.pl/download/gfx/portalinformacyjny/en/defaultaktualnosci/3576/4/1/1/raport_opracowanie_metodyki_i_oszacowanie_kosztow_zewnetrznych_emisji_zanieczyszczen.pdf
[27] Transport&Enviroment. Boom for registration of luxury cars in Poland due to a tax system that favors polluting cars (in Polish). 2022. https://www.transportenvironment.org/discover/boom-na-rejestracje-samochodow-luksusowych-w-polsce-przez-system-podatkowy-ktory-faworyzuje-zanieczyszczajace-pojazdy/
[28] Trzaskowski D, Wasiak M. ENThe effect of current financing methods on vehicle replacement policy – a case study (in Polish). Prace Naukowe PW Transport. 2017;119:477-492.
[29] Tsakalidis A, Krause J, Julea A, Peduzzi E, Pisoni E, Thiel C. Electric light commercial vehicles: are they the sleeping giant of electromobility? Transport Res D-TR E. 2020;86: 102421. https://doi.org/10.1016/j.trd.2020.102421
[30] Vujanović D, Momčilović V, Vasić M. A hybrid multi-criteria decision making model for the vehicle service center selection with the aim to increase the vehicle fleet energy efficiency. Therm Sci. 2018;22(3):1549-1561. https://doi.org/10.2298/TSCI170530208V

Prof. Emilian Szczepański, DSc., DEng. – Faculty of Transport, Warsaw University of Technology, Poland.
e-mail: *emilian.szczepanski@pw.edu.pl*

Prof. Roland Jachimowski, DSc., DEng. – Faculty of Transport, Warsaw University of Technology, Poland.
e-mail: *roland.jachimowski@pw.edu.pl*

Tomasz Rudyk, MSc. – PhD student at the Faculty of Transport, Warsaw University of Technology, Poland.
e-mail: *tomasz.rudyk@rudykon.pl*

Article citation info:
Siadkowska K, Barański G. Combustion stability for early and late direct hydrogen injection in a dual fuel diesel engine. Combustion Engines. 2024;196(1):89-98. https://doi.org/10.19206/CE-171390

Ksenia SIADKOWSKA
Grzegorz BARAŃSKI

Combustion Engines
Polish Scientific Society of Combustion Engines

Combustion stability for early and late direct hydrogen injection in a dual fuel diesel engine

ARTICLE INFO

Received: 1 June 2023
Revised: 11 July 2023
Accepted: 19 August 2023
Available online: 16 September 2023

The paper presents an analysis of the experimental results of direct hydrogen injection in a dual-fuel diesel engine. The test object is a four-cylinder, four-stroke ADCR engine. The parameters like: indicated mean effective pressure, peak pressure, angle of maximum pressure and released heat were analyzed. Statistical analysis of the obtained results was carried out for each cylinder separately for four different hydrogen doses. Both early and late direct hydrogen injection were analyzed. The significance of the differences for each of the analyzed parameters and type of injection was determined. The stability of the combustion process was evaluated using the coefficient of variation CoV(IMEP).

Key words: *diesel engine, direct hydrogen injection, dual fuel, combustion engine, hydrogen*

1. Introduction

The changed market trends for the further development of internal combustion engines [22] and alternative fuels in vehicles [20] have not stopped research work in this area. In particular, the use of hydrogen, both in the combustion process in internal combustion engines [1, 11, 12] and its obtaining [6, 22] has been consistently popular among scientists. Ongoing research involves both spark-ignition [21] and compression-ignition engines [9, 10]. The experiments conducted just a few years ago let us identify high-pressure direct injection and cryogenic injection technologies in internal combustion engines for further development [7, 8]. Although it is the automotive field internal combustion engines that have led the way over the past decades, they can be applied much more wider, i.e. in aviation [3, 5, 18], marine [2] and stationary applications [14, 15], which justifies their further research. The internal combustion engine emissions admittedly are problematic, but modern fuel cell electric vehicles also require much research and development [4].

The results presented in this publication are a continuation of the research that includes the analysis of the combustion process in a dual-fuel diesel engine with direct hydrogen injection.

The paper [16] presents the results of the study that compares particulate emissions in early and late hydrogen direct injection. The particulate emissions were investigated with a Semtech Ecostar exhaust gas analyzer. In general, the particulate emissions were lower for late hydrogen injection than for early, especially for lower hydrogen doses and loads. Overall, late hydrogen injection resulted in a 23% decrease in particulate emissions relative to early injection. Increasing the hydrogen dose resulted in a multiple increase in particulate emissions and approaching the engine rumble limit.

Combustion process analysis was continued in the paper [17] and the following parameters were studied then: indicated mean effective pressure, maximum pressure, peak pressure angle and heat released. This analysis focused on determining whether there are significant differences between early and late injection. The study case was a single cylinder.

The statistical analysis in the designed experimental plan was globally performed for the various measurement points and indicated that there were no significant differences between early and late hydrogen injection. However, when the selected conditions were separately analyzed, the differences were statistically significant. The relatively large standard deviations for some measurement points may indicate instability in the combustion process. As the load and the share of hydrogen increased, the unrepeatability of the operating process increased. There was a clear phenomenon that required a more detailed analysis so, it was decided to check how the combustion process proceeded in each cylinder separately at the highest engine load. The results of the analysis are presented in this paper.

2. Materials and methods

The test object is an ADCR, 4-cylinder, 4-stroke engine with a displacement of 2,636 cm^3 and a compression ratio 17.5. The glow plugs were replaced by injectors of compressed hydrogen. A view of the test stand is shown in Fig. 1, and a schematic diagram is shown in Fig. 2.

The indicated mean effective pressure, peak pressure, the angle it occurs at and the heat released for four cylinders and four different doses of hydrogen were investigated. The unchanging parameter was the pilot dose of diesel fuel and the initiating torque was experimentally determined as the maximum for the research object. The research plan assumed changing only one parameter – hydrogen injection time, i.e. early (40° after TDC, E symbol) and late (160° after TDC, L symbol) injection. Thus, the effect of just this single parameter on the combustion process was evaluated. The hydrogen injection pressure was 1.2 MPa. During the tests, each point was recorded three times. The addition of hydrogen caused rumbling at some measurement points, despite the experimental being designed within a safety limit. The tests were planned for the 1500 rpm. This rotational speed was selected from the results of tests determin-

ing the load profile where the highest share has the engine load up to 40%, which is 1480 rpm for research object [16].

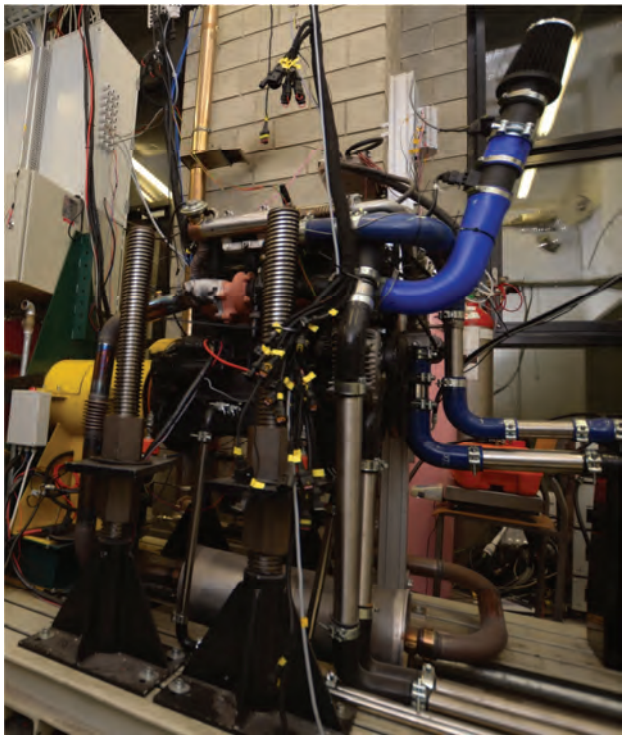

Fig. 1. Test bench

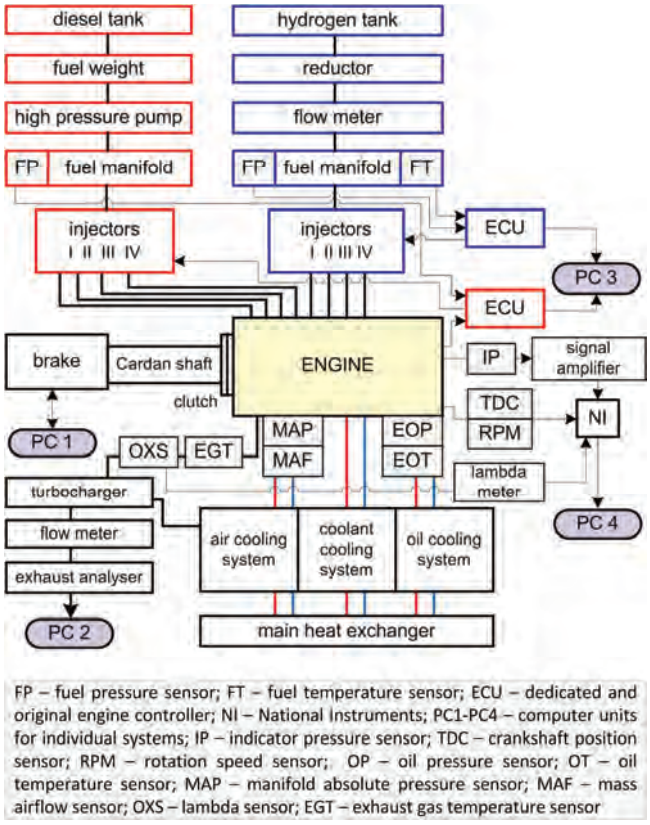

Fig. 2. Diagram of the dynamometer stand

The unrepeatability of the individual cylinders was analyzed and the significance of the differences was determined for the two types of direct hydrogen injection: early and late. Although hydrogen was supplied directly to the combustion chamber, the so-called early injection is similar to indirect injection. Late injection was specified from the preliminary tests of the object, in order to maximize the obtained power and not disrupt the combustion process.

3. Results and discussion

Observing the average values of the results only highlights differences between cylinders and injection times but their nature is unknown. This situation makes it difficult to analyze injection and its effect on the combustion process so box-and-whisker plots were made. Fig. 3 shows how the measurement points were marked.

Fig. 3. Measuring points

Fig. 4–7 show the mean, standard error and standard deviation for the analyzed combustion parameters for each cylinder separately (C1–C4). Each measurement point was repeated and recorded three times. Fig. 4 shows the average values of the indicated mean effective pressure, Fig. 5 shows the maximum pressure values, Fig. 6 shows the values of the maximum pressure occurrence angles, and Fig. 7 shows the released heat for each cylinder separately (C1–C4). The first point is the values obtained for diesel fuel only (H0), the subsequent ones should be considered in pairs (H1E-H1L). The first is early injection (E), the second is late injection (L). The results are shown for four increasing hydrogen shares (H1–H4) and one initial torque for diesel T4 (150 Nm). The maximum torque obtained was 180 Nm at maximum hydrogen flow (H4).

The above graphs suggest the need for a closer analysis of the phenomena occurring in the individual cylinders. At certain measurement points, large standard deviations are apparent. The combustion process in the C4 cylinder deviates from the others at the highest shares of hydrogen. The combustion process needs to be examined in detail to understand the nature of the observed phenomena.

The pressure was measured using AVL GH14D pressure sensors installed in the combustion chamber. The indicated pressure in all cylinders and the crankshaft position were recorded. The heat release during combustion depends mainly on the fuel injection process in the combustion chamber. The heat release rate is determined by the volume of fuel burned per 1 CAD [13]. This value is used to determine the cumulative heat release. Calculation of the heat release rate is carried out based on the equation [24]:

$$\frac{dq_s}{d\alpha} = \frac{1}{\kappa - 1} \cdot \left(V_x \cdot \frac{dp}{d\alpha} + \kappa \cdot p \frac{dV}{d\alpha} \right) \quad (1)$$

where: p – in-cylinder combustion pressure; α – crank angle; q_s – heat release during combustion; κ – the ratio of the specific heats (c_p/c_v) at constant pressure and constant volume, respectively, $\kappa = 1.3$; V_x – in-cylinder volume.

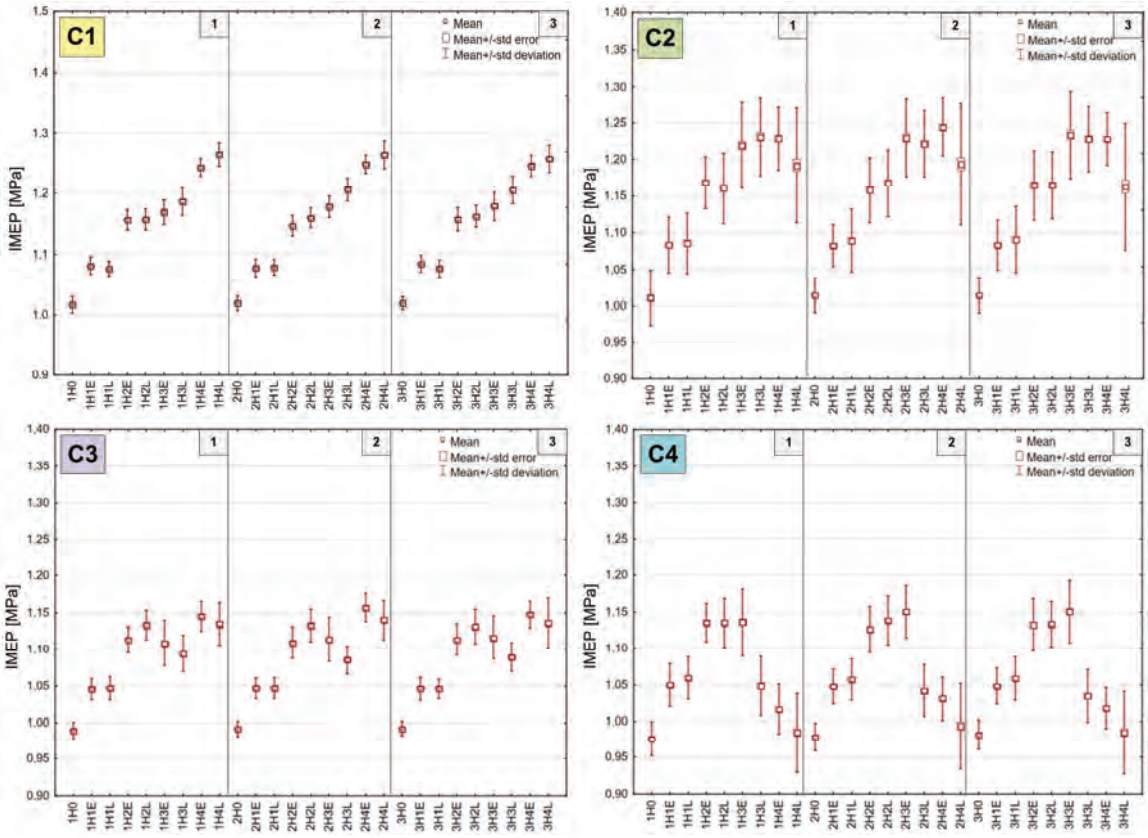

Fig. 4. Box-whisker for the IMEP in all cylinders

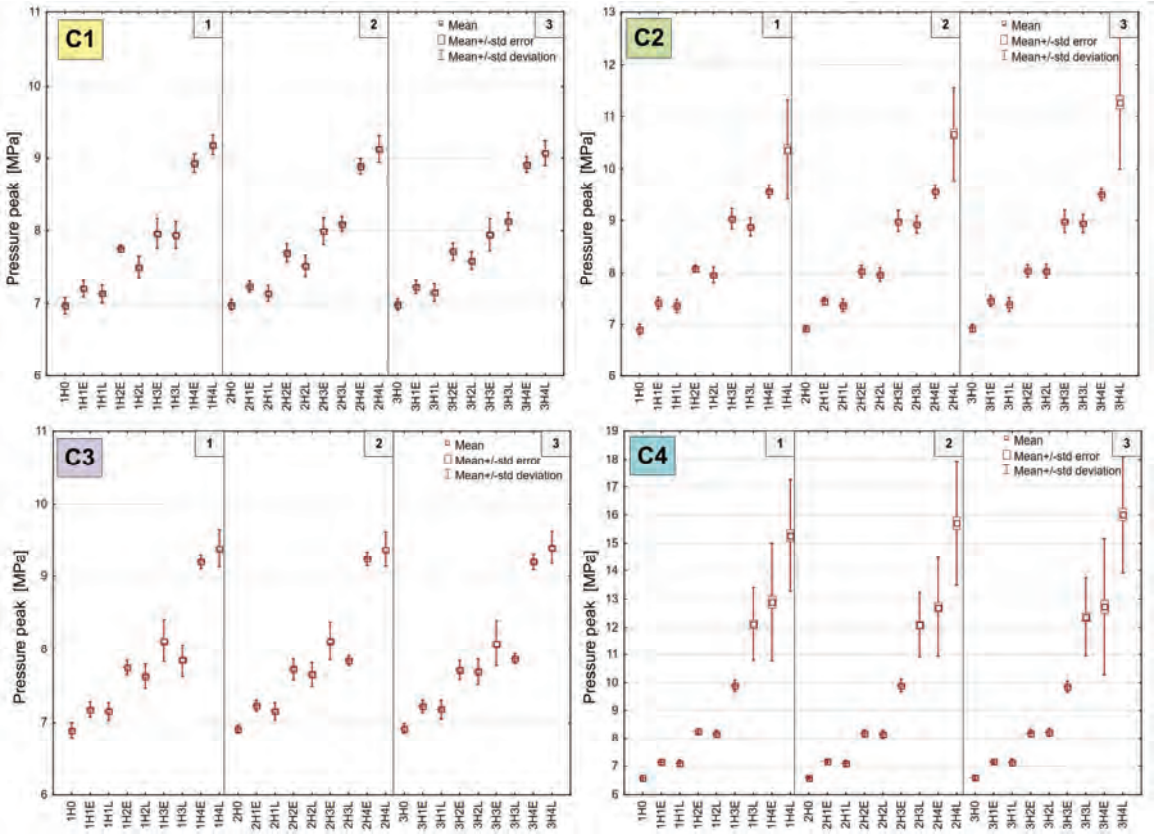

Fig. 5. Box-whisker for the pressure peak in all cylinders

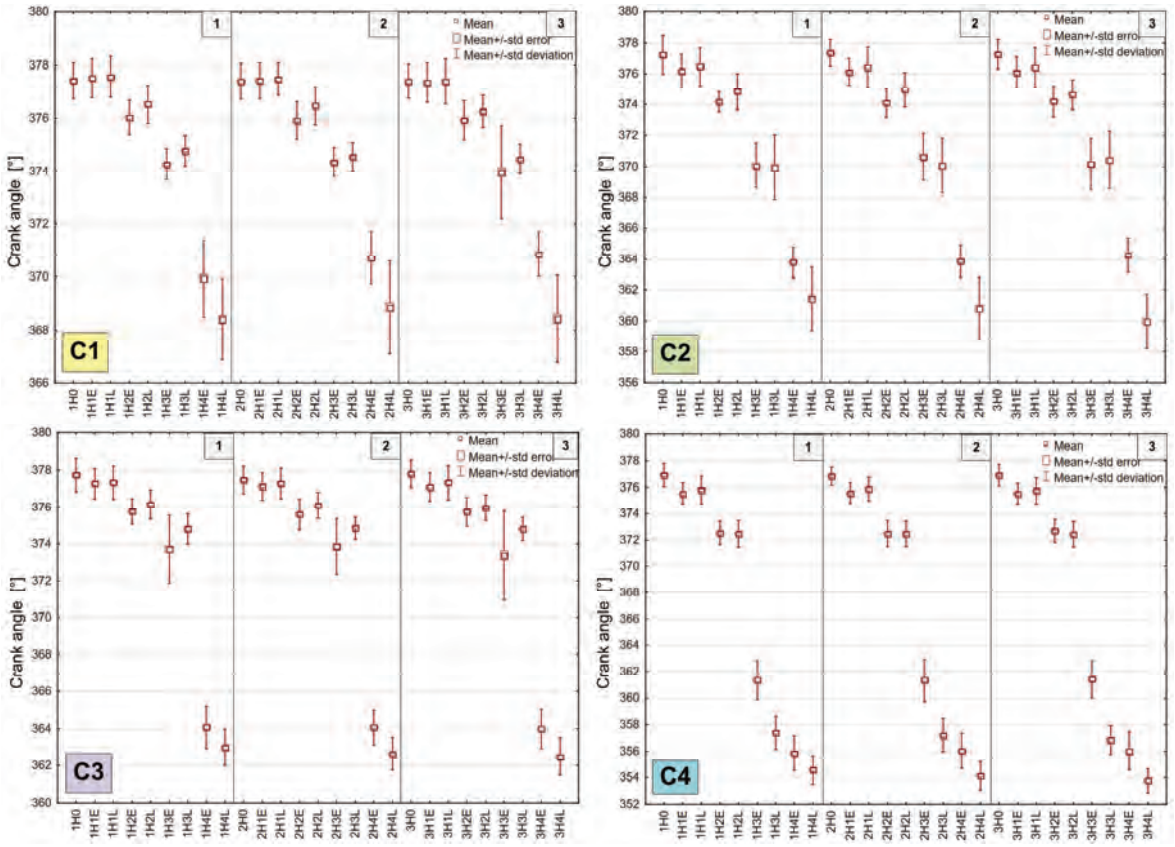

Fig. 6. Box-whisker for the crank angle of pressure peak in all cylinders

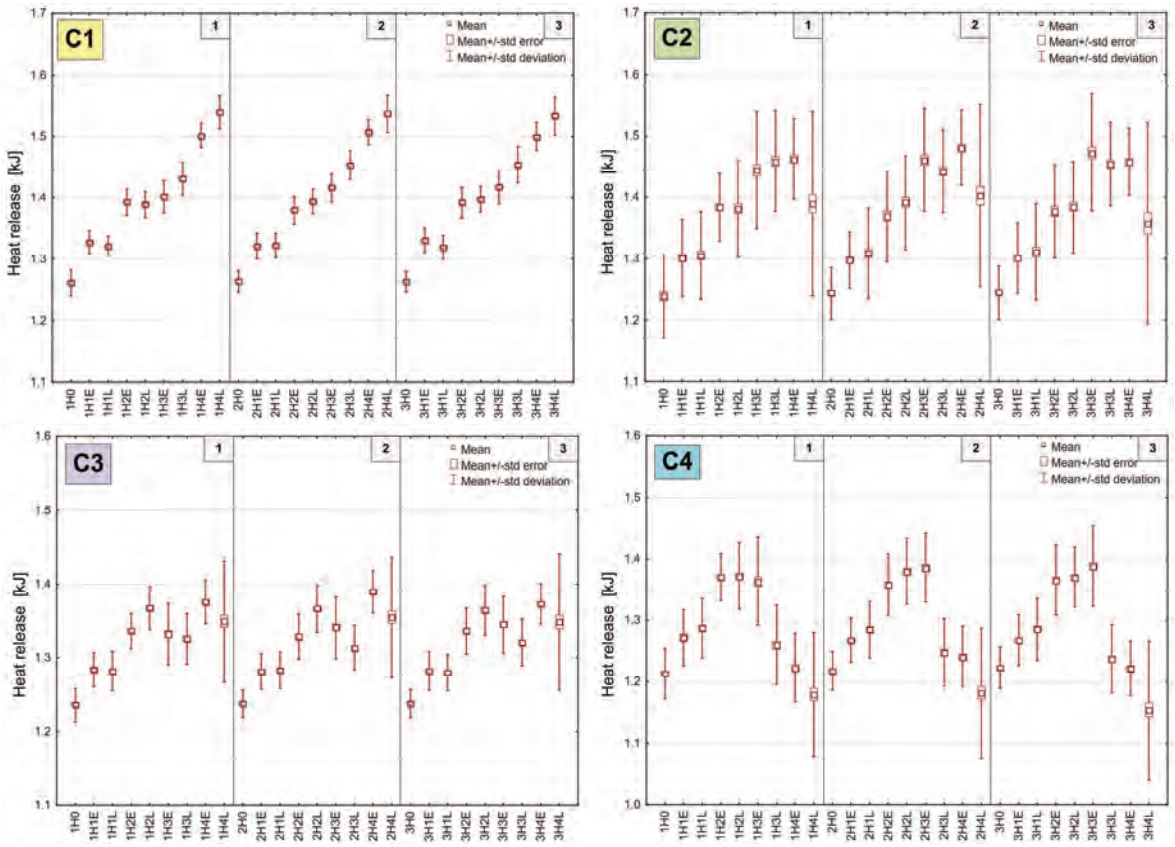

Fig. 7. Box-whisker for the heat released in all cylinders

4. Analysis

The main purpose of the analysis is to determine whether there are significant differences between early and late hydrogen injection for a single cylinder for the selected combustion process parameters. A comparison of the combustion process between cylinders is also an important part of the study.

A Student's t-test analysis was performed for this purpose, and the significance of differences between the analyzed parameters was determined. The null hypothesis of the absence of significant differences between groups was put forward in the following form:

$$H0: \beta i = \beta i^*$$

and the alternative (there are differences between the groups):

$$H1: \beta i \neq \beta i$$

A significance level of $\alpha = 0.05$ was chosen. For the indicated significance level, $t_\alpha = 1.984$ was the boundary value.

The same methodology was followed for all the conducted analyses. The Student's t-distribution tables let us claim that:

1. The results of the analysis are not in the critical area, as $t_i < t_\alpha$ for the analyzed parameters. This means that, according to the analysis, there are no significant differences between the analyzed groups so at a significance level of $\alpha = 0.05$, there are no grounds to reject the null hypothesis H0 in favor of the alternative hypothesis H1.

or

2. The results of the analysis are in the critical area, since $t_i > t_\alpha$. This means that, according to the analysis, there are significant differences between the studied groups so at a significance level of $\alpha = 0.05$, there are reasons to reject the null hypothesis H0 in favor of the alternative hypothesis H1.

The results of the analyses are shown in the following plots for the individual cylinders when the time of hydrogen injection changed and when only diesel fuel (H0) was burnt. Both single artifacts and instability throughout the entire measurement can be seen. To compare the effect of injection timing, early vs. late hydrogen injection pairs were analyzed. To discuss the combustion uniformity, the six pairs of cylinders (cylinder to cylinder) were analyzed.

Figures 8–11 shows the indicated mean effective pressure to compare the early and late injection for four cylinders and four hydrogen doses, i.e. for 16 pairs of early vs. late. The IMEP curves illustrate a regular combustion process for C1 cylinder. In the other cases, cyclic fluctuations or singular irregularities are apparent.

In seven cases, the Student's t-test did not reject the hypothesis of equality, i.e. it did not detect significant differences between early and late injection, but four of these seven cases involve all four cases for C2 cylinder only, while the remaining three cases involve one each for cylinders C1, C3 and C4 for hydrogen dosage H1 or H2 (1H2, 3H1, 4H2). The reason for such an interpretation of the test

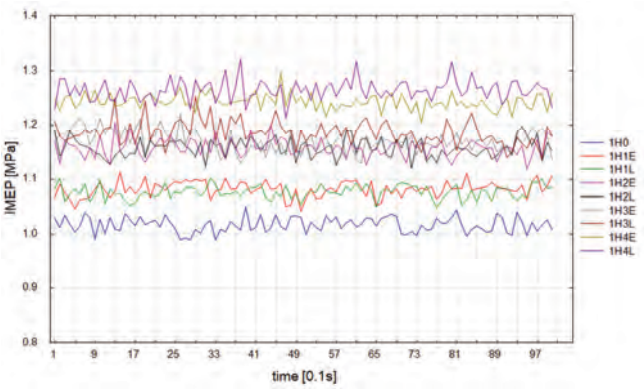

Fig. 8. The IMEP in C1 cylinder

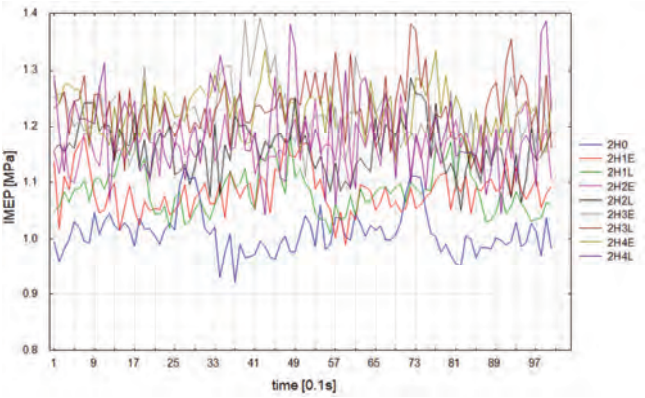

Fig. 9. The IMEP in C2 cylinder

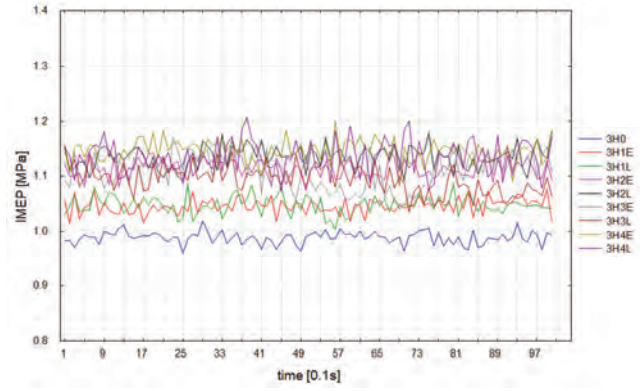

Fig. 10. The IMEP in C3 cylinder

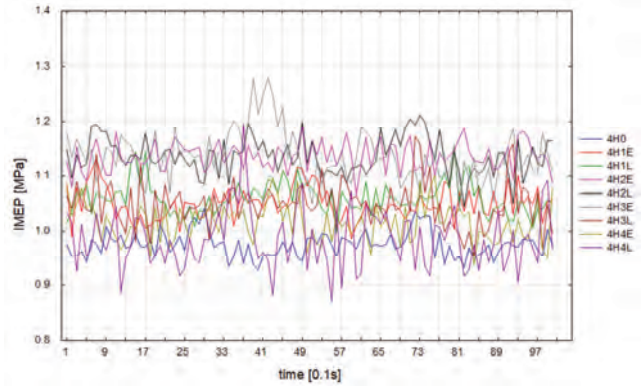

Fig. 11. The IMEP in C4 cylinder

may be more due to large standard deviations than none of differences, which shows the Fig. 4. The application of higher hydrogen doses (H3, H4) shows significant differences for six of the eight measurement points, and for lower doses (H1, H2) for three of the eight points. It can be concluded that the time of injection was statistically significant for IMEP in nine of the sixteen cases of early vs. late injection pairs analyzed.

The indicated mean effective pressure in the individual cylinders was also analyzed for diesel fuel only in order to assess the combustion homogeneity (Fig. 12).

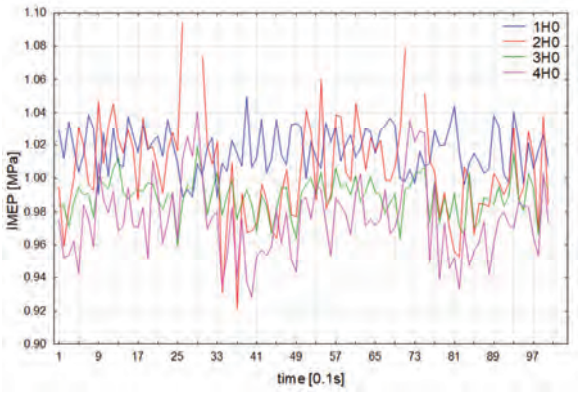

Fig. 12. The IMEP in all cylinders only for diesel fuel

In five of the six cases of the analyzed comparisons, the Student's t-test indicated statistically significant differences. This fact suggests the need to consistently analyze the combustion process independently for each cylinder. The differences may be related to the adopted method of analysis or to the non-uniformity of the test injectors, which may be influenced by the research controller software.

To determine combustion stability and evaluate the differences between early and late injection, coefficient of variation analysis was performed [19]. To evaluate combustion stability, the coefficient of variation of the indicated mean effective pressure CoV(IMEP) is usually taken. This is the standard deviation of the measurement divided by the mean value. CoV(IMEP) was separately determined for each cylinder at successive measurement points. The values of CoV(IMEP) below about 5 % are usually considered desirable since such levels of cyclic fluctuation guarantee smooth engine operation. Figure 13 shows the CoV(IMEP) levels for the recorded operating points. For late injection in the two cylinders at the maximum hydrogen dose, the desired levels of CoV(IMEP) were exceeded, whereas at the other measurement points, the combustion process was stable.

The next analyzed parameter was maximum pressure (Fig. 14–17). Following the same methodology, for maximum pressure, significant differences did not occur only in two cases out of the sixteen analyzed early vs. late injection pairs (1H3, 3H1). This means that the timing of early or late injection in almost 90 % of the analyzed measurement points (14 out of 16) was statistically significant for the maximum pressure values. For the largest applied hydrogen content in the C2 cylinder, single deviations are evident for late injection. In the C4 cylinder, both early and late hydrogen. injection was accompanied by rumbling at the highest (H4) hydrogen dose.

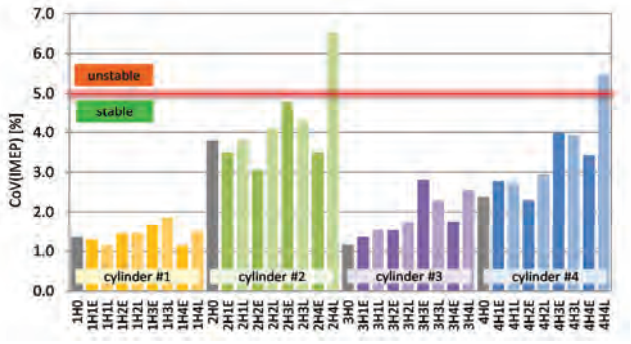

Fig. 13. Coefficient of variation of IMEP for all operating points

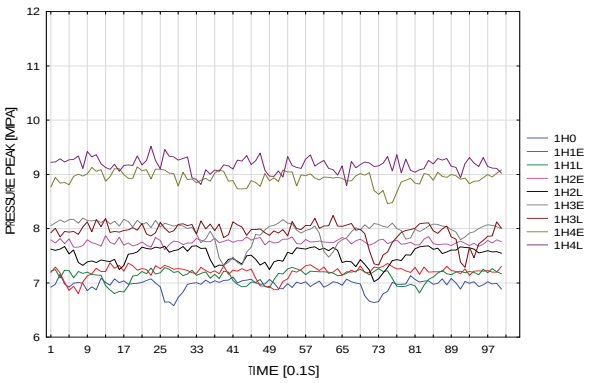

Fig. 14. Peak pressure in C1 cylinder

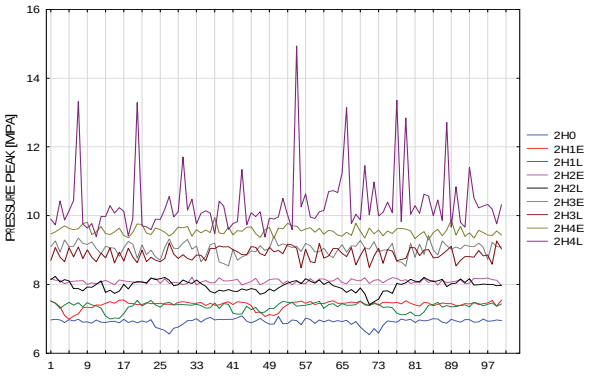

Fig. 15. Peak pressure in C2 cylinder

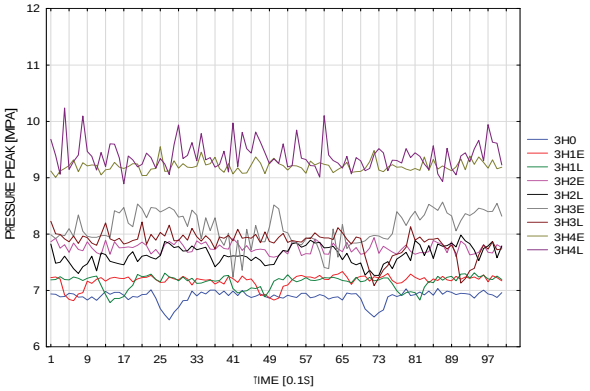

Fig. 16. Peak pressure in C3 cylinder

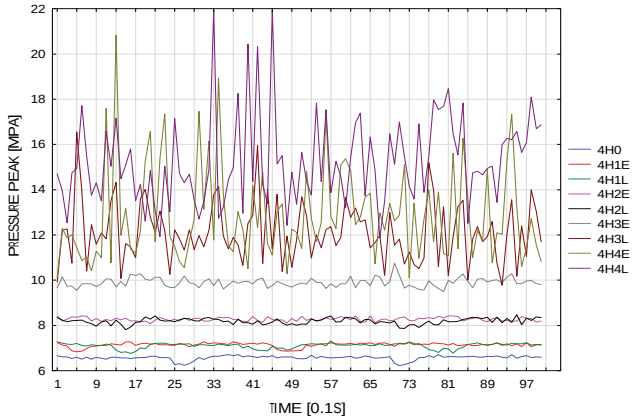

Fig. 17. Peak pressure in C4 cylinder

The maximum pressure in each cylinder was analyzed only when diesel fuel was supplied (Fig. 18). Two pressure fluctuations were observed whose timing matches the IMEP peak in the C2 cylinder. It can also be seen that the maximum pressure in the C4 cylinder is lower than in the other three cylinders.

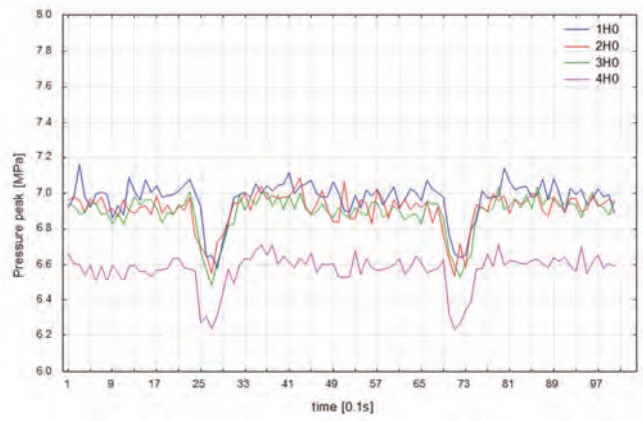

Fig. 18. Peak pressure in all cylinders only for diesel fuel

In five out of the six cases for the four groups analyzed, the Student's t-test indicated statistically significant differences.

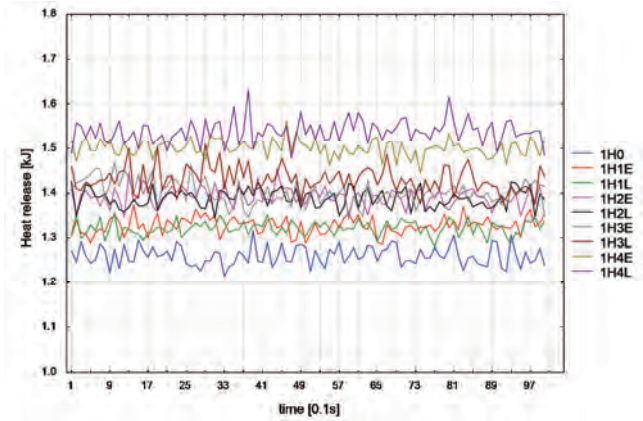

Fig. 19. Heat released in C1 cylinder

The next parameter analyzed was the heat released during combustion in each cylinder and for different hydrogen doses (Fig. 19–22). In the case of C1 cylinder, there are no artifacts, in C3 cylinder they are single, while in C2 and C4 cylinders irregularities in the combustion process for the highest hydrogen doses are well visible. While the early injection caused an increase in heat release, the later injection of hydrogen disrupted the combustion process. The hydrogen dose was not probably completely burned.

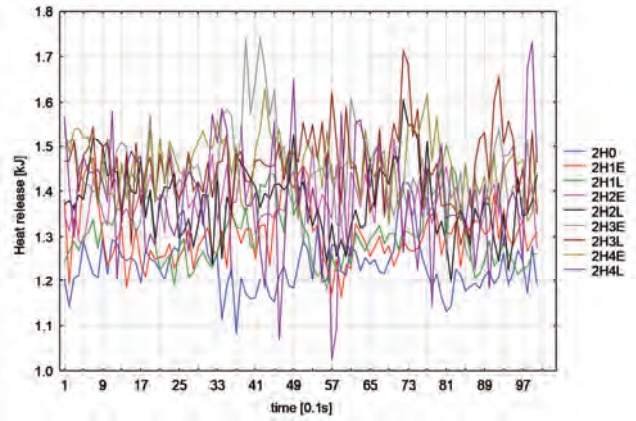

Fig. 20. Heat released in C2 cylinder

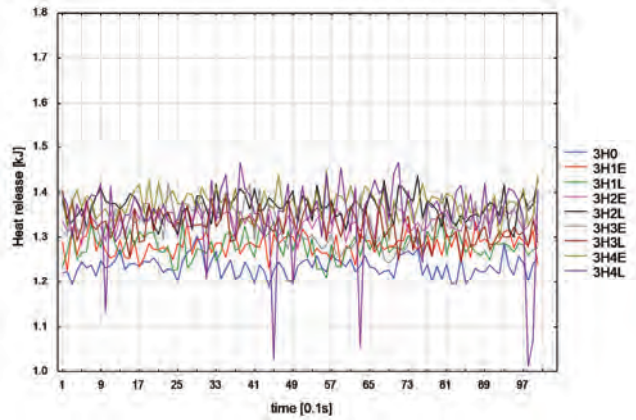

Fig. 21. Heat released in C3 cylinder

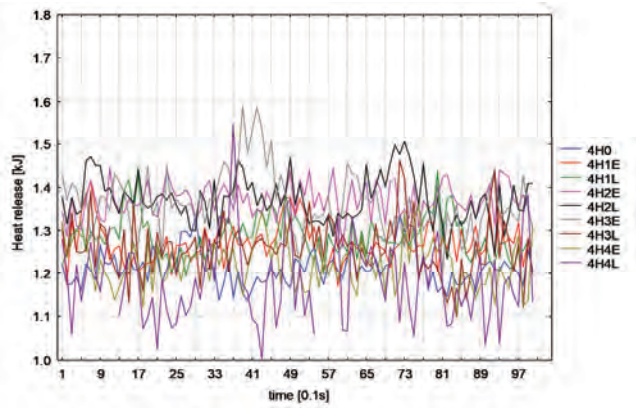

Fig. 22. Heat released in C4 cylinder

The amount of heat released in the individual cylinders on diesel fuel only was analysed (Fig. 23). A heat peak in

the C2 cylinder is clear and coincides in time with a local decrease in maximum pressure.

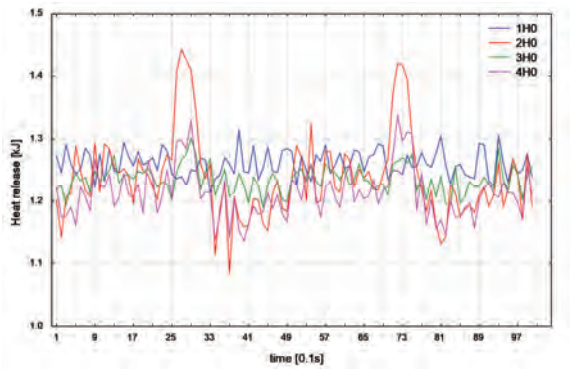

Fig. 23. Heat released in all cylinders only for diesel fuel

In five out of the six cases, the Student's t-test indicated statistically significant differences.

The last parameter analyzed is the angle of maximum pressure occurrence for early and late hydrogen injection (Fig. 24–27). The dominant value for most measurement points is approx. 375 CAD. An increase in the proportion of hydrogen makes maximum pressure occur faster by up to 20 CAD. The late hydrogen injection decreased this value more than the early injection, i.e. it made maximum pressure occur faster.

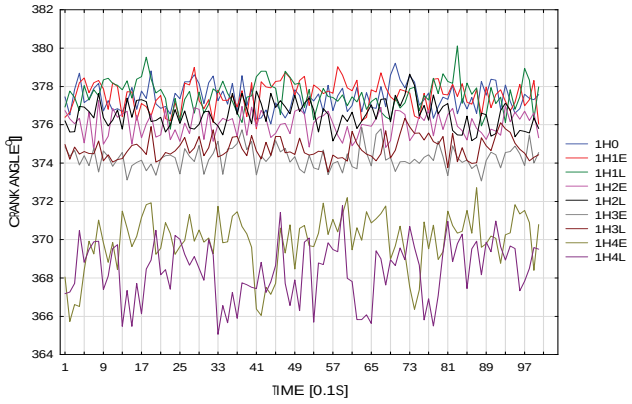

Fig. 24. Crank angle of pressure peak in C1 cylinder

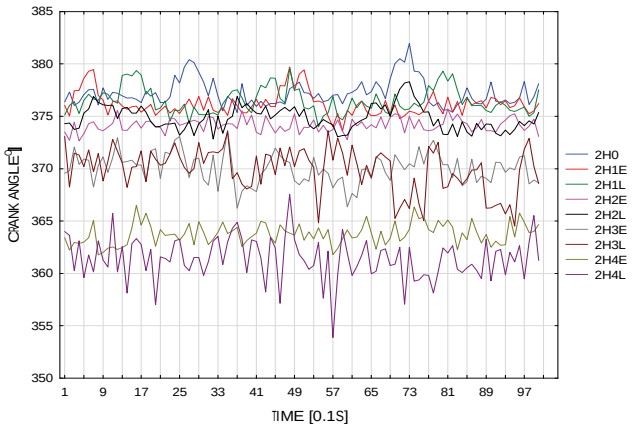

Fig. 25. Crank angle of pressure peak in C2 cylinder

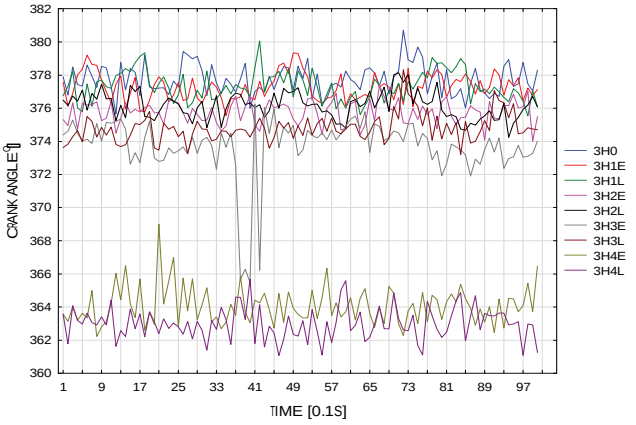

Fig. 26. Crank angle of pressure peak in C3 cylinder

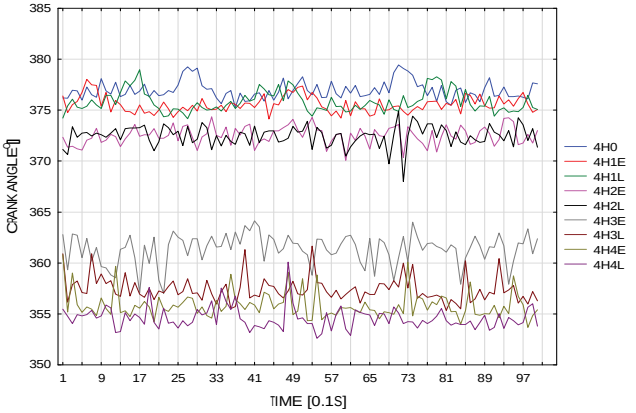

Fig. 27. Crank angle of pressure peak in C4 cylinder

The peak pressure angle in the individual cylinders fed with diesel fuel only was also analyzed (Fig. 28). Here, too, the evident irregularity in the C2 cylinder temporarily disturbed the combustion process. In four of the six cases, the Student's t-test indicated statistically significant differences between the cylinders.

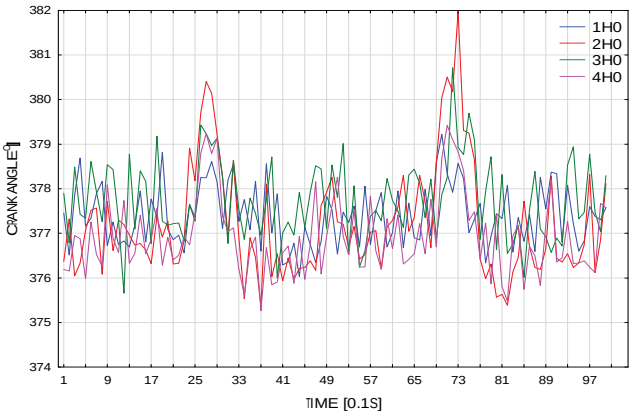

Fig. 28. Crank angle of peak pressure in all cylinders only for diesel fuel

5. Conclusions

The conclusions drawn from the research and analysis carried out are that if the combustion process is investigated, it is advisable to consider separately and multidimensionally the phenomena occurring in individual cylinders of an internal combustion engine. When a research object is

holistically analyzed, it can be difficult, even for single-cylinder units, to determine the causes of the phenomena occurring. This is especially important in the case of research work using innovative propulsion systems. We should examine source data that is as raw as possible because such an approach helps us draw more comprehensive conclusions on processes that occur in the research engine. Any additional factor and transformation can distort the interpretation of the combustion process. The choice of data processing methods is not indifferent to results obtained, which may be the reason behind research diversity in evaluating the soundness of direct hydrogen injection in diesel engines.

Certain specific conclusions about the measurement points studied have been drawn from the analysis:

– There are statistically significant differences between the tested combustion process parameters for early and late injection based on the analysis by the Student's t-test at $\alpha = 0.05$: IMEP: 9 out of the 16 cases (56%), peak pressure: 14 out of 16 (88%), heat released: 9 out of 16 (56%), crank angle for peak pressure: 9 out of 16 (56%).
– In 34 out of the 36 (94%) measurement points, the coefficient of variation of the IMEP did not exceed 5%, which means a stable combustion process.
– It can be concluded that the change of direct hydrogen injection timing from early to late has an effect on the combustion process only. The significance of this effect depends, among other things, on the hydrogen dose and initial torque. In the analyses, when the highest hydrogen doses were supplied, the limit of the maximum load acting on the research object was nearly reached and rumbling began to occur, which may explain the irregularities in the presented results. This justifies further research on using hydrogen in diesel engines.

Nomenclature

CAD	crank angle degree
CoV	coefficient of variation
CI	compression ignition
DI	direct injection
E/L	early/late hydrogen injection
H0–H4	hydrogen dose
IMEP	indicated mean effective pressure

Bibliography

[1] Bayramoğlu K, Yılmaz S. Emission and performance estimation in hydrogen injection strategies on diesel engines. Int J Hydrogen Energ. 2021;46(57):29732-29744. https://doi.org/10.1016/j.ijhydene.2020.08.135

[2] Berthelot JM, Cole JM. Composite materials: mechanical behavior and structural analysis. Springer, New York1998.

[3] Brzezański M, Noga M, Szalek A. Operation of the fuel cell electric vehicle in moderate and low-temperature ambient conditions. SAE Technical Paper 2022-01-1129. 2022. https://doi.org/10.4271/2022-01-1129

[4] Carlucci AP, Ficarella A, Laforgia D, Trullo G. Multiobjective optimization of the breathing system of an aircraft two stroke supercharged diesel engine. Enrgy Proced. 2015;82: 31-37. https://doi.org/10.1016/j.egypro.2015.11.879

[5] Dopona M, Foxhall N, Dutzler C. 912iS fuel injected aircraft engine. SAE Technical Paper 2012-32-0049. 2012. https://doi.org/10.4271/2012-32-0049

[6] European Commission. European Hydrogen & Fuel Cell Technology Platform. Strategic Research Agenda 2005.

[7] Gerke U. Numerical analysis of mixture formation and combustion in a hydrogen direct-injection internal combustion engine. Swiss Federal Institute of Technology 2007.

[8] Green Car Congress. High-pressure direct-injection hydrogen engine achieves efficiency of 42 %; on par with turbodiesels. Energy, technologies, issues and policies for sustainable mobility. 2009. http://www.greencarcongress.com/2009/03/high-pressure-d.html

[9] Hernández JJ, Salvador JB, Cova-Bonillo A. Autoignition of diesel-like fuels under dual operation with H2. Adv Mech Eng. 2019;11(6):1-8. https://doi.org/10.1177/1687814019856781

[10] Jamrozik A, Grab-Rogaliński K, Tutak W. Hydrogen effects on combustion stability, performance and emission of diesel engine. Int J Hydrogen Energ. 2020;45(38):19936-19947. https://doi.org/10.1016/j.ijhydene.2020.05.049

[11] Lata DB, Misra A. Theoretical and experimental investigations on the performance of a dual fuel diesel engine with hydrogen and LPG as secondary fuels. Int J Hydrogen Energ. 2010;35:11918-11931. https://doi.org/10.1016/j.ijhydene.2010.08.039

[12] Liu X, Srna A, Yip HL, Kook S, Chan QN, Hawkes ER. Performance and emissions of hydrogen-diesel dual direct injection (H2DDI) in a single-cylinder compression-ignition engine. Int J Hydrogen Energ. 2021;46(1):1302-1314. https://doi.org/10.1016/j.ijhydene.2020.10.006

[13] Puzdrowska P. Analysis of changes in the temperature of the working medium in the cylinder and in the exhaust gas duct of a diesel engine for diagnostic purposes - state of research (in Polish). Journal of Polish CIMEEAC. 2020;15(1):89-101.

[14] Saravanan N, Nagarajan G. An experimental investigation of hydrogen-enriched air induction in a diesel engine system. Int J Hydrogen Energ. 2008;33(6):1769-1775. https://doi.org/10.1016/j.ijhydene.2007.12.065

[15] Serio De D, De Oliveira A, Sodré JR. Effects of EGR rate on performance and emissions of a diesel power generator fueled by B7. J Braz Soc Mech Sci Eng. 2017;39:1919-1927. https://doi.org/10.1007/s40430-017-0777-x

[16] Siadkowska K. Experimental study of particulate emissions for direct hydrogen injection in a dual fuel diesel engine. SAE Technical Paper 2020-01-2197. 2020. https://doi.org/10.4271/2020-01-2197

[17] Siadkowska K, Barański G, Sochaczewski R, Wendeker M. Experimental investigation on indicated pressure and heat release for direct hydrogen injection in a dual fuel diesel engine. Adv Sci Technol Res J. 2022;16(3):54-66. https://doi.org/10.12913/22998624/149300

[18] Siadkowska K, Czajka B, Ścisłowski K, Wendeker M. Analysis of propulsion units dedicated to test stands for aviation systems. Combustion Engines. 2021;185(2):39-43. https://doi.org/10.19206/CE-139405

[19] Soltic P, Hilfiker T, Hutter R, Hanggi S. Experimental comparison of efficiency and emission levels of four-cylinder lean-burn passenger car-sized CNG engines with different ignition concepts. Combustion Engines. 2019;176(1):27-35. https://doi.org/10.19206/CE-2019-104
[20] Stępień Z. Synthetic automotive fuels. Combustion Engines. 2023;192(1):78-90. https://doi.org/10.19206/CE-152526
[21] Subramanian B, Thangavel V. Experimental investigations on performance, emission and combustion characteristics of diesel-hydrogen and diesel-HHO gas in a dual fuel CI engine. Int J Hydrogen Energ. 2020;45(46):25479-25492. https://doi.org/10.1016/j.ijhydene.2020.06.280
[22] Szumska EM, Jurecki R. Technological developments in vehicles with electric drive. Combustion Engines. 2023; https://doi.org/10.19206/CE-168219
[23] Tira HS. Impact of alternative fuels and hydrogen – enriched gaseous fuel on combustion and emissions in diesel engines. Doctoral Thesis. 2013. https://etheses.bham.ac.uk//id/eprint/4376/1/Tira13PhD.pdf
[24] Wajand JA, Wajand JT. Medium- and high-speed internal combustion piston engines (in Polish). WNT. Warsaw 2005.

Siadkowska Ksenia, MEng. – Faculty of Mechanical Engineering, Lublin University of Technology, Poland.
e-mail: *k.siadkowska@pollub.pl*

Barański Grzegorz, DEng. – Faculty of Mechanical Engineering, Lublin University of Technology, Poland.
e-mail: *g.baranski@pollub.pl*

Article citation info:
Krzemiński A, Jaworski A, Kuszewski H, Woś P. A comparative study on selected physical properties of diesel–ethanol–dodecanol blends. Combustion Engines. 2024;196(1):99-105. https://doi.org/10.19206/CE-170267

Artur KRZEMIŃSKI
Artur JAWORSKI
Hubert KUSZEWSKI
Paweł WOŚ

Combustion Engines
Polish Scientific Society of Combustion Engines

A comparative study on selected physical properties of diesel–ethanol–dodecanol blends

ARTICLE INFO

Received: 8 June 2023
Revised: 21 July 2023
Accepted: 2 August 2023
Available online: 20 September 2023

The article presents findings of the comparative analyses of the selected physicochemical parameters of diesel fuel and diesel-ethanol blends with the addition of dodecanol, used to stabilise the blend Diesel fuel and the blends were tested for density, flash point, and cold filter plugging point. The physicochemical properties were assessed in seven samples with different proportional volumes of ethanol contained in diesel fuel. Homogeneous blends were produced by adding 5% dodecanol to blends containing between 5% and 30% ethanol. The study was conducted to assess the selected physicochemical properties of diesel-ethanol blends with the addition of dodecanol and to compare the obtained results with the requirement of EN590:2022-08.

Key words: *diesel fuel, ethanol, dodecanol, alternative fuels, physicochemical properties*

1. Introduction

The emission of toxic compounds produced during the combustion of fuel by internal combustion engines is a major source of environmental pollution. In order to reduce the negative impact of vehicles powered by internal combustion engines, increasingly stringent standards are being introduced for the emission of harmful compounds contained in exhaust gases [24]. This leads to further advancements in internal combustion engines, which consequently results in increased complexity of their design and the widespread use of electronics to enable precise control and diagnostics [25]. Toxic emissions can be reduced for instance by optimizing the shape of combustion chamber and the fuel injection parameters [6, 27, 28].

Another way to reduce emissions of carbon dioxide (CO_2) and toxic compounds such as particulates and nitrogen oxides (NO_x), generated by diesel engines, is to use alternative fuels [29, 30]. These fuels, associated with low environmental risks, should originate from renewable resources and they should be readily available. Within this group of fuels, those of plant origin, mainly alcohols, are becoming increasingly popular because of their high oxygen content (about 35%), low viscosity and good atomization. Furthermore, alcohols such as ethanol, methanol, propanol, butanol and pentanol can be produced during the process of biomass fermentation.

Ethanol is the most widely used alcohol because it is obtained from renewable resources in the course of a simple and cost-effective production process, and it has high oxygen content [2, 8].

There are three main ways of using ethanol to power a diesel engine. These are: direct injection of ethanol into the intake manifold, direct injection of ethanol into the cylinder by a separate injector, and the use of diesel–ethanol or ethanol–biodiesel blends [4, 9]. Compared to the first two, the latter method has considerable advantages owing to its simplicity. The use of this type of blend makes it possible to avoid costly changes to the engine design, and may only require certain adjustments to be made [2, 23]. However, the miscibility of ethanol in diesel fuel is limited and depends on temperature changes and water content in the fuel; even a small amount of water can lead to stratification of the blend. To improve miscibility and avoid stratification of the blend, it is possible to apply dodecanol ($C_{12}H_{26}$). It is obtained by reducing methyl esters [32]. It is a colorless water-insoluble solid with a melting point of 24°C. It exhibits good solubility in both of the aforementioned fuels and has been used as a stabilizer in diesel-ethanol blends [7]. Homogeneous blends were produced by adding 5% dodecanol to blends containing between 5% and 30% ethanol. This proportional content of dodecanol was used to ensure miscibility [19, 22].

Experimental studies show that a higher concentration of ethanol in a diesel blend results in a reduction of nitrogen oxides and particulates, but can lead to an increase in exhaust gas temperature, carbon monoxide (CO) emissions at low and medium engine load and an increase in the amount of unburned hydrocarbons (HC) [2, 3, 10].

Alternative fuels differ in terms of physicochemical parameters from conventional fuels. It is important to identify the differences in the basic physicochemical parameters of alternative fuels because they determine behavior of a given medium in different conditions. To this end, the experimental tests were carried out to:

- measure the density at 15°C
- fraction composition
- calorific value
- measure the flash point (FP)
- measure the cold filter plugging point (CFPP).

The density of fuel is an important parameter, as it influences the amount of fuel injected into the combustion chamber. Consequently, a decrease in fuel density can lead to reduced engine power, increased fuel consumption, and alterations in the emission of toxic compounds in exhaust gases. Additionally, density can affect the rate of pressure build-up in the cylinders, gas-dynamic processes, the range of the sprayed fuel stream, the fuel pressure in the injection lines, and the fuel spray digestion time.

Substitute fuels differ in calorific value compared to diesel fuel. An appropriate correction of the injection time should be selected to guarantee an equivalent amount of fuel injected into the combustion chamber. The distillation characteristics are determined by normal distillation, during which the fuel is separated into fractions with different boiling points. The fractional composition determines the volatility of diesel fuel, which affects its ignition properties and determines the course and completeness of the combustion process. Another parameter that determines the usability of the fuel is the cold filter plugging point temperature, which defines the lowest temperature at which the fuel can be used.

The flash point does not directly affect the combustion process in diesel engines. It classifies the fuel into the appropriate fire hazard class.

Since that the aforementioned parameters affect the operational properties and safety of handling this type of fuel, and considering the lack of research on this fuel type, this issue is discussed in this article.

2. Description of research methods

The physicochemical properties were assessed in seven samples with different proportional volumes of ethanol contained in diesel fuel. The fuels subjected to the analyses are shown in Table 1. Homogeneous blends were produced by adding 5% dodecanol to blends containing between 5% and 30% ethanol. This proportional content of dodecanol was used to ensure the miscibility of the blends [20, 22]. The samples were made from diesel fuel, the selected parameters of which are presented in Table 2 as well as dehydrated ethanol with the main properties shown in Table 3. The selected parameters of dodecanol are presented in Table 4.

The fuels prepared for testing were stored in closed containers due to the hygroscopic nature of ethanol.

Table 1. List of fuels subjected to tests

Sample description	Percentage [% v/v]		
	Dodecanol	ON	Ethanol
ON	0	100	0
ON-ET5	5	90	5
ON-ET10	5	85	10
ON-ET15	5	80	15
ON-ET20	5	75	20
ON-ET25	5	70	25
ON-ET30	5	65	30

Table 2. Properties of diesel fuel [32]

Parameter	Unit	Value
Cetane number	–	51.7
Viscosity (40 °C)	mm^2/s	2.516
Polycyclic aromatic hydrocarbons content	%(m/m)	2
Sulfur content	mg/kg	5.9
Water content	%(m/m)	0.008
Density	g/cm^3	0.833

Table 3. Basic properties of ethanol [17]

Parameter	Unit	Value
Alcohol content (20°C)	%	99.9
Autoignition temperature	°C	425
Water content	% (m/m)	≤ 0.1
Methanol content	mg/100 cm^3	< 0.6
Ester content	mg/100 cm^3	< 0.2
Density	g/cm^3	0.789

Table 4. Basic properties of dodecanol [18]

Parameter	Value	Unit
Melting/freezing point at a pressure of 101.3 kPa	24	°C
Autoignition temperature	275	°C
Flash point	134.8	°C
Solubility in water (25°C)	0.037	g/l
Density (25°C)	0.843	g/cm^3

Density was measured using DMA 4500 M apparatus (Fig. 1), with the following technical parameters [14]:

– measuring range: density 0–3 g/cm^3, temperature from 0 to 90°C
– accuracy: $5 \cdot 10^{-5}$ g/cm^3, 0.03°C
– sample volume: minimum 1 ml.

Density of the blends was determined by the standard PN-EN ISO12185:2002. Figure 1 shows the screen of DMA 4500 M apparatus, which can be used to measure density following the standard, during the measurement of the parameter in ON-ET20 blend at 15°C.

Fig. 1. Density meter DMA 4500 M

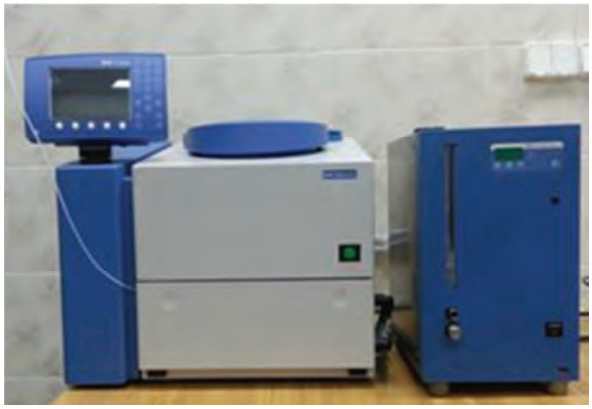

Fig. 2. Calorimetr IKA C5000

The study of the higher heating value (HHV), based on which the Lower Heating Value (LHV) of the fuel was determined, was carried out using the isobaric method using a measuring system with the IKA C5000 calorimeter (Fig.

2). The device is characterized by the following selected parameters [11]:
- oxygen filling station integrated with the calorimeter and automatic emptying of the bomb after the measurement
- measurement range: max. 40 000 J (corresponds to the temperature increase of the calorimetric vessel to approx. 40 K)
- measurement accuracy: ±0.0001 K
- measurement time: adiabatic method 14–18 min, isoperibolic method 20–22 min, dynamic method 8 min.

Fig. 3. Distillation analyzer OptiDist

The fractional composition of the tested blends was determined using the OptiDist apparatus (Fig. 3). The apparatus is characterized by the following parameters [15]:
- volume of the tested sample: initial volume range 0–103%, resolution 0.03 ml, accuracy ±0.1 ml, automatic calculation of distillation residue
- vapor temperature: range 0–450°C, Pt 100 sensor IEC 751
- receiver chamber: temperature range 0–40°C.

The test apparatus was configured for the 4th group, which corresponds to a typical diesel oil, thanks to which the main parameters of the apparatus configuration were the same for each of the tested blends. Such a setup of the apparatus made it possible to carry out comparative tests of the tested fuels with diesel oil.

Another physicochemical parameter impacting the possibility of using fuel at low temperatures is the factor known as CFPP. Another physicochemical parameter affecting the possibility of using the fuel at low temperatures is the CFPP coefficient, which was determined based on the standard PN-EN 116:2015-09. The value of the cold filter plugging point corresponds to the temperature at which the final completed filtration process starts. The measurement of the cold filter plugging point was performed using the automatic apparatus FPP 5Ds (Fig. 4) with the following parameters [12]:
- sample temperature measuring range: –69–+35°C
- sample volume: 45 ml
- programming of the negative pressure of the drawn sample.

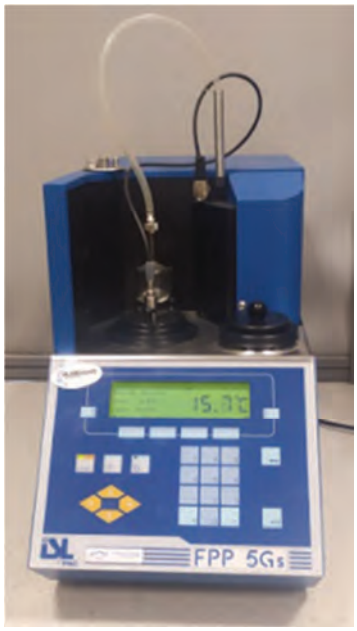

Fig. 4. CFPP tester FPP 5Gs

Measurement of flash point was performed following PN-EN ISO2719:2016-08.

Measurement of the flash point was performed using HFP 339 tester (Fig. 5) with the following parameters [14]:
- sample temperature measuring range: 0–400°C, resolution 0.1°C
- the rate of heating: 0.5–14°C/min – depending on the test method
- ignition source: electrical coil igniter; frequency of ignition depends on the selected method 0.5–5°C.

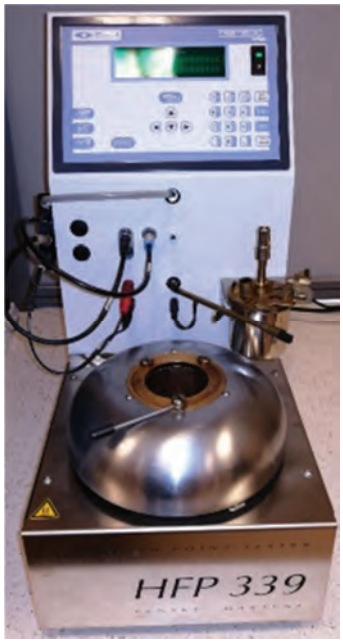

Fig. 5. Flash point tester HFP 339

3. Results and analysis

Fuel density impacts engine performance characteristics [16]. A change in fuel density affects engine power output because of the different weight of the fuel injected [1]. Density was measured at a temperature of 15°C, in line with PN-EN ISO12185:2002.

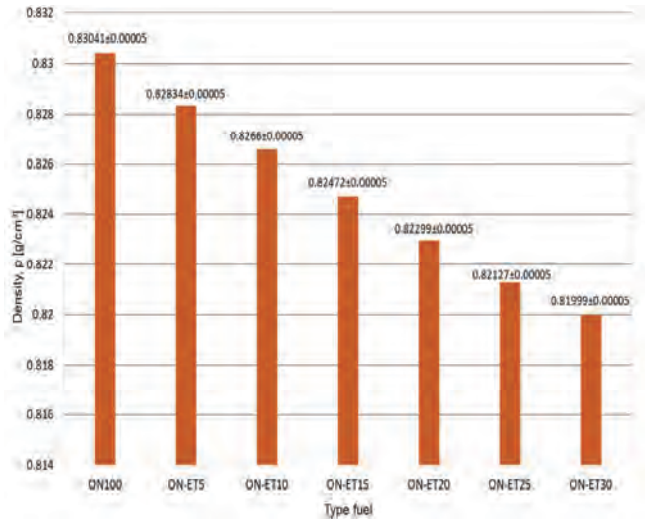

Fig. 6. Density of the fuel samples tested (at 15ºC)

Based on the results presented in Fig. 6, it can be observed that an increase in the proportional content of ethanol results in an approximately 0.2% decrease in density. The lowest density was identified in the ON-ET30 blend, containing 30% ethanol and 5% dodecanol; in this case, there was approximately a 1.2% decrease in density relative to the reference diesel fuel sample. All the fuels, with the exception of ON-ET30, met the density requirements defined by the regulations [26]. The uncertainty of (±0.00005 g/cm^3) was established by the test device supplier.

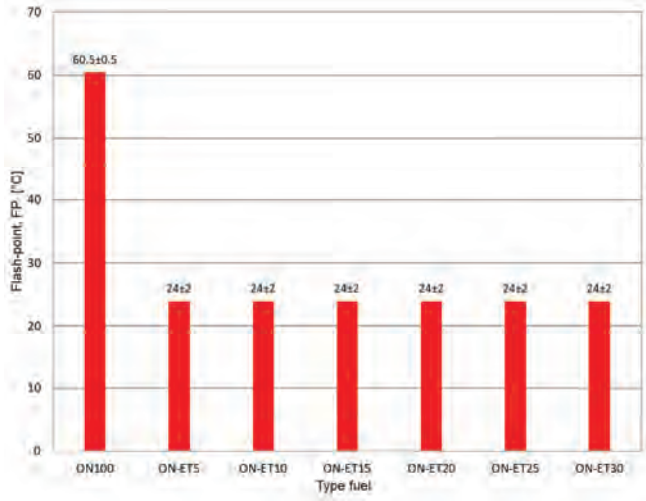

Fig. 7. Flash point of the fuel samples tested

FP is a decisive factor in establishing the necessary precautions for fuel handling.

The FP was taken as the lowest temperature at which the ignition of the flammable blend with air occurred.

The highest value of flash point, identified in diesel fuel sample, was 60.5°C ±0.5 (Fig. 7). In contrast, all the blends formed vapours that ignited at an ambient temperature of 24 ±2°C. All samples with the addition of ethanol ignited at ambient temperature during the test immersion of the igniter (without heating the sample).

CFPP determines the lowest temperature at which a fuel can be used. Based on the value of CFPP, diesel fuels are designated to be used in specific seasons, depending on weather conditions. The CFPP value quantitatively indicates the solidification of paraffinic hydrocarbons, where excessive paraffinic hydrocarbon crystals can obstruct the flow of fuel through the fuel system. The present study applied winter diesel fuel ON100 as the reference sample. The tests performed in line with PN-EN116:2015-09 produced results presented in Fig. 8, which show that in the case of diesel fuel ON100 the value of CFPP was −25°C. Compared to all the samples investigated, the fuel ON-ET10, with 10% ethanol content, was found with the lowest value of cold filter plugging point amounting to −30°C. The improvement of low-temperature properties may result from the addition of dodecanol, which improves low-temperature properties for low concentrations of ethanol in diesel fuel [21]. This blend meets Grade F requirements for temperate climates and Grade 1 requirements for Arctic climates, as does the fuel sample ON-ET5. On the other hand, the highest cold filter plugging point values of −17°C, and −18°C were measured in the case of ON-ET30 and ON-ET25 samples, respectively. These blends meet Grade E requirements defined for temperate climates. The remaining fuels also satisfy Grade F requirements for temperate climate.

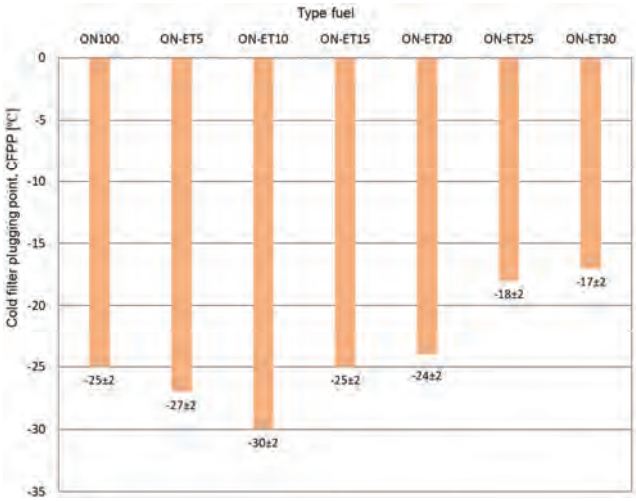

Fig. 8. Cold filter plugging point of the fuel samples tested

Figure 9 displays the higher heating value results for the tested blends. Among them, ON100 fuel exhibits the highest heat of combustion value at 44.25 MJ/kg, while the lowest value of 38.62 MJ/kg is observed for the ON-ET30 fuels.

In Fig. 10, the results of the lower heating value for all tested blends are shown. Diesel fuel demonstrates the highest calorific value of 41.74 MJ/kg. As the ethanol concentration increases, the calorific values decrease. The mixture

of ON-ET30 has the lowest calorific value at 37.58 MJ/kg compared to the other fuels.

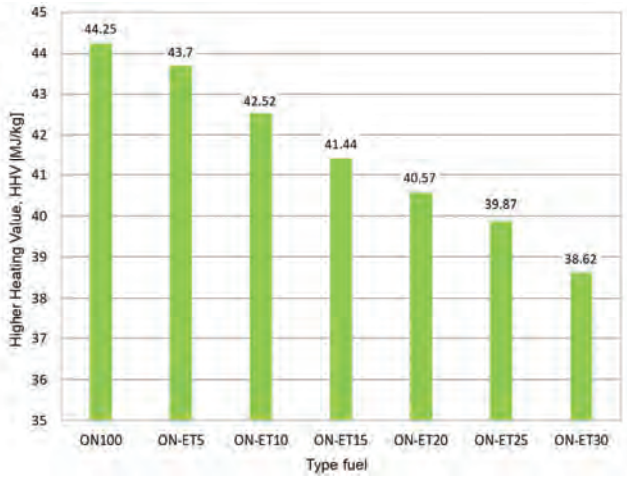

Fig. 9. Higher heating value for the tested blends

An important indicator determining the operational value is the fractional composition of fuels. On its basis, it is possible to determine not only the volatility affecting the speed of starting the engine but also its tendency to form vapor locks that cause interruptions in its operation.

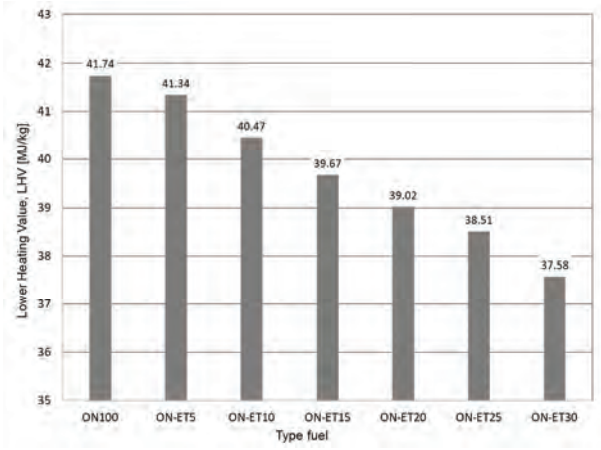

Fig. 10. Lower heating value for the tested blends

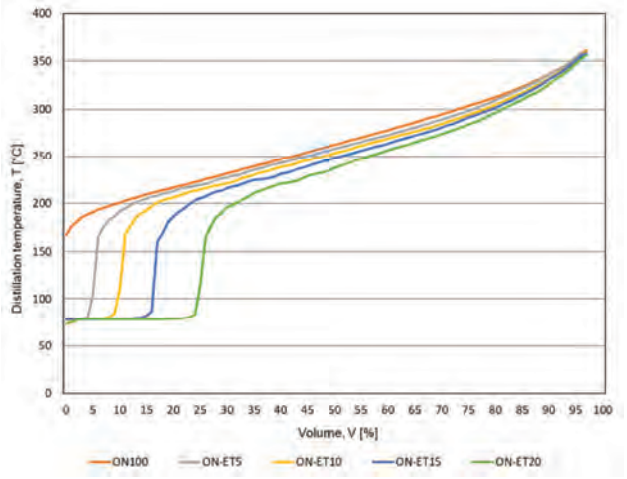

Fig. 11. Distillation curves for the tested fuels

In Table 5 presents the values temperatures corresponding to the subsequent stages of their evaporation, while Fig. 11 presents them graphically using distillation curves.

Table 5. Degree of fuel evaporation as a function of temperature

Parameter	T_S	$T_{10\%}$	$T_{50\%}$	$T_{90\%}$	T_F
	°C	°C	°C	°C	°C
ON	167.19	200.87	262.30	335.96	361.87
ON-ET5	77.77	191.87	258.03	335.35	358.74
ON-ET10	77.78	109.09	253.21	331.62	359.99
ON-ET15	78.09	78.72	248.07	331.16	355.75
ON-ET20	73.63	78.43	237.69	326.32	352.60
ON-ET25	–	–	–	–	–
ON-ET30	–	–	–	–	–

The obtained distillation curves (Fig. 11) show that up to the temperature of 180°C the following were distilled: 1% of ON100 fuel, 7% ON-ET5, 12% ON-ET10, 18% ON-ET15, 27% ON-ET20. Up to the temperature of 250 °C, 42% ON100, 44% ON-ET5, 47% ON-ET10, 51% ON-ET15, 56% ON-ET20 were distilled. The highest distillation start temperature was recorded for ON100, amounting to 167.11°C, and the lowest, amounting to 75.46°C, for the ON-ET20 mixture. The requirements of the norm for the result of distillation of 95% of the fuel fraction to the temperature of 360°C were met by all blends for which distillation was possible. Only for fuels marked ON-ET25 and ON-ET30 the distillation curves could not be determined. In order to obtain distillation curves for these fuels, it would be necessary to perform the measurement under reduced pressure distillation conditions, which would require the use of other apparatus.

4. Conclusions

Based on the experimental tests and analysis of the results, the following conclusions have been formulated:

– based on the obtained results, it can be concluded that fuel blends in which the ethanol content does not exceed 25% meet the requirements of the EN 590:2022-08 standard regarding density and cold filter plugging point;
– increase in ethanol content resulted in approximately 0.2% decrease in the density, and the lowest density was identified in the fuel blend with 30% ethanol and 5% dodecanol; in this case, density was approximately 1.2% lower than in diesel fuel;
– the fuel sample ON-ET30 did not meet the fuel density-related requirements specified in the regulation of EN 590:2022-08;
– the flash point, which is an indicator for precautions to be taken when handling the product, has decreased from 60.5°C in diesel fuel to 24°C in the case of all the diesel-ethanol blends, changing the classification of these fuels from Class III to Class II fire hazard. None of the mixtures of diesel fuel with ethanol and dodecanol meet the requirements of the standard EN 590:2022-08;
– cold filter plugging point tests have shown that fuels with ethanol content up to 25% can be used in winter; on the other hand the blends with 25% content of ethanol or higher can be used during transitional periods;

– increase in the share of ethanol in fuel sources of reduced heating value and calorific value. The lowest calorific value was reduced by approx. 10% compared to diesel oil was obtained for the ON-ET30 blend. The ON-ET5 blend obtained the highest calorific value of the tested blends of diesel oil and ethanol and was lower by 1% in relation to the base diesel oil;
– fuels containing ethanol additives exhibit the lowest initial distillation temperature of 10% of the mixture, which proves the high presence of the light fraction in the fuel. This can lead to a significant increase in pressure within the cylinders, ultimately impacting the engine's durability and noise levels in a negative manner. It may intensify the combustion process and result in significant increases in cylinder pressure, which in turn adversely affects the durability and noise level of the engine operation. It can also lead to the formation of vapor locks in the fuel system, which can disrupt the injection process and consequently impact the deterioration of engine performance parameters;
– fuels containing 5% to 20% volume of ethanol are characterized by lower distillation temperatures ($T_{50\%}$) compared to diesel fuel. This can influence the reduction in the time needed to form the fuel-air mixture, consequently enhancing the combustion process.

Acknowledgements

The research leading to these results has received funding from the commissioned task entitled "VIA CARPATIA Universities of Technology Network named after the President of the Republic of Poland Lech Kaczyński" contract no. MEiN/2022/DPI/2578, action entitled "ISKRA – building inter-university research teams".

Nomenclature

$C_{12}H_{26}$	dodecanol	HHV	higher heating value
CFPP	cold filter plugging point	LHV	lower heating value
FP	flash point	ρ	density

Bibliography

[1] Alptekin E, Canakci M. Determination of the density and the viscosities of biodiesel–diesel fuel blends. Renew Energ. 2008;33(12):2623-2630. https://doi.org/10.1016/j.renene.2008.02.020
[2] Atmanli A, Yilmaz N. A comparative analysis of n-butanol/diesel and 1-pentanol/diesel blends in a compression ignition engine. Fuel. 2018;234:161-169. https://doi.org/10.1016/j.fuel.2018.07.015
[3] Beck NJ, Uyehara OA, Johnson WP. Effects of fuel injection on diesel combustion. SAE Technical Paper 880299. 1988. https://doi.org/10.4271/880299
[4] Boretti A. Advantages of converting diesel engines to run as dual fuel ethanol–diesel. Appl Therm Eng. 2012;47:1-9. https://doi.org/10.1016/j.applthermaleng.2012.04.037
[5] Brzeżański M. Carbon dioxide emissions in the aspect of applied engine fuels. Combustion Engines. 2007;131(4):62-67. https://doi.org/10.19206/CE-117319
[6] Channappagoudra M, Ramesh K, Manavendra G. Comparative study of standard engine and modified engine with different piston bowl geometries operated with B20 fuel blend. Renew Energ. 2019;133:216-232. https://doi.org/10.1016/j.renene.2018.10.027
[7] Di Y, Cheung C,S, Huang Z. Experimental study on particulate emission of a diesel engine fueled with blended ethanol–dodecanol–diesel. J Aerosol Sci. 2009,40(2):101-112. https://doi.org/10.1016/j.jaerosci.2008.09.004
[8] Emiroglu AO, Sen M. Combustion, performance and emission characteristics of various alcohol blends in a single cylinder diesel engine. Fuel. 2018;212:34-40. https://doi.org/10.1016/j.fuel.2017.10.016
[9] Fraioli V, Mancaruso E, Migliaccio M, Vaglieco BM. Ethanol effect as premixed fuel in dual-fuel CI engines: experimental and numerical investigations. Appl Energ. 2014; 119:394-404. https://doi.org/10.1016/j.apenergy.2014.01.008
[10] Gnanamoorthi V, Devaradjane G. Effect of compression ratio on the performance, combustion and emission of DI diesel engine fueled with ethanol–diesel blend. J Energy Inst. 2015,88(1):19-26. https://doi.org/10.1016/j.joei.2014.06.001
[11] Device manual C5000. Inkom Instruments, Warszawa 2011.
[12] Device manual FPP 5Gs. Inkom Instruments, Warszawa 2011.
[13] Device manual HFP 339. Inkom Instruments, Warszawa 2011.
[14] Device manual DMA 4500 M. Inkom Instruments, Warszawa 2011
[15] Device manual OptiDist. Inkom Instruments, Warszawa 2011
[16] Joshi RM, Pegg MJ. Flow properties of biodiesel fuel blends at low temperatures. Fuel. 2007;86(1-2):143-151. https://doi.org/10.1016/j.fuel.2006.06.005
[17] Safety data sheet: Ethyl alcohol completely contaminated. Alpinus 2016.
[18] Safety data sheet: 1-dodecanol ≥ 98% for synthesis. Carl Roth GmbH + Co KG. Karlsruhe 2016.
[19] Kuszewski H, Krzemiński A, Ustrzycki A. Influence of ethanol addition on kinematic viscosity of diesel fuel. Publishing House Rzeszow University of Technology. Series: Transport. Rzeszow 2016.
[20] Kuszewski H, Krzemiński A, Ustrzycki A. The effect of alcohol hydration on the cetane test derivative of the oil with ethanol in the propulsion system and add dodecanol. Series: Transport. Publishing House Rzeszow University of Technology. Rzeszow 2017.
[21] Krzemiński A, Lejda K, Ustrzycki A. Influence of dodecanol addition on cold filter plugging point for the mixtures of diesel oil with ethanol. Conf Ser Mater Sci. 2018; 421:042043. https://doi.org/10.1088/1757-899X/421/4/042043
[22] Krzemiński A, Lejda K, Ustrzycki A. Influence of dodecanol addition on the energy value of diesel oil mixture with ethanol. Viśniki Narodowy Uniwerystet Transportu. 3(45), Kijów 2019.

[23] Lotko W. Influence of the type of fuel on the fuel pressure in the injection pipe and the nozzle needle lift in a diesel engine. The Archives of Automotive Engineering. 1997:1–2.
[24] Mickevicius T, Labeckas G, Slavinskas S. Experimental investigation of biodiesel-n-butanol fuels blends on performance and emissions in a diesel engine. Combustion Engines. 2022;188(1):90-95. https://doi.org/10.19206/CE-142030
[25] Pielecha I, Czajka J, Borowski P, Wisłocki K. Research-based assessment of the influence of hydrocarbon fuel atomization on the formation of self-ignition spots and the course of pre-flame processes. Combustion Engines. 2014;157(2): 22-35. https://doi.org/10.19206/CE-116942
[26] Regulation of the Minister of Economy of 9 October 2015 r. on quality requirements for liquid fuels. Journal of Laws 2015, position 1680.
[27] Sanli BG, Uludamar E, Ozcanli M. Evaluation of energetic-exergetic and sustainability parameters of biodiesel fuels produced from palm oil and opium poppy oil as alternative fuels in diesel engines. Fuel. 2019;258:116116. https://doi.org/10.1016/j.fuel.2019.116116
[28] Sitnik LJ, Sroka ZJ, Andrych-Zalewska M. The impact on emissions when an engine is run on fuel with a high heavy alcohol content. Energies. 2021;14(1):41. https://doi.org/10.3390/en14010041
[29] Yasilyurt MK. The effects of the fuel injection pressure on the performance and emission characteristics of a diesel engine fuelled with waste cooking oil biodiesel-diesel blends. Renew Energ. 2019;132:649-666. https://doi.org/10.1016/j.renene.2018.08.024
[30] Yilmaz N, Ileri E, Atamanli A, Deniz Karaoglan A, Okkan U, Sureyya KM. Predicting the engine performance and exhaust emissions of a diesel engine fueled with hazelnut oil methyl ester: the performance comparison of response surface methodology and LSSVM. J Energ Resour-ASME. 2016;138(5):052206. https://doi.org/10.1115/1.4032941
[31] www.hmdb.ca/metabolites/HMDB0011626
[32] www.orlen.pl

Artur Krzemiński, MEng. – Department of Automotive Vehicles and Transportation Engineering, Rzeszow University of Technology, Poland
e-mail: *artkrzem@prz.edu.pl*

Artur Jaworski, DEng. – Department of Automotive Vehicles and Transportation Engineering, Rzeszow University of Technology, Poland.
e-mail: *ajaworsk@prz.edu.pl*

Hubert Kuszewski, DSc., DEng. – Department of Automotive Vehicles and Transportation Engineering, Rzeszow University of Technology, Poland
e-mail: *hkuszews@prz.edu.pl*

Prof. Paweł Woś, DSc., DEng. – Department of Automotive Vehicles and Transportation Engineering, Rzeszow University of Technology, Poland.
e-mail: *pwos@prz.edu.pl*

Article citation info:
Stajuda L, Levchenko D, Kubiak P, Siczek K, Boguslawski G, Kuchar M et al. Composition, features, problems, and treatment related to cooling fluid – a review. Combustion Engines. 2024;196(1):106-125. https://doi.org/10.19206/CE-169185

Lukasz STAJUDA
Dmytro LEVCHENKO
Przemyslaw KUBIAK
Kamil SICZEK
Grzegorz BOGUSLAWSKI
Maciej KUCHAR
Marek WOZNIAK
Mateusz SZYMCZYK
Gustavo OZUNA
Krzysztof SICZEK

Combustion Engines
Polish Scientific Society of Combustion Engines

Composition, features, problems, and treatment related to cooling fluid – a review

ARTICLE INFO

Received: 20 May 2023
Revised: 1 July 2023
Accepted: 3 July 2023
Available online: 6 July 2023

Vehicle coolant is one of the most important operating fluids. Along with changes in the design of engines, the composition of the coolant has also changed. The main function of the coolant is heat transfer (HT). It absorbs up to one-third of the heat energy generated by the engine. The coolant is also responsible for protecting the cooling system from damage caused by corrosion, scaling and deposits. The unfavorable working environment of the engine is also affected by smaller capacities of the cooling systems (CSs) of the drive units, extreme temperatures and increased pressure in the CS, enhancing the importance of the fluid composition. The coolant must be replaced every three years or 100,000 kilometers or every five years or 250,000 kilometers with the Organic Acid Technology (OAT). It is worth remembering that coolant of unknown composition or low quality used for a long time can expose the system to engine overheating, corrosion, deposits and restriction of liquid flow. This can lead to engine failure, in extreme cases even engine seizure. Currently, many types of fluids, including nanocoolants with different compositions, are available on the cooling market. The article presents these fluids, describe the most common failures of CSs, present the currently used methods of fluid replacement in the engine and proposes an innovative method based on the pressure method, which allows both replacing the fluid in the entire system and cleaning it.

Keywords: *combustion engine, hybrid and electric vehicles, cooling system, nanocoolant, device for coolant change*

1. Introduction

Recently, the development of internal combustion engines (ICEs) has been accompanied by the enhancement in their aggregate power strongly affected by their average effective pressure and speed, and the extensive use of electronic control units (ECUs). The mentioned engine power enhancement is accompanied by raised thermal and mechanical loads on the components of the engine systems. The high reliability of ICE needs the proper balance for the parameters of the fuel supply, pressurization, lubrication and cooling in an engine. The selection and provision of the needed parameters during engine operation are conducted by engine control systems linked to the onboard computer. The introduction of the new engine to the market, its modernization or even repair is accompanied by studies focused on improving automatic systems, devices and software for adjustment of the ICE thermal state and factors of engine cooling to provide their reliability with raising thermomechanical loads [179].

The ICE CS should ensure the best thermal state of its parts and assemblies. The operational engine temperature (ET) should be close to optimum, to allow retaining the material strength of engine components, very good lubricity and load-bearing ability of engine oil, and minimum heat loss via the CS [179].

About 70% of fuel energy is transferred and lost to the engine and vehicle CSs, the exhaust gas, and frictional parts [100]. The design of a CS of an ICE usually allows for removing as much heat as possible. A car's CS comprises two regions: the hot part and the cold part. The latter comprised zones where the coolant fluid quits the radiator and flows to the engine; the hot part comprised zones where the fluid quits the engine, after the heat deletion, and flows to the radiator [10].

The CS removes 30–35% of total heat [125]. Nowadays, the liquid- and air-CSs appear in vehicles. Most automobiles and trucks use liquid-CSs [161].

In an air-CS, the engine block is covered with a set of fins made of Al alloy (for example, AA204) conducting the heat away from the cylinder. A powerful fan forces airflow over the fins, cooling the engine by transferring the heat to the air [65].

The amount of such transferred heat is affected by the total area of the fin surfaces, the velocity/amount of the cooling air (0–25 m/s), and the temperature of both the fins (up to 72°C) and the cooling air (20–40°C) [65].

Air-cooling is mostly used in fewer horsepower engines, including motorcycles, scooters, small cars and small aircraft engines, the forward motion provides enough airflow (speed) to cool the engine. The air-CS is also applied in some small industrial engines [25].

It was noticed that the tendency to enhance the temperature level of ICE cooling [139, 145] and the ever-wider use of high-temperature CSs (HTCS) in diesel engines [27, 42, 120, 180]. The coolant temperature (CT) of the ICEs manufactured by MAN B&W Diesel Ltd, Caterpillar, General Motors, Wartsila/Sulzer, Deutz AG, Barnaultransmash OJSC ranged from 115 to 126°C [26].

Cupiał et al. [45] described a gas engine with a two-stage compressed mixture water cooler with an outer venti-

lator to cool down the compressed hot air-biogas mixture to a temperature of about 40°C before delivering it to the inlet manifold and the cylinders. This tubular-type cooler comprised tubes and a package of flat ribs made of copper.

Various electric and hybrid vehicles utilize electric motors (EMs) cooperating with various battery sets. They operate best under narrow temperature variations provided by cooling and heating systems [72]. Some of them utilize various coolants. The goal of the present paper was to review problems related to vehicle liquid fluid-based CSs.

2. Cooling systems of electric and hybrid vehicles

The electric car battery can be cooled with phase change material (PCM), fins, air, or a liquid fluid [49]. Chen et al. [37] considered four battery-cooling methods: air-based, direct liquid-based, indirect liquid-based, and fin-based.

PCM absorbs much heat energy by modifying the state from solid to liquid under little temperature change. Application of such materials is limited due to the volume change occurring at a phase change (PC), pure absorption without transferring of the heat generated away, which slows down limiting overall temperature compared to other systems [49]. Several studies were conducted on PCM-based CSs [67, 102, 166, 177] comparing battery and PC cold storage in a PV CS in various climates. PCMs are unfavorable for use in vehicles but can lower internal temperature fluctuations and peak cooling loads, improving thermal performance (TP) in buildings or infrastructure devices, such as battery rooms, power supply stations, or so-called energy tanks [49].

Cooling fins have high surface area to increase the HT rate from the battery pack (BP) to them, then to the atmosphere. The fins are used in electronics and additional CSs on ICE vehicles. However, they are inefficient for the electric car battery sets due to the fins weight outweighing the profits from their high thermal conductivity (TC) [49].

Air cooling (AC) transfers heat from the BP to air running over its surface. AC appeared in earlier electric cars like the Nissan Leaf. Despite, its simplicity and easiness, AC is not efficient compared to liquid cooling (LC), causing safety issues in hot climates [49]. Several studies were conducted on ACs [38–41, 54, 73, 108, 109, 171].

Liquid coolants possess better TC and heat capacity than air, compact structure, and ease of arrangement. They best ensure the correct temperature range and uniformity of a BP. LCs cause safety problems relevant to leaking and disposal under improper coolant (glycol) handling. They currently appear in Tesla, Jaguar, and BMW, to name a few [49]. Several studies were conducted on LCs.

Chen et al. [37] reported that an air-based CS needed up to 3 more energy than others to provide the same temperature. An indirect liquid-based one exhibited the lowest maximum temperature rise. A fin-base one rose by 40% in weight of the heaviest battery when the four kinds of CSs were of the same volume. Indirect liquid-based one was more usable than a direct liquid-based one despite its slightly lower cooling efficiency.

Huang et al. [76] stated that EMs in hybrid electric vehicles (HEVs) generate considerable heat depending on the operating conditions. Thus, an effective motor CS is needed to keep the temperature within a prescribed range. The classical coolant-based system is efficient but spends energy on driving the coolant pump and radiator fan. The authors studied a hybrid CS linking heat pipes with conventional coolant in a compact thermal cradle. Such a system allowed heat removal via an integrated thermal pathway by regulating centrifugal fans, radiator pumps, and fans to minimize energy use. The EM temperature was maintained close to the 70°C. Additionally, a higher energy amount was saved than in case of a conventional LC systems.

Operation of an EV with high effectiveness needs maintaining the best temperature range for the EM, the power electronics and the BP. This is realized with a thermal management (TM) system using:

- a refrigerant-based system consisting of a condenser, evaporator and an unit comprising battery cells, cooling plate and electric auxiliary heater. It utilizes the refrigerant from the air-conditioning system (ACS) and is managed apart via valves and temperature sensors.
- coolant and refrigerant-based flow-path subdivided into several sections, each comprising an individual low-temperature cooler, a coolant pump, a thermostat and a coolant stop valve. The refrigerant flow-path of the ACS is also linked via a chiller. A HV coolant heater allows proper battery temperature management at low external temperatures.

The CT for the EM and the power electronics is kept under 60°C inside an individual flow-path via a low-temperature cooler. The CT of the battery should be in the range of 15–30°C. At too-low temperatures, the coolant is warmed via an auxiliary HV heater. At too-high temperatures, it is cooled via a low-temperature cooler. When necessary, a chiller linked into both the coolant and refrigerant paths further lowers the CT. The refrigerant of the ACS passes via the chiller, further cooling down the coolant also passing via the chiller. The control is realized via separate thermostats, sensors, pumps and valves.

The ACS operation inside the vehicle is affected by the engine operation because of the mechanically driven compressor with a belt from the engine. When the engine stops, the temperature at the evaporator outlet of the ACS rises after just 2 seconds. The accompanied low rise in the temperature of the air blown in by the ventilation and the humidity rise is nasty for passengers. To avert low temperatures of accumulators, so-called storage evaporators comprising an evaporator and an accumulator block are used. The refrigerant passes via both blocks in the start-up phase or the engine running. Meanwhile, a latent fluid in the evaporator is chilled up to freezing. When the engine stops the warm air passing via the evaporator cools down, and a heat exchange (HX) occurs until full melting of the latent fluid. Once the vehicle carries on the process repeats [72].

Three temperature management options are used [72]:

Option 1 – air is drawn in from the air-conditioned vehicle interior and cools the battery. The cool air extracted from the vehicle interior has a temperature below 40°C. This air circulates around the accessible surfaces of the BP.

Option 2 – a specialized evaporator plate inside the battery is linked to the vehicle ACS using the decomposition process on the high-pressure and low-pressure side via pipelines and an expansion valve. The evaporator inside the

vehicle and the battery evaporator plate are linked to the same flow-path. While the interior CS contains the comfort requests, the HV battery should be chilled with various intensities according to the driving situation and the ambient temperature. The particular design of the evaporator plate and its linking to the battery provide a great contact surface for the HX. This prevents reaching the temperature above 40°C. Evaporator plates directly linked to the battery are not separately replaceable. Their damage needs the battery exchange.

Option 3 – to enable additional heating at very low temperatures, the battery is linked into a secondary flow-path, ensuring maintaining the operating temperature in the range of 15–30°C at all times. Coolant (water/glycol blend) passes via a cooling plate linked to the battery block. At lower temperatures, the coolant is quickly warmed by a heater. The latter is shut off if the temperature in the battery increases under the use of the hybrid functions. The coolant is then chilled via a battery cooler in the vehicle's front end or a low-temperature cooler using the airstream from the vehicle driving.

At high external temperatures, the coolant passes via a HX unit. Therein, refrigerant from the vehicle ACS is evaporated. The heat is delivered from the secondary flow-path to the evaporating refrigerant. An additional re-chilling of the coolant is executed [72].

Due to high cooling effectiveness, compact structure and flexible geometry, heat pipes were applied in various cooling systems of the EV battery CS [57, 78, 103, 164]. Zhao et al. [176] studied the TP of a mini-channel liquid-cooled cylinder for cylindrical power Li-ion battery (LIB) affected by channel quantities, mass flow rate, flow direction and entrance size. Zhang et al. [174] studied temperature distributions for the BP with liquid flow in the cooling process. Saw et al. [138] investigated the open cell Al foams forms with various porosity for the LIB CS. Xu et al. [172] studied the mini-channel cooling preventing thermal runaway of the LIBs. De Vita et al. [47] investigated the influence of various CSs on the transient thermal behavior of the LIB pack. Al-Zareer et al. [11–14] elaborated a TM system using boiling cooling for high-powered LIB packs for HEV. Bai et al. [23] studied the TM performance of the PCM/water cooling plate used for the LIB module. Rao et al. [127] investigated the influence of variable contact surface on the liquid TP of the cylindrical LIB module. Deng et al. [46] tested the cooling effectiveness of the power LIB with various coolants and cooling manners. Wang et al. [165] studied a forced gas cooling flow-path packaging with a liquid plate for the TM of LIBs. Tan et al. [123, 151] elaborated the carbon-fiber composites with 2D microvascular panels for battery cooling (BC). Jiaqiang et al. [89] tested the effect of LC structure on the cooling effect in battery thermal management (BTM) system. Tian et al. [155] studied the integrated TM system with BC and motor waste heat recovery for EV. Zhao et al. [175] studied the thermal behavior of discharging/charging cylindrical LIB module cooled by channeled liquid flow. Shahid and Chaab [143, 167] developed a technique to improve air-cooling and temperature uniformity in a BP for cylindrical batteries and hybrid cooling. Gillet et al. [64] tested an automotive multi-evaporator ACS and battery CS. Li et al. [96] studied the water-cooling-based strategy for LIB pack dynamic cycling for the TM system. Malik et al. [111] tested the TP and electrical performance of the set of LIBs with LC.

There are several Thermal Management (TM) approaches used to control and limit the temperature offset for high voltage (HV) BPs applied in HEVs end EVs dependent on the heat transfer (HT) medium used: air [110, 173], liquid or PCM [8, 9, 92, 101, 116]. The choice of the transfer medium is a trade-off between vehicle topology, performance, durability and costs.

In the case of Plug-in Hybrid Electric Vehicles (PHEVs), only PCM is inapplicable [92] and often either AC or LC is needed. While AC systems are simpler and cheaper, LC ones offer higher efficiency in HT and higher precision in temperature adjustment [122]. The complex liquid CSs with intricate pipe architecture utilize a TM control way that engaged the numerous electrical pumps, valves and fans to keep the battery sets within the best operation range, spending minimum electrical energy [106, 107, 113, 178].

Interestingly, Catuneanu et al. [33] reported the existence of a practical thermal limit to traditional Intelligent power modules within electric vehicle (EV IPM) HX units. Thus, the traditional LC strategies can be insufficient to cool the next generation of EV IPMs as semiconductor technology transitions from Si IGBTs, to SiC MOSFETs and GaN power HEMTs, with progressively decreasing die areas. However, until now, no violations of this thermal limit have been noticed.

Vijaya et al. [162] developed a battery monitoring and management system to control the temperature, voltage, current, charge and discharge cycle of LIB sets in EVs. Such a system possesses a liquid CS with a coolant tube inserted between battery cells to cool them when overheated.

Ayers et al. [22] elaborated a CS for the power electronics of HEVs. A common automotive refrigerant R-134a (1,1,1,2 tetrafluoroethane) is applied as the coolant in a system that can be used as either part of the existing car ACS or independently of the existing air conditioner.

The cooling of the vehicle's battery set can also be realized using nanocoolant (NC). Wiriyasart et al. [168] studied the temperature distribution and pressure drop (PD) using NCs flowing in the corrugated mini-channel of the EV BC module. They found that temperature distributions in the module are strongly affected by the flow direction, mass flow rate, and types of coolant. Using NC allowed a reduction of 28% of the maximum temperature compared to the typical cooling module. However, the PDs also enhanced. The NCs provided a cooling capacity greater than that of water.

Summarizing, one can note that various systems for cooling HV BPs in HEV and EVs are under development. Various coolants like water, EG or their mixtures, and others, including NCs are applied to them. Also, various TM approaches are under development.

3. Cooling systems of vehicles with ICEs

In the liquid-cooled ICE, coolant fills a CS and acts as a HX fluid. It flows only within the cooling circuit via rub-

ber hoses from the radiator to the engine. It does not appear in air-cooled engines [147].

According to [100], the engine CS (ECS) should keep the engine operating at the best temperature with the minimal fuel consumption. The radiator design should provide compactness and low PD and costs.

According to [135], there are two types of modern ECSs:

– pump circulation system – in this arrangement, a coolant circulates efficiently from the cylinder block to the radiator and back using a centrifugal pump driven by the engine v-belt or electric pump operating a part of the engine.
– pressurized CS – it is an amelioration over the pump circulation system of cooling. Such a system comprises a special radiator cap having a spring-loaded pressure valve and a vacuum valve.

The cap is gas-tight, so when the engine is heated, coolant vapor is formed, which cannot go out. Therefore, the boiling point of water in the system is enhanced so the engine operating temperature also increases, providing higher thermal efficacy.

The pressure valve opens when the pressure in the system surpasses a certain predetermined value (often 0.05 MPa), allowing the steam to escape, preventing undue pressure formation. When the engine is chilled the vacuum valve opens and compensates for the loss of coolant or air.

The scheme of the ECS similar to the one of those described in [28] is presented in Fig. 1.

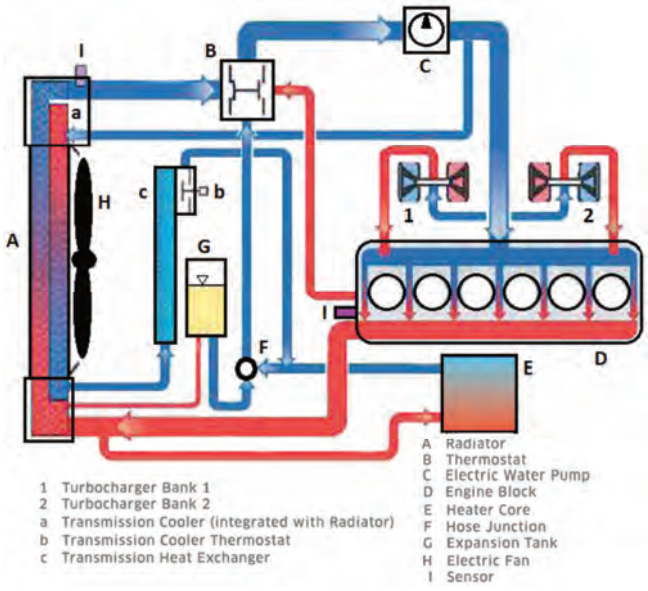

Fig. 1. The scheme of the ECS

Romero-Piedrahita et al. [131] stated that CS regulates ET within a prescribed range. This system facilitates the engine reaches the temperature quickly and evenly. Under cool weather, the CS should not over-perform as cold engines wear more rapidly, pullulate more, exhibit worsen fuel economy, and produce less power. Under-performing systems are prone to failures including burst hoses and warped metallic components. The too-cool engine operation worsens the passenger comfort in cool weather, while the too-hot one causes discomfort on warm days. However, for a better combustion performance achieving a very consistent operating temperature is beneficial. CS performance is somewhat proportional to engine power, so improving the engine requires enhancing the capacity of the CS. The ECS layout is particular for each application and is mainly determined by the engine warm-up strategies as well as the position of the heater core, oil cooler, and EGR cooler in the branches of the CS. The coolant is driven to the engine water jacket by the action of the coolant pump. At the exit of the engine, the coolant is conveyed to the water box, from which the flow is diverted through four branches connected in parallel: to the radiator (as the thermostat opens with the CT increase), to the expansion tank, to the heater core, and to the bypass, which is the shortest way to the engine inlet.

Additives comprised in coolant protect the CS against corrosion, cavitation and scaling. The blending of inconsistent coolants causes the additives to "drop out" of the solution and form radiator sludge or slime. A failed head gasket or cracked cylinder head allows oil and coolant to blend, also causing a sludge. In vehicles with automatic transmissions, where the ECS also cools the transmission, failure of such a system contaminates coolant with transmission fluid. When an imbalanced coolant chemically reacts with metallic surfaces causes corrosion, forming reddish deposits appearing as sludge or slime [16].

According to [125], a CS comprises above ten devices and parts presented further in the chapter and Fig. 1.

The temperature of the engine coolant (EC) is checked with Coolant Temperature Sensor (CTS). The signal from this sensor is utilized by the ECU to regulate fuel injection and ignition time. Some engines have numerous CTSs, while some have just one. The signal from CTS is also used to control the radiator fan and update the driver console's temperature gauge. Most CTSs are of the negative temperature coefficient type with resistance decreasing with the temperature rise. The CTS can have a two- or three-pin type, depending on the vehicle [53]. The sensor must stay in a specific resistance range to satisfy the computer operating program. If such values are out of range the computer turns the engine check procedure on and produced a trouble code pointing to a needed sensor replacement [180]. The CTS is a high failure item needing replacement when decreased fuel mileage, engine overheating, reduced engine power, or backfires appear [181].

The radiator core is produced from flattened Al tubes with Al strips/fins arranged in zigzag mode betwixt the tubes. The fins shift the heat from the tubes into the air stream carried out to the atmosphere. On each end of the radiator core, there is a plastic reservoir covering the radiator ends. The tubes can be arranged horizontally with the plastic reservoir on either side or vertically with the reservoir on the top and bottom. On radiators with plastic end caps, the gaskets between the Al core and the plastic reservoirs seal the system and prevent coolant leaks [10, 53].

A crack or leak from the radiator can lead to a significant loss of coolant or antifreeze. Without these fluids in the CS, air bubbles start developing [75].

One or two electric cooling fans within a housing, which protects fingers and directs the airflow are positioned on the back of the radiator on the side nearest to the engine. These fans keep the airflow via the radiator under automobile slow driving or stoppage with the engine operating [10, 53].

The radiator fan defect is often caused by wear and tear, compromising bearings. Much deteriorated bearings induce a fan improper operation. An EM fan assembly is eager to fatigue as well. Sometimes, a radiator fan can become non-active when struck by debris from the road. It also happens that a wrong motor mounting causes a slight engine tilt was leading the fan blades to hit surrounding vehicle components [30].

A bad or failing cooling fan motor displays symptoms:

- cooling fans do not turn on due to the cooling fan motors burning out or failing,
- the cooling fan motors failing allows the rise of the ET until the engine overheats,
- a blowing cooling fan circuit fuse occurs when the motors fail or surge, to protect the rest of the system from any sort of damage due to electrical surges. The fuse replacement usually allows restoring functionality to the fans [132]. However, faulty relays and damaged wiring also prevent motor operation. The long-term lack of the noise of a radiator fan motor usually hearable within a few seconds after an engagement, can signal motor malfunctions [30].

As a radiator fan also sucks air via the HVAC (heating, ventilation, air conditioning) system's A/C (air/conditionning) condenser, an ineffective fan causes an inadequate cabin chilling. This issue occurs especially at slow vehicle speeds, as condenser airflow is highly restricted [30].

The unforeseen turn on a car's temperature warning light can indicate the cooling fan's fault due to a non-enough airflow in the radiator leading to overheating. Sometimes, coolant can boil signaled by steam coming from beneath the radiator [30].

A reservoir tank prevents coolant cavitation at too high engine speed, causing unstable CS pressure, leading to system overheating or damage. It maintains high radiator efficiency and control CS pressure, thus preventing temperature rises [117]. Thick white smoke emanating from the exhaust pipe indicates low antifreeze levels in the coolant reservoir [75].

The radiator pressure cap maintains pressure in the CS up to a certain value. If the pressure exceeds such a set value, it is released by a calibrated spring-loaded valve [10]. A faulty pressure cap is signaled by coolant leaks, a reservoir overflowing, a radiator hose collapse, the air in the CS, and engine overheating [21].

A water/coolant pump keeps the coolant circulation as long as the engine operates and is affixed on the engine front. The pump can be driven by the engine via:

- a fan belt driving an alternator or power steering pump;
- a serpentine belt driving the alternator, power steering pump or/and AC;
- the timing belt driving one or more camshafts [125].

Coolant pumps withstand varying temperatures (–40°C to 120°C), speeds (500–8000 rpm) and pressures of up to 3 bars, thus requiring high bearing and sealing resistance. The mechanical pump comprises the drive wheel and impeller made of plastic and metal installed on a common shaft mechanically sealed towards the outside. The rotating impeller drives continuous coolant circulation within the CS. The coolant provides lubrication and cooling of the shaft mechanical seal. The shaft bearing strain is lower with plastic wheels not too liable to cavitation. However, plastic wheels become brittle over time. Due to design limits, small amounts of coolant can reach the free space after the sealing ring and escape at the pump's relief bore [72].

The electric one and its integrated electronic control operate independently of the engine and as required. Not initially running under a cold start, allows the engine to achieve its operating temperature faster. Even at idle or stopping the engine, the electric pump provides adequate cooling power. This lowers power consumption, friction losses and fuel consumption, thus reducing engine emissions [72].

The brushless electric pump is installed separately and out of the engine. It is lightsome and maintenance-free. At a voltage of 12–360 volts, it achieves outputs of 15 to 1000 watts. Coolant lowers the temperature of the pump's EM. Using a pulse-width modulated (PWM) signal, its flexible control facilitates keeping the cooling temperature constant. According to the drive type (ICE, hybrid, electric) and the system, one or many pumps can be applied [72].

Vehicles with diesel engines can lower their fuel consumption using the 48 V technology, particularly a 48 V motor, to propel the coolant pump on a 13-L diesel engine applied in the commercial vehicle class [91].

Low pressure in the CS strongly affects the operation of the pump. This is usually caused by a faulty radiator pressure cap, leaking hose, clogged radiator, compromised seals, and low fluid levels [149].

A coolant pump failure can be accompanied by noise, loss of coolant, poor cooling and engine overheats. Such failure can be caused by electrical damage (short circuit/interruption) or/and mechanical damages including impeller lose or breaking, defects of bearing or seal, drive wheel damage, canal cross-section constricting because of corrosion or sealant cavitation, impeller failure resulting from creation or decay of steam bubbles in the coolant [72].

The drive wheel damage or loose drive wheel ring is caused by the too high strain of the timing belt or its insufficient orientation. The broken pump bearing, or its cage is induced by intensive oscillations caused by a defective Visco clutch. Coolant leakage results from worn-out or cracked seals. Sealant mass residues can enter the cooling circuit and injure the slide ring seal. Corrosion in the whole CS can result from faulty cylinder head sealing allowing engine emissions to reach the CS. The wrong pH value of coolant also facilitates corrosion development. The impeller, housing, slide ring seal and shaft can be seriously injured by pinholing caused by the action of old coolant with a significant quantity of chlorides under higher temperatures. Excessive coolant leakage at discharge boring can be induced by corrosion in the CS [72]. Incorrect coolant water mixture or contaminated coolant can cause deposits in the water pump [149].

Huang et al. [77] stated that the limited engine radiator volume leads to excessive coolant flow resistance making

engine water pumps inclined to cavitation. Accordingly, air bubbles easily permeate into the EG, highly lowering the performance, reliability and service life of the engines. The authors studied the effects of the EG amount in coolant in the engine water pump on the coolant-supply capability and cavitation temperature at the occurrence of air or burnt gas in the system. They found that engines exhibit a higher tolerance to air bubbles at lower speeds. At a fixed speed, the tolerable cavitation temperature of an engine's water pump fell slowly with enhancing of the quantity of air bubbles.

The thermostat has two main functions [131]:

- restricting the coolant flow to the radiator at low operating temperatures,
- keeping CTs within pre-defined limits.

The thermostat is a valve controlling the CT. If warm fairly, it opens allowing the coolant to pass via the radiator. In the contrary case, the passing via the radiator is locked, and the coolant is guided to a bypass system allowing the coolant to return directly to the engine. The bypass system keeps the coolant flow via the engine to equalize the temperature and exclude hot points. As passing via the radiator is locked, the engine reaches operating temperature faster and, on a chilly day, allows the heater to start pressing hot air into the interior faster. Thermostats keep the temperature of the coolant in a range from 192 to 195 degrees. The engine operation at such hotter temperatures lowered emissions. Additionally, moisture condensation within the engine is fast incinerated prolonging engine life and allowing an entire combustion increasing fuel saving. The thermostat comprises a sealed Cu cup containing wax and a metal pellet. When the thermostat warms up, the hot wax broadens, shoving a piston against spring pressure to unlock the valve and allow coolant circulation. The thermostat is often positioned on the engine front top in a coolant outlet housing ,also the linking point for the upper radiator hose. The thermostat housing is joined to the engine with pair of bolts and a gasket sealing it against coolant escapes [125].

Various configurations of thermostats are available on the market. For example, Valeo offers three main thermostat types: conventional wax thermostats with pre-defined opening temperature, electrically heated wax thermostats with variable opening temperature and quick responding due to optional current feed, electrically actuated thermostats allowing full control of the CS independently of CT [157].

The failing thermostat can be marked by various symptoms including overheating or overcooling, coolant leaking, irregular temperature changes, strange sounds and heater problems [71], rust and deposit build-up, and inefficient engine running [48].

The bypass system allows the coolant to bypass the radiator and return to the engine. Some engines utilize a rubber hose or a fixed steel tube. The other uses a cast-in passage built into the water/coolant pump or front housing. When the thermostat is shut, coolant is guided to the bypass and back to the water/coolant pump, sending the coolant back into the engine omitting cooling by the radiator [125]. When an O-ring or gasket sealing the bypass tube to the engine wear out or tear, coolant leaking from the bypass tube producing a coolant smell from the vehicle's engine bay. The bypass tube can leak also due to excessive corrosion. The coolant bypass tube failure can induce engine overheating and serious engine injury [133]. A bad bypass valve is indicated by a coolant leak, engine overheating and electronic fails. The latter appears if software problems lead to the bypass valve malfunction. If so, the check engine light illuminates and persists until the problem disappears [160].

During the manufacturing of an engine block, a special sand sculpture maps the configuration of the coolant passages therein. This sand sculpture is located within a mold and then washed with molten metal (cast iron or Al alloy) in a casting process. Such a metal fills the space between the mentioned sand sculpture and the walls of the hole made in the molding sand previously thickened by churning in the casting mold. After the cooled metal maps the shape of the engine block, the sand is unfastened and taken out via holes in the engine block casting letting be the passages that the coolant passes via. Such passages should be closed using so-called freeze plugs [53, 125].

The machined flat mating surfaces between the engine block and one- or two-cylinder heads are sealed with the head gasket. Sometimes, additional gasket seals similar surfaces between the engine block and inlet manifold. The mentioned gaskets possess holes allowing coolant flow in the CS and preventing its leaks [53, 125]. In the case of a damaged, cracked, or weakened head gasket, antifreeze liquid leak and air bubbles develop leading to rapid overheating and other serious engine issues [75].

Providing needed heat to the vehicle interior is realized using the hot coolant flowing via a heater core linked to the CS with a pair of rubber hoses. One hose guides hot coolant from the water pump to the heater core and the other one gives the coolant back to the engine top [53, 125].

A set of several rubber hoses connects the components of the CS. The main hoses are called the upper and lower radiator hoses. Such two hoses are about 2 inches in diameter and direct coolant between the engine and the radiator [53, 125]. Over time, the hoses grow weaker or may develop cracks and holes resulting in coolant leaks [75].

White exhaust is related to leaks in your CS, which in turn causes the coolant fluid to get burned up by extremely high temperatures [75].

Various CSs including ECS, EGR coolers, air conditioning, frictional components (brakes, gearbox and bearings) CS, and electronic equipment CS were discussed in [100], mainly regarding minimizing fuel consumption.

Absorption cooling allows the effective reusing of the exhaust gas energy to drive the ACS for the compartment. However, the coefficient of performance (COP) of the absorption cooling is very weak.

Electronic CSs play an important role in electric/hybrid vehicles. However, some electronic equipment components operate under very low temperatures. For example, the operating temperature of a battery is below 55°C. Therefore, some new cooling manners need to be applied including PCM as a coolant in the battery CS.

With enhancing vehicle power, much heat produced in the frictional elements can be transferred to the atmosphere only with a separate CS.

The design of the ECS is strongly affected by the enhancing power and the space limitation in cars. Especially radiator

dimensions should be optimized to provide more heat removed from the engine within limited space within a car.

To summarize, CSs become more and more complex with the development of vehicles due to the necessity of minimizing fuel consumption, reduction of exhaust gases and negative influence on the environment in case of coolant leaks.

4. Coolant types

4.1. Battery and power electronic (PE) coolants

Many innovative solutions related to hybrid and electric vehicles have been introduced on the market. Some of them need intensive cooling of electric/electronic components.

Coolants for HEVs, PHEVs, and battery electric vehicles (BEVs) are typically the same coolants used in the ICE. One should use a new, pre-mixed 50/50 coolant upon refilling the CS. In the contrary case, there can occur:

- cooling fin corrosion inside the heat-generating PE components causing low heatsink performance, overheating, and even failure,
- restricted passages inside the HV BC/heating plates causing overheating, setting Diagnostic Trouble Codes (DTC), and HV system shutdown,
- loss of HV isolation at a battery coolant heater element, causing DTCs and HV system shutdown.

The coolant should be replaced:

- the pink-colored Toyota Super Long-Life Coolant (SLLC) in the:
- ICE, every 10 years or 160,000 km and then every 5 years or 80,000 km afterward.
- PE, every 15 years or 240,000 km and then every 5 years or 80,000 km afterward.
- the orange-colored General Motors (GM) DEX-COOL every 5 years or 241,400 km.
- the blue-colored premixed Nissan Long Life Coolant used in their BEVs every 15 years or 200,000 km.
- the purple-colored Tesla G-48 ethylene-glycol Hybrid Organic Acid Technology (HOAT) coolant in their BEVs should be replaced every eight years or 160,000 km.

The coolant most often applied in engines is a blend of water with an antifreeze (usually ethylene glycol – EG). Such antifreeze prevents water from freezing in cold climates and increases the fluid's boiling point [10].

4.2. Classic coolants for vehicles with ICEs

When ICE generates the power necessary to overcome the vehicle's resistance to motion, a high amount of energy is wasted as heat. The latter should be extracted from the engine mechanisms end efficiently transferred to the outside air and dissipated therein. This is usually done using different coolants, despite their low convective HT rates. An ideal coolant should exhibit small viscosity, great thermal capacity, chemical inactivity and cheapness [124], additionally without causing or promoting corrosion of the CS.

In the early state, ICEs were cooled with water with a very high specific heat value, high boiling temperature and low cost. However, a water freezing temperature of 0°C excluded it from engines utilized in cold climate zones. The water within a radiator expanded during the freezing process can destroy any water-only chilled ICEs in winter. Water also promotes corrosion generating metal oxides or rust with the materials applied in engines and radiators [43].

Although branded engine coolants (BEC) allow for mitigating problems related to elevated freezing point, low boiling point, inadequate pH and high corrodent effect of water, many drivers still apply water for chilling engines [152].

To prevent the results of coolant freezing, the methyl alcohol (methanol) can be blended with water and hence reduce its freezing temperature. However, such an antifreeze also reduces the boiling temperature of the water, which boils at 100°C. Engines reach operating temperatures at or over the 100°C and can readily boil water. The reduced boiling point of adopting methanol for antifreeze was thus unaccepted [43].

The next antifreeze generation was based on glycerol. It reduced the freezing temperature of the water but with enough efficiency down to only –37.8°C. It was not quite low enough for some winter climate conditions [43].

Next EG-based coolant generation became the new antifreeze of choice for ICEs. EG has almost one-half the specific heat value of water. When blended with water the heat portion retainable by a unit volume of such a blend is weakened. Such blends need to circulate more intensively to carry the similar heat portion that water alone would do. It is cheaper to produce, has a slightly higher boiling and flash point, and has a lower viscosity than propylene glycol (PG). Its freezing point is lower than that of PG and is around –11.5°C. It crystallizes at low temperatures and has a lower heat absorption capacity than PG. As EG is diluted, its freezing point decreases. Therefore, it is mixed with water [105].

The next coolant generation was PG-based, well adapted to automotive coolant purposes and non-toxic in moderate amounts. However, when included in coolant blends, it is eager to expand bacterial and fungal growth gradually, which can be limited by special additives [43]. PG is more expensive than EG, but less toxic, and does not crystallize, but thickens with decreasing temperature until it does not flow at all. It is less commonly used than EG. The lowest possible freezing point is achieved with a 68% glycol content in the water. Exceeding this value in either direction increases the freezing point [105].

Also, the chemical, glycerol, has recently been considered as a possible non-toxic replacement for EG [43].

Hull et al. [79] and Canter [32] noticed that engine coolants often include EG (1,2 ethanediol) or PG (1,2 propanediol). Such compounds have been the cheapest chemical bases for engine antifreeze/coolants for a long time [50].

According to [20] ECs comprised mainly: glycol (EG or PG), deionized water, and corrosion inhibitors. The features of ECs were strongly affected by the quality of each component.

The glycols in coolant mainly protect against freeze, albeit water gives the best HT [62].

FAL [61] reported that antifreeze solutions in automobile coolants typically have an EG content of 50%.

EG is more widely used in coolant than PG [128]. It has a lower viscosity, higher density, and better TC. However, despite its environmental benefit, PG is very expensive.

The coolants must effectively withstand high temperatures. Pure glycols can withstand over 180°C before boiling. Standard coolants can withstand 105 to 110°C. Adding a small amount of glycol slightly rises the boiling point [105].

Fuel Cell Electric (FCEV) and battery electric vehicle need low conductivity coolants designed for use with passivated HX units. When utilized in systems with unpassivated heat exchanges the coolant conductivity can vary during vehicle operation. It can be applied GuardIon coolant with low initial conductivity below 5 μS (microsiemens). Such coolant is diluted in a 50/50 proportion and cannot be blended with other antifreeze/coolants. The use of such a coolant provides freeze and anti-boil protection together with general corrosion protection in contact with aluminum, steel, copper, and brass surfaces [58].

Antifreeze producers utilize their own additives to enhance antifreeze life, greatly diminish corrosion, increase water pump efficiency and reduce foaming. Commonly antifreeze comprises a corrosion inhibitor, tolyl triazole, facilitating the detection of antifreeze leaks by smelling [43].

Corrosiveness is affected by the concentration of corrosive ions, such as chloride and sulfate [163].

Coolants comprise various additives called corrosion inhibitors, which inhibit corrosion and scale formation in the ECS [3, 34, 36, 150].

According to [68], corrosion inhibitors belong to general classes, like phosphates, silicates, and organic acids.

Coolant additives may comprise organic acids, silicates and phosphates, nitrites, defoamers, and bittering agents. Penrite Green OEM Coolant is recommended for vehicles with electric drivetrains systems for use in either the ICE CS or the BTM system in an electric-powered vehicle [121].

Li [97] also reported that silicates and phosphates are extensively utilized inhibitors. Jointly with molybdates and tungstates, they form the inhibitors reported in lots of recent patents [136]. Such inhibitors [5], including borates [44], are from inorganic sources.

Both organic and inorganic compounds are extensively utilized as corrosion inhibitors. Many inorganic compounds are poisonous and environment-unfriendly; thus, strictly limiting their application as corrosion inhibitors due to enhanced ecological awareness and strict environmental regulations. Many organic compounds get activated when adsorbed on the metallic surface [142]. Organic products like carboxylates are the main components in the additive package of Organic Acid Technology (OAT) coolants [18].

4.2.1. Ongoing use of various antifreeze/coolant types

It is necessary to choose from full-strength antifreeze or a 50–50 blend of antifreeze and water. The former needs blending with distilled water before introducing it into the ECS. A 50/50 blend operates for cold climates securing against freezing down to –37.2°C. A 60/40 blend of antifreeze to water for excessive cold can secure reduced temperature freeze protection [43].

Blending antifreeze with tap water is forbidden due to dissolved chemicals and/or chlorine can seriously disrupt the operation of CSs [43]. Tap water contains large amounts of calcium, which are deposited on the walls of coolers, while distilled water causes rapid corrosion of the walls. The best water for radiators is water treated with inhibitors (anti-corrosion agents) [105].

An empty CS cannot be refilled with 100% antifreeze, as the concentrated antifreeze can freeze at –12.2°C rather than the –37.2°C reached with a 50/50 mix.

Coolants are colored to facilitate the identification of the coolant in an engine. The lack of its brilliant color indicates that a coolant starts finishing its service life [43].

There are some colour groups for coolants applied in combustion engines [43] (Table 1) including:

1. IAT (Inorganic Acid Technology) – Bright Green

These coolant blends were utilized by automobile manufacturers through 1994, and by Ford continuing through 2002. Asian and European car manufacturers have withdrawn it from use since 1990. IATs contain phosphates and silicates and mate properly with cast iron engine blocks and Cu or Al radiators. They should be reconditioned every 2 years or 36,000 miles. If it remained in an engine above these restrictions, the unavoidable creation of clogging solids can weaken a CS's performance. Heater core obliterations occurred under the irregular coolant replacement [43].

IATs contain silicates and nitrates, which form a protective barrier over the entire surface of the CS from the inside. Such fluids quickly lose their properties, and if not replaced for a long time, they form deposits and sediments blocking water channels. They are predestined for ICEs with a cast iron block and an aluminum head, as long as they are replaced at least every two years [105]. IATs comprise inhibitors in the form of silicates [159]. IATs are rarely used as factory fill-in ICEs due to the fast depletion rate of their additives enhancing the needed frequency of changing for such coolants, usually every two years or 24,000 miles [1].

2. OAT (Organic Acid Technology) – Orange, Red, Blue, or Dark Green

Such coolants comprised no phosphates or silicates were applied in many cars produced after 1994. A benefit of these coolants was an prolonged coolant life until 5 years or 150,000 miles [43]. OATs comprise inhibitors in the form of organic acids and are applied in engines of GM, Saab, and VW vehicles [159]. OATs are typically changed every five years or 50,000 miles [1]. They form a much thinner protective layer than IAT coolants, no less effective. Thanks to this, they receive and give off heat more easily than IAT. OAT fluids are used in engines where there are no lead solders in the coolers, as organic acids very negatively affect such connections, causing their destruction, which results in leaks [105].

FleetGuard [59] point out that all Organic Acid Technology (OAT) or Extended Life Coolants (ELC) products are easier to maintain and more tolerant of contamination (brazing flux, hard water, etc.) than older technology products. However, liner pitting performance and elastomer compatibility varies on the types and quantity of organic additives used. 2-ethylhexanoate (2-EH) commonly used organic additive in both light and heavy-duty applications, have a negative impact on silicone elastomers, including head gaskets, rocker cover housing gaskets and silicone hoses. 2-EH induces degradation of the silicone elastomers

over time, with the gasket and hose material shrinking and becoming brittle. The failed silicone head gaskets allow exhaust gas to bypass the gasket, leading to acidification of the coolant and enhanced corrosion. Silicone head gaskets are most common in high-horsepower applications, but silicone hoses are common in various less-power automobiles.

According to Cummins Engineering Standard 14603 (CES14603), coolants should be compatible with silicone elastomers. All Fleetguard coolants are 2-EH-free and meet the requirements of CES14603 [59].

Nitrite-free OAT products are less effective at protecting liners from pitting than nitrite-containing coolants. However, the formulation of the nitrite-free Fleetguard ES Compleat OAT provided maintaining liner protection close to that of a nitrite-containing coolant. The ES Compleat OAT is Nitrite, Amine, Phosphate and Silicate Free and provides an effective 1000000 millages of the engine. It provides antifreeze and anti-boil protection, very good liner pitting and corrosion protection, and is superior for contact with aluminum and solders [60].

3. Si-OAT (Silicated HOAT) – Purple

They contain inhibitors in the form of Silicates and Organic Acids and are applied in engines of Mercedes-Benz, Audi, VW, Porsche and other vehicles [159].

4. HOAT (Hybrid Organic Acid Technology) – Yellow, Turquoise, Pink, Blue, or Purple.

These coolant blends liebetween the IAT and OAT types and are often applied in newer Chrysler products besides in European and Asian automobiles [43]. HOATs contain organic additives and silicate agents to replace IAT fluids for better corrosion protection and longer drain intervals [105]. HOATs comprise inhibitors in the form of organic acids and silicates and are applied in the engines of Ford, Chrysler and European vehicles [159]. Such coolants are typically changed every five years or 50,000 miles, although in some cases intervals as long as ten years or 150,000 miles are also met [1].

5. HOAT (Hybrid OAT, Phosphate-free) – Turquoise

They contain NAP Free inhibitors and are applied in engines of BMW, Volvo, Tesla, Mini, and others [159].

6. P-HOAT (Phosphated HOAT) – Pink or Blue

They contain inhibitors in the form of Phosphates & Organic Acids and are applied in the engines of Toyota, Nissan, Honda, Hyundai, KIA & other Asian vehicles [159].

7. Dex-Cool – Orange

Being of an OAT type, they were introduced in 1995 for GM cars. When drivers faultily inserted green coolant into systems comprising the Dex-Cool system, obliterations often appeared. However, Dex-Cool is a plausible coolant but cannot be blended with other antifreeze [43].

Although some producers offer a so-called 'universal' 150,000-mile prolonged life coolant (yellow in color) [158, 159], introducing this to the ECS is risky. When any antifreeze is required, it is better to use the type predestined for a given engine [43]. Dex-Cools should be replaced every 3-5 years [35].

Table 1. Properties and marks for various coolant

Type	Inhibitor	Vehicles	Color	Periods between coolant change	Refs
IAT (Inorganic Acid Technology)	Silicates	Older Vehicles	Green	2 yrs/24,000 miles	[130, 159]
OAT (Organic Acid Technology)	Organic Acids	GM, Saab, VW, Opel	Orange	5 yrs/50,000 miles	[130, 159]
HOAT (Hybrid OAT)	Silicates & Organic Acids	Ford, Chrysler, European	Yellow	5 yrs/50,000 miles	[130, 159]
HOAT (Hybrid OAT, Phosphate-free)	NAP Free	BMW, Volvo, Tesla, Mini, Audi, Jaguar, Mercedes, Porsche, Rolls-Royce, Saab, VW	Turquoise		[130, 159]
P-HOAT (Phosphated HOAT)	Phosphates & Organic Acids	Toyota, Nissan, Honda, Hyundai, KIA & other Asian vehicles	Pink/ Blue		[130, 159]
Si-OAT (Silicated HOAT)	Silicates & Organic Acids	Mercedes-Benz, Audi, VW, Porsche, Bentley, Lamborghini	Purple	5 yrs/150,000 miles (LAppl) 3 yrs/300,000 miles (HAppl)	[130, 159]

According to [130], engines made in Asia have had issues with poor HT. Therefore, their coolants, instead silicates, utilize phosphates and carboxylates as the anticorrosive additive. Engines made in Europe utilized silicates and carboxylates instead of phosphates, as hard water, comprising calcium and magnesium, reacts with phosphate inhibitors in EC, inducing the scale to settle on engine inner surfaces.

Some physical properties of various coolants are presented in Table 2 [19, 95, 154].

Hyper Lube [130] proposed three coolant additives:

1. Hyper Cool Radiator Cleaner and Super Flush formula consistent with all petrol and diesel engines. The coolant can purge and secure the engine within 30 minutes. Such a heavy-duty formula can contact all CS elements, including plastic and Al ones. It effectively removes rust, scale, residue and solder bloom. This formula also comprises water pump lubricant and corrosion inhibitors, promoting keeping the cleaner engine running.
2. Hyper Lube's Diesel Super Coolant, a supplemental coolant additive (SCA) is compatible with any standard diesel EC. It is predestined to secure present, turbocharged and intercooled diesel engines. It enhances HT and lowers engine part temperature by up to 9°C. A 50/50 blend of glycol and water lower an ET to 197.8°C, while that mix with super coolant added decreased it to 192.8°C. Just water lowers an ET to 194.4°C, while a blend of water and supper coolant decreases it to 181.1°C. This coolant improves the effectiveness of regular coolant, enhances fuel economy by up to 2%, boosts power and acceleration and secures against corrosion.
3. Hyper Cool Super Coolant, an EC system additive compatible with nearly every type of EC. It can lower ETs

by up to 25°C. A 50/50 blend of antifreeze and water lowers an ET to 110°C, while a 50/50 mid and super coolant decreases it to 105.6°C. Water only decreases an ET to 103.9°C, while a mix of water and super coolant lower in a decreased temperature of 90°C. Hyper Cool Super Coolant enhances engine power and ameliorates engine warm-up in chill environments.

According to [153], present water-based engine coolants (WBEC) are obtained by introducing corrosion inhibitors (CI) and anti-freezing agents (AFA) to water first deionized to eliminate corrosion factors (CF). They compared properties including CI, CF and AFA of water-extract from fermented ground maize (WEFGM) to water as the base fluid (BF) for the production of WBEC. The CF found in two WEFMG samples, exhibited pH values of 2.82 and 2.67, conductivity of 1941 and 1786 μs/cm, Pb of 0.06 and 0.05 mg/L, and Zn of 0.74 and 0.89 mg/L, respectively. CI existed were 12.25 and 22.51 mg/L of phosphates and 5 and 6 mg/L of nitrates, while AFA appeared were 5.29 and 2.38 mg/L of EGs and 4.74 and 2.15 mg/L of PGs from the 2 samples, respectively. The WEFGM was a cheaper BF for WBEC than water due to the occurrence of CI and AFA in the former.

In case of unexpected traffic issues, one can add distilled water to the CS. However, this is a temporary fix, and the system leak must be inspected, and the coolant blend either amended to rebuild preservation or the system rinsed and replenished. A new coolant can be added to the old one only when the former is of the identical type and color as the present antifreeze in an ECS. Non-adhering to this principle can induce the failure of the engine [43].

The most sensitive to improper mixing of coolants are inhibitors, which, depending on the type, are effective only at a certain pH. Mixing unsuitable fluids and changing the pH environment not only deteriorates corrosion protection but also allows the formation of an aggressive substance [105].

Introducing inappropriate antifreeze to the ECS can lead to coagulation of the coolant and clogging the radiator or the whole system. If badly clogged, the system cannot be readily rinsed and may require an expensive full deinstallation for decontamination [43].

According to [35] a coolant needs to be changed when:

- the coolant light coming on points out reduced coolant levels as well as the engine operating too hot. This can be caused by a coolant leak
- temperature on the gauge is higher than normal. If the needle moves upward or downward, a CS is compromised
- the tell-tale puddles of colored toxic fluid appear below the vehicle
- sweet smell near the car can also point out coolant leakage
- the heater fails due to a leak of enough coolant amount
- coolants tested periodically with chemical strips exhibited acidic pH levels.

The coolant levels need to be checked every time refueling or at least once every two weeks. At least this level should be checked once every 6 months, i.e., before both summer and winter. If the level is under the max line, this can result from natural and gradual loss and the need to top up the reservoir with the manufacturer's recommended coolant. However, if the level falls under the minimum mark, one needs to refill the reservoir and inspect for a few days if the level dips under the max line every time to the point of the necessity to refill every time. This may point out a leak in the system.

EG antifreeze is highly poisonous when exposed via fumes, skin contact, and ingestion.

Coolants aggregate heavy metal contamination during circulation through the engine. It is necessary to apart store contaminated and uncontaminated antifreeze. Recycling coolant contaminated by gas or engine oil is impossible at regular recycling facilities. Uncontaminated antifreeze should be recycled, but contaminated ones should be directed to a hazardous chemical disposal facility.

Summarizing this part, it can be noticed that the unsuitable freezing temperature of the coolant can cause its freezing under low temperatures leading to damage to the radiator or engine block. The unsuitable boiling temperature of the coolant can provide the sudden growth of air/steam pressure in the CS resulting in the destruction of its components or their arrangement.

Table 2. Physical properties of coolants

Coolant	k	c	ν				ρ	T_B	T_{FP}
			T_1	T_2	T_3	T_4			
W	2.21	4181	-	1.79	0.68	0.28	1000	100	0
50/50 W/EG	1.3	3284	19.34	8.48	2.39	0.71	1082	107.8	-37.8
40/60 W/EG	1.45	3473	13.76	6.09	1.87	0.61	1073	105.5	-23.9
60/40 W/EG	1,17	3088	30.08	12.68	3.03	0.78	1102	110	-47.8
50/50 W/PG	1.22	3535	61.82	19.52	3.34	0.81	1061	105.5	-33.3
40/60 W/PG	1.39	3707	40.92	13.12	2.4	0.66	1054	103.8	-21.1
60/40 W/PG	1.06	3343	114.9	33.68	4.62	0.94	1068	107.2	-50.6
(k [W/m^{2}K] – TC at the temperature of 98.9°C, c [J/kg K] – specific heat at the temperature of 21.1°C, ν [cP] – kinematic viscosity at temperature: T_1 = –17.8°C, T_2 = –1.1°C (0°C for W), T_3 = 37.8°C, T_4 = 98.9°C, ρ [kg/m^3] – density at the temperature of –1.1°C (0°C for W), T_B [°C] – boiling point, T_{FP} [°C] – freezing point)									
W/EG – Water/Ethylene Glycol blend, W/PG – Water/Propylene Glycol blend									

The admissible crossing period of coolant exploitation causes paraffin releases and a fall in heater patency. Insufficient level of coolant in a CS reduces its efficiency and leads to the engine overheating.

4.3. Nanocoolants

A very innovative direction in the development of CSs is the application of nanoparticles (NPs) to coolants.

Ibrahim et al. [86] noted that ICE radiators use forced convection during the HT process under coolant circulation. In addition to water, glycerol, and EG, also various nanofluids (NFs), and nanocellulose are used in such radiators.

According to Naraki et al. [115], using a car radiator with NC under laminar flow provided the overall HT coefficient much more than that of the BF.

According to [15], enhanced thermal efficiency of the NCs resulted from many mechanisms including TC intensification, gravity, inter-phase frictional force, sedimentation, dispersion, ballistic phonon advection, non-uniform shear rate, nanoparticle migration induced by viscosity gradient and layering at the solid-liquid interface. The hydrothermal characteristics of NFs are sensitive toward particle size and shape, material and percentage strength, BF features and pH value, fluid temperature and additives.

NCs belong to the class of NFs, taking the form of base liquids with dispersed NPs of size less than 100 nm [104]. As a base liquid, the most often used water (W), EG and their mixtures in various proportions. NPs having a high TC, when suspended in conventional liquids, improve the TC and HT efficiency of such liquids. This enhances the HT rates while also changing the property of the resulting fluids allowing them to be the next generation of HT fluids called nanocoolants (NCs) [112].

Many studies were conducted regarding the enhancement of the convective HT performance using NPs [80], [137]. However, the application of NFs, due to their enhanced heat-carrying capacity, needs a decrease in the pumping power required despite increased resistance to flow compared to fluids without NPs.

Among the most widely presented and studied NPs in the composition of NFs in the scientific literature, the following types can be distinguished:

Metals: Cu, Ag, Au, etc. The particle size is ranged from 10 to 110 nm. For example, Gopa et al. [66] reported the overall effectiveness of the radiator improvement by 14% with a 0.01% volume fraction Cu NPs-based coolant (size of Cu NPs about 57 nm).

Oxides: Al_2O_3, CuO, ZnO, MgO, SiO_2, ferrofluid and magnetized ferrofluids (containing Fe oxides at various levels of oxidation). This NP type has been studied both theoretically and experimentally. The peak of scientific interest in the application of this NP type as a component of NF for engine cooling approximately began between 2010 and 2019.

Carbon: Diamond, SWCNT, MWCNT, Graphene. The history of application and research of this NP type in ICEs began almost simultaneously with the discovery of the corresponding particles. At the initial stage, the use of particles of this type was largely represented in studies regarding the cooling and lubrication of an internal combustion engine with engine oil with the addition of carbon particles of various types. As some types of carbon NPs (for example, graphene) have very high TC (up to 1000 W/mK [129]) their use as an additive to NF coolant is logical.

In addition to NPs and BFs, a NF can contain various surfactants. For example: Anionic like Sodium Dodecyl Sulphate (SDS), Cationic like Cetyl Trimethyl Ammonium Bromide (CTAB), Non-ionic like Gum Arabic GA, Triton X-100, Amphoteric like lecithin, hydroxylamine, etc. [29].

Summary of the TC, theoretical and experimental investigations for NFs as a coolant for automotive engine radiators were comprehensively performed by Karaar Mahdi Al-Araji et al. [6]. It seems rational to build the literature analysis of NFs in this paper in a similar way where investigations are mainly divided into theoretical (mathematical, numerical modeling and simulation) and experimental studies, but giving more recent references and adding information about emerging trends in this field.

Considering early theoretical studies one should mention the following publications: [156] (Al_2O_3, CuO/W-EG), [31] (CuO/W), [81] (CuO/EG), [134] (Al_2O_3/W), [70] (TiO_2, Fe_2O_3, CuO/W), [2] (Al_2O_3, Au, CuO, TiO_2/W), from which one can draw the following general conclusions that use of Al_2O_3 NPs enables greater extent HT coefficient comparing to TiO_2, Au, CuO, and Fe_2O_3. NPs impact on laminar to turbulent flow transition and allow to enhance Brownian motion. Further theoretical studies were performed by [51] (Al_2O_3, CuO/W), [56] (Al_2O_3, CuO/W), [82] (MWCNT–Fe_3O_4/W), [85] (Al_2O_3/W), [74] (Al_2O_3/W, EG), [17] (Al_2O_3/W, EG), [63] (MgO, ZnO/W, EG), [83] (TiO_2/W), [52] (Al_2O_3, CuO/W), [90] (Al_2O_3, TiO_2, ZnO, SiO_2/W), [99] (SiO_2/W), [114] (Cu/EG), [140] (Al_2O_3/EG), [141] (TiO_2/EG-W (1:3)), [119] (Al_2O_3/W), [10] (Al_2O_3, CuO/EG). Summarizing those studies one can notice that the efficiency of the HT process is linearly related to the fraction of NPs in the range of volume concentrations from 1 to 6% (depending on the NP type), which gives an increase of HT coefficient by e.g. 17.1% at 3% concentration of ZnO and MgO NFs, 10% for CuO/W NF at 2%, 12.03% and 14.31% at 4% concentration of Al2O3/W comparing to a BF for given conditions. The friction coefficient and PD rise with utilizing NFs considerably. For instance, at Re of 1750 and NP amount of 0.07, they rose by 271 and 267% for Al2O3/W and 266 and 226% for CuO/W, respectively [52].

The authors of Refs: [4] (TiO_2/W), [7] (MWCNT, CuO, Al2O3), [24] (Al_2O_3/W), [69] (ZnO/W), [84] (SiO_2), [93] (Fe-magnetised NPs), [98] (SiC-MWCNTs), [99] (SiO_2/W), [118] (CaC2/W), [124] (Fe_2O_3, CuO/W), [126] (CuO, Al_2O_3/W, EG), [140] (Al_2O_3/EG), [144] (Al_2O_3/W, EG), [146] (MWCNT), [148] (Al_2O_3/W, EG), performed experimental studies on the impact of NFs on car radiator performance. Summarizing and generalizing the research outcomes one can notice that:

- major share in HT increase is flow rate for NF and volume fraction of NPs. The increase in HT due to the inlet temperature of the coolant is insignificant. Considerable increase in TC and specific heat of the fluid leads to an increase of Nusselt number.
- for many NF types, the concentration level of 0.5–1.0% (volume) brings positive effect. For instance: NC with 0.5% ZnO yields the biggest overall HT coefficient than

other NFs or the BFs [69]; on the other hand: the maximum values of friction factor enhanced to 22% for SiO_2 NPs dispersed in water with 2.5% volume concentration. The biggest Nusselt number rise up to 40% obtained for SiO_2 NPs in water. The Nusselt number of 1% SiO_2 NF at 80°C has 52% deviation than pure water but 32% at 60°C [84]. Thus, an increase in the volume fraction above 1%vol highly rises friction leading to higher energy consumption of the pump. The more NP concentration the higher chance that the suspended particles fall into the sediment.

– use of NF allows designing compact-size radiators which also reduces the weight of the system.

Jadeja et al. [88] represented a profound review study for NF as a coolant in internal combustion engines. The authors noticed that among the various NFs the use of NCs with MWCNTs, Al_2O_3 and CuO can augment heat transport rate taking into account the balance between operating costs and efficiency. Also, they pay attention to the existing two NFs fabrication methods: (i) one-step technique and (ii) two-step technique. The two-step one is prevalent for oxide NPs. It is less valuable with metallic particles than the single-step one. They emphasized the need for the proper identification of surface functionality, crystal structure, crystalline character, and stability of NPs inside the BF.

Considering the latest trends and challenges HT application using hybrid nanofluids (HNFs) one should notice the recent 2023 study Kumar et al. [94], where the authors have come to the following remarks from the extensive review:

1) The classical models applied to assess the rheological and HT efficiency of mono NFs cannot rate the HNF features precisely. Particularly, these deviations are more at higher percentage strengths.
2) Flow properties of HNFs are improved by the addition of hybrid NPs (HNPs). The relative viscosity of the HNF rose because of the formation of nanoclusters in the BF. These nanoclusters induce rises in the hydraulic diameters of HNPs enhancing the relative viscosity with the risen temperature, inter particles' cohesive force was weakened and subsequently the viscosity was reduced.
3) TC of HNFs is significantly more than BF and mono NFs of individual constituents. In the HNFs, metallic NPs form a new nanolayer on the metal oxide particle surface and create the thermal interfaces between grain boundaries of HNPs and BF, so that TC rise is considerably higher. As the temperature of NF increases the particles move at a faster rate, which intensifies Brownian motion and rises the TC.
4) HT characteristics of mono NFs are ameliorated by the addition of NPs as result of their refined thermos-physical properties and this amelioration is more for the HNFs.
5) Friction factor and PD are relatively more for the HNFs than for mono NFs and BF. The inclusion of HNPs develops more wall shear enhancing with volume fraction.

Interestingly, Ettefagi et al. [55] studied ECs comprising biodegradable carbon quantum dots (CQDs) in concentrations varying from 100 to 1000 ppm. For 200-ppm CQDs concentration, the coefficients of TC (k) and of convection HT (h) were improved by 5.7% and 16.2% compared to these of the BF, respectively.

In conclusion, it should be noted that the only increase in the efficiency of cooling processes in an ICE is not capable of leading to a significant energy effect for the propulsion system as a whole. First of all, this is due to the fact that even the best results of NFs, which give good increases in the HT coefficient, cannot compete with cooling methods based on the phase transition of the coolant (where huge values of HT coefficients are achieved during evaporation or condensation). Therefore, it seems extreme perspective combines the positive effects of NF with phase transition cooling schemes, where the removed heat is recuperated for increasing engine performance. The stability of NPs in ECs plays a very important role.

5. Pressure device for coolant change

A new device [169] for the coolant changes in vehicles up to 3500 kg was developed after some observations.

The classic method of coolant change comprising the hose's disassembly from the radiator, unscrewing the plug from the engine block, and down the fluid cannot assure 100% removal of coolant.

The ITALCOM device [87], shown in Fig. 2, allows the removal of used coolant, rinsing the CS, and filling it with fresh coolant using the hypotensive method. Before the realization of coolant change with such a device, the equalizing tank of the CS is open to lower in-system pressure, and then the used coolant flows away to tank 4. The EM 1 and monometer 7 steering operation of the pomp 2 is connected to the vehicle battery by switch 8. When the pressure in the CS falls below 400 hPa, what follows after the unlocking of the CS thermostat, it causes starting of engine 1 driving pump 2. The latter presses fresh coolant to the radiator of the system. The fresh coolant is pressed into the CS cyclically, which is realized by locking and unlocking the thermostat. In one cycle, about 1,5 liter of fresh coolant is pumped into the CS. When the pressure in the CS grows up to 600 hPa, what follows after the thermostat lock, relay 6 causes the separation of engine 1 from the battery and disconnection of coolant pump 2. The use of under-pressure can cause clamps of pipes during coolant change, which causes a pause in flow.

The new device [169] to change the coolant in the CS (Fig. 3 and 4) also contains tank 3 with fresh coolant connected by a pipe with electric pomp 2 connected via a pipe to the vehicle radiator, similar to the scheme in Fig. 2. The pump 2 is connected with the EM 1 possessing pins to link to the outer power supply. The pump 2 is connected simultaneously by the relay with the manometer possessing pins to link to the external power source supply (e.g., vehicle battery), but the EM and manometer are separately connected with the external power source. The pump 2 is connected via a rubber pipe and its connector to the vehicle radiator. The EM 1 is connected simultaneously by relay 6 with manometer 7 possessing pins to connect to the vehicle battery. The EM 1 and monometer 7 are connected to the battery by switch 8. The device also contains tank 4 for waste coolant connected via a rubber pipe and its connector to the vehicle thermostat. The new device allows the cool-

ant change by the pressure method, eliminating the pipe clamping during the coolant change process.

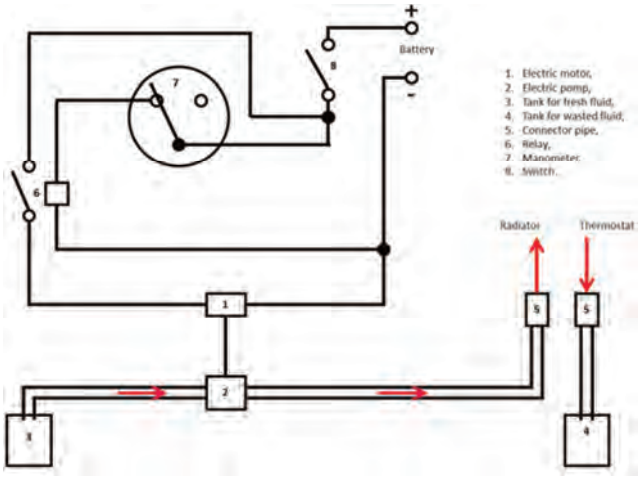

Fig. 2. The scheme of device for cooling fluid change

Fig. 3. The device for coolant changes and the control pressure gauge with start switch

Fig. 4. The device for coolant connected to the vehicle.

Summary

Various CSs are developed in classical ICE vehicles and hybrid and electrical ones. Various systems for cooling HV BPs in HEV and EVs using various coolants and TM approaches are under development. The existence of various coolants used for ICEs and HV BPs can hinder the identification of leak sources, especially in HEVs.

The use of NCs in CSs may be hampered by the tendency of NPs to agglomerate, favoring the local accumulation of deposits in the flow channels, which may even lead to their clogging. The effect of the addition of oleic acid, which is one of the stabilizers preventing NPs agglomeration [170] is not well recognized in the case of NCs. In addition, the influence of adding NPs to base coolants on changing their toxicity is unknown. Therefore, further research is needed on these issues.

Various devices facilitating coolant changes and differing complexity and costs are under development.

Nomenclature

AC	air cooling
ACS	air conditioning system
BC	battery cooling
BF	base fluid
BP	battery pack
BTM	battery thermal management
BEC	branded engine coolant
BEV	battery electric vehicle
CF	corrosion factor
CI	compression ignition; corrosion inhibitor
COP	coefficient of performance
CQD	carbon quantum dot
CS	cooling system
CT	coolant temperature
CTS	coolant temperature sensor
DTC	diagnostic trouble codes
EC	engine coolant
ECS	engine cooling system
ECU	electronic control unit
EG	ethylene glycol
EGR	exhaust gas recirculation
EM	electric motor
ET	engine temperature
EV	electric vehicle
FCEV	fuel cell electric vehicle
HEV	hybrid electric vehicles
HNF	hybrid nanofluid
HOAT	hybrid organic acid technology
HNP	hybrid nanoparticle
HT	heat transfer
HTCS	high-temperature cooling system
HV	high voltage
HVAC	heating, ventilation, air conditioning
HX	heat exchange
IAT	inorganic acid technology
ICE	internal combustion engine
LIB	lithium-ion battery
LC	liquid cooling

NC	nanocoolant
NF	nanofluid
NP	nanoparticle
OAT	organic acid technology
PC	phase change
PCM	phase change material
PD	pressure drop
PG	propylene glycol
PHEV	plug-in hybrid electric vehicle
TC	thermal conductivity
TM	thermal management
TP	thermal performance
W	water
WBEC	water-based engine coolant
WEFGM	water-extract from fermented ground maize

Bibliography

[1] AAA (the American Automobile Association, Inc.). Engine Coolant 101 The Right Coolant for Your Vehicle. https://www.aaa.com/autorepair/articles/engine-coolant-101-the-right-coolant-for-your-vehicle

[2] Abbasi M, Baniamerian Z. Analytical simulation of flow and heat transfer of two-phase Nanofluid (stratified flow regime). Int J Chem Eng. 2014;2014. https://doi.org/10.1155/2014/474865

[3] Accepta. Cooling System Scale & Corrosion Inhibitors. https://accepta.com/water-treatment-chemicals/cooling-water-treatment-chemicals/scale-corrosion-inhibitors-cooling-water-treatment-chemicals

[4] Ahmed SA, Ozkaymak M, Sözen A, Menlik T, Fahed A. Improving car radiator performance by using TiO_2-water nanofluid, Engineering Science and Technology. 2018; 21(5):996-1005. https://doi.org/10.1016/j.jestch.2018.07.008

[5] Alajaili, H. Corrosion inhibitors for cooling/ heating water-based systems. MSc Thesis. McGill University, Montreal. October 2016.

[6] Alaraji KM, Hachim DM, Almoussawi MA. Nano-fluids as a coolant for automotive engine radiators: review study. Al-Furat J Innov Mech Sustain Energy Eng. 2021;1(2):64. https://doi.org/10.52262/130221-05

[7] Al-Araji KM, Almoussawi MA, Alwana KJ. The heat transfer performance of MWCNT, CuO, and Al_2O_3 nanofluids in an automotive engine radiator. E3S Web Conf. 2021;286:1-10. https://doi.org/10.1051/e3sconf/202128601009

[8] Al-Hallaj A, Selman JR. Thermal modeling of secondary lithium batteries for electric vehicle/hybrid electric vehicle applications. J Power Sources. 2002;110(2):341-348. https://doi.org/10.1016/S0378-7753(02)00196-9

[9] Al-Hallaj S, Kizilel R, Lateef A, Sabbah R, Selman JR. Passive Thermal Management Using Phase Change Material (PCM) for EV and HEV Li-ion Batteries. Proc. IEEE Veh. Power Propulsion Conf. 1-5. https://doi.org/10.1109/VPPC.2005.1554585

[10] Alves LOFT, Henríquez JR, da Costa JAP, Abramchuk V. Comparative performance analy-sis of internal combustion engine water jacket coolant using a mix of Al_2O_3 and CuO-based nanofluid and ethylene glycol. Energy. 2022: 250:123832. https://doi.org/10.1016/j.energy.2022.123832

[11] Al-Zareer M, Dincer I, Rosen MA. Novel thermal management system using boiling cooling for high powered lithium-ion battery packs for hybrid electric vehicles. J Power Sources. 2017;363:291-303. https://doi.org/10.1016/j.jpowsour.2017.07.067

[12] Al-Zareer M, Dincer I, Rosen MA. Performance assessment of a new hydrogen cooled prismatic battery pack arrangement for hydrogen hybrid electric vehicles. Energy Convers Manag. 2018;173:303-319. https://doi.org/10.1016/j.enconman.2018.07.072

[13] Al-Zareer M, Dincer I, Rosen MA. A novel phase change based cooling system for prismatic lithium ion batteries. Int J Refrigeration. 2018;86:203-217. https://doi.org/10.1016/j.ijrefrig.2017.12.005

[14] Al-Zareer M, Dincer I, Rosen MA. Development and evaluation of a new ammonia boiling based battery thermal management system. Electrochim Acta. 2018;280:340-343. https://doi.org/10.1016/j.electacta.2018.05.093

[15] Ambreen T, Kim MH. Heat transfer and pressure drop correlations of nanofluids: A state of art review. Renew Sust Energ Rev. 2018;91:564-583. https://doi.org/10.1016/j.rser.2018.03.108

[16] AMSOIL. Why is there sludge/slime in my radiator? August 2018. https://blog.amsoil.com/why-is-there-sludgeslime-in-my-radiator/

[17] Anis S, Kayunda YC, Kusumastuti A, Simanjutak JP. Simulation study of Al_2O_3-H_2O nanofluids as radiator coolant using computational fluid dynamics method. IOP Conf Ser Earth Environ Sci. 2022;969. https://doi.org/10.1088/1755-1315/969/1/012026

[18] Arteco Engine Coolants. OAT coolants. https://www.arteco-coolants.com/en/products/engine-coolants/oat-coolants

[19] ASHRAE Handbook 2009 Fundamentals, physical properties of secondary coolants. American Society of Heating, Refrigerating and Air-Conditioning Engineers, Inc. Atlanta 2009.

[20] ASME D3306-19 Standard specification for glycol base engine coolant for automobile and light-duty service. https://standards.globalspec.com/std/13302102/ASTM%20D3306-19

[21] Autolady Synergy Coy Ltd. 5 Common Signs of a Faulty Radiator Cap. https://medium.com/@autoladysynergy/5-common-signs-of-a-faulty-radiator-cap-358f4941d1a6

[22] Ayers CW, Conklin JC, Hsu JS, Lowe KT. A unique approach to power electronics and motor cooling in a hybrid electric vehicle environment. 2007 IEEE Vehicle Power and Propulsion Conference. Arlington 2007, 102-106. https://doi.org/10.1109/VPPC.2007.4544107

[23] Bai F, Chen M, Song W, Feng Z, Li Y, Ding Y. Thermal management performances of PCM/water cooling-plate using for lithium-ion battery module based on non-uniform internal heat source. Appl Therm Eng. 2017;126:17-27. https://doi.org/10.1016/j.applthermaleng.2017.07.141

[24] Balitskii A, Kindrachuk M, Volchenko D, Abramek KF, Balitskii O, Skrypnyk V et al. Hydrogen containing nanofluids in the spark engine's cylinder head cooling system. Energies 2022;15(1):59. https://doi.org/10.3390/en15010059

[25] Banco India. Automotive ESC introduction. June 2017. http://www.bancoindia.com/wp-content/uploads/2017/06/automotive-ecs-introdution.pdf

[26] Barros CP, Peypoch N. Technical efficiency of thermoelectric power plants. Energy Economics. 2008;30(6):3118-3127. https://doi.org/10.1016/j.eneco.2008.04.007

[27] Bezyukov O, Zhukov V, Zhukova O. Effectiveness of liquid cooling systems in motors and manufacturing equipment. Russian Engineering Research. 2008;28(11):1055-1057. https://doi.org/10.3103/S1068798X08110063

[28] Bimmerworld. BMW cooling System. https://www.bimmerworld.com/About-Us/BMW-Cooling-System-Tech/
[29] Borode AO, Ahmed NA, Olubambi PA. Surfactant-aided dispersion of carbon nanomaterials in aqueous solution surfactant-aided dispersion of carbon nanomaterials in aqueous solution. Physics of Fluids. 2019;071301. https://doi.org/10.1063/1.5105380
[30] Boyd J. 5 symptoms of a bad radiator fan (and replacement cost) 2022. https://cartreatments.com/bad-radiator-fan-symptoms/
[31] Bozorgan N, Krishnakumar K, Bozorgan N. Numerical Study on Application of CuO-water nanofluid in automotive diesel engine radiator. Modern Mechanical Engineering 2012;2(4):130-136. https://doi.org/10.4236/mme.2012.24017
[32] Canter N. Heat transfer fluids: selection, maintenance and new applications. Tribol Lubricat Technol. 2009;65:28-32.
[33] Catuneanu A, Burgers JG, Fleury P, Zhang WJ, Ng WT. Practical limits of liquid cooling electric vehicle power modules. 33rd International Symposium on Power Semiconductor Devices and ICs (ISPSD). 2021 May 30-Jun 03; Nagoya 2021. 379-382. https://doi.org/10.23919/ISPSD50666.2021.9452221
[34] Chapter 24 – Corrosion control-cooling systems. Water technologies and solutions. https://www.watertechnologies.com/handbook/chapter-24-corrosion-control-cooling-systems
[35] ChemGroup. Antifreeze: The ultimate guide. https://chem-group.com/antifreeze-the-ultimate-guide/
[36] ChemTreat. Cooling water corrosion inhibitors. https://www.chemtreat.com/cooling-systems-corrosion-inhibition/
[37] Chen D, Jiang J, Kim GH, Yang C, Pesaran A. Comparison of different cooling methods for lithium ion battery cells. Appl Therm Eng. 2016;94:846-854. https://doi.org/10.1016/j.applthermaleng.2015.10.015
[38] Chen K, Wang C, Song M, Chen L. Configuration optimization of battery pack in parallel air-cooled battery thermal management system using an optimization strategy. Appl Therm Eng. 2017;123:177-186. https://doi.org/10.1016/j.applthermaleng.2017.05.060
[39] Chen K, Wang S, Song M, Chen L. Structure optimization of parallel air-cooled battery thermal management system. Int J Heat Mass Transf. 2017;111:943-952. https://doi.org/10.1016/j.ijheatmasstransfer.2017.04.026
[40] Chen K, Chen Y, Li Z, Yuan F, Wang S. Design of the cell spacings of battery pack in parallel air-cooled battery thermal management system. Int J Heat Mass Transf. 2018;127: 393-401. https://doi.org/10.1016/j.ijheatmasstransfer.2018.06.131
[41] Chen K, Song M, Wei W, Wang S. Structure optimization of parallel air-cooled battery thermal management system with U-type flow for cooling efficiency improvement. Energy. 2018;145:603-613. https://doi.org/10.1016/j.energy.2017.12.110
[42] Cheng C, Cheung C, Chan T, Lee S, Yao C, Tsang K. Comparison of emissions of a direct injection diesel engine operating on biodiesel with emulsified and fumigated methanol. Fuel. 2008;87(10-11):1870-1879. https:// doi.org/10.1016/j.fuel.2008.01.002
[43] Coddington R. Understanding the different types (and colors) of coolant. December 26, 2022. https://cartreatments.com/types-of-coolant/
[44] Cui J, Yang Y, Li X, Yuan W, Pei Y. Toward a slow-release borate inhibitor to control mild steel corrosion in simulated recirculating water. ACS Applied Materials & Interfaces. 2018;10(4):4183-4197. https://doi.org/10.1021/acsami.7b15507
[45] Cupiał K, Dużyński A, Grzelka J. Damage of the air-fuel cooler in the biogas supercharged engine. Combustion Engines 2006;2(125):78-81. https://doi.org/10.19206/CE-117356
[46] Deng Y, Feng C, Jiaqiang E, Zhu H, Chen J, Wen M et al. Effects of different coolants and cooling strategies on the cooling performance of the power lithium ion battery system: a review. Appl Therm Eng. 2018;142:10-29. https://doi.org/10.1016/j.applthermaleng.2018.06.043
[47] De Vita A, Maheshwari A, Destro M, Santarelli M, Carello M. Transient thermal analysis of a lithium-ion battery pack comparing different, cooling solutions for automotive applications. Appl Energy. 2017;206:101-112. https://doi.org/10.1016/j.apenergy.2017.08.184
[48] Dey A. 5 crucial symptoms of a failing car thermostat. GoMechanic Oct 2021. https://gomechanic.in/blog/failing-car-thermostat-symptoms/
[49] Dober. Electric vehicle cooling systems. https://www.dober.com/electric-vehicle-cooling-systems
[50] Eaton E, Boon W, Smith C. Chemical base for engine coolant/antifreeze with improved thermal stability properties. U.S. Patent 6818146 B2. 2004.
[51] Elbadawy I, Elsebay M, Shedid M, Fatouh M. Reliability of nanofluid concentration on the heat transfer augmentation in engine radiator. Int J Automot Technol. 2018;19:233-243. https://doi.org/10.1007/s12239-018-0022-3
[52] Elsebay M, Elbadawy I, Shedid MH, Fatouh M. Numerical resizing study of Al_2O_3 and CuO nanofluids in the flat tubes of a radiator. Appl Math Model. 2016;40:6437-6450. https://doi.org/10.1016/j.apm.2016.01.039
[53] Engineering Learn. Types of cooling system in car engine: components & function. https://engineeringlearn.com/types-of-cooling-system-in-car-engine-components-function/
[54] Erb DC, Kumar S, Carlson E, Ehrenberg IM, Sarma SE. Analytical methods for determining the effects of lithium-ion cell size in aligned air-cooled battery packs. J Energy Storage. 2017;10:39-47. https://doi.org/10.1016/j.est.2016.12.003
[55] Ettefagi E, Rashidi A, Ghobadian B, Najafi G, Khoshtaghaza MH, Sidik NAC et al. Experi-mental investigation of conduction and convection HT properties of a novel nanofluid based on carbon quantum dots. Int Commun Heat Mass. 2018;90:85-92. https://doi.org/10.1016%2Fj.icheatmasstransfer.2017.10.002
[56] Farooq MS, Farid EMM, Ali U, Mukhtar T. Comparative analysis of nanofluid coolant in a car radiator using CFD. The International Journal of Thermal & Environmental Engineering (IJTEE). 2021;18(1):1-8. https://doi.org/10.5383/ijtee.18.01.001
[57] Feng L, Zhou S, Li Y, Wang Y, Zhao Q, Luo C et al. Experimental investigation of thermal and strain management for lithium-ion battery pack in heat pipe cooling. J Energy Storage. 2018;16:84-92. https://doi.org/10.1016/j.est.2018.01.001
[58] FleetGuard. GuardIon low conductivity antifreeze/coolant. https://www.cumminsfiltration.com/sites/default/files/LT37042.pdf
[59] FleetGuard. The ES compleat OAT advantage. https://www.cumminsfiltration.com/sites/default/files/ES%20Compleat%20OAT%20advantage.pdf
[60] FleetGuard. ES compleat OAT nitrite, amine, phosphate & silicate free. https://www.cumminsfiltration.com/sites/default/files/LT36796_ES%20Compleat%20OAT%20Flyer.pdf

[61] Franklin Associates Ltd. Life cycle assessment of ethylene glycol and propylene glycol based heat transfer fluids. Final Report and Peer Review, Prepared for Union Carbide Corporation. 1995.

[62] Fritz P. Learning coolant basics. Machinery Lubrication (Noria Publication) 2006;1:841.

[63] Gamal M, Radwan MS, Elgizawy IG, Shedid MH. Heat transfer performance and exergy analyses of MgO and ZnO nanofluids using water/ethylene glycol mixture as base fluid. Numer Heat Transf Part A Appl. 2021;80:597-616. https://doi.org/10.1080/10407782.2021.1962631

[64] Gillet T, Andres E, El-Bakkali A, Lemort V, Rulliere R, Haberschill P. Sleeping evaporator and refrigerant maldistribution: an experimental investigation in an automotive multi-evaporator air-conditioning and battery cooling system. Int J Refrigeration. 2018;90:119-131. https://doi.org/10.1016/j.ijrefrig.2018.04.004

[65] Gomes CL, Arruda CAM, Sian JGA, Schaeffer LC, Favalessa LB, Monhol FAF. Finned surfaces in air-cooled internal combustion engine: influence of geometry and flow conditions. SAE Technical Paper 2019-36-0160. 2019. https://doi.org/10.4271/2019-36-0160

[66] Gopa P, Kumar CR, Vadivelu. Experimental investigation on heat transfer enhancement in automotive radiator using copper nano particles in engine coolant. J Chem Pharm Sci. 2015;SI6:282-287.

[67] Greco A, Jiang X. A coupled thermal and electrochemical study of lithium-ion battery cooled by paraffin/porous-graphite-matrix composite. J Power Sources. 2016;315:127-139. https://doi.org/10.1016/j.jpowsour.2016.03.018

[68] Garbutt PC. Water coolant chemistry – part II. November 2013. http://www.overlockers.com

[69] Handoyo EA, Soeyanto CI, Sutrisno. Experimental study on effect of nano ZnO on the cooling performance of motorcycle radiator. J Adv Res Fluid Mech Therm Sci. 2022;100: 169-180. https://doi.org/10.37934/arfmts.100.2.169180

[70] Hatami M, Ganji DD, Gorji-Bandpy M. CFD simulation and optimization of ICEs exhaust heat recovery using different coolants and fin dimensions in heat exchanger. Neural Comput Appl. 2014;25:2079-2090. https://doi.org/10.1007/s00521-014-1695-9

[71] Hawley D. Symptoms of a bad or failing thermostat. J.D. Power Sept 2022. https://www.jdpower.com/cars/shopping-guides/symptoms-of-a-bad-or-failing-thermostat

[72] Hella Tech World. Thermal management in electric and hybrid vehicles. https://www.hella.com/techworld/au/Technical/Car-air-conditioning/Thermal-management-in-electric-and-hybrid-vehicles-1725

[73] Hong S, Zhang X, Chen K, Wang S. Design of flow configuration for parallel air-cooled battery thermal management system with secondary vent. Int J Heat Mass Transf. 2018; 116:1204-1212. https://doi.org/10.1016/j.ijheatmasstransfer.2017.09.092

[74] Hossen A, Sakib N. Numerical analysis on heat transfer with nanofluid in an automotive radiator. International Conference on Mechanical, Industrial & Energy Engineering (ICMIEE-2020) 19-21 December 2020. ICMIEE20-127.

[75] HPAutomotive. The top 8 common cooling system issues to look out hp auto for. March 2021. https://hpautomotive.com.au/2021/03/the-top-8-common-cooling-system-issues-to-look-out-for/

[76] Huang J, Naini SS, Miller RS, Rizzo DM, Sebeck K, Shurin S et al. A hybrid electric vehicle motor cooling system – design, model, and control. IEEE Transactions on Vehicular Technology 2019;68(5):4467-4478. https://doi.org/10.1109/TVT.2019.2902135

[77] Huang KD, Tzeng SC, Ma WP. Effects of anti-freeze concentration in the engine coolant on the cavitation temperature of a water pump. Appl Energ. 2004;79(3):261-273. https://doi.org/10.1016/j.apenergy.2004.01.004

[78] Huang Q, Li X, Zhang G, Zhang J, He F, Li Y. Experimental investigation of the thermal performance of heat pipe assisted phase change material for battery thermal management system. Appl Therm Eng. 2018;141:1092-1100. https://doi.org/10.1016/j.applthermaleng.2018.06.048

[79] Hull WC, Robertson C, Mullen J, Stradling J, Sidwell B. Analysis of ethylene glycol-basedengine coolant as a vehicle fire fuel. Proceedings of the International Symposium on Fire Investigation Science and Technology, National Association of Fire Investigators. Sarasota 2008, 1-12.

[80] Huminic G, Huminic A. Heat transfer capability of the hybrid nanofluids for heat transfer applications. J Mol Liq. 2018;272:857-870. https://doi.org/10.1016/j.molliq.2018.10.095

[81] Huminic G, Huminic A. Numerical analysis of laminar flow heat transfer of nanofluids in a flattened tube. Int Commun Heat Mass Transf. 2013;44:52-57. https://doi.org/10.1016/j.icheatmasstransfer.2013.03.003

[82] Huminic G, Huminic A. Numerical analysis of hybrid nanofluids as coolants for automotive applications. Int J Heat Technol. 2017;35:288-292. https://doi.org/10.18280/ijht.35Sp0139

[83] Hussein AM, Dawood HK, Bakara RA, Kadirgamaa K. Numerical study on turbulent forced convective heat transfer using nanofluids TiO_2 in an automotive cooling system. Case Studies in Thermal Engineering. 2017;9:72-78. https://doi.org/10.1016/j.csite.2016.11.005

[84] Hussein AM, Bakar RA, Kadirgama K. Study of forced convection nanofluid heat transfer in the automotive cooling system. Case Stud Therm Eng. 2014;2:50-61. https://doi.org/10.1016/j.csite.2013.12.001

[85] Hussain T, Javed MT. A numerical simulation of heat transfer enhancement using Al_2O_3 nanofluid. Nanoscience & Nanotechnology-Asia. 2020;10(5):610-621. https://doi.org/10.2174/2210681208666181108102041

[86] Ibrahim, NI, Sazali N, Jamaludin AS, Ramasamy D, Soffie SM, Othman MHD. A review on vehicle radiator using various coolants. Journal of Advance Research in Fluid Mechanics and Thermal Sciences. 2019;59(2):330-337. https://www.akademiabaru.com/submit/index.php/arfmts/article/view/2622

[87] Italcom. Equipment for oils and fluids. https://italcom.com.pl/kategoria-produktu/urzadzenia-do-olejow-i-plynow/

[88] Jadeja KM, Bumataria R, Chavda N. Nanofluid as a coolant in internal combustion engine–a review. Int J Ambient Energy. 2022;148(5):2189-2206. https://doi.org/10.1080/01430750.2022.2127891

[89] Jiaqiang E, Han D, Qiu A, Zhu H, Deng Y, Chen J et al. Orthogonal experimental design of liquid-cooling structure on the cooling effect of a liquid-cooled battery thermal management system. Appl Therm Eng. 2018;132:508-520. https://doi.org/10.1016/j.applthermaleng.2017.12.115

[90] Khan TA, Ahmad H. CFD-based comparative performance analysis of different nanofluids used in automobile radiators. Arab J Sci Eng. 2019;44:5787-5799. https://doi.org/10.1007/s13369-019-03750-9

[91] Kiesenhofer M. Assessment of an electrical coolant pump on a heavy-duty diesel engine. SN Appl Sci. 2021;3:349. https://doi.org/10.1007/s42452-021-04340-x

[92] Kim GH, Gonder J, Lustbader J, Pesaran A. Thermal management of batteries in advanced vehicles using phase-

change materials. The World Electric Vehicle Journal. 2008;2(2):134-147. https://doi.org/10.3390/wevj2020134
[93] Kocheril R, Elias J. Fuel efficiency enhancement by addition of nano sized magnetised ferro particles in cooling system of internal combustion engines. Mater Today Proc. 2020;21: 722-726. https://doi.org/10.1016/j.matpr.2019.06.746
[94] Kumar RM, Raju AVSR, Varma KPVK, Prasad PVD. Emerging trends and challenges in heat transfer applications using hybrid nanofluids – a comprehensive review. Gradiva Review Journal. 2021;7(11):252-276.
[95] Laird thermal systems. Common coolant types and their uses in liquid cooling systems. Laird thermal systems application note. March 2017. https://lairdthermal.com/thermal-technical-library/application-notes/common-coolant-types-and-their-uses-liquid-cooling-systems
[96] Li K, Yan J, Chen H, Wang Q. Water cooling based strategy for lithium ion battery pack dynamic cycling for thermal management system. Appl Therm Eng. 2018;132:575-585. https://doi.org/10.1016/j.applthermaleng.2017.12.131
[97] Li L. An improved method for determination of corrosion inhibitors in engine coolants. Chemistry. 2011:203690851. https://www.semanticscholar.org/paper/An-Improved-Method-for-Determination-of-Corrosion-Lang/00bf62eaba02cf58fe80e21936b8aa2d83429d85
[98] Li X, Wang H, Luo B. The thermophysical properties and enhanced heat transfer performance of SiC-MWCNTs hybrid nanofluids for car radiator system. Colloids Surfaces A Physicochem Eng Asp. 2021;612:125968. https://doi.org/10.1016/j.colsurfa.2020.125968
[99] Lim K. Study of forces convection nanofluid heat transfer in the automotive cooling system. Technical Report. 2016. https://doi.org/10.13140/RG.2.1.3463.7202
[100] Lin W, Sundén B. Vehicle cooling systems for reducing fuel consumption and carbon dioxide: literature survey. SAE Technical Paper 2010-01-1509. 2010. https://doi.org/10.4271/2010-01-1509
[101] Lin Z, Zhu C, Liu W, Yan S. Study on heat dissipation system of phase change heat storage liquid-cooled lithium-ion battery pack. 4th International Conference on Intelligent Control, Measurement and Signal Processing (ICMSP), Hangzhou 2022;419-423. https://doi.org/10.1109/ICSP55950.2022.9859140
[102] Ling Z, Cao J, Zhang W, Zhang Z, Fang X, Gao X. Compact liquid cooling strategy with phase change materials for Li-Ion batteries optimized using response surface methodology. Appl Energy. 2018;228:777-788. https://doi.org/10.1016/j.apenergy.2018.06.143
[103] Liu F, Lan F, Chen J. Dynamic thermal characteristics of heat pipe via segmented thermal resistance model for electric vehicle battery cooling. J Power Sources. 2016;321:57-70. https://doi.org/10.1016/j.jpowsour.2016.04.108
[104] Liu Z, Fu R, Yuying Y. Chapter 2 – Preparation and evaluation of stable nanofluids for heat transfer application. Ali HM (ed.). Advances in Nanofluid Heat Transfer. 2022:25-57. https://doi.org/10.1016/B978-0-323-88656-7.00013-1
[105] Lobodzinski M. Autokult. manuals and mechanics. Fluids for car radiators – composition, types and operation. 2014. https://autokult.pl/plyny-do-chlodnic-samochodowych-sklad-rodzaje-i-eksploatacja,6809059043883137a
[106] Lopez-Sanz J, Ocampo-Martinez C, Alvarez-Florez J, Moreno-Eguilaz M, Ruiz-Mansilla R, Kalmus J et al. Nonlinear model predictive control for thermal management in plug-in hybrid electric vehicles. IEEE T Veh Technol. 2017; 66(5):3632-3644. https://doi.org/10.1109/TVT.2016.2597242
[107] Lopez-Sanz J, Ocampo-Martinez C, Alvarez-Florez J, Moreno-Eguilaz M, Ruiz-Mansilla R, Kalmus J et al. Thermal management in plug-in hybrid electric vehicles: a real-time nonlinear model predictive control implementation. IEEE T Veh Technol. 2017;66(9):7751-7760. https://doi.org/10.1109/TVT.2017.2678921
[108] Lu Z, Meng XZ, Wei LC, Hu WY, Zhang LY, Jin LW. Thermal management of densely-packed EV battery with energy forced air cooling strategies. Procedia. 2016;88:682-688. https://doi.org/10.1016%2Fj.egypro.2016.06.098
[109] Lu Z, Yu X, Wei L, Qiu Y, Zhang L, Meng X et al. Parametric study of forced air cooling strategy for lithium-ion battery pack with staggered arrangement. Appl Therm Eng. 2018;136:28-40. https://doi.org/10.1016/j.applthermaleng.2018.02.080
[110] Mahamud R, Park C. Reciprocating air flow for Li-ion battery thermal management to improve temperature uniformity. J Power Sources. 2011;196(13):5685-5696. https://doi.org/10.1016/j.jpowsour.2011.02.076
[111] Malik M, Dincer I, Rosen MA, Mathew M, Fowler M. Thermal and electrical performance evaluations of series connected Li-ion batteries in a pack with liquid cooling. Appl Therm Eng. 2018;129:472-481. https://doi.org/10.1016/j.applthermaleng.2017.10.029
[112] Manikandan S, Jancirani J. Heat transfer enhancement of thermal system using nanofluids. J Chem Pharm Sci. 2014;4:38-40.
[113] Masoudi Y, Azad NL. MPC-based battery thermal management controller for Plug-in hybrid electric vehicles. 2017 American Control Conference (ACC), Seattle 2017:4365-4370. https://doi.org/10.23919/ACC.2017.7963627
[114] Mohammadpoor M, Sabbaghi S, Zerafat MM, Manafi Z. Investigating heat transfer properties of copper nanofluid in EG synthesized through single and two-step routes. International Journal of Refrigeration. 2019;99:243-250. https://doi.org/10.1016/j.ijrefrig.2019.01.012
[115] Naraki M., Peyghambarzadeh SM, Hashemabadi SH, Vermahmoudi Y. Parametric study of overall heat transfer coefficient of CuO/water nanofluids in a car radiator. Int J Therm Sci. 2013;66:82-90. https://doi.org/10.1016/j.ijthermalsci.2012.11.013
[116] O'Keefe M, Bennion K. A comparison of hybrid electric vehicle power electronics cooling options. 2007 IEEE Vehicle Power and Propulsion Conference, Arlington 2007:116-123, https://doi.org/10.1109/VPPC.2007.4544110
[117] Okuyama Auto Sports Developer. Reservoir tank. https://www.carbing.co.jp/international/products/tank/reservoir.shtml
[118] Oni T, Ajayi R, Faluru E. Heat transfer augmentation using CaC_2-water nanofluid. American Journal of Engineering Research (AJER). 2018;7(6):260-268. http://www.ajer.org/papers/Vol-7-issue-6/ZG0706260268.pdf
[119] Oyedepo SO, Ezeuduji D, Araoyinbo AO, Kilanko O, Efewikekwe UK, Dirisu JO et al. Numerical modeling of heat transfer performance and optimization of car radiator using (H_2O/Al_2O_3) nanofluids as coolant. Numer Heat Transf Part B Fundam. 2022;82:185-198. https://doi.org/10.1080/10407790.2022.2083854
[120] Pastor JV, García-Oliver JM, Pastor JM, Ramírez-Hernández JG. Ignition and combustion development for high speed direct injection diesel engines under low temperature cold start conditions. Fuel. 2011;90(4):1556-1566. https://doi.org/10.1016/j.fuel.2011.01.008
[121] Pentrite Oil Company Pty Ltd. Green OEM Coolant Concentrate. https://penriteoil.com.au/products/green-oem-coolant-concentrate

[122] Pesaran AA. Battery thermal management in EVs and HEVs: Issues and solutions. Advanced Automotive Battery Conference, Las Vegas 2001;43.
[123] Pety SJ, Tan MHY, Najafi AR, Barnett PR, Geubelle PH, White SR. Carbon fiber composites with 2D microvascular networks for battery cooling. Int J Heat Mass Transf. 2017; 115: 513-522. https://doi.org/10.1016/j.ijheatmasstransfer.2017.07.047
[124] Peyghambarzadeh SM, Hashemabadi SH, Naraki M, Vermahmoudi Y. Experimental study of overall heat transfer coefficient in the application of dilute nanofluids in the car radiator. Appl Therm Eng. 2013;52(1):8-16. https://doi.org/10.1016/j.applthermaleng.2012.11.013
[125] Prudhvi G, Vinay G, Babu GS. Cooling systems in automobiles & cars. International Journal of Engineering and Advanced Technology (IJEAT). 2013;2(4):688-696.
[126] Rafi AA, Haque R, Sikandar F, Chowdhury NA. Experimental analysis of heat transfer with CuO, Al_2O_3/water-ethylene glycol nanofluids in automobile radiator. AIP Conf. 2019;2121. https://doi.org/10.1063/1.5115878
[127] Rao Z, Qian Z, Kuang Y, Li Y. Thermal performance of liquid cooling based thermal management system for cylindrical lithium-ion battery module with variable contact surface. Appl Therm Eng. 2017;123:1514-1522. https://doi.org/10.1016/j.applthermaleng.2017.06.059
[128] Recochem. HD expert premium antifreeze/coolant. https://www.recochem.com/products/hd-expert-premium-antifreeze-coolant/
[129] Renteria JD, Nika DL, Balandin AA. Graphene thermal properties: applications in thermal management and energy storage. Appl Sci. 2014:525-547. https://doi.org/10.3390/app4040525
[130] Rislone. How to choose the right coolant for your car. https://rislone.com/blog/cooling/how-to-choose-the-right-coolant-for-your-car/
[131] Romero-Piedrahita CA, Carranza-Sánchez YA, Mejía-Calderón LA. Engine heat transfer in mechanical engineering curriculum. 23rd ABCM International Congress of Mechanical Engineering. December 6-11, 2015, Rio de Janeiro. COB-2015-1422.
[132] Ruelas E. Symptoms of a bad or failing cooling/radiator fan motor. YourMechanic. 2016. https://www.yourmechanic.com/article/symptoms-of-a-bad-or-failing-cooling-radiator-fan-motor
[133] Ruelas E. Symptoms of a bad or failing heater bypass tube. YourMechanic. 2016. https://www.yourmechanic.com/article/symptoms-of-a-bad-or-failing-heater-bypass-tube
[134] Safikhani H, Abbassi A. Effects of tube flattening on the fluid dynamic and heat transfer performance of nanofluids. Adv Powder Technol. 2014;25:1132-1141. https://doi.org/10.1016/j.apt.2014.02.018
[135] Saif M. Types of cooling system in automobile engines (I.C Engine). The engineers post. 2021. https://www.theengineerspost.com/cooling-system-for-ic-engine/?utm_content=cmp-true
[136] Saji VS. A review on recent patents in corrosion inhibitors. Recent Pat Corrosion Sci. 2010;2:6-12. https://doi.org/10.2174/1877610801002010006
[137] Sajid MU, Hafiz MA. Recent advances in application of nanofluids in heat transfer devices: a critical review. Renew Sust Energ Rev. 2019;103(10):556-592. https://doi.org/10.1016/j.rser.2018.12.057
[138] Saw LH, Ye Y, Yew MC, Chong WT, Yew MK, Ng TC. Computational fluid dynamics simulation on open cell aluminium foams for Li-ion battery cooling system. Appl Energy. 2017;204:1489-1499. https://doi.org/10.1016/j.apenergy.2017.04.022
[139] Schneider S, Stehlig J, Eilemann A. Cascaded charge air cooling for PC diesel engines. MTZ Worldwide 2014;75(6):4-9. https://doi.org/10.1007/s38313-014-0155-3
[140] Seraj M, Yahya SM, Badruddin IA, Anqi AE, Asjad M, Khan ZA. Multi-response optimization of nanofluid-based I. C. engine cooling system using fuzzy PIV method. Processes. 2020;8(1):30. https://doi.org/10.3390/pr8010030
[141] Seraj M, Yahya SM, Anas M, Sutrisno A, Asjad M. Integrated Taguchi-GRA-PCA for optimising the heat transfer performance of nanofluid in an automotive cooling system. Grey Systems: Theory and Application. 2021;11(1):152-165. https://doi.org/10.1108/GS-09-2019-0036
[142] Serdaroğlu G, Kaya S. Organic and inorganic corrosion inhibitors. Organic Corrosion Inhibitors. Verma C, Hussain CM (eds). Ebenso 2021. https://doi.org/10.1002/9781119794516.ch4
[143] Shahid S, Chaab MA. Development and analysis of a technique to improve air-cooling and temperature uniformity in a battery pack for cylindrical batteries. Therm Sci Eng Prog. 2018;5:351-363. https://doi.org/10.1016/j.tsep.2018.01.003
[144] Sharma V, Kumar RN, Thamilarasan K, Bhaskar GV, Devra B. Heat reduction from IC engine by using Al_2O_3 nanofluid in engine cooling system. American Journal of Engineering Research (AJER). 2016;3(4):173-177.
[145] Shatrov M, Krichevskaya T, Yakovenko A, Solovyev A. The IT based internal combustion engines integrated teaching complex. Auer M, Tsiatsos T (eds). The Challenges of the Digital Transformation in Education. Advances in Intelligent Systems and Computing. 2018;916:333-343. https://doi.org/10.1007/978-3-030-11932-4_32
[146] Sica LUR, Contreras EMC, Filho EPB, Parise JAR. Cold start analysis of an engine coolant-MWCNT nanofluid: Synthesis and viscosity behavior under shear stress. P I Mech Eng D-J Aut. 2022;236:366-380. https://doi.org/10.1177/09544070211019217
[147] Stauffer E, Dolan JA, Newman R. Chapter 14 – Other possible examinations conducted on fire debris. Stauffer E, Dolan JA, Newman R (eds). Fire Debris Analysis. Academic Press 2008:529-578. https://doi.org/10.1016/B978-012663971-1.50018-X
[148] Subhedar DG, Ramani BM, Gupta A. Experimental investigation of heat transfer potential of Al_2O_3/water-mono ethylene glycol nanofluids as a car radiator coolant. Case Stud Therm Eng. 2018;11:26-34. https://doi.org/10.1016/j.csite.2017.11.009
[149] Sundralingam D. Car water pump failure: signs to pay attention to before it's too late. CarSome May 2022. https://www.carsome.my/news/item/car-water-pump-failure
[150] Szilágyi B. Corrosion inhibitors in antifreeze coolants. 44th International Petroleum Conference, Bratislava 2009.
[151] Tan MHY, Najafi AR, Pety SJ, White SR, Geubelle PH. Multi-objective design of microvascular panels for battery cooling applications. Appl Therm Eng. 2018;135:145-157. https://doi.org/10.1016/j.applthermaleng.2018.02.028
[152] Taofeek Y. A study on the factors influencing preferred use of water over the branded engine coolant among automobile users. International Journal of Trend in Research and Development. 2017;4(6):68-70.
[153] Taofeek Y, Bukola B, Ismaila, Olasunkanmi I. Analytical test of water-extract from fermented ground maize as an alternative base for engine coolants. Walailak Journal of Science and Technology. 2017;14(2):75-82.
[154] The Engineering Toolbox. Ethylene glycol heat-transfer fluid properties. https://www.engineeringtoolbox.com/ethylene-glycol-d_146.html

[155] Tian Z, Gan W, Zhang X, Gu B, Yang L. Investigation on an integrated thermal management system with battery cooling and motor waste heat recovery for electric vehicle. Appl Therm Eng. 2018;136:16-27. https://doi.org/10.1016/j.applthermaleng.2018.02.093
[156] Vajjha RS, Das DK, Namburu PK. Numerical study of fluid dynamic and heat transfer performance of Al_2O_3 and CuO nanofluids in the flat tubes of a radiator. Int J Heat Fluid Flow. 2010;31:613-621. https://doi.org/10.1016/j.ijheatfluidflow.2010.02.016
[157] Valeo Service. Car thermostats. https://www.valeoservice.com/en-com/passenger-car/cooling-system-air-management-technologies/car-thermostats
[158] Valvoline. Valvoline multi-vehicle antifreeze coolant. https://sharena21.springcm.com/Public/Document/18452/823b8057-fe75-e711-9c10-ac162d889bd3/9069eb8c-e29c-e711-9c10-ac162d889bd3
[159] ValvolineGlobal. Choosing the right engine coolant for your car. https://www.valvolineglobal.com/en/engine-coolant/
[160] VEHQ. What are the symptoms of a bad coolant bypass valve. 2022. https://vehq.com/symptoms-bad-coolant-bypass-valve/
[161] Vijay T. A short article on engine cooling systems. 2017. https://www.linkedin.com/pulse/short-article-engine-cooling-systems-vijay-tharad/
[162] Vijaya GG, Aruna N, Janadharani S, Varshini ND, IoT based lithium-ion battery monitoring system in electric vehicle. 3rd International Conference on Artificial Intelligence and Smart Energy (ICAIS), Coimbatore 2023:1092-1096. https://doi.org/10.1109/ICAIS56108.2023.10073696
[163] Walters J, Duke D. Effective use of recycled water in cooling towers with new green technology. West Basin Municipal Water District, Carson CA & Water Conservation Technology International. Temecula 2009:1-59.
[164] Wang Q, Jiang B, Xue QF, Sun HL, Li B, Zou HM et al. Experimental investigation on EV battery cooling and heating by heat pipes. Appl Therm Eng. 2015;88:54-60. https://doi.org/10.1016%2Fj.applthermaleng.2014.09.083
[165] Wang S, Li Y, Li YZ, Mao Y, Zhang Y, Guo W et al. A forced gas cooling circle packaging with liquid cooling plate for the thermal management of Li-ion batteries under space environment. Appl Therm Eng. 2017;123:929-939. https://doi.org/10.1016/j.applthermaleng.2017.05.159
[166] Wang X, Dennis M. A comparison of battery and phase change cool storage in a PV cooling system under different climates. Sustain Cities Soc. 2018;36:92-98. https://doi.org/10.1016/j.scs.2017.09.035
[167] Wei Y, Chaab MA. Experimental investigation of a novel hybrid cooling method for lithium-ion batteries. Appl Therm Eng. 2018;136:375-387. https://doi.org/10.1016/j.applthermaleng.2018.03.024
[168] Wiriyasart S, Hommalee C, Sirikasemsuk S, Prurapark R, Naphon P. Thermal management system with nanofluids for electric vehicle battery cooling modules. Case Studies in Thermal Engineering. 2020;18:100583. https://doi.org/10.1016/j.csite.2020.100583
[169] Wozniak M. Urządzenie do wymiany płynu chłodzącego w układzie chłodzenia pojazdów samochodowych/Tool to change coolant fluid in coolant system in passanger vehicles. PL Patent 394224. 2013.
[170] Wulandari AD, Sutriyo S, Rahmasari R. Synthesis conditions and characterization of superparamagnetic iron oxide nanoparticles with oleic acid stabilizer. J Adv Pharm Technol Res. 2022;13(2):89-94. https://doi.org/10.4103%2Fjaptr.japtr_246_21
[171] Xie J, Ge Z, Zang M, Wang S. Structural optimization of lithium-ion battery pack with forced air cooling system. Appl Therm Eng. 2017;126:583-593. https://doi.org/10.1016/j.applthermaleng.2017.07.143
[172] Xu J, Lan C, Qiao Y, Ma Y. Prevent thermal runaway of lithium-ion batteries with minichannel cooling. Appl Therm Eng. 2017;110:883-890. https://doi.org/10.1016/j.applthermaleng.2016.08.151
[173] Yuksel T, Michalek J. Development of a simulation model to analyze the effect of thermal management on battery life. SAE Technical Paper 2012-01-0671. 2012. https://doi.org/10.4271/2012-01-0671
[174] Zhang T, Gao Q, Wang G, Gu Y, Wang Y, Bao W et al. Investigation on the promotion of temperature uniformity for the designed battery pack with liquid flow in cooling process. Appl Therm Eng. 2017;116:655-662. https://doi.org/10.1016/j.applthermaleng.2017.01.069
[175] Zhao C, Cao W, Dong T, Jiang F. Thermal behavior study of discharging/charging cylindrical lithium-ion battery module cooled by channeled liquid flow. Int J Heat Mass Transf. 2018;120:751-762. https://doi.org/10.1016/j.ijheatmasstransfer.2017.12.083
[176] Zhao J, Rao Z, Li Y. Thermal performance of mini-channel liquid cooled cylinder based battery thermal management for cylindrical lithium-ion power battery. Energy Convers Manag. 2015;103:157-165. https://doi.org/10.1016/j.enconman.2015.06.056
[177] Zhao R, Gu J, Liu J. Optimization of a phase change material based internal cooling system for cylindrical Li-ion battery pack and a hybrid cooling design. Energy. 2017;135:811-822. https://doi.org/10.1016/j.energy.2017.06.168
[178] Zhu C, Lu F, Zhang H, Mi CC. Robust predictive battery thermal management strategy for connected and automated hybrid electric vehicles based on thermoelectric parameter uncertainty. IEEE J Em Sel Top P. 2018;6(4):1796-1805. https://doi.org/10.1109/JESTPE.2018.2852218
[179] Zhukov V, Melnik O, Logunov N, Chernyi S. Regulation and control in cooling systems of internal combustion engines. E3S Web Conf. 2019;135:02015. https://doi.org/10.1051/e3sconf/201913502015
[180] Zhukov V, Pulyaev A, Melnik O, Nyrkov A. Ensuring the permissible temperature state of parts of the cylinder-piston group of forced diesels. 2019 IEEE Conference of Russian Young Researchers in Electrical and Electronic Engineering (EIConRus); Saint Petersburg and Moscow 2019:385-388. https://doi.org/10.1109/EICONRUS.2019.8657247
[181] 2CARPROS. Symptoms of a bad coolant temperature sensor. 2022. https://www.2carpros.com/articles/symptoms-of-a-bad-coolant-temperature-sensor

Lukasz Stajuda, MSc. – Ecotechnology Team, Lodz University of Technology, Poland.
e-mail:*lukasz.stajuda@lodzkie.pl*

Dmytro Levchenko, DEng. – Ecotechnology Team, Lodz University of Technology, Poland.
e-mail: *dmytro.levchenko@p.lodz.pl*

Przemyslaw Kubiak, DSc. DEng. – Ecotechnology Team, Lodz University of Technology, Poland.
e-mail: *przemyslaw.kubiak@p.lodz.pl*

Mateusz Szymczyk, DEng. – Department of Vehicles and Fundamentals of Machine Design, Lodz University of Technology, Poland.
e-mail: *ks670907@p.lodz.pl*

Kamil Siczek, MSc. – Faculty of Law and Administration, University of Lodz, Poland.
e-mail: *kamilkkk000000@tlen.pl.*

Prof. Gustavo Ozuna – Department of Industrial Engineering and Systems, University of Sonora, Mexico.
e-mail: *gozuna@industrial.uson.mx.*

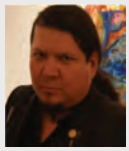

Marek Wozniak, DEng. – Department of Vehicles and Fundamentals of Machine Design, Lodz University of Technology, Poland.
e-mail: *marek.wozniak.1@p.lodz.pl*

Grzegorz Bogusławski, DEng. – Ecotechnology Team, Lodz University of Technology, Poland.
e-mail: *grzegorz.boguslawski@p.lodz.pl*

Maciej Kuchar, DEng. – Department of Vehicles and Fundamentals of Machine Design, Lodz University of Technology, Poland.
e-mail: *maciej.kuchar@p.lodz.pl*

Krzysztof Siczek, DSc. DEng. – Department of Vehicles and Fundamentals of Machine Design, Lodz University of Technology, Poland.
e-mail: *ks670907@p.lodz.pl*

Article citation info:
Wesołowski M, Hamid M, Mońka P, Janicka A. Analysis of the potential of electro-waste as a source of hydrogen to power low-emission vehicle powertrains. Combustion Engines. 2024;196(1):126-133. https://doi.org/10.19206/CE-169494

Mateusz WESOŁOWSKI
Mohamad HAMID
Piotr MOŃKA
Anna JANICKA

Combustion Engines
Polish Scientific Society of Combustion Engines

Analysis of the potential of electro-waste as a source of hydrogen to power low-emission vehicle powertrains

ARTICLE INFO

Received: 31 May 2023
Revised: 18 June 2023
Accepted: 11 July 2023
Available online: 4 August 2023

The decarbonisation of transport is one of the key aspects in the context of environmental protection. These emissions are particularly noticeable in highly urbanised areas, where the possibility of dispersal of harmful substances is much lower. A way to improve emission factors is the introduction of hydrogen vehicles. Burning hydrogen in engines significantly reduces emissions of harmful substances into the atmosphere compared to the combustion of conventional fuels used today. Hydrogen can be obtained by gasifying waste in a steam atmosphere. Electronic waste is a special type of waste characterised by a high degree of commingling, which makes it difficult to treat. The volume of this type of waste is increasing year on year. As a result of this process, we are able to obtain syngas. This gas, after separation processes, can be a source of hydrogen, an energy carrier that could prove crucial in low-carbon energy or transport applications. This paper presents the results of the gasification of electronic waste, the composition of the syngas obtained in the process and an assessment of the potential of this waste treatment technology to power means of transport.

Key words: *gasification, hydrogen drives, hydrogen, low-carbon transport, e-waste*

1. Introduction

Transportation development progress is key to the growth of societies which branches and consolidate the different elements of their sectors. For all intents and purposes, it is the "bloodstream" that distributes the goods produced. Developing countries are characterized by a burgeoning service sector, a thriving industry and, consequently, a growing transportation sector. A growing transportation sector can cause increasing emissions of harmful substances, particularly nitrogen oxides. As indicated by the European Environment Agency, the share of transportation in total greenhouse gas emissions is 28.5%. Road transport accounts for the largest share of all emissions at 20.5% [4].

To prevent such problems, new technologies are being developed to decarbonize modes of transportation and, consequently, the entire transportation sector. Both familiar conventional drives are being upgraded, but new vehicle concepts are also being developed. Recent years have seen particular growth in the electric vehicle market, but there is also a growing emphasis on increasing the share of hydrogen vehicles. The development of these two competing technologies is having a positive impact on the concept of decarbonizing the transportation sector. The aforementioned technologies can be applied to road and rail transportation, where they are already successfully occurring in many parts of the world. The use of hydrogen in vehicles can have two facets. The use of hydrogen can give a second life to internal combustion engines used in transportation vehicles, but it can also be used in hydrogen cells. The potential of hydrogen technologies is particularly studied by the countries of northern and western Europe [8].

Electric and hydrogen vehicle technologies are competitors for each other in the market. However, hydrogen technologies in means of transportation have features that can be qualified as their strengths. First and foremost among these features, it is worth noting the short refueling time of the vehicles and the greater range of the vehicles. Thus, they seem to be an ideal alternative to electric vehicles for long distances [7]. In addition, the use of hydrogen in traditional internal combustion engines means that we will have a modern fuel in a proven propulsion design, making it easier to operate and reducing unwanted events.

Hydrogen vehicle technologies also have advantages in terms of propulsion system design. Hydrogen tanks monitored in the vehicles do not require rare elements for their construction, which distinguishes them from electric vehicle traction batteries. The world's supply of lithium, among other elements, is a serious constraint on the construction of electric vehicles and thus can be a major barrier to their development. Hydrogen vehicles have no such barrier, and the various ways of producing hydrogen through renewable and conventional processes provide ample access to the energy carrier.

According to the study by Ściążko et al. [19] hydrogen vehicles will already account for about 10% of total vehicles in 2030, and in 2050 their share of the automotive market will be about 60%. The study also indicates that electric vehicles will develop their market share but from 10% in 2030 to 25% in 2050 [19]. The disparity between the technologies being developed clearly shows that hydrogen vehicles are the future of low-carbon transportation. These technologies can keep classic internal combustion engines in use, and the development of green technologies for hydrogen generation, could prove crucial for the transportation sector and improving the quality of life.

2. Streams and characterization of e-waste as a potential source of hydrogen

The characterization of electronic waste as a potential source of hydrogen would have to be divided into two main axes. In order for this waste to be useful in terms of its use as a feedstock for the gasification process, it is important to

know the characteristics of electronic waste and to know the streams of this type of waste. In particular, the second axis is very important in terms of potentially estimating the possibility of converting electronic waste in the gasification process.

2.1. Characteristics of electronic waste

Electronic waste is a very diverse group of goods, and consequently its composition can vary greatly depending on what type of equipment we are dealing with. According to the study by Forti, Baldé, Kuehr and Bel, we can distinguish 6 basic groups of electronic waste [6]. They include:

- temperature exchange equipment
- screens and monitors
- lamps
- large equipment
- small equipment
- small IT and Telecommunication equipment.

As can be seen, the waste groups can be characterized by different sizes and thus, by different shares of individual components in the product composition. There are particular problems in the department known as "large equipment". This waste is often generated, but there are numerous problems with its recovery. This type of electronic waste is deposited in places unsuitable for it, in wild dumps, and thus can negatively impact the local environment and threaten to contaminate the soil or water.

Electronic waste is characterized by a complex, integrated structure. Separating the various component fractions of devices is energy-intensive work. The development of the concept of gasification in a steam atmosphere makes it possible to solve the problem of both disassembling the individual components of the device and gaining access to reusable components. This allows easy access to rare or valuable elements such as copper [9].

Examples of electronic waste, the number of which is growing every year, are cell phones. They have the typical characteristics of electronic waste, that is, for example, an integrated structure. The stream of this type of waste is increasing due in part to technological advances and growing consumerism in rich countries.

The material composition of the sample phone is shown in Fig. 1.

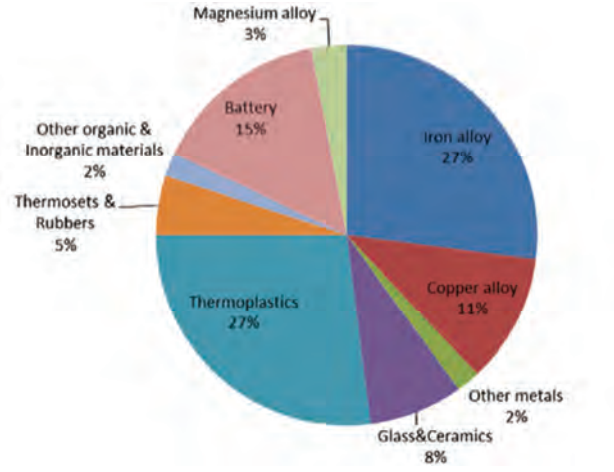

Fig. 1. Example of percentage material composition for a Nokia phone [20]

As Figure 1 shows, the composition of a standard cell phone is very complex. Most of the phone's composition is made up of various types of metals, with iron alloys making up the largest percentage. Thermoplastics account for the same percentage. The third component of the phone with the highest mass is the battery. Due to the large stream of this type of waste and the high proportion of polymeric materials in its composition, it can be a good substrate for the gasification process. In addition, the product after the gasification process is ready for material recycling of such components as copper alloys or magnesium alloys, among others. The process of gasification in a steam atmosphere has a positive effect on the process of disassembly of individual product components. Under the action of high temperature coming from steam, plastic components decompose and, with the gasification agent form syngas, which can be a hydrogen source after separation. This makes the plastic components, which are heavy to process, degrade, and can already be, in the form of a gas, an important element in terms of energy [20, 23].

Virtually every modern device is equipped with a printed circuit. This is one of the wastes that can be a substrate in the gasification process. In addition to it, devices are often equipped with various types of controllers, RAM or processors. This makes this type of waste stream advantageous in terms of its ability to be used as a potential source of hydrogen [23].

RAM may prove to be a particularly interesting waste. The popularity of RAM is increasing year by year. They are no longer used only in personal computers. The use of RAM can also be seen in modern vehicles, everyday devices such as smart coffee makers and televisions, and even smartwatches. The construction of RAM consists of two components, namely printed circuit boards and integrated circuits mounted on them. Materials in the form of RAM can be packaged in many ways, for example, using ceramic material [14].

Printed circuits can be characterized by different composition, which varies with the quality and proportion of materials used. According to the study "Valorization of Printed Circuit Boards from Electrical and Electronic Waste by Pyrolysis and Electronic Equipment by Pyrolysis", copper has the largest share in the construction of printed circuit boards and amounts to up to 27% by mass of the product. Metals account for about 40% of the product's mass and can be recovered in recycling after gasification. About 30% by mass is made up of plastics of various types, such as polyethylene and polyester. These plastics are very valuable in terms of treating electronic waste as a substrate in the gasification process. Their thermal decomposition in a steam atmosphere produces syngas [22].

2.2. Electronic waste streams

Electronic waste is growing every year, and the rate of increase in WEEE waste production is increasing. Parts of the world considered highly developed have a much higher per capita waste production. According to the study by Forti et al. [6], very high contrast in this regard is seen between Europe and Africa. Electro-waste generated per person in Europe is 16.2 kg, while for Africa, it is only 2.5 kg per person. At the same time, Europe is the leader of all

continents in terms of the amount of electronic waste generated per person. Asia has the largest amount of electronic waste, with 24.9 Mt. The second largest amount of electronic waste is generated in North and South America, with 13.1 Mt. This shows a very large disproportion, and allows us to conclude that Asian countries such as Japan, South Korea and China place great emphasis on the development of electronic and electrical equipment, and are world leaders in this field, and therefore generate the most electronic waste [6].

We can conclude that the purchasing power of a selected part of the population clearly influences purchasing behavior, and, consequently the generation of electronic waste. This is related to a number of factors, one of which is certainly the standard of living that the selected groups prefer. A greater number of electronic equipment significantly increases the comfort of life, which in turn increases opportunities for development. We can observe a particular increase in the number of electronic equipment according to earnings in the case of laptops and cell phones. These relationships are shown in Fig. 2.

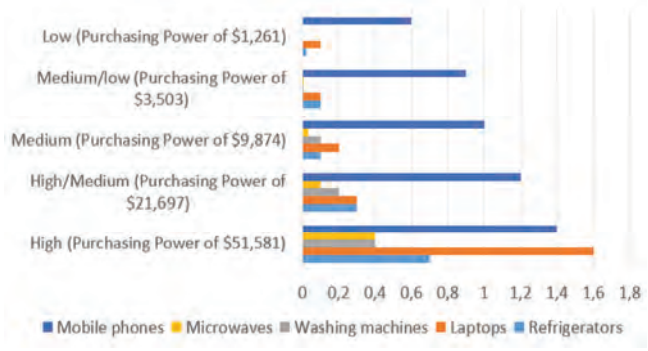

Fig. 2. Effect of purchasing power on the number of electronic devices owned [6]

As the graph in Fig. 2 shows, technological advances are making a significant contribution to increasing e-waste streams, thereby increasing the number of potential substrates that can be used in the gasification process [6].

The development of technology can be seen very well from the growth of the various sections of electronic waste. The increments were studied over the period from 2014–2019. During the period under review, electronic waste qualified as "Temperature exchange equipment" grew the most, with a 7% increase [6]. This indicates a pronounced trend in replacing equipment responsible for maintaining thermal comfort indoors. The new devices are characterized by higher efficiencies and lower energy consumption, which is beneficial from the point of view of consumers. In addition, the trend of using reversible heat pumps may increase the waste stream in this area, as may the increasingly popular use of photovoltaic panels. Photovoltaic panels are included in the division of large equipment, which growth in the period under review is 5%. In addition to them, the division includes washing machines and clothes dryers, for example. These are usually large appliances, problematic in terms of their transportation to waste disposal sites. The aforementioned photovoltaic panels are a very interesting and forward-looking type of waste. The popularity of the development of photovoltaic installations is very high especially for private entities. Taking into account the life cycle of photovoltaic panels and their decreasing efficiency with age will make them a large waste stream in 15–20 years. Increases in this area are already evident, as the first photovoltaic installations are just reaching the end of their life cycle. The amount of waste photovoltaic panels is shown in Fig. 3.

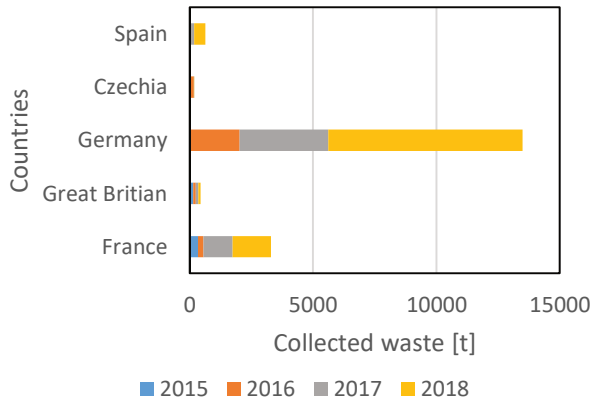

Fig. 3. Collected photovoltaic panels in selected countries in 2015–2018 [5]

3. Reverse logistics of e-waste

The issue of the amount of waste generated is only one component in the context of electronic waste management. An equally important issue is the aspect of waste collection and "recovery" after the device has completed its life cycle. This factor is very important, since it is not the number of wastes generated that really matters for the treatment process, but the number of wastes retrieved after the device has completed its useful life.

Europe compares very well with the world, where the amount of collected and reused electronic waste oscillates around 5.1 Mt, which is about 42.5% of the generated electro-waste. This result compares very well with other continents. In comparison, the percentage of electronic waste collection and reuse is 11.7% for Asia, and only 0.9% for Africa. This shows that the level of electronic waste collection stands at a low level in the world. Even in the case of Europe, it shows that 57.5% of electronic waste is not re-collected and reused [6].

According to the study by Nowakowski, the level of waste collection in Poland in 2015 was 38.38% [15]. Juxtaposing this with the previous figures, it appears that Poland compares quite positively with the world in terms of the amount of electronic waste re-collected, but further, the numbers are far from the high efficiency of electronic waste return logistics.

While the level of bulky waste collection is not at a low level, as it is about 41.84% in Poland as of 2015, the mass of waste that remains uncollected is by far the largest, at about 154 608 t [15]. This shows that bulky waste collection has a very large impact on the electrical and electronic waste stream and can be a very important source both in terms of recycling metals and also being a substrate in the gasification process.

Several issues are important in the development of e-waste reverse logistics systems. The subject of electronic waste should be approached holistically both by developing people's awareness in the context of environmental education and the scope of their responsibilities in the context of electronic waste, as well as an information campaign on waste collection points or treatment options. It would also be advisable to consider forms of gratification for people for fulfilling their obligations to segregate waste, especially electronic waste, as they can be a threat to the environment. The gratification concept could include, among other things, reducing the tax on the purchase of new electronic devices, assuming documented e-waste donation or reducing the waste disposal fee.

An important element in reverse logistics is the inspection stage of the received product. Not all previously used equipment or machinery has to be disposed of. Many components can be reused after appropriate processing or certain modifications. It is therefore important that the equipment is thoroughly inspected and properly categorized. This makes it possible for some machine and equipment components to have a longer life cycle and last longer as part of a new product [3, 15].

The use of mobile apps as an enhancement to the electronic waste collection process seems to be an interesting idea. The use of this method requires proper preparation of the application, or website. The idea is that any interested person can report the need to donate e-waste via the Internet. The database collects information on the type of waste and its mass or size, and the company's dispatch center makes a decision on the scheduled transport. An ideal improvement would be to incorporate artificial intelligence or neural networks into the operation of such a system. This would reduce the need for human labor, and the neural networks, after repeated processing, would be able to match optimal routes and means of transportation for the selected type of electronic waste [16].

E-waste reverse logistics, therefore, needs a highly interdisciplinary approach based on the cooperation of both transportation, IT and environmental specialists. The joint efforts of these aforementioned industries are able to guarantee an increased volume of waste received, and thus increase the stream of potential substrates for hydrogen production.

4. The gasification process.

Gasification is a process in which a given raw material is converted into a gas with the help of an oxidizing agent. It is the oldest technology for obtaining hydrogen. It is stated to be an intermediate process between combustion and pyrolysis. The temperature of the process is between 600 and 1000^{o}C and the raw materials for the process can be either waste, biomass or fossil fuels. The composition of the gas resulting from the aforementioned process depends on a number of factors, which are its components. The composition of the gas depends on the substrate used in the experiment, the temperature of the process, the pressure used and the agent used for gasification. Among the reactants we can distinguish oxygen, steam, air or carbon dioxide, among others [9]. Processes based on the steam medium reach a hydrogen level of about 40% in the syngas mixture [12].

The gasification process is particularly useful in the processing of integrated products whose components may be valuable. The use of gasification for the processing of electronic waste makes it possible to obtain syngas from which, after appropriate transformation, we are able to obtain pure hydrogen and recover rare raw materials from the residue of the substrate after the gasification process. The composition of syngas is hydrogen, carbon monoxide, methane, carbon dioxide, nitrogen and steam [9].

Gasification may be carried out in the presence of a catalyst to improve the synthesis process and eliminate organic phases [9]. The use of a suitable catalyst is very important when it comes to creating syngas. Among the most important features of a suitable catalyst we must certainly include its price and availability on the market. Among the catalytic deposits, it is worth mentioning such active substances as dolomite, calcium oxide or iron oxide [18].

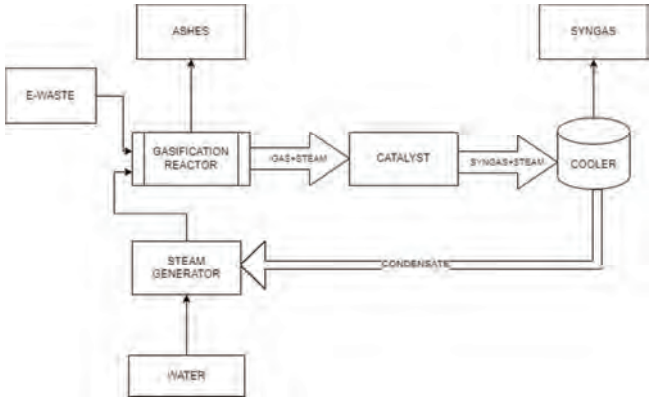

Fig. 4. Gasification process of electronic waste in a steam atmosphere

As shown in Fig. 4, the electronic substrate gasification scheme has its own closed circuit. The weakest point in the process appears to be the steam generator. It needs a power source, and thus a good solution would be to couple the gasification plant with a source of renewable energy. This would lower the economic cost of producing hydrogen, and the use of electricity from renewable energy sources would also lower the carbon footprint.

The gasification process supported by renewable energy sources is a very interesting concept. The cost of producing a kilogram of hydrogen by gasification is between $1.21–$3.5 and could be reduced by using renewable sources in the process [12]. Research on this topic includes both solar, wind and geothermal energy concepts. Concepts are also being developed for hybrid or cogeneration systems using waste heat of the process. Geothermal systems are a particularly interesting alternative for Polish conditions knowing our conditions regarding geothermal deposits. In addition, biomass, both waste and energy crops, can be used in the substrate gasification process. This makes the process capable of coming from renewable sources, and the resulting hydrogen can be an important factor in balancing energy systems [12, 13].

Current global trends promote low-carbon energy and low-carbon transportation. The gasification process seems

to be an ideal solution to such problems. It makes it possible to manage various types of waste, such as electronic waste, plastics or sewage sludge, which can become substrates for the process. The process makes it possible to produce hydrogen, the use of which can be very wide, both in low-emission transportation, including internal combustion engines, as well as in the power industry for fueling gas turbines.

5. Separation of hydrogen from syngas.

The final product of the gasification process is syngas, which is a mixture of various elements, including hydrogen, carbon dioxide, methane, carbon monoxide or nitrogen. Among the side effects of the process, we can distinguish tars or ashes [17].

To obtain a carrier of clean energy in the form of hydrogen from syngas, several separation steps are needed. For industrial-scale systems, the first step is to use water reforming to increase the proportion of hydrogen in the mixture. The next step is to use one of three hydrogen purification and separation methods. These methods are PSA (Pressure Swing Adsorption), cryogenic distillation, and membrane techniques. Depending on needs, the hydrogen energy carrier can also be further purified using specialized equipment [2].

Among the methods mentioned, membrane separation methods are particularly noteworthy. The main division of membranes is the composition of their structure. Thus, we can distinguish between organic, inorganic and composite membranes. The advantage of their use is the absence of waste, as they are a physical barrier. Other advantages of such methods include the ease of operation of the hydrogen separation plant or the possibility of producing hydrogen in a continuous process. This is very important in the context of building a gasification plant with the possibility of continuous batching on a process scale. The sequestration of hydrogen in a continuous process allows the possibility of continuous production to be maintained, and thus gasification can be a stable process that does not destabilize the energy system or hydrogen-based transportation systems [2].

In the separation of hydrogen from syngas, it is also possible to use so-called chemical loops. The first step, as with the previous methods, is hydrogen enrichment by water reforming. The water reforming process is responsible for the conversion of carbon monoxide into carbon dioxide, which is automatically absorbed by the calcium oxide sorbent. Then, in the regeneration stage, the gas with oxygen is fed into the gasification reactor. The gas is designed to oxidize the iron-based catalyst. During this time, the sorbent that previously absorbed the carbon dioxide is decomposed by the acting heat and releases the previously stored compound. Thus, the separation process contains two chemical loops, one involving the activity in the catalyst reactor, the other involving the action of the sorbent [10].

6. Gasification of electronic waste

The gasification of electronic waste was performed according to the scheme shown earlier in Fig. 4. The substrate in the gasification process was RAM memory. The experimental system is divided into a gasification zone, where the feedstock lands, and a catalyst zone, which in the case of the study conducted was dolomite. The gasification agent was steam. Two survey samples were conducted. The table below summarizes the parameters of the two test samples.

Table 1. Results of the gasification process

Process components	Experiment 1	Experiment 2	Units
Mass of the charge before the process	120.54	194.56	[g]
Mass of the charge after the process	92.6	156.15	[g]
Mass loss	27.94	38.41	[g]
Mass loss	23.18	19.74	[%]
Mass of water placed in the steam feeding flask	398.21	279.35	[g]
Mass of water remaining in the steam feeding flask	18.37	194.74	[g]
Mass of water given in the process	379.84	84.61	[g]
Steam feeding time	295	293	[min]
Average steam output	1.29	0.29	[g/min]
Condensate mass	267.15	35.1	[g]
Steam/water loss	112.69	49.51	[g]

As can be seen in Table 1, samples containing RAM had different weights. In the case of the first experiment, a higher proportion of the gasification medium was also evident, with a consequent increased amount of condensate. Figure 5 and 6 show the gasification process waveforms.

Figure 5 and 6 show that gasification in experiment two took less time than in example one. The reactor heating rate was the same for both experiments. The maximum reactor and catalyst temperatures for both experiments were the same. We can also deduce from Fig. 5 and 6 that the steam feeding started 28 minutes earlier in experiment 2 than in experiment 1. In the case of experiment 1, there were spikes in the temperature of the catalyst, while in experiment two the temperature course was harmonic. The P1 sample for experiment 1 was taken 88 minutes after the start of steam injection, while the P1 sample for experiment 2 was taken 53 minutes after the start of steam injection. Despite this difference, the samples have similar compositions. Table 2 shows the composition of the gases that are the product of the gasification process.

Table 2. The results of the analysis of gases produced from the gasification process

	Experiment 1		Experiment 2			Units
Gas analysis	Sample P1	Sample P2	Sample P1	Sample P2	Sample P3	
CO	17.32	1.33	17.51	12.66	11.05	[%Vol]
CO_2	50.62	28.1	57.24	58.2	60.74	[%Vol]
0_2	5.96	7.09	3.44	4.13	3.74	[%Vol]
HC	667	26	1050	402	142	[ppm Vol]
NO	–34*	–8*	7	9	–21*	[ppm Vol]
Lambda	0.939	1.144	0.918	0.957	0.966	–
Gas flow rate	2.0	0.9	–	1.4	1.4	[dm^3/min]
Estimated share of H_2	27.71	2.13	28.02	20.26	17.68	[%Vol]
*The minus results are due to the measuring range of the instrument.						

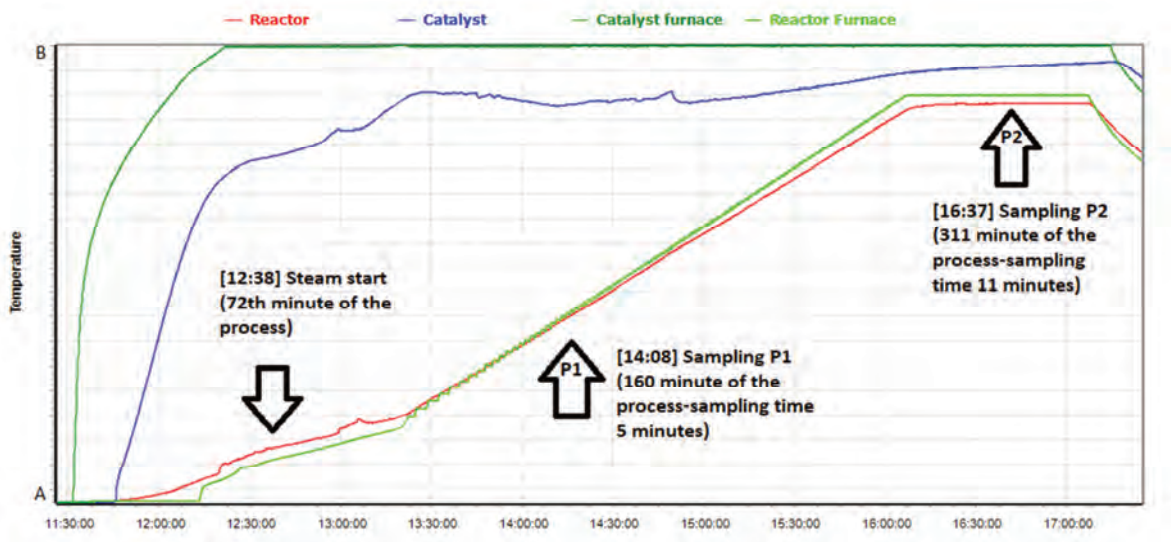

Fig. 5. The course of the gasification of the first experiment

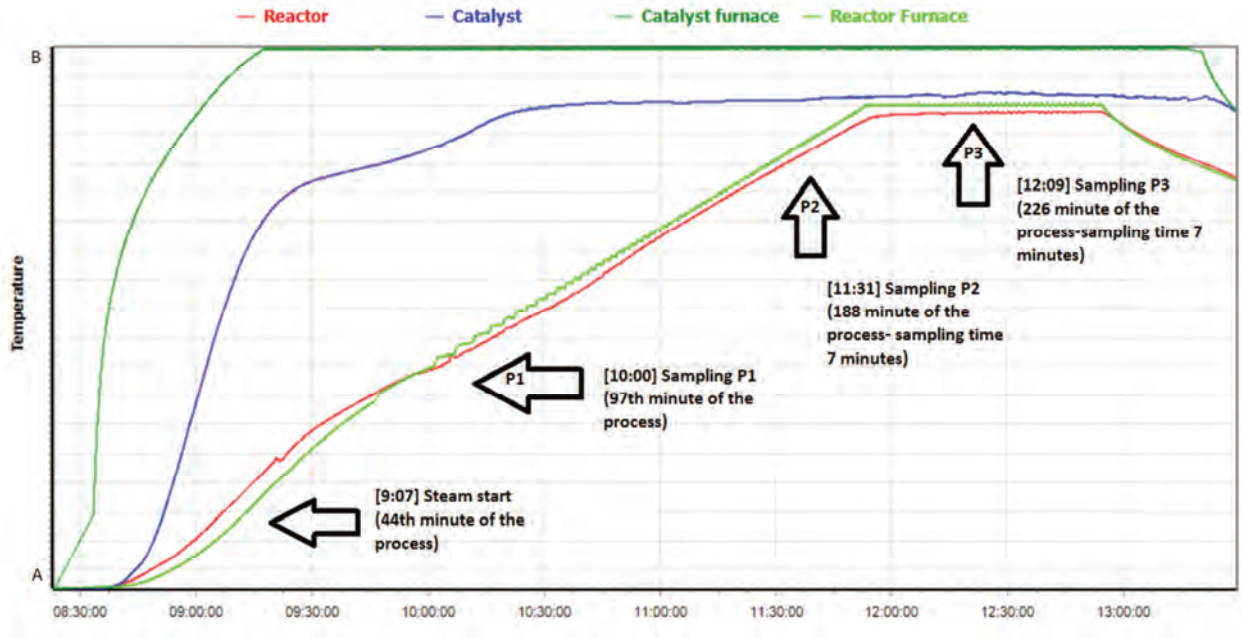

Fig. 6. The course of the gasification of the second experiment

The first gas samples were taken while the catalyst was heating up, when its performance was at a high level. This can be seen in the higher gas flux values. Once the catalyst reaches heating, its efficiency decreases over time, as does the gas flow rate. The initial phases of gasification also release the most hydrocarbons, which are the source of our interest. Over time, the presence of carbon oxides in the mixture also decreases. The highest flow rate is about 2 dm^3/min, which would yield about 0.55 dm^3 of hydrogen per minute. The estimated proportion of hydrogen was calculated by knowing the ratio of H_2 to CO. According to the literature, this ratio is 1.6 [12]. These values should be considered indicative, taking into account possible measurement errors when examining the gas composition and the potential inaccuracy of the method.

The materials lost between 19–23% of their mass after the gasification process. The remaining materials were characterized by a black color, visible copper layer of RAM. Behind the catalyst, chromium precipitated as a yellow precipitate. The material is recyclable, and the plastics have mostly oxidized to form syngas.

7. Summary and conclusions

Waste gasification technologies are a very important step towards sustainable and low-emission transport, especially since most of the hydrogen is produced in the process of reforming fossil resources [11]. Using waste, especially electronic waste, as a source of hydrogen for vehicles seems to be a solution with many advantages. In particular, we manage waste, a thing unnecessary for the environment, and get the opportunity to recover important raw materials

from the waste, and as a gaseous product, a fuel that can power vehicles.

The use of purely hydrogen-powered engines is an object of further research and requires a lot of money, while the use of engines combining hydrogen with diesel fuel is already a possible implementation. Such engines can achieve peak efficiencies of up to 50%, which compares very well with internal combustion engines powered by conventional fuels. The use of such a fuel mix also reduces emissions in the city, which is crucial in the context of sustainable urban development and low-carbon transportation systems, especially urban transportation [1]. In addition, hydrogen blended with biogas can further reduce the share of hydrocarbons in emissions and this is also one potential avenue for development [21].

Electronic waste as a process input is characterized by a high flux, and thus a high level of availability. The gasification process is an ideal solution for both the energy use of this waste and its disposal, thus offsetting its environmental impact. Plastic materials or epoxy resins used in electronic products are a very important part of the syngas that is formed afterwards. By combining the gasification process with renewable energy sources, the cost of the process is reduced and the emission burden will be even lower. The ecological process of producing hydrogen, as well as the characteristics of this energy carrier, make the application of the process a future-proof solution worthy of further study, and hydrogen is a great element for application in both the professional energy and automotive markets.

Nomenclature

WEEE	Waste of Electrical and Electronic Equipment	RAM	random-access memory
PSA	pressure swing adsorption	E-waste	electronic and electrical waste
IT	information technology		

Bibliography

[1] Boretti A, Hydrogen internal combustion engines to 2030. Int J Hydrogen Energ. 2020;45(43):23692-23703. https://doi.org/10.1016/j.ijhydene.2020.06.022

[2] Chmielewski AG, Wawryniuk K, Antczak J. Separation of syngas components using polymer and metallic membrane. http://www.eko-dok.pl/2012/13.pdf (accessed on 30 April 2023).

[3] Doan LTT, Amer Y, Lee S-H, Phuc PNK, Dat LQ. E-waste reverse supply chain: a review and future perspectives. Appl Sci. 2019;9:5195. https://doi.org/10.3390/app9235195

[4] European Environment Agency. 2022. www.europarl.europa.eu (accessed on 22.04.2023).

[5] Eurostat database. https://ec.europa.eu/eurostat/databrowser/view/ENV_WASELEE__custom_4322723/default/table?lang=en (accessed on 23.04.2023).

[6] Forti V, Baldé CP, Kuehr R, Bel G. The global e-waste monitor 2020: quantities, flows and the circular economy potential. United Nations University (UNU)/United Nations Institute for Training and Research (UNITAR) – co-hosted SCYCLE Programme, International Telecommunication Union (ITU) & International Solid Waste Association (ISWA), Bonn/Geneva/Rotterdam.

[7] Gis M, Gis W. Alternative ways of driving and powering vehicles, Transport Samochodowy, 2015;4:79-95.

[8] Gis M, Gis W. The current state and prospects for hydrogenisation of motor transport in Northwestern Europe and Poland. Combustion Engines. 2022;190(3):61-71. https://doi.org/10.19206/CE-144560

[9] Gurgul A, Szczepaniak W, Zabłocka-Malicka M. Thermal process of recovery of raw materials from electronic waste – steam gasification, Towards a circular economy Industry perspective. Kulczycka J, Głuc K (ed.). Publishing House IGSMiE PAN; Kraków 2017:41-48.

[10] Kai S, Le Q, Zhang T. Separation of hydrogen from syngas using a chemical-looping cycle. Fuel. 2012;98:80-87. https://doi.org/10.1016/j.fuel.2012.03.020

[11] Kotowski JW, Augustynowicz A. A growing position of methanol and hydrogen as energy carriers in the global economy. Combustion Engines. 2009;39(4):61-67. https://doi.org/10.19206/CE-117169

[12] Lepage T, Kammoun M, Schmetz Q, Richel A. Biomass-to-hydrogen: A review of main routes production, processes evaluation and techno-economical assessment. Biomass Bioenerg. 2021;144(105920):105920. https://doi.org/10.1016/j.biombioe.2020.105920

[13] Li H, Zhang X, Liu L, Wang S, Zhang GQ. Proposal and research on a combined heating and power system integrating biomass partial gasification with ground source heat pump. Energ Convers Manage. 2017;145:158-168. https://doi.org/10.1016/j.enconman.2017.04.090

[14] Mońka P, Szczepaniak W, Zabłocka-Malicka M. Gasification of RAM memory waste. Czasopismo Techniczne. Chemia, 2011;108:119-126.

[15] Nowakowski P. Identification of factors affecting the efficiency of the reverse logistics chain of waste electrical and electronic equipment. Knosala R (ed.). Innovations in management and production engineering. T.2 (in Polish). Publishing House of the Polish Society of Production Management. Opole 2017.

[16] Nowakowski P, Szwarc K, Supporting of the mobile collection of waste electrical and electronic equipment based on a web application with the integrated database. Conference: Transport Problems – VIII International Conference and V International Symposium of Young Researchers. 2016;801-810.

[17] Stepien P, Pulka J, Bialowiec A. Estimation of lower heating value and higher heating value of syngas from carbonized sewage sludge gasification. Ochrona Srodowiska. 2018;40(1):45-50.

[18] Szczepaniak W, Zabłocka-Malicka M, Zielińska A. Method for high-temperature recovery of materials composed of waste and system for high-temperature recovery of materials composed of waste. Patent description PL 235360, 2014.

[19] Ściążko M, Smółka B, Wenecki T. Prospects for hydrogen in transport and energy. Nowa Energia. 2018;3:7-11.

[20] Tanskanen P. Management and recycling of electronic waste. Acta Mater. 2013;61(3):1001-1011. https://doi.org/10.1016/j.actamat.2012.11.005

[21] Tira H, Gill S, Theinnoi K, Shenker J, Lau C, Tsolakis A et al. The study of simulated biogas on combustion and emission

characteristics in compression ignition engines. Combustion Engines. 2010;141(2):47-55. https://doi.org/10.19206/CE-117146

[22] Williams PT. Valorization of printed circuit boards from waste electrical and electronic equipment by pyrolysis. Waste Biomass Valori. 2010;1:107-120. https://doi.org/10.1007/s12649-009-9003-0

[23] Woynarowska A. Thermal utilization of electronic waste in a fluidized bed reactor. Doctoral Thesis. Publishing House of the Cracow University of Technology. Kraków 2014.

Mateusz Wesołowski, MEng. – Faculty of Mechanical Engineering, Wrocław University of Science and Technology, Poland.
e-mail: *mateusz.wes12@wp.pl*

Mohamad Hamid, PhD student – Faculty of Mechanical Engineering, Wrocław University of Science and Technology, Poland.
mail: *mohamad.hamid@pwr.edu.pl*

Piotr Mońka, DEng. – R&D departament, EKO PM Sp. z o.o, Poland.
e-mail: *pm@ekopm.pl*

Prof. Anna Janicka, DSc., DEng. – Faculty of Mechanical Engineering, Wrocław University of Science and Technology, Poland.
e-mail: *anna.janicka@pwr.edu.pl*

Article citation info:
Wendeker M, Grabowski Ł. Investigations of the city bus powertrain efficiency. Combustion Engines. 2024;196(1):134-139. https://doi.org/10.19206/CE-172819

Mirosław WENDEKER
Łukasz GRABOWSKI

Combustion Engines
Polish Scientific Society of Combustion Engines

Investigations of the city bus powertrain efficiency

ARTICLE INFO

Received: 7 June 2023
Revised: 15 September 2023
Accepted: 22 September 2023
Available online: 10 November 2023

Research work on the energy efficiency of vehicles is driven, among other things, by limits related to fuel consumption and carbon dioxide emissions. This also applies to city buses, where fuel consumption averages between 25 and 30 dm^3 per 100 km, which can be converted into approximately 87 kg CO_2 per dm^3. This article, therefore, presents the results of a study of the total efficiency of the power train of a city bus, taking into account the internal combustion engine, transmission, torque converter, and tire friction on the rollers. The test object was a 12-metre city bus equipped with diesel engines and an automatic gearbox. The tests were carried out on a chassis dynamometer by implementing the World Harmonized Vehicle Cycle (WHVC). The WHVC driving test is a synthesis of the vehicle's on-road speeds and consists of three stages: Urban, Rural, and Motorway. During the tests, the fuel consumption, vehicle speed, and power generated at the wheels of the bus were recorded. From this, efficiency was calculated as the ratio of the power measured at the wheels of the bus to the power contained in the fuel supplied to the engine. Efficiency was shown to range from 5 to 22%.

Key words: *efficiency, city bus, diesel engine*

1. Introduction

The efficiency of a vehicle's powertrain depends mainly on the design and efficiency of the engine, drivetrain i.e. gearbox, and main transmission [9, 14]. Despite the limitations associated with plans to phase out internal combustion engines from transport, research is still being carried out in this area [9, 10]. Modern compression-ignition engines are characterized by high thermodynamic efficiency due to, among other things, the use of high-pressure fuel injection systems, turbocharging, and emission control systems [1, 13]. The gearboxes are usually automated gearboxes whose control algorithms are adapted to the optimal engine operating conditions. In addition, the efficiency of the fuel energy conversion process on board the bus is influenced by the resistance to motion of the vehicle operating in urban conditions, i.e. the uphill resistance and inertia resistance, which will contribute to changes in the kinetic and potential energy of the vehicle. Consequently, the internal combustion engine installed as the vehicle's source of propulsion operates under varying load conditions. This is due to the varying intensity of vehicle traffic or the slope of the road. At the same time, the manner of operation has a significant impact on fuel consumption [15], and in particular the driving technique, i.e. the way the accelerator lever is operated.

These factors affect average fuel consumption. This is because, under road conditions, the engine operates at different overall efficiencies. Therefore, some studies have proposed a methodology for applying dynamic correction factors to steady-state engine data. Example results are included in the paper [7]. It was shown that, in the case of a conventionally powered vehicle, the average difference between the real-world energy demand and the values obtained for a vehicle operated in Switzerland was approximately 22% more than during the running test.

Regarding the compression-ignition engine, it should be mentioned that processes such as acceleration, start/stop and cold-start systems must be considered when determining efficiency. Another important factor influencing the transient operation of an IC engine is the turbocharger lag [5, 8].

Under steady-state conditions, the only parameters on which the actual value of the efficiency of converting fuel energy into mechanical power depends are the crankshaft speed and the torque generated by the engine, representing the engine loads. In the case of urban autobahn operation, the resistance to motion is constantly changing. The only state that can be considered a steady state is engine idling. Engine idling can comprise up to 45% of the total operating time of a city bus [2]. However, in the case of transients, characterized by varying engine load and crankshaft speed, the engine efficiency may be lower than that specified by steady-state characteristics.

One method of transient vehicle testing is the use of drive cycles. This is a repeatable representation of the road load conditions mapped. Examples include the popular driving cycle, SORT (Standardised On-Road Tests cycles) [4], or WHVC (World Harmonised Vehicle Cycle). These are time series of post-run speeds recorded at consecutive (equally spaced) time points [11]. They represent typical vehicle driving patterns in urban and non-urban conditions. Driving cycles are the result of a synthesis of real-world driving conditions such as speed, acceleration or road gradient. Driving cycles are often used in vehicle tests on a chassis dynamometer. Thanks to the controlled loading of the vehicle, it is possible to carry out repeated tests, e.g. on exhaust emissions. This allows emission tests to be carried out and compliance with exhaust emission standards to be assessed, which is still the subject of developmental research in internal combustion engine vehicles.

The World Harmonized Heavy Vehicle Cycle test was also used to measure emissions. The formaldehyde (HCHO) emissions from heavy diesel vehicles (HDVs) were presented in the work [11]. The purpose of using the WHVC test is to evaluate HCHO emissions from HDVs under controlled laboratory conditions and compare them

with other test cycles, such as the Harmonized Light Vehicle The WHVC test was performed at different temperatures (5°C and 23°C) to evaluate the impact of ambient temperature on HCHO emissions This study aimed to provide insight into real-time measurements of HCHO emissions from modern vehicles, and WHVC testing formed an essential part of the experimental tests conducted about this issue.

The efficiency of a vehicle's powertrain, relevant to the evolution of transport and plans to eliminate internal combustion engines, is a multidimensional issue. It involves both the design of the engine and its dynamic operation under changing road conditions. Modern internal combustion engines achieve high efficiency through advanced technologies such as high-pressure fuel injection system, turbocharging, and emission control systems. However, in reality, this efficiency is subject to fluctuations due to varying engine loads caused by vehicle traffic and road load.

A key factor affecting powertrain efficiency is driving technique and traffic conditions such as hill resistance and inertia. It is therefore necessary to take these variables into account when assessing fuel consumption and average driveline efficiency. The use of driving cycles, such as SORT or WHVC, allows repetitive testing under road conditions, which is important for evaluating exhaust emissions and testing the efficiency of internal combustion engines under different operating conditions. It is worth noting that, despite plans to phase out internal combustion engines, research into their efficiency and emissions is still being conducted to optimize today and future vehicles.

According to the Diesel Forum website, as of December 2022, 77% of all public transport buses in operation were powered by a diesel engine. Of these, 51% are the latest generation of advanced diesel engine technology that achieves near-low emissions of greenhouse gases, particulates, and nitrogen oxides compared to previous generation buses.

Therefore, the aim of the present study was to test the overall efficiency of a city bus's powertrain, taking into account the combustion engine, transmission, torque converter, and tyre friction on the rollers.

2. Scope of study

The research involved performing a driving test on a chassis dynamometer. The test chosen was the World Harmonised Vehicle Cycle. The WHVC is generally used for emissions and fuel consumption studies of different types of HDVs. It is a dynamometer test based on the data set used to develop the WHTC international harmonised non-stationary cycle. The WHVC test is a cycle used for heavy-duty vehicles (HDV) and is based on an emissions-oriented, engine-harmonised test cycle performed on the WHTC engine dynamometer. It is contained in regulations issued by the European Economic Commission. It is a synthesis of on-road vehicle speeds and consists of three stages: Urban, Rural, and Motorway. It is used during vehicle testing and modelling. Results from the WHVC driving cycle can be used for research purposes to compare individual levels of toxic emissions and fuel consumption.

The duration of the entire WHVC test is 1800 seconds (Fig. 1). The test consists of three stages representing urban, non-urban, and motorway driving:

– Stage I (Urban) – 900 s, 0–900 s – represents urban driving at an average speed of 21.3 km/h with a top speed of 66.2 km/h. This stage includes frequent starting, stopping, and idling.
– Stage II (Rural) – 481 s, 900–1381s – represents off-road driving at an average speed of 43.6 km/h with a top speed of 75.9 km/h.

The average speed of stages I and II is 29 km/h.

– Stage III (Motorway) – 419 s, 1381–1800 s – represents driving on the motorway at an average speed of 76.7 km/h with a top speed of 87.8 km/h.

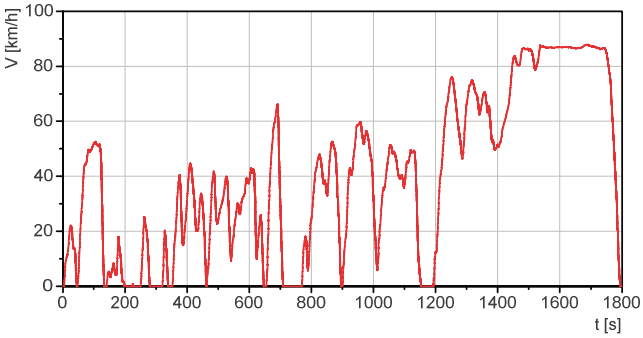

Fig. 1. Vehicle speed profile of the WHVC

During the tests, stages I and II, named Urban and Rural, and part of stage III were carried out. This is due to the fact that stage III of the WHVC driving cycle involves speeds that do not occur during urban bus operation. At the same time, the powertrain control system of the test vehicle limited the maximum speed. The test was carried out in triplicate and the averaged run was analyzed. During the tests, time series were recorded at a frequency of 10 Hz. These were as follows:

– vehicle speed – V [km/h]
– effective wheel power – P_e [kW]
– fuel consumption – F_c [dm^3/h]
– accelerator pedal position – APP [%].

The instantaneous vehicle speed value corresponded to the assumed profile with an accuracy of 1.5 km/h. In addition, a regression was developed as a compilation of the speed assumed in the profile and that obtained during the tests. A regression analysis was performed to verify the test. A coefficient of determination of 0.99 indicates correctness.

3. Test stand and research object

The tests were carried out on the MAHA LPS 3000 LKW chassis dynamometer. This device allows the simulation, under test bench conditions, of drive train operating conditions similar to those encountered on the road (this applies to both steady and transient states). By realizing the tests, independence from atmospheric conditions and the need for the test vehicle to travel to the control road section was achieved. In addition, the bench conditions increase the possibility of using measuring equipment and ensure the repeatability of test conditions, which is very difficult to achieve under road conditions.

The MAHA LPS 3000 LKW chassis dynamometer was used to simulate road conditions. It is a testing and diagnostic device for vehicles tested under load. The device is intended for trucks and buses with a maximum permissible axle load of 15,000 kg. It is capable of testing heavy vehicles with a power of up to 660 kW. This chassis allows classic performance measurements with a recording of engine mechanical power, torque, engine speed, and wheel speed. The LPS 3000 permits realization driving tests (e.g. NEDC, SORT2, WHVC) to be set up in simulation mode. The recording of additional vehicle operating state parameters is made possible by connecting external devices such as a Diesel MDO 2 toxic gas emission meter or a fuel consumption meter. The basic technical data of the dynamometer is summarised in Table 1.

Table 1. Technical data of the MAHA LPS 3000 LKW chassis dynamometer

Axle load	15,000 kg
Roller stand dimensions	4550 × 1100 × 625 mm
Roll length	900 mm
The diameter of the rollers	318 mm
Centre distance of rollers	565 mm
Min. wheel diameter of the vehicle	400 mm
Max. speed	200 km/h
Wheelbase min/max	820/2620 mm
Max. wheel power standard/increased	300/600 kW
Tractive effort standard/increased	15,000/25,000 N
Wheel power measurement error	2%
Measuring system	Strain gauge
Electric power supply	400 V/50 Hz/63 A
Total weight	2350 kg

The test object was a 12 m-long MAXI-class city bus, a Mercedes Conecto (Fig. 2). Buses in this class are low-floor vehicles with a gross vehicle weight without passengers in the range of 11,000 to 13,000 kg and a length of 10 to 12 m. The total permissible weight including passengers of such a vehicle is 18,000 kg. The passenger capacity of a particular model can vary depending on the interior configuration and version of the bus. In general, it can be assumed that the buses in this family can accommodate between approximately 60 and over 80 passengers, depending on length and seating arrangement.

Fig. 2. Mercedes Conecto LF city bus on a chassis dynamometer

Mercedes Conecto is a two axial, with a rear drive axle. The engine is connected to a four-speed automatic transmission via a torque converter. The vehicle was manufactured in 2009. The bus had a power unit with the designation OM 926 LA. It is an in-line, 6-cylinder, compression-ignition engine with a displacement of 7.23 dm^3. It produces a maximum output of 205 kW (278 HP). Average fuel consumption is 39 dm^3 per 100 km. The emission standard the vehicle meets is Euro IV.

The data recording system is based on National Instruments hardware and software. The NI cRIO-9024 real-time controller was used, along with the required measurement cards. This included the NI 9862 CAN card, which allows the recording of operating parameters available in the bus diagnostic system. Fuel consumption measurement was based on the communication protocol of the Profibus network available in onboard diagnostic defined by the DIN 19245 was used to measure data. The use of the FMS transmission standard made it additionally to record: vehicle speed, engine crankshaft speed, and accelerator lever position.

The temperature of the drive axle tires and the engine temperature were kept stable during the tests. For this purpose, two blowers set up on two sides of the bus were used. An external source of compressed air for the brake system was also used. This made it possible to eliminate interference from the compressor, which is driven by the engine.

4. Results

Figure 3 shows the test results obtained during the WHVC test on a chassis dynamometer. These are in turn: power, accelerator pedal position, fuel consumption, engine speed, and vehicle speed. The results are described detailed in detail in the paper [6].

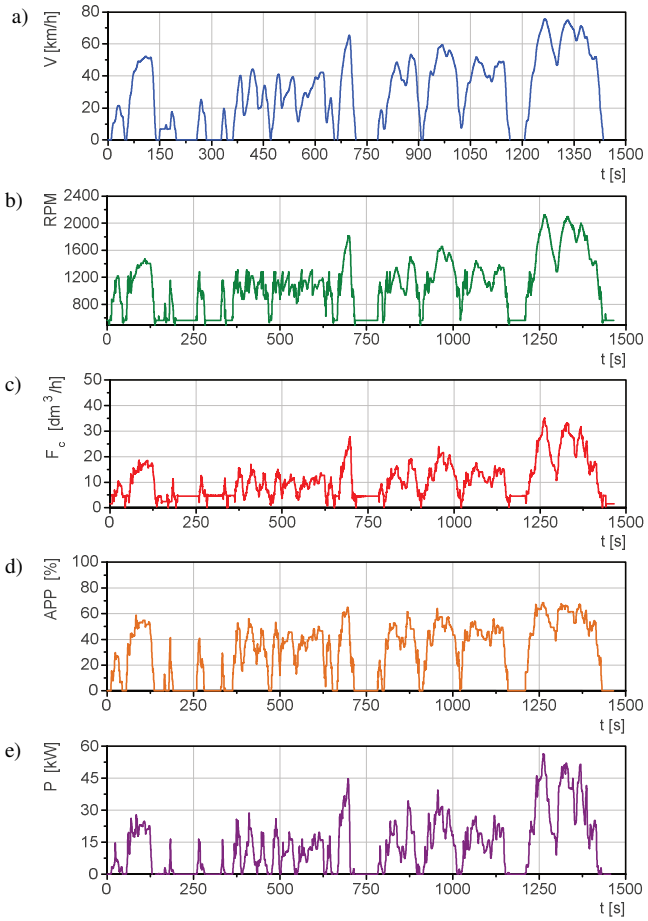

Fig. 3. Time courses of measured values: a) vehicle speed, b) engine speed, c) fuel consumption, d) accelerator pedal position, e) wheel power [6]

The mechanical power generated ranged from –5 to 55 kW. Values below zero occurred during engine braking, with fuel consumption equal to 0. The cycle stages named Urban and Rural were characterized by maximum powers of 40 kW. The Motorway stage was a maximum of 68 kW. Fuel consumption in the first and second stages did not exceed 30 dm^3/h. During the Motorway, it increased to 35 dm^3/h. Changes in the position of the accelerator lever ranged from 0 to 70%. Engine speed peaked during the last phase of the cycle at around 2100 rpm. Acceleration position pedal signal obtained a maximum value of around 60%

The recorded vehicle speed during the test was compared with the speed given as a reference. The mapping of the obtained speed against the theoretical one was verified by performing regression analysis. The obtained values of the coefficient of determination of 0.97 and the directional coefficient of the straight line of 1.01 are within acceptable ranges.

5. Data analysis

The first step in the analysis was to calculate instantaneous efficiency values. This was done using the recorded time waveforms. Referring to the purpose of this study, the analysis determined the efficiency of converting the power contained in the fuel supplied to the engine into mechanical power obtained at the wheels of the bus – Eq. (1). It should be mentioned that the calculated efficiency is only the power conversion efficiency and refers to operating states in which there is a transfer of effective power to the wheels of the vehicle. In road traffic, the phenomena associated with the accumulation of energy in the mass of the vehicle must also be taken into account. This is required for a complete energy balance of vehicle motion. However, in this case, based on the results obtained on a chassis dynamometer, the conversion efficiency of the power flowing from the fuel to the wheels was analyzed.

$$\eta = \frac{P_e}{P_f} \tag{1}$$

The power contained in the fuel was calculated using eq. 2, taking into account the density of the fuel $\rho = 0.82$ kg/dm^3 and heating value $W_o = 42$ MJ/kg = 11.94 kWh/kg.

$$P_f = F_c \cdot \rho \cdot W_o \tag{2}$$

The time series of fuel power is presented in Fig. 4. The fuel power delivered is dependent on the speed defined by the WHVC cycle. Speed influences the resistance to motion and the power required to overcome it. The lowest values were found in the past phase of the cycle. Fuel power was a maximum of 170 kW. In the second phase, it increased to 260 kW. By contrast, in the third phase of the driving cycle, where the highest vehicle speeds occurred, wheel power reached a maximum of 360 kW.

Figure 5 shows the time course of the power conversion efficiency of the city bus propulsion system. Due to the method of analysis adopted, which relates wheel power to fuel power, an efficiency of zero was obtained for zero vehicle speed and engine idling. The efficiency value varied from 0 to a maximum of 25%. It can be seen that any starting process is associated with the lowest values of efficiency, which increases with speed. Such low efficiency values may be due to slippage occurring in the torque converter. Above 10 km/h, efficiency varies between 5 and 25%.

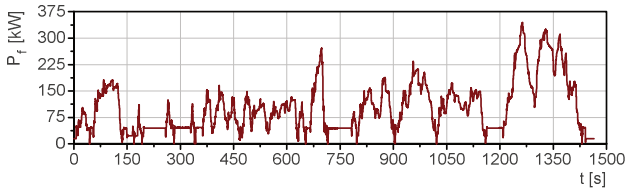

Fig. 4. Time course of measured fuel power

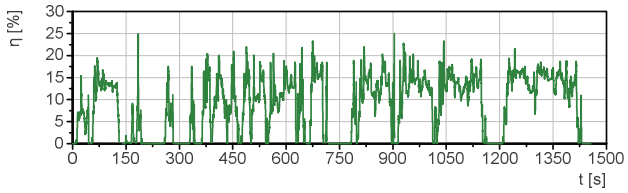

Fig. 5. Time course of the measured power conversion efficiencies in the drive system

Figure 6 provides a comprehensive depiction of the intricate relationship between power conversion efficiency and vehicle speed. The data unequivocally reveals a discernible augmentation in efficiency with escalating vehicular velocity. This empirical observation substantiates the presence of a dynamic state during vehicular acceleration, prominently manifesting within the speed spectrum ranging from 0 to 40 km/h. Within this range, the efficiency experiences a conspicuous flux, underscoring the complex of forces and energy conversion involved during vehicle powertrain system. Beyond this threshold of 40 km/h, the efficiency stabilizes, oscillating within a relatively consistent range of 10–20%. Those phenomenon, underscores the critical significance of optimizing vehicular dynamics for enhanced energy efficiency.

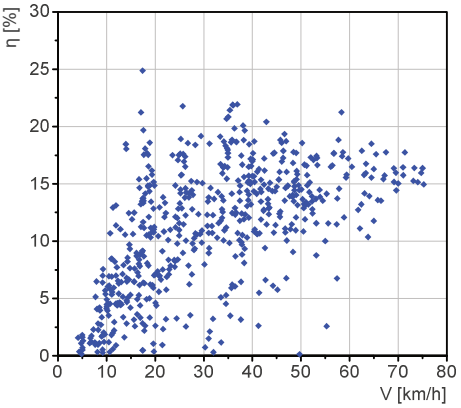

Fig. 6. Power conversion efficiency as a function of vehicle speed

A similar relationship can be seen by analysing Fig. 7, showing the dependence of the efficiency of the power conversion on the power at the wheels. Again, the lowest values were obtained in the range from 0 to about 30 kW. There is a range that corresponds to the acceleration and deceleration of the vehicle. At the same time, this could also be the result of slippage occurring on the torque converter. This may indicate that dynamic states are character-

ised by lower efficiency. This occurs during the acceleration of the vehicle due to the fact that the efficiency of the individual components of the system is lower than the static characteristics of the individual components. Above 30 kW of power measured at the wheels, the efficiency ranges from 15 to 20%. The range of variation is much smaller as it relates to higher speeds, which can also be inferred from Fig. 6.

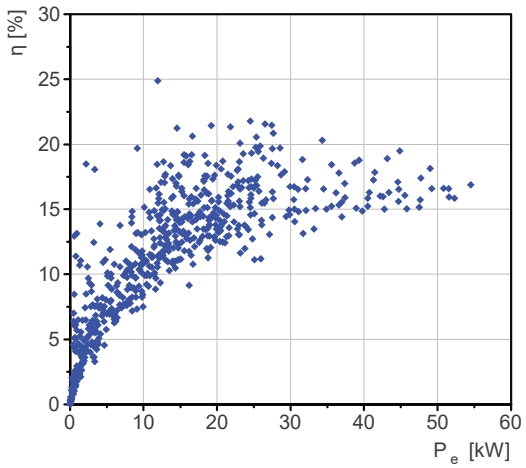

Fig. 7. Wheel power conversion efficiency shown as a function of wheel power

The average value of the conversion efficiency of fuel power to effective power at the wheels of the vehicle was 11.26% (Fig. 8). Figure 8 shows the calculated incidence of efficiency as a function of efficiency and power generated at the wheels of the bus. Three peak values can be observed. The first peak value is for efficiency values of 0–3% with the lowest power at the wheels. The second peak value frequencies around 5% are for efficiencies of around 1% and powers of 10–20 kW. In the context of the analysis presented, the third peak, constituting approximately 3% of the total dataset, manifests as a significant property. This specific peak is concomitant with power output levels of around 30 kW, concurrently yielding an efficiency of the drive train equal to 15%.

Figure 8 accentuates a dependence between efficiency and the power generated by the vehicle's wheels. A conspicuous trend is observed, wherein efficiency ascends up to the 30 kW power, subsequently maintaining a plateau-like constancy within the range of approximately 30 kW to 55 kW. It presents a characteristic of the drive train system under scrutiny.

As a conclusion of the results analysis, it should be noted that, due to the tests carried out on the chassis dynamometer, the calculated efficiencies concerned only the operating states in which power flowed from the engine to the wheels of the vehicle. Real-world road traffic also requires the phenomena of energy storage in the vehicle mass to be considered for a full energy analysis of the movement. However, the analysis based on the results from the chassis dynamometer focused on the efficiency of power conversion from the fuel to the vehicle wheels.

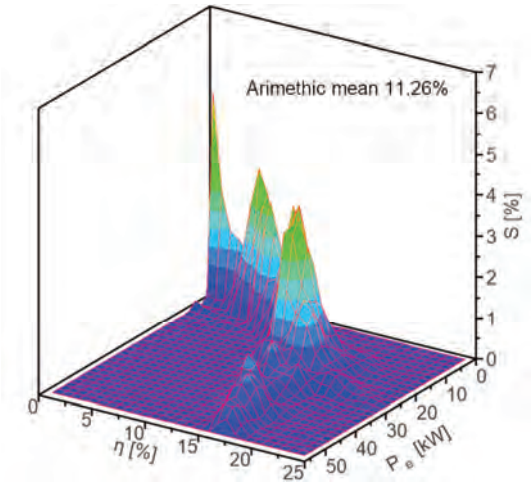

Fig. 8. Incidence of efficiency as a function of efficiency and power generated at the wheels of the bus

The power conversion efficiency of the city bus powertrain varied from 0% to 25%, depending on the vehicle speed. The results showed that the acceleration processes had a lower efficiency, which increased with increasing vehicle speed. This phenomenon could be related to slippage in the torque converter. Above 10 km/h, efficiency remained in the range of 5% to 25%. The analysis showed that efficiency increased with increasing vehicle speed and power at the wheels.

6. Summary

The work carried out on the analysis of the energy conversion process in the powertrain of a city bus showed that:

- the tests carried out on the chassis dynamometer do not fully take into account the energy storage in the vehicle mass
- the average overall efficiency was about 11%
- the efficiency achieved varied with the vehicle load, i.e. the vehicle speed achieved
- as the load increased, the efficiency increased, reaching a maximum of approximately 22%.

In conclusion, it should be noted that more than 80% primary energy of diesel fuel could be dissipated in the powertrain of city buses.

Acknowledgments

This research has been financed by the Polish National Centre for Research and Development, PBSII, under Grant Agreement No. 209379.

Nomenclature

APP	accelerator pedal position
F_c	fuel consumption
HCHO	formaldehyde
HDV	heavy-duty vehicles
P_f	fuel power
P_e	effective power

SORT	Standardised On-Road Tests cycles	W_o	fuel heat value
V	velocity	ρ	fuel density
WHVC	World Harmonised Vehicle Cycle	η	efficiency

Bibliography

[1] Far M, Gallas D, Urbański P, Woch A, Mieżowiec K. Modern combustion-electric PowerPack drive system design solutions for a hybrid two-unit rail vehicle. Combustion Engines. 2022;190(3):80-87. https://doi.org/10.19206/CE-144724

[2] Gęca M, Wendeker M, Grabowski Ł. A city bus electrification supported by the photovoltaic power modules. SAE Technical Papers 2014-01-2898. 2014. https://doi.org/10.4271/2014-01-2898

[3] Giakoumis EG, Alafouzos AI. Study of diesel engine performance and emissions during a transient cycle applying an engine mapping-based methodology. Appl Energ. 2010; 87(4):1358-1365. https://doi.org/10.1016/j.apenergy.2009.09.003

[4] Gis W, Kruczyński S, Taubert S, Wierzejski A. Studies of energy use by electric buses in SORT tests. Combustion Engines. 2017;170(3):135-138. https://doi.org/10.19206/CE-2017-323

[5] Gómez A, Fernández-Yáñez P, Soriano J, Sánchez-Rodríguez L, Mata C, Garcia-Contreras R et al. Comparison of real driving emissions from Euro VI buses with diesel and compressed natural gas fuels. Fuel. 2021;289:119836. https://doi.org/10.1016/j.fuel.2020.119836

[6] Grabowski Ł. Conversion of fuel chemical energy into electrical energy in city bus with diesel engine (in Polish). Lublin University of Technology Publishing House. Lublin 2023. https://www.bc.pollub.pl/dlibra/publication/14168/edition/13825

[7] Küng L, Bütler T, Georges G, Boulouchos K. How much energy does a car need on the road? Appl Energ. 2019; 256:113948. https://doi.org/10.1016/j.apenergy.2019.113948

[8] Rakopoulos CD, Michos CN, Giakoumis EG. Study of the transient behavior of turbocharged diesel engines including compressor surging using a linearized quasi-steady analysis. SAE Technical Papers 2005-01-0225. 2005. https://doi.org/10.4271/2005-01-0225

[9] Rosero F, Fonseca N, López J, Casanova J. Real-world fuel efficiency and emissions from an urban diesel bus engine under transient operating conditions. Appl Energ. 2022; 261:114442. https://doi.org/10.1016/j.apenergy.2019.114442

[10] Rosero F, Fonseca N, López J, Casanova J. Effects of passenger load, road grade, and congestion level on real-world fuel consumption and emissions from compressed natural gas and diesel urban buses. Appl Energ. 2021;282:116195. https://doi.org/10.1016/j.apenergy.2020.116195.

[11] Suarez-Bertoa R, Selleri T, Gioria R, Melas AD, Ferrarese C, Franzetti J et al. Real-time measurements of formaldehyde emissions from modern vehicles. Energies. 2022; 15(20):7680. https://doi.org/10.3390/en15207680

[12] Tamsanya S, Chungpaibulpatana S, Limmeechokchai B. Development of a driving cycle for the measurement of fuel consumption and exhaust emissions of automobiles in Bangkok during peak periods. Int J Auto Techn. 2019;10: 251-264. https://doi.org/10.1007/s12239-009-0030-4

[13] Weissbäck M, Howlett M, Ausserhofer N, Krapf S. The efficiency engine – cost-effective alternative to downsizing. Combustion Engines. 2012;149(2):3-9. https://doi.org/10.19206/CE-117034

[14] Xu H, Tu R, Li T, Chen H. Interpretable bus energy consumption model with minimal input variables considering powertrain types. Transport Res D-Tr E. 2023;119:103742. https://doi.org/10.1016/j.trd.2023.103742

[15] Zhao Q, Chen Q, Wang L. Real-time prediction of fuel consumption based on digital map API. Appl Sci. 2019;9: 1369. https://doi.org/10.3390/app9071369

Łukasz Grabowski, DSc., DEng. – Faculty of Mechanical Engineering at the Lublin University of Technology, Poland.
e-mail: *l.grabowski@pollub.pl*

Prof. Mirosław Wendeker, DSc., DEng. – Faculty of Mechanical Engineering at the Lublin University of Technology, Poland.
e-mail: *m.wendeker@pollub.pl*

Article citation info:
Noga M, Moskal T. Evaluation of a pressure sensing glow plug in terms of its application possibility to control the combustion process of a hydrogen-powered spark-ignition engine. Combustion Engines. 2024;196(1):140-145. https://doi.org/10.19206/CE-172820

Marcin NOGA
Tomasz MOSKAL

Combustion Engines
Polish Scientific Society of Combustion Engines

Evaluation of a pressure sensing glow plug in terms of its application possibility to control the combustion process of a hydrogen-powered spark-ignition engine

Article Info

Received: 2 June 2023
Revised: 14 September 2023
Accepted: 22 September 2023
Available online: 11 November 2023

The article contains the results of an analysis of the suitability of a pressure sensing glow plug for use in a hydrogen engine control system. Due to the properties of hydrogen, the process of its combustion in spark-ignition engines is significantly different from the classic fuels. It is planned to use the pressure sensor signal to control the combustion process to obtain high power and efficiency, with the lowest possible emission of nitrogen oxides, which is the main harmful component of hydrogen engines. After an initial assessment of suitability, it was decided to use a pressure sensing glow plug. This choice is dictated by the low price, good availability and high durability of these sensors. The preliminary tests were carried out using a low-power single-cylinder SI engine coupled with a 48 V generator. The tests were carried out for several values of engine speed and load of the generator and for classic gasoline with a research octane number (RON) of 95. To obtain an increased pressure rise rate in the cylinder, as for hydrogen fueling, the engine operation was also tested with unmodified light gasoline used as solvent, which is characterized by a significantly lower RON value. The use of a reference pressure sensor in the cylinder made it possible to determine the behavior of the PSG in various operating conditions. The tests revealed that the differences in the pressure waveforms registered with both sensors can be systematized depending on the engine speed and its load.

Key words: *pressure sensing glow plug, in-cylinder pressure, engine control, spark ignition, hydrogen fuel*

1. Introduction

Fossil fuel depletion and stricter emission regulations drive the search for alternative fuels that can both meet the pollution requirements but still be suitable for piston engines that still developed [19], and are in a majority of vehicles currently in use not only for road transport [9], but also, to a large extent, in rail transport [3, 14].

Various types of alternative fuels are still being developed to decrease emissions [2, 15, 16], although uniquely hydrogen is a fuel that inherently does not produce carbon-related emissions when combusted, thus serving as a suitable substitute to classic liquid fuels [5, 7, 8, 21]. The combustion of hydrogen still requires minimization of nitrogen oxide emissions, and the distinct nature of hydrogen as a fuel in comparison to gasoline requires advanced control methods to enhance the efficiency of the process. Table 1 presents a comparison of fuel properties according to [1, 18].

Table 1. Comparison of hydrogen and gasoline properties as a fuel

Parameter	Unit	Hydrogen	Gasoline
Density	kg/m^3	0.090 (gas)	735
Lower Heating Value (LHV)	MJ/kg	120.1	44
LHV of stoichiometric mixture	MJ/kg	3.4	2.81
Laminar flame speed	m/s	2.4	0.4
Stoichiometric air-fuel ratio (AFR)	kg/kg	34.3	14.7
Research octane number	–	130	95
Diffusion coefficient in air	cm^2/s	0.61	0.05
Minimum energy of ignition in air	mJ	0.02	0.24
Self-ignition temperature	K	858	510–744
Flame temperature in air	K	2318	2470
Flammability range (relative AFR)	–	0.14–10	0.3–1.67

Advanced combustion control methods, also known as smart combustion control, have already been approached, with tailored pressure sensors for this purpose [4, 20].

To achieve a similar goal, an application of in-cylinder pressure signal is proposed with the use of a pressure-sensing glow plug, commonly found in current diesel engines, making it a lower-cost alternative to bespoke sensor systems.

The PSG of choice was the PSG006 sensor made by BERU (BorgWarner). To evaluate its suitability and extend previous research on applying a PSG as a stand-alone pressure sensor [6, 17], a comparative study against a laboratory-grade pressure sensor – Optrand D822D6-SP – has been conducted. Tables 2 and 3 present the available technical data for the sensors used.

Table 2. Beru PSG parameters as per [10]

Parameter	Unit	Value
Pressure range	bar	0–200
Accuracy	–	±2%
Resolution	steps/cycle	700
Sensor principle	–	piezo-resistive

Table 3. Optrand D822D6-SP parameters [11]

Parameter	Unit	Value
Pressure range	psi (bar)	0–1500 (0–100)
Sensitivity	mV/psi (mV/bar)	2.66 (38.58)
Sensor principle	–	optical

2. Test stand

As part of the research topic, it is planned to use the PSG sensor for a four-cylinder liquid-cooled engine. Since testing the suitability of the sensor requires two pressure sensors to be mounted together in the engine combustion chamber, it was decided to use a low-power single-cylinder air-cooled engine for the initial stage of the research. The engine selected for the tests was used to drive the 48 V-range extender developed a few years ago at the Cracow University of Technology [12, 13]. The range extender is

attached to a light commercial electric vehicle Melex and can charge its traction battery. The view of the test stand based on the engine of the range extender developed for the Melex vehicle is shown in Fig. 1.

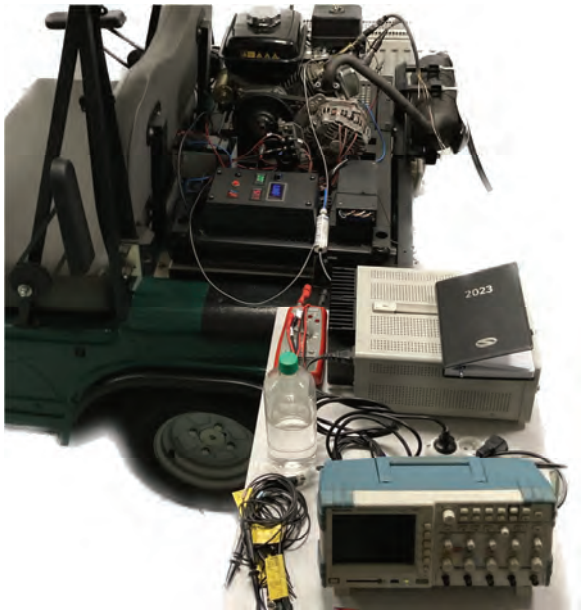

Fig. 1. Test stand consisting of a Melex cart with a range extender ICE

Charge current can be set via a regulator mounted next to the engine. This allows smooth adjustment of the engine load. Maintaining a constant engine speed is carried out by a centrifugal governor. The main technical specifications of the range extender are presented in the Table 4.

Table 4. Range extender technical data

Engine model	WEIMA 168FA
Engine type	four-stroke, SI, single cylinder
Engine displacement	163 cm^3
Engine maximum power	3.8 kW at 3600 rpm
Ignition timing	fixed, 27°CA BTDC
Generator type	Synchronous 3-phase AC
Nominal voltage	48 V
Continuous output power	2200 W
Peak overall efficiency	18.8%

During the tests, the actual ignition timing was also measured for various engine speeds. The angle of ignition is fixed and set to 27°CA BTDC which is a slightly higher value than declared in the available technical specifications of the engine (25°CA BTDC).

The engine was equipped with a crank angle sensor and two in-cylinder pressure sensors – a BorgWarner PSG and an Optrand D822D6-SP (Fig. 2 and Fig. 3).

Fig. 2. PSG mounted inside the spark-plug fitting adapter next to a PSG

Fig. 3. Tip view of the PSG next to the adapter

To install the pressure sensors, a brass adapter (Fig. 2) has been designed and manufactured at Cracow University of Technology. The glow plug seals on its conical surface inside the adapter. The adapter has an axial channel to house the tip of the glow plug, as seen in Fig. 3. A threaded channel on a side wall of the adapter has been prepared, to provide a fitting for the reference sensor. Both channels form a single volume so that both sensors face the same pressure conditions. The equipped adapter is shown in Fig. 4.

Fig. 4. Both sensors fitted to the adapter

The adapter with two pressure sensors has been mounted into the factory spark plug fitting, while the spark plug itself has been installed in an additional fitting that was made in the cylinder head for the installation of a second spark plug as part of previous research and development, as shown in Fig. 5.

Fig. 5. Adapter mounted to the cylinder head. Note: combustion chamber view (right) does not show the additional spark plug fitting – a standard cylinder head shown

Pressure sensors are supplied by a linear power supply. Sensor readings were observed through a 4-channel digital oscilloscope Tektronix TPS2024 and registered onto external memory for further processing. A diagram of the test stand is presented in Fig. 6.

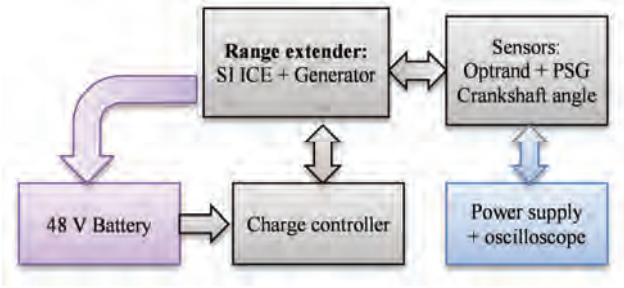

Fig. 6. Test stand block diagram

Data processing has been conducted on a PC with MATLAB software.

3. Sensor response analysis

To compare the two outputs of the sensors, two fuels were used – RON 95 gasoline and a solvent with a significantly lower RON than gasoline. The solvent used for research is a hydrotreated light petroleum fraction (light gasoline). Several test runs were conducted, at varying engine speeds and charge currents. Between each test run, cart electric loads were operated to discharge the battery, and thus, equalize tests conditions.

Figures 7 and 8 show two examples of smoothed sensor readouts. Raw data has been smoothed with the use of a built-in MATLAB function, based on local regression using weighted linear least squares and a 2nd degree polynomial model. This process has been done to facilitate the data processing, while maintaining key signal characteristics, i.e., dynamics and local maxima.

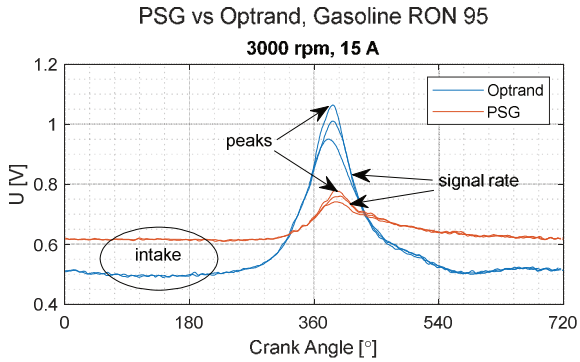

Fig. 7. Sensor response comparison – RON95 gasoline run

The key is to determine the pressure in both the intake phase, as well as in the most crucial, combustion phase. The figures show that for both fuels the PSG sensor readout is significantly weaker, and the sensor response for increasing pressure is slightly delayed by ~3°CA degrees. Additionally, the post-peak signal level tends to drop at a slower rate for the PSG compared to the optical sensor.

In Fig. 7 and 8 it can be observed that there are multiple pressure readouts – for a single measurement multiple engine cycles were observed, and thus, pressure pulses. After recalculating them into the crank angle domain, they all appear in the same spot on the crank angle axis.

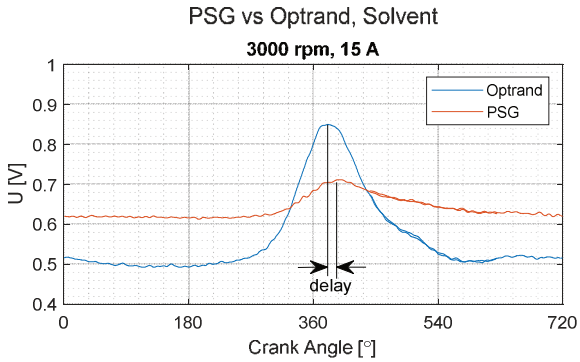

Fig. 8. Sensor response comparison – solvent run

3.1. Test methodology

Since the PSG sensor datasheet is proprietary to its manufacturer, the following approach to convert the voltage values to pressures was proposed. For each fuel, a transfer function

$$U = a_{fuel} \cdot U_{PSG} + b_{fuel} \quad (1)$$

can be determined, according to which the pressure reading from the PSG sensor is recalculated to the voltage levels of the Optrand sensor. The transfer function has been chosen so that the signals correspond to each other in the intake phase (≈ atmospheric pressure), as well as the peak pressure phase.

Firstly, the intake phase signal level from both sensors at 100°CA was extracted. Next, the peak pressure signal levels were noted down. Using the two pairs, both a_{fuel} and b_{fuel} coefficients were determined for each data series. In case a test run possessed multiple pressure peaks, the first peak and a preceding intake phase were considered.

Figure 9 shows the data points used for the recalculation. In this case, the two higher peaks that are visible in both plots, have occurred later in time than the marked ones and were omitted.

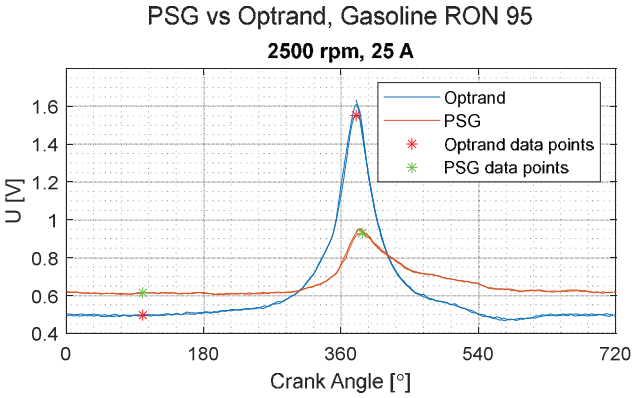

Fig. 9. Example of data with selected points used for signal recalculation

3.2. Sensor voltage recalculation

The recalculation of the coefficients for a variety of test runs (between 1500 and 3500 rpm, and 10 to 25 A of load current) proved that the coefficients form into planes in relation to both parameters, as seen in Fig. 10 and 11 in the form of blue asterisks.

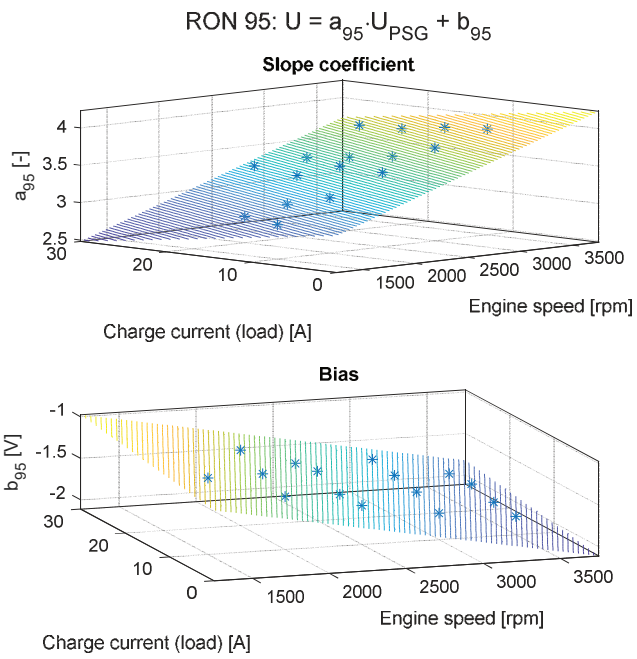

Fig. 10. Approximated coefficient maps for RON95 gasoline

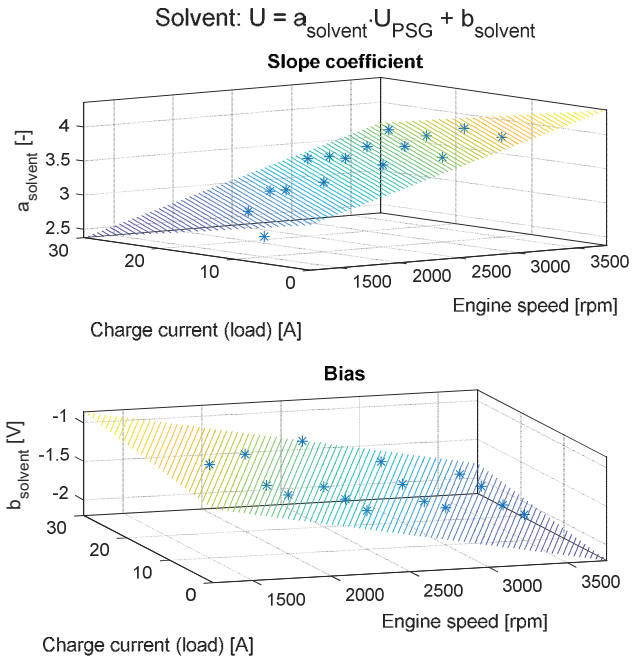

Fig. 11. Approximated coefficient maps for solvent fuel

Hence, it was assumed that coefficients a_{fuel} and b_{fuel} are linear functions of the engine speed and the engine load, expressed in the charge current of the battery.

Using the least squares method, two planes were identified, corresponding to a_{fuel} and b_{fuel} coefficients, and their equations are as follows:

$$a_{95} = 5.03 \cdot 10^{-4} \cdot n - 0.0164 \cdot I_c + 2.35 \quad (2)$$

$$b_{95} = -3.39 \cdot 10^{-4} \cdot n + 0.0096 \cdot I_c - 0.84 \quad (3)$$

$$a_{solvent} = 5.29 \cdot 10^{-4} \cdot n - 0.0221 \cdot I_c + 2.38 \quad (4)$$

$$b_{solvent} = -3.80 \cdot 10^{-4} \cdot n + 0.0130 \cdot I_c - 0.78 \quad (5)$$

The planar approximations have the following coefficients of determination: 0.9306, 0.9143, 0.8044 and 0.7893.

The calculated planes have been depicted in each plot in Fig. 10 and 11 in the form of contour lines.

By obtaining the planar function equations, the PSG sensor readouts could be calculated for any running condition, without the necessity of recording a measurement from the reference sensor. This assumption is only valid within the range of tested charge currents and engine speeds.

4. Results

The method proves to be satisfactorily accurate to recalculate the pressure signal from a pressure-sensing glow plug to Optrand pressure signal levels.

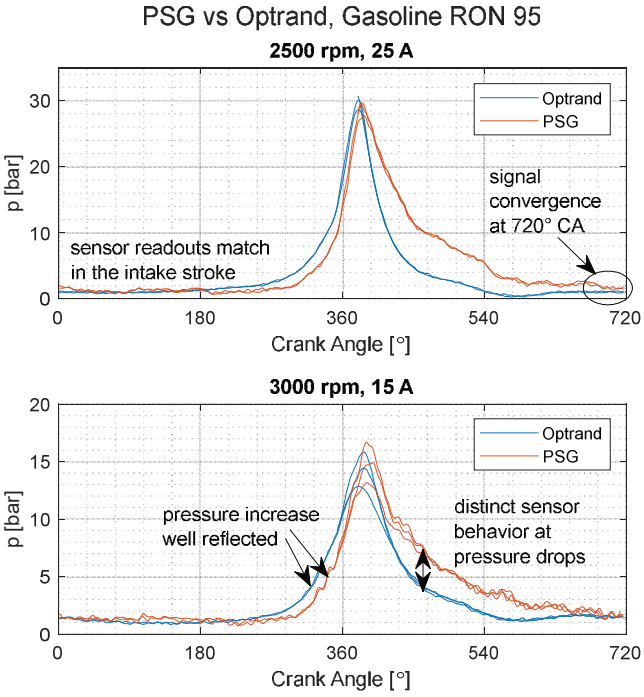

Fig. 12. Recalculated signals for RON95 gasoline

In Fig. 12, it can be visible that both the intake as well as the peak pressure correspond well to each other from both sensor readouts.

Results from the solvent run prove to be satisfactory as well. However, due to poorer coefficients of determination, less accurate signal recalculations can be observed.

In Fig. 13, it can be observed that for the run at 2500 rpm with a 25 A charge current, the intake pressure is poorly reflected. Similar artifacts were observed for both fuels for most outlying runs from the calculated planes, for lowest engine speed and charge current set, i.e., 1500 rpm and 10 A.

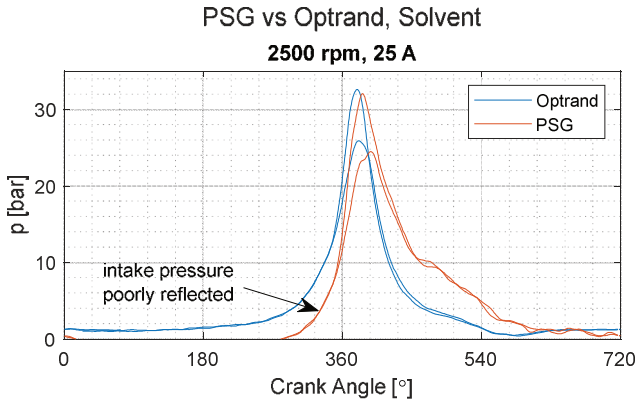

Fig. 13. Recalculated signals for solvent run

As for the sensor comparison, after the recalculation, it can be observed that the pressure reading from the PSG is slower to drop after peak pressure is achieved, which was not clearly visible before recalculation. The sensor readouts converge at the end of the exhaust stroke, around 720°CA.

5. Conclusions

The method proves to be suitable for recalculating the PSG sensor readouts to known Optrand sensor voltage levels. During the tests, it was revealed that the sensitivity of the pressure-sensing glow plug depends on the load and engine speed. It was also shown that the value of the signal also depends on the rate of pressure rise, which was increased by using fuel with a low octane number. The collected data shows that there is a linear dependency between both sensor readouts of different working principle, which can be approximated by planar equations in the domain of engine load and engine speed.

However, the analysis of the results of the tests carried out allowed for obtaining systematized transition functions from the measured PSG signal to the actual value of the pressure measured in the cylinder. This confirms the possibility of using an affordable PSG sensor to control the combustion process in a hydrogen engine. It should be noted that the obtained relationships are preliminary, confirming only the initial assumptions.

To use the sensor in a developed control system, a similar calibration must be performed on the target engine. This is due to the fact that the load carried out on the test stand was measured as the generator charging current and cannot be directly transposed to, for example, the brake mean indicated pressure for the engine.

Nomenclature

AC alternating current
BTDC before top dead center
PSG pressure-sensing glow plug
RON research octane number
SI spark ignition

Bibliography

[1] Al-Dabbas MA, Al-Rousan AA. The simulation of using hydrogen in gasoline internal combustion engines. Pacific Journal of Science and Technology. 2009;10(1):93-106.
[2] Balasubramanian D, Annamalai M. A study on performance, combustion and emission behaviour of diesel engine powered by novel nano nerium oleander biofuel. J Clean Prod. 2018;196:74-83. https://doi.org/10.1016/j.jclepro.2018.06.002
[3] Bondarenko I, Lukoševičius V, Keršys R Neduzha L. Investigation of dynamic processes of rolling stock–track interaction: experimental realization. Sustainability. 2023;15:5356. https://doi.org/10.3390/su15065356
[4] Chłopek Z, Stasiak P. The analysis of an unrepeatability of cylinder pressure signal in internal combustion engines. Combustion Engines. 2005;120(1):31-39. https://doi.org/10.19206/CE-117409
[5] Gis M, Gis W. The current state and prospects for hydrogenisation of motor transport in Northwestern Europe and Poland. Combustion Engines. 2022;190(3):61-71. https://doi.org/10.19206/CE-144560
[6] Lijewski P, Fuć P, Grzeszczyk R, Molik P, Rymaniak Ł, Ziółkowski A. The use of an integrated combustion chamber sensor for engine cylinder pressure measurement (in Polish). Logistyka. 2014;3:3765-3770.
[7] Longwic R, Tatarynow D, Kuszneruk M, Wozniak-Borawska G. Preliminary tests of a Diesel engine powered by diesel and hydrogen. Combustion Engines. 2023;195(4):35-39. https://doi.org/10.19206/CE-169485
[8] Matla J. Possible applications of prechambers in hydrogen internal combustion engines. Combustion Engines. 2022;191(4):77-82. https://doi.org/10.19206/CE-148170
[9] Menes M. Program initiatives of public authorities in the field of hydrogenation of the economy in a global perspective, as of the end of 2020. Combustion Engines. 2022;189(2):18-29. https://doi.org/10.19206/CE-142170
[10] New glow plug technology from the world market leader. BERU Technical briefs. Available from: https://www.beruparts.eu/content/dam/marketing/emea/beru/brochure/en-psg-pressure-sensor-glow-plug.pdf
[11] Noga M. Selected issues of the indicating measurements in a spark ignition engine with an additional expansion process. Appl Sci. 2017;7(3):295. https://doi.org/10.3390/app7030295
[12] Noga M, Gorczyca P. Development of the range extender for a 48 V electric vehicle. Combustion Engines. 2019;177(2):113-121. https://doi.org/10.19206/CE-2019-220
[13] Noga M, Gorczyca P, Hebda R. The effects of use of the range extender in a small commercial electric vehicle. Automotive Experiences. 2021;4(1):5-19. https://doi.org/10.31603/ae.4137
[14] Pavelčík V, Dižo J, Blatnický M, Ishchuk V, Molnár D. Analysis of the test bench design influence on the cooling performance of a rail vehicle brake disc. Communications – Scientific Letters of the University of Žilina. 2023;25(2):194-200. https://doi.org/10.26552/com.C.2023.048
[15] Pielecha I, Wierzbicki S, Sidorowicz M, Pietras D. Combustion thermodynamics of ethanol, n-heptane, and n-butanol in a Rapid Compression Machine with a Dual Direct Injection (DDI) supply system. Energies. 2021;14:2729. https://doi.org/10.3390/en14092729
[16] Stępień Z. Synthetic automotive fuels. Combustion Engines. 2023;192(1):78-90. https://doi.org/10.19206/CE-152526

[17] Szczurowski K, Walczak D, Zieliński Ł. Use of pressure sensor glow plug for the control of combustion process (in Polish). Zeszyty Naukowe Instytutu Pojazdów. 2014;99: 139-144.
[18] Szwaja S. Combustion pressure fluctuations study in the hydrogen fueled internal combustion engine (in Polish). Częstochowa University of Technology Publishing House. Częstochowa 2010.
[19] Szwaja S, Szymkowiak M. The Szymkowiak's over-expanded cycle in the rocker engine with the variable compression ratio – kinematics. Combustion Engines. 2022; 189(2):68-72. https://doi.org/10.19206/CE-143157
[20] Vollberg D, Wachter D, Kuberczyk T, Schultes G. Cylinder pressure sensors for smart combustion control. Journal of Sensors and Sensor Systems. 2019;8:75-85. https://doi.org/10.5194/jsss-8-75-2019
[21] Wesołowski M, Hamid M, Mońka P, Janicka A. Analysis of the potential of electro-waste as a source of hydrogen to power low-emission vehicle powertrains. Combustion Engines. https://doi.org/10.19206/CE-169494

Marcin Noga, DSc., DEng. – Faculty of Mechanical Engineering, Cracow University of Technology, Poland.
e-mail: *marcin.noga@pk.edu.pl*

Tomasz Moskal, MEng. – Faculty of Mechanical Engineering, Cracow University of Technology, Poland.
e-mail: *tomasz.andrzej.moskal@gmail.com*

Article citation info:
Kęska A, Dziubek M, Michalik D. The economic aspects of vehicle operation in the context of electromobility strategies. Combustion Engines. 2024;196(1):146-152. https://doi.org/10.19206/CE-172821

Aleksandra KĘSKA
Mateusz DZIUBEK
Dawid MICHALIK

Combustion Engines
Polish Scientific Society of Combustion Engines

The economic aspects of vehicle operation in the context of electromobility strategies

ARTICLE INFO

Received: 30 May 2023
Revised: 13 September 2023
Accepted: 22 September 2023
Available online: 10 November 2023

The transformation of the automotive industry towards electromobility is a key step in achieving a sustainable transportation system. To analyze the economic feasibility of electric vehicles (EVs) compared to internal combustion engine vehicles (ICEs), this study assessed the operating costs of both types of vehicles, including fueling and charging costs on a selected theoretical route. The analysis of economic aspects also examined the development of fueling and charging infrastructure and the impact of government programs promoting electromobility. The study employs a comparative analysis of ICE and EV based on fuel and electricity prices, insurance costs, and servicing expenses. The results of the analysis indicate that adopting EVs can lead to significant economic benefits, especially when coupled with government incentives and well-developed charging infrastructure. The network of charging stations and fuel infrastructure serves as an indicator of the market conditions for vehicles equipped with either internal combustion engines or electric powertrains, and forecasts help anticipate their future directions. The decreased pace of new petrol stations being established may indicate a weakening market for internal combustion engine vehicles compared to previous periods. This study highlights the economic aspects of electromobility strategies aimed at accelerating the transition towards a sustainable transportation system.

Key words: *life cycle assessment, electric vehicle, internal combustion engine vehicle, transportation economy*

1. Introduction

Internal combustion engines are one of the most widespread technologies in the automotive sector. Spark-ignition and compression-ignition engines have been used in commercial and passenger vehicles for over a hundred years. They have become a major factor in shaping culture and have also transformed and organized social life. Mobility, spatial planning, and consumer habits are largely structured according to the requirements and capabilities offered by cars. Cars are widely prevalent in developed countries. In Poland, the number of vehicles amounts to 687 cars per 1000 inhabitants [14]. Economic growth in developing countries is strongly correlated with increased access to cars [7], leading to a continuous growth in the size of the global automotive fleet.

Over the years, efforts have focused on diversifying and improving engines. Internal combustion engines (ICE) are fundamental to the automotive industry's development, with ongoing work to enhance their efficiency and performance. However, their high efficiency does not align with low pollutant emissions. Countries are implementing legal concepts to minimize the environmental impact of these engines. The Green Deal, EURO standards, and EU regulations have compelled manufacturers to adopt new strategies. The need to reduce emissions has led to the introduction of new technical solutions for internal combustion engines. “Zero-emission vehicles” are crucial for sustainable mobility and have gained importance through improved performance and infrastructure development. The continuous efforts of EU countries to mitigate the negative impacts of CO_2 emissions resulted in a significant reduction of CO_2 equivalents per inhabitant emissions in 2020 by 13.6% compared to 2019, reaching the levels of 1990 [5]. The term "zero-emission cars" is commonly used to describe electric vehicles, emphasizing their environmental benefits. However, it's a simplification as these vehicles are not entirely zero-emission. Emissions can still occur during energy production, battery manufacturing, tire wear, and the use of air conditioning or heating systems. While electric cars are more environmentally friendly than their internal combustion engine counterparts, achieving true zero emissions requires further advancements in energy production and battery sustainability. However, many researchers emphasize the overall carbon footprint that includes resource extraction, production of car components including batteries, electricity generation, and maintenance of electric vehicles in the context of a specific EU country [2].

The examination of the progress of electromobility pertaining to technical infrastructure, software systems, motor design, construction techniques, and related aspects is the focal point of investigation for numerous scientific research teams [4, 9, 11]. At the same time, the cost-effectiveness of electric vehicles, compared to traditional internal combustion engine vehicles, is a sensible step forward in adopting electric transportation, and it serves as a subject of analysis for the environmental, technical, and economic conditions of individual countries. [6, 8, 12]. The level of development of the energy infrastructure, such as photovoltaics, in a given country is also subject to consideration in the economic analysis of the cost-effectiveness of electric vehicles [1].

The availability of an adequate number of charging stations plays a vital role in encouraging private users to embrace electric cars. Despite efforts made, certain regions in Poland still lack adequate infrastructure for charging electric cars, especially considering their limited range. However, the development of new technologies and the construction of additional charging stations and supporting infra-

structure provide hope for ensuring sufficient availability of charging stations in all regions of Poland [3].

The designs of internal combustion engines and electric engines are diversified. Combustion engines emit environmentally degrading substances, while zero-emission vehicles produce no pollutants during their operation. This difference in adapted technology also impacts the vehicles usage. One of the factors significant for users is the cost associated with operating a particular propulsion system, which plays a crucial role in choosing a suitable vehicle. Lower operating costs make a potential vehicle more appealing to customers.

Electric vehicles have a relatively shorter range compared to vehicles powered by combustion engines. This is due to the limited energy storage capabilities. In a conventional vehicle, fuel is burned inside the engine chamber. In contrast, electric vehicles store converted energy using batteries.

2. Economic analysis of operating a combustion engine and electric engine from the user's perspective

In this article, we embark on a comprehensive exploration of the factors influencing the choice between Internal Combustion Engine vehicles and Electric Vehicles within the context of Poland. Two representative cars, the Toyota Corolla XII and the Volkswagen ID 3 PRO S, have been selected to illustrate the contrasting aspects of ICE and EV technology. Our investigation covers critical aspects such as purchase price, maintenance costs, insurance expenses, travel expenditures, and the evolving charging infrastructure in Poland. Additionally, we explore the strategies and visions of leading automotive manufacturers as they shift towards electric mobility solutions.

2.1. Car service costs

In order to identify the operating costs of ICE and EV vehicles, two cars were selected and used to calculate the operating costs based on a proposed tourist route in Poland.

The representative of internal combustion engines was the Toyota Corolla XII in the sedan version (Fig. 1). The market value of the model in the comfort version is 124,999 PLN (Q2 2022). The Toyota Corolla vehicle has a displacement of 1.490 cm^3. It is equipped with a gasoline engine, which has a maximum torque of 153 Nm at 4800 rpm (Table 1).

Fig. 1. Compared ICE vehicle – Toyota Corolla XII [15]

The representative of EV vehicles is the 2022 Volkswagen ID 3 PRO S (Fig. 2). In 2017, the Volkswagen brand announced plans to focus on electric vehicles. The strategy of the company includes introducing at least 30 EV models to the market by 2025 and achieving 20–25% of total annual sales (2–3 million) from electric vehicles. The ID model is the first series of electric cars by the VW group, designed from scratch as electric vehicles. According to Volkswagen, ID stands for "Intelligent Design, Identity, and Visionary Technologies". The market value of the model is 187,990 PLN (Q2 2022). The Volkswagen ID 3 PRO S vehicle is equipped with an electric motor, with a maximum torque of 310 Nm (Table 1).

Fig. 2. Compared EV vehicle – Volkswagen ID 3 PRO S [16]

Table 1. Comparison of selected parameters of ICE and EV vehicles [15, 16]

Parameter	ICE	EV
Name	Toyota Corolla XII	Volkswagen ID 3 PRO S
Number of doors	4	4
Number of seats	5	4
Turning diameter	10.4 m	10.2 m
Production year	Since 2019	Since 2020
Engine type	Petrol	Electric
Engine power	132 HP	204 HP
Maximum torque (electric)	153 Nm	310 Nm
Engine displacement	1490 cm^3	–
Battery capacity	–	77 kWh
Length	4630 mm	4261 mm
Width	1780 mm	1809 mm
Height	1435 mm	1552 mm
Wheelbase	2700 mm	2770 mm
Front wheel track	1530 mm	1536 mm
Rear wheel track	1545 mm	1513 mm

The selected vehicles are representatives of the C segment, which is the medium-sized car class. Despite similar parameters, the purchase price of both vehicles differs significantly. The cost of purchasing an ICE vehicle is 33.5% cheaper than that of an electric drive. Servicing is an important aspect of operating each vehicle, and due to differences in vehicle designs, the price varies. Example repairs related to the combustion engine and their prices are presented in Table 2.

Table 2. Prices for service of an internal combustion car (Q2 2022)

Service	ASC	Non-ASC (A)	Non-ASC (B)	Non-ASC (C)
Engine oil and filter replacement	622	231	217	604
Spark plug replacement	320	216	–	176
Air filter replacement	147	72	71	64
Cabin filter replacement	131	67	86	26
Fuel filter replacement	121	100	130	102
Coolant replacement	–	–	120	175
Brake fluid replacement	150	52	110	148
A/C refrigerant replacement	150 + refrigerant	175 + refrigerant	318	80 + refrigerant
Air conditioning disinfection	80–100	included in the price of a refrigerant exchange	included in the price of a refrigerant exchange	50
Suspension check (checking clearances and alignment)	250	57 (check) 145 (alignment)	115	included in the inspection price
Inspection of the braking system	80 (cleaning) 180 (cleaning with brake pads dismantling)	228	70	included in the inspection price
Total [PLN]	**2071**	**1343**	**1237**	**1415**

The highest costs for a user of a vehicle equipped with an internal combustion engine are incurred when using an authorized service centre (ASC). The lowest price for servicing a car is approximately 1237 PLN.

Brand new vehicles do not require frequent servicing. In the event of such a situation, the manufacturer's warranty usually applies. However, after the warranty period, annual costs can be high. These costs can be effectively reduced by using non-authorized service centres, but for calculation purposes, only the costs from ASC have been considered.

In the case of an electric vehicle, the amount of maintenance required is significantly lower. The batteries need to be replaced after approximately 8 years. Recommended maintenance procedures along with their prices at ASC are presented in Table 3.

Table 3. Prices for service of an electric car (Q2 2022)

Service	ASC
Air filter replacement	149
Cabin filter replacement	119
Coolant and brake fluid replacement	225
Traction battery test	49
Disinfection and replacement of air conditioning refrigerant	299
Inspection activities	199
Total [PLN]	**1040**

The annual maintenance at an authorized service centre costs 1040 PLN. This amount is 50% lower compared to internal combustion engine vehicles. The difference is noticeable in terms of the number of tasks performed during the service. In EVs, the quantity of fluids and oils is much lower, resulting in lower overall costs. In ICE vehicles, the most expensive tasks are related to the engine operation, spark plug replacement, filters, and engine oil change.

2.2. Insurance expenses

Among the operating costs, we can mention car insurance. Prices vary depending on the vehicle, the user, selected packages, and the insurance company. For the analyzed vehicles, insurance costs (third-party liability + comprehensive motor insurance + personal accident insurance with assistance package) were determined based on the following assumptions:

– the first user was born on May 25, 1987, and has held a driver's license since 2006
– the second driver was born on May 3, 1986, and has held a driver's license since 2004.

It was also assumed that the car owners had not caused any collisions since obtaining their licenses. This factor is crucial as it allows for cost minimization compared to individuals with an accident history. The total insurance cost for both types of cars was verified with a reputable insurer. The cost of insuring an electric vehicle is significantly higher and amounts to 3703 PLN. In the case of a conventional combustion engine vehicle, the price is 2204 PLN. The difference of 1499 PLN is due to the higher purchase cost of an EV and a higher comprehensive insurance premium. This is because total loss claims are more frequently accepted for electric vehicles, requiring the payout of the full insured value. Another cause is that repairs for electric cars are often uneconomical, and specific components are very expensive and hard to obtain.

2.3. Travel expenses

To conduct an economic analysis of ICE and EV vehicles, a travel route was established. The starting point was Wrocław, while the final stage of the journey was determined in close proximity to Bieszczady mountains (Fig. 3).

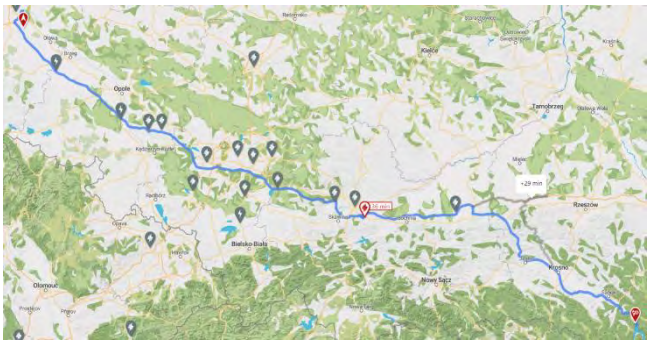

Fig. 3. Travel route – Wrocław–Solina [17]

The optimal distance between Wrocław and Solina is 518 km. The A4 motorway section covers 81% of the route, while the remaining part is traversed in urban and mountainous conditions. The Toyota Corolla XII has the following fuel consumption parameters:

– highway conditions – 6.2 dm^3/100 km
– urban and mountainous conditions 7.3 dm^3/100 km.

The travel time of a vehicle equipped with an internal combustion engine is approximately 5 hours and 49

minutes. The travel costs were determined based on the average fuel price on May 20, 2022, which was 7.21 PLN per litre.

The fuel tank capacity of the ICE vehicle is 55 litres. This value, combined with the fuel consumption parameters of the Toyota Corolla model, allows for covering the designated distance without the need for refuelling breaks. During the journey, 36.29 litres of gasoline will be consumed. The cost of the 518-kilometer trip will amount to 233.25 PLN.

Vehicles using electric power units during the journey must undergo the charging process. The stop will be made in the town of Wieliczka, at a fast-charging station. The proximity of charging points near the highway sections does not affect the maximization of the covered distance. The length of the route is 522 km, which is 4 km more than in the case of an ICE vehicle. Well-developed charging infrastructure along the A4 highway allows for minimizing the mileage. By using special software that takes into account the terrain conditions and the EV-specific specifications, the battery consumption level has been determined. The charging time during the stop is 36 minutes. The battery will be replenished using a CHAdeMO connector with a power of 44.5 kWh.

In the case of an electrically powered vehicle, the total cost of covering the designated distance is 138.8 PLN. The cost of charging using dedicated infrastructure is significantly higher than home charging conditions. Charging the battery using charging points is 2.02 kWh/PLN more expensive. Charging time is one of the crucial factors. The use of superchargers allows for charging at a rate of 44.5 kW within a 36-minute period. In home conditions, using the provided charger, charging the vehicle to its initial state can take up to 28 hours. This time is not included in the total travel time, as the charging process will take place upon reaching the destination.

The total travel time is 6 hours and 17 minutes. The charging process took 36 minutes. The duration of the journey was determined based on a best-case scenario, assuming that the charging station would not be occupied by another user. In the analyzed scenario, the driving time was 5 hours and 41 minutes. In the Wrocław–Wieliczka route, the EV vehicle completes the journey with a battery level of 20% and will then be charged up to 81%. The EV device will reach the final destination with a battery charge level of 10%. A buffer of 10% is maintained in case of unforeseen road circumstances.

The vehicle equipped with an internal combustion engine (ICE) exhibits a shorter travel time on the Wrocław–Solina route. The duration of this distance for electric vehicles was 7% longer (28 minutes). The faster arrival of ICE vehicles is due to the absence of the need for mandatory stops, allowing for continuous driving.

Despite the longer travel time, the cost of the journey for an electric vehicle (EV) is significantly lower. The total price amounts to 138.8 PLN. Reducing the charging costs of EVs is possible by using a charger in home conditions. However, minimizing costs may maximize charging time. The adopted charging structure for the vehicle through home conditions and charging points is the most probable scenario. The cost per kilometre of travel is as follows: 0.27 PLN/km for EV and 0.45 PLN/km for ICE.

Table 5 presents the annual fees that need to be covered for each vehicle type. The annual operating costs of different vehicle types are diversified. Internal combustion engines have higher values, which are caused by current gasoline prices. Low insurance costs, servicing, and covering a distance of 10,000 kilometers generate significant expenses. In the longer term, EVs are more advantageous. The low cost-effectiveness of the covered distances does not minimize the total price presented in Table 4. The annual cost value is due to expensive insurance, which accounts for approximately 50% of all operating expenses. The costs of powering EVs can be eliminated by using home charging connectors. The high price of purchasing an electric vehicle results in a low return rate. Under current conditions, the value of an EV may be recouped after approximately 47 years. However, the average lifespan of an electric vehicle is relatively shorter. In Scandinavian countries, 54% of EVs are deregistered after 2–3 years.

Table 4. Annual maintenance costs – EV and ICE (Q2 2022).

Type of cost	**EV**	**ICE**
Service maintenance	1040	2071
Insurance	3703	2204
Travel (10,000 km)	2700	4500
Total [PLN]	**7443**	**8775**

2.4. Forecasting fuel and charging infrastructure in Poland

An essential element of the comparative analysis of the economic viability of EVs and ICE vehicles is the infrastructure of fuel stations and charging points. The increase in the number of vehicles on the roads contributes to the demand for and development of this network. Its condition reflects the trends and preferences of users. Based on historical data, a forecast regarding the number of points in the future has been developed. The number of vehicle charging stations located within the territory of Poland is presented in Table 4 [13].

Table 5. The number of refuelling and charging stations in Poland [1]

Year	The number of retail fuel outlets	The number of charging stations
2010	6755	–
2011	6771	–
2012	6756	–
2013	6746	–
2014	6486	119
2015	6591	298
2016	6803	324
2017	6643	552
2018	7765	836
2019	7628	884
2020	7739	1792
2021	7852	2811

The fuel infrastructure has been developed for over a decade. The difference between 2010 and 2021 shows an overall increase of 1097 stations. The first charging points were established only in 2014. The growth is characterized

by a much more dynamic form compared to the distribution of fossil fuels.

Exponential smoothing is the most widely used class of procedures for smoothing discrete time series in order to forecast the near future. Its idea is to reduce the influence of the original series. It utilizes the moving average of the smoothed series to forecast future values. The forecast is constructed based on exponentially weighted averages of past observations. The highest weight is assigned to the current observation, a lower weight to the preceding observation, and an even lower weight to the earlier observation [10]. Exponential smoothing was used to estimate the forecast of the development of fuel and charging station infrastructure. The selected model has a relative error of 4.8%.

By 2025, the number of fuel stations will experience a slight increase. The diversification of the actual and modelled values is due to difficulties associated with the growth and decline of the discussed infrastructure elements. The forecast focuses on balancing the challenging-to-predict trends. The trend line predicts a decrease in the number of stations to 7,535 in 2022, followed by a gradual increase in the subsequent years:

- 2022 – 7535 objects
- 2023 – 7596 objects
- 2024 – 7658 objects
- 2025 – 7720 objects.

The increasing number of registered vehicles is correlated with the development of fuel station infrastructure. The Polish market is characterized by a high average age of vehicles and a small share of EV devices compared to Western countries. The well-developed fuel infrastructure does not require immediate expansion. The existing facilities meet the demand for such services.

The charging station infrastructure in Poland has been developed since 2014. The relatively new type of facilities creates favorable conditions for growth. It should be noted that the increasing number of electric vehicles creates a strong demand for expanding the charging station network. For the year 2022, the model indicates just under 3,981 points. In the following years, the number of charging stations will increase significantly, reaching 13,666 by 2025. Compared to the developed countries, the number of 13,000 facilities is relatively low. Currently, there are 59,410 active charging stations in Germany. Poland is likely to reach this number only after 2025.

The fuel infrastructure and charging station network reflect the market conditions of ICE or EV vehicles. The forecast allows for predicting their development directions. The decreasing pace of new petrol stations indicates a weakening market for combustion engine vehicles compared to previous years. Currently, the automotive industry focuses on reducing emissions. These efforts lead to minimizing fuel consumption levels, which correlates with the overall number of fuel distribution points. On the other hand, the charging station network is constantly expanding. The rapid growth is driven by the increasing number of electric vehicles on the roads.

Table 6. Electrification strategies of automotive manufacturers.

Manufacturer	Strategy
Jaguar	British luxury car brand Jaguar announced in February 2022 that starting from 2025, it will fully utilize electric power. The brand has committed to achieving zero carbon dioxide emissions by 2039. The first fully electric model of Land Rover is expected to debut in 2024, with the ultimate goal of phasing out internal combustion engines.
Audi	From 2026 onwards, all new models manufactured by the German car producer Audi will be powered by batteries. Vehicles with gasoline, diesel, and hybrid engines produced before 2026 will continue to be manufactured and sold until the beginning of 2030. The company, which belongs to the Volkswagen Group, will cease the development of internal combustion engines by 2033.
Alfa Romeo	Italian car manufacturer Alfa Romeo has announced that from 2027 onwards, it will be selling battery-powered cars in Europe, North America, and China.
Rolls-Royce	Luxury car manufacturer Rolls-Royce announced in September 2021 that it will exclusively produce electric vehicles by 2030. The brand, which is owned by BMW, is set to unveil its first fully electric car named "Spectre" by the end of 2023. By 2030, Rolls-Royce will no longer produce or sell any products powered by internal combustion engines.
Mini	The brand belonging to BMW announced in March 2021 that it will exclusively produce battery-electric vehicles by the end of the decade. The last model with an internal combustion engine will be released in 2025.
Volvo	The car manufacturer Volvo has committed to producing exclusively fully electric vehicles by 2030. By 2025, they aim for approximately 50% of their cars sold worldwide to be battery-powered, with the remaining 50% being hybrids.
Mercedes-Benz	Mercedes-Benz, a subsidiary of Daimler, aims to fully embrace electric power by the end of the decade. The company has taken actions focused on ensuring that battery-electric vehicles and plug-in hybrids account for 50% of its global sales by 2025.
Fiat	The Italian car manufacturer, owned by Stellantis, is taking steps towards a complete departure from the production of vehicles equipped with internal combustion engines by the end of 2029. The CEO of Fiat announced that between 2025 and 2030, cars of this brand will gradually be equipped exclusively with electric propulsion.
Ford	The American car manufacturer Ford has announced that by 2030, all of its passenger cars in Europe will be fully electric. The company expects that by the same year, 40 to 50% of its global sales will be comprised of electric vehicles with battery power. In September, Ford Motor and its Korean partner SK Innovation announced plans to build an electric vehicle assembly plant and three battery factories in the United States, scheduled to open in 2025. This $15.7 billion investment plan represents the largest manufacturing investment in Ford's 118-year history.
Volkswagen	By 2035, the German car manufacturer VW has committed to selling only battery electric vehicles in Europe. It plans to discontinue the sale of combustion engine cars in the United States and China at a slightly later date. VW aims to make its entire fleet carbon-neutral by no later than 2050 in terms of CO_2 emissions.

2.5. Strategies and visions of automotive manufacturers

The visions and strategies adopted by automotive manufacturers reflect the consumer needs of specific target groups. The visions often align with the main goals of the pro-environment policies in European countries, which aim to shift away from traditional sources of energy towards alternative ones. Harnessing solar, wind, and hydro energy is at the core of the modern energy revolution.

Planned changes to the existing paradigms strongly impact the transportation sector as well. In recent times, the automotive industry has been taking steps towards the mass introduction of electrified vehicles into the market. Table 6 presents the electrification strategies of car manufacturers, along with their declarations regarding the future and the development of transportation.

Each car manufacturer intends to increase its sales share in the zero-emission vehicle market in the future. British brands such as Mini, Jaguar, and Rolls-Royce plan to completely phase out internal combustion engines. However, the automotive industry is divided between the European market and the USA along with China. Ford and Volkswagen declare their intention to introduce only electric vehicles on the European continent while continuing to produce combustion engines in other countries. Mercedes-Benz aims to combine the advantages of both types of engines, creating modern hybrids. Audi stands out with an interesting aspect, as it is the only manufacturer that officially declares the development of combustion technologies until 2033.

3. Conclusions

The conducted economic analysis allowed for the identification of the electric propulsion system as more advantageous in terms of efficiency and operating costs. The problematic area lies in the range of vehicles, which is limited by the number of charging stations and low consumer awareness. The costs of purchasing new vehicles are diversified. Devices equipped with internal combustion engines are still less capital-intensive. However, ICE vehicles generate high financial and environmental costs. The price of acquiring an ICE vehicle and insurance costs are determining factors for their selection by consumers.

The conducted analysis of the number of fuel and charging infrastructure for both types of engines indicates intermediate directions for the automotive industry's development. The fuel infrastructure shows a small growth in the future. This may be attributed to the changing market share of internal combustion and electric vehicles. Most designs in the future aim for full or partial electrification. This fact organically reduces the consumption of fossil fuels while simultaneously increasing the demand for electric energy. The rapid development of charging points indicates the maximization of electric vehicle numbers. The evolving pro-environmental policies and the pursuit of carbon neutrality proclaim the emergence of efficient charging networks. Infrastructure investment is crucial for achieving emissions reduction and transportation system efficiency improvements. Governments need to provide regulatory frameworks and support for upgrading charging infrastructure to make EVs convenient for consumers.

Nomenclature

ASC authorized service centre
CEO Chief executive officer
CHAdeMO CHArge de Move (DC charging technology)
EV electric vehicle
EU European Union
ICE combustion engine

Bibliography

[1] Bienek F, Szczygiel I, Rutczyk B. Economical analysis of electric vehicles in Poland. Combustion Engines. 2023; 192(1):55-62. https://doi.org/10.19206/CE-151941

[2] Borkowski A, Zawiślak M. Comparative analysis of the life-cycle emissions of carbon dioxide emitted by battery electric vehicles using various energy mixes and vehicles with ICE. Combustion Engines. 2023;192(1):3-10. https://doi.org/10.19206/CE-147159

[3] Dižo J, Blatnický M, Semenov S, Mikhailov E, Kostrzewski M, Droździel P, Šťastniak P. Electric and plug-in hybrid vehicles and their infrastructure in a Particular European Region. Transp Res Proc. 2021;55:629-636. https://doi.org/10.1016/j.trpro.2021.07.029

[4] Islam S, Iqbal A, Marzband M, Khan I, Al-Wahedi A. State-of-the-art vehicle-to-everything mode of operation of electric vehicles and its future perspectives. Renew Sust Energ Rev. 2022;166:112574. https://doi.org/10.1016/j.rser.2022.112574

[5] Jere N, Corselli-Nordblad L, Ford-Alexandraki E, Xenelli G. Key figures on European Transport – 2022 edition. Publications Office of the European Union. 2023.

[6] Joshi A, Sharma R, Baral B. Comparative life cycle assessment of conventional combustion engine vehicle, battery electric vehicle and fuel cell electric vehicle in Nepal. J Clean Prod. 2022;379:134407. https://doi.org/10.1016/j.jclepro.2022.134407

[7] Klanjčić M, Gauvin L, Tizzoni M, Szell M. Identifying urban features for vulnerable road user safety in Europe. EPJ Data Sci. 2022;11(27):1-15. https://doi.org/10.1140/EPJDS/S13688-022-00339-5

[8] Liu Z, Song J, Kubal J, Susarla N, Knehr KW, Islam E et al. Comparing total cost of ownership of battery electric vehicles and internal combustion engine vehicles. Energ Policy. 2021;158:112564. https://doi.org/10.1016/j.enpol.2021.112564

[9] Moon S, Lee Y, Lee D. A cost-effectiveness analysis of fuel cell electric vehicles considering infrastructure costs and greenhouse gas emissions: an empirical case study in Korea. Sustainable Energy Technologies and Assessments. 2022; 54:102777. https://doi.org/10.1016/j.seta.2022.102777

[10] Ostertagová E, Ostertag O. The simple exponential smoothing model. Modelling of Mechanical and Mechatronic Systems. 380-382. The 4th International Conference, Herľany: Technical University of Košice 2011.

[11] Rostad S. Mobility at the crossroads – electric mobility policy and charging infrastructure Lessons from across Europe. Transport Res A-Pol. 2022;157:144-159. https://doi.org/10.1016/j.tra.2022.01.010
[12] Suttakul P, Wongsapai W, Fongsamootr T, Mona Y, Poolsawat K. Total cost of ownership of internal combustion engine and electric vehicles: a real-world comparison for the case of Thailand. Energy Reports. 2022;8:545-553. https://doi.org/10.1016/j.egyr.2022.05.213
[13] The Polish Organization of Petroleum Industry and Trade. https://popihn.pl/stacje-paliw-w-latach-2016-2023 (accessed on 29.5.2023)
[14] Eurostat. Passenger cars per 1000 inhabitants. https://ec.europa.eu/eurostat/databrowser/view/road_eqs_carhab/default/table?lang=en (accessed on 25.5.2023)
[15] Toyota Corolla Sedan (2023). https://www.wyborkierowcow.pl/toyota-corolla-sedan-2020-opis-wersji-i-cennik (accessed on 22.5.2023)
[16] Downstream: sportowe sprężyny H&R do VW ID.3! https://www.tuningblog.eu/pl/kategorien/autos-von-a-z/sportfedern-vw-id3-312481 (accessed on 25.5.2023)
[17] Routeplanner. https://abetterrouteplanner.com/?plan_uuid=73153f79-389d-44d2-aa8c-0b3793d03040 (accessed on 24.5.2023)

Aleksandra Kęska, DEng. – Faculty of Mechanical Engineering, Wroclaw University of Science and Technology, Poland.
e-mail: *aleksandra.keska@pwr.edu.pl*

Dawid Michalik, MEng. – Faculty of Mechanical Engineering, Wroclaw University of Science and Technology, Poland.
e-mail: *gadaki198@gmail.com*

Mateusz Dziubek, MEng. – Faculty of Mechanical Engineering, Wroclaw University of Science and Technology, Poland.
e-mail: *mateusz.dziubek@pwr.edu.pl*

Article citation info:
Idzior M, Karpiuk W, Smolec R. Investigation of a novel ceramic materials (Al_2O_3 and SSiC) for high-pressure pumps' delivery sections. Combustion Engines. 2024;196(1):153-160. https://doi.org/10.19206/CE-174315

Marek IDZIOR
Wojciech KARPIUK
Rafal SMOLEC

Combustion Engines
Polish Scientific Society of Combustion Engines

Investigation of novel ceramic materials (Al_2O_3 and SSiC) for high-pressure pumps delivery sections

ARTICLE INFO

Received: 27 July 2023
Revised: 4 September 2023
Accepted: 19 October 2023
Available online: 23 November 2023

In this paper, a comparative analysis of structural materials used in the construction of high-pressure pumps delivery sections was carried out. The focus was on a comparison of the ceramic materials such as corundum (alumina, Al_2O_3) and silicon carbide (solid-state sintered) – SSiC with bearing alloy steel 100Cr6, that is the most common material used to make pistons and cylinders of the delivery section of common rail injection pumps. Simulations performed using the finite element method have proven that ceramic materials have a number of advantages and could therefore be an interesting substitute for materials traditionally used in this area.

Key words: *ceramic, injection systems, common rail, fuel pump, FEM*

1. Introduction

A common feature of the high-pressure pumps used in passenger cars from all manufacturers is the use of fuel as a lubricant. During pump operation, fuel is supplied to both the delivery sections and the drive train (shaft–cam). It is therefore necessary to ensure proper lubrication parameters that will allow the formation of an oil film and thus the separation of the cooperating surfaces.

The lubricity of fuels is determined using the HFFR method. It consists of determining the maximum diagonal imprint resulting from a ball wear test using the test fuel as a lubricant. Figure 1 shows the relationship between running time and wear on pump components (expressed in micrometres of material layer loss). Analyzing the data, a clear relationship can be seen between the HFFR parameter and the durability of pump components. If the HFFR is above 600 µm, there is a very rapid increase in wear, leading to the destruction of the pump. For this reason, the fuel delivered to filling stations must meet the requirements of the standard [21], which sets an upper limit for the HFFR parameter of 460 µm. It should be emphasized that the addition of rapeseed oil fatty acid methyl esters to diesel effectively improves its lubricating properties due to the very favorable HFRR coefficient, which for pure rapeseed oil fatty acid methyl esters is below 200 µm.

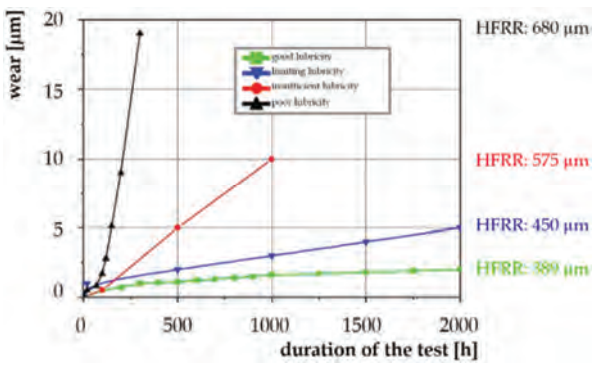

Fig. 1. The dependence of the wear of the pump components on the duration of the test [22]

One of the primary causes of pump failures is insufficient fuel quality. This conclusion is related to the lubricity issue described. It should be noted, however, that the inadequate design of both the low-pressure feed pump and the high-pressure pump is also a factor in the formation and progression of injection system failures. Thus, in terms of use, the increased forces occurring in the pump drive system must not translate into increased wear in the precision pair of cylinder and piston and the cam and tappet area. It is these structural components that are responsible for the pump's correct operation. Their durability can be increased by using modern materials in the field of engineering ceramics. To properly select such materials, it seems necessary to know the nature of their operation and the damage that occurs in their working area.

2. Causes of damage and functional problem

The main cause of wear in high-pressure injection systems is contamination. The destruction of precision components, whose steel surfaces are finely machined, is influenced by hard mineral particles (silica, alumina) [5]. They can get into the pump system in the form of impurities along with fuel or lubricating oil. Surface pressures in the case of tappet and roller or plain bearings are the result of the negative effect of excessive clearances and unevenness. This leads to a rapid expansion of wear, and the products, i.e. metal particles including steel, increase the amount of contamination in the lubricating oil and fuel. On the other hand, the formation of fretting corrosion is favored by water getting into the oil. Such a process significantly accelerates the wear of rubbing or rolling steel surfaces. As a result, hematite (Fe_2O_3), a product of wear, enters the fuel or lubricating oil, impairing its lubricating properties. It is often observed that the oil changes its consistency into a dense mixture of heavy hydrocarbons with impurities and water particles. This has a detrimental effect on mating pump components, causing deposits to form, e.g. on cylinder walls [5].

Damage to the surfaces of cams and eccentrics and the tappet rollers that roll over them is also a major problem. Particularly unfavorable are larger cavities, chipping of the

surface layer of metal, the presence of developed corrosion and localised collapsing of the cam distorting its profile, especially at the transition from the cam's tangential surface to its apex. The tappet spring is subject to surface scratching, corrosion and cracking. Other parts of the pump, the design of which depends on the variety and type of pump, are closely related to the potential for a variety of damage. They also depend on the operating conditions of the high-pressure pump. Such elements are: precision pairs, high pressure connections, hoses, valves, and control sleeves [5].

An example of a pump where the failure rate is mainly based on precision pair wear is the Bosch CP1 pump. This is only an example illustrating the problem – Siemens VDO pumps, for instance, are characterised by a similar design. In the case of the Bosch, the defect is caused by the negative effect of the design itself in combination with the load. The problem lies in the pivoting position of the tappet relative to the rotating cam on the pump shaft. This position of the tappet results in a tangential force to the cam in addition to the normal force. Under unfavorable conditions and insufficient lubrication, in addition to the force perpendicular to the piston axis, the frictional force has a negative effect [17]. This forces stresses into the mating components and results in material breakage. The resulting wear products can enter the piston-cylinder precision pairs, causing their destruction through abrasive wear and the formation of cracks (Fig. 2). Noticeable scratches then occur on the cylindrical surface of the piston, resulting, in a later stage of wear, in leakage in the working area of the pump [9, 18].

Fig. 2. Pump section piston with scratches on the side surface [10]

Torn-off material particles can also enter the part of the pump where the roller rotates. Material loss occurs on the side surface of the tappet due to the occurrence of cavitation and shearing due to contact between roughness vertices [11]. The cavitation mentioned can occur within the pump and high-pressure lines. It involves the formation of vapor bubbles due to the action of varying pressure and implosion, which, when occurring close to the walls, causes damage to the walls. The high energy density contributes to the formation of cavitation pits [11].

Some swarf also enters the high-pressure pump from the pre-pumping pump. This is usually a gear pump characterised by a discharge pressure of 300–600 kPa. The contact area between the teeth and the pump raceway is exposed to frictional forces resulting in tribological wear.

A sensitive area is the inlet and outlet valves from the delivery section. A frequent cause of damage in this area is particles from dirt in the pumped oil. The discharge valve is made up of a ball embedded in a seat. The loss of tightness of this association is caused by erosion and distortion of both components. Defects can also occur in the throttling hole safety valve used to distribute fuel between the discharge section and the pump's lubrication and cooling circuit, under the influence of pressure variations in the low-pressure circuit. Defects in this area result in reduced cooling of the delivery section and consequent heating of the components [11].

The drive shaft of the pump is also susceptible to damage. During the transmission via the coupling, run-out of the cam shaft can occur, as well as its rubbing under the sealing ring. Wear occurs at the point of connection between the shaft and the coupling (Fig. 3) [11]. The seals also deteriorate under pressure and contaminants present, resulting in fuel leaking outside the pump body. The high pressures generated by the pump contribute to high loads on the shaft itself and the eccentric placed on it, as well as on the plain bearings in the body. The highest loads from the pressure forces occur when reaching the top extreme position of the piston. The loads are transferred at the bearing locations. These are characterised by varying wear of the roller surfaces. Micro-cutting and furrowing occur at those locations adjacent to the shortest radius of the eccentric [1].

Fig. 3. Examples of damage to the pump cam shaft [10]

3. Ceramics as a material for precision pump pairs

For the material analysis, ceramic materials such as corundum (alumina, Al_2O_3) and silicon carbide (solid-state sintered) – SSiC were used and compared with 100Cr6 alloy bearing steel, i.e. the most popular of the materials from which the pistons and cylinders of the pumping sections of the pumps are made common rail injection system.

Alumina, also called corundum, especially in the stable polymorphic form alpha (α-Al_2O_3), is characterized by properties suitable for construction purposes [12, 18]. The variety mentioned here, crystallized in the hexagonal system, has good strength and tribological properties, although it should be mentioned that they depend on the course of the sintering process [8]. Valuable properties in terms of strength are also shown by silicon carbide, which is characterized by similar and even more favorable material parameters than Al_2O_3. Its advantages are greater hardness and

resistance to thermal shock, and better mechanical properties, including, for example, durability. When choosing a material for a specific application, its mechanical properties should be taken into account. The materials of the elements of precision pairs should behave appropriately under the influence of occurring loads.

Ceramic materials are prone to brittle fracture, which is different from metals, where a certain range of plastic deformation is noticeable. The reason lies in the structure of the ceramic, where the covalent bonds are directional. In addition, there are defects in the form of cracks, pores and voids, and the samples are destroyed already in the range of elastic deformations [8, 16]. These discontinuities in the structure contribute to a lower resistance to tensile loading and cracking due to tensile stresses that are lower than those assumed based on interatomic bonds. Then, the aforementioned empty spaces are expanded, which in turn leads to a reduction in the load-carrying capacity [15]. Ceramics are characterized by higher compressive strength compared to tensile strength ($R_c \cong 15 \cdot R_m$) [20]. Therefore, it is advantageous to use engineering ceramics in section pump pistons, but also in rollers, because due to the nature of work, these elements transfer compressive loads. The most important mechanical properties of the analyzed materials from the point of view of the conducted considerations are presented in Table 1.

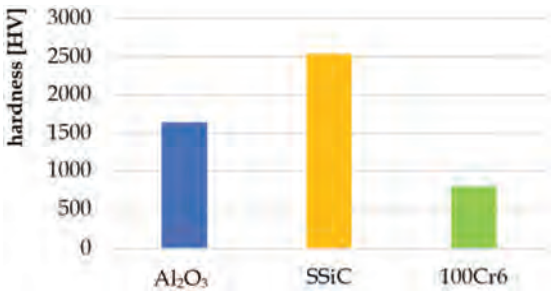

Fig. 4. Comparison of the hardness of ceramics and steels [24]

The characteristic features of ceramic materials are their high hardness and abrasion resistance. This is due to the structure in which the network with ionic bonds resists dislocations [19]. It is very difficult to initiate their movement, and permanent plastic deformation occurs through these linear defects. The determination of hardness by various available methods is also the determination of the state of plasticity, so it can be considered through deformation. To activate the dislocation, high stresses are needed in the tangential direction of the bonds, which results in their tearing [9]. The critical stress of alumina ceramics that initiates dislocation slipping is high, of the order of E/30, while for metals it is only E/1000 [3]. A comparison of the hardness of ceramics and steel is shown in Fig. 4. An analogous combination concerning Young's modulus is shown in Fig. 5.

In the case of Al_2O_3 alumina with ionic bonds, the movement of atoms in certain directions is complete, so the resistance is lower [3, 9]. Note the high hardness of SSiC, even greater than Al_2O_3, far exceeding the level typical for metals. The associated Young's modulus E, which determines the resistance to elastic deformation, is about 430 GPa. At the same time, it is not dependent on the load operation time. Hardness and strength, which are dependent properties, are affected by the type of structure-building bonds. As mentioned, these are covalent bonds resistant to activation and dislocation [23]. Like alumina, silicon carbide has a certain strength distribution, describing the possibility of failure even under stresses at which it should withstand the load.

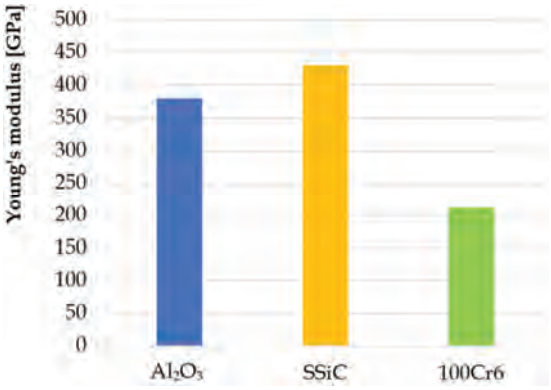

Fig. 5. Comparison of Young's modulus of ceramic materials and steel [24]

An important parameter from the point of view of injection pumps is the stress intensity factor K1C. Its value for ceramic materials is more than three times lower than for 100Cr6 steel. According to the definition of the parameter, this indicator determines the load causing uncontrolled crack development in sections [7]. This is the adverse effect of hindering dislocation slippage. Ceramic materials are characterized by lower fracture toughness than metals due to the limited plastic deformation capacity, and thus lower impact strength. The high brittleness of engineering ceramics can be the main obstacle in the structural applications of the designed elements. Products made of it are often destroyed during use or their premature damage is noticeable. It is therefore important to avoid structure discontinuities, e.g. micro-cracks, by maintaining a low tolerance for defects [14]. Even micro-scale cracks, within the tolerance range, smaller than critical cracks, can develop and contribute to their further propagation [20]. Compressive and flexural strengths should also be closely monitored – ceramic materials withstand pressure loads much better than metals [9, 14, 20, 25].

Table 1. Mechanical properties of the analyzed materials

Material	Standardised hardness HK0.1 [GPa]	Vickers hardness [HV]	Stress intensity factor K_{1C} [MPa $m^{1/2}$]	Compressive strength R_c [MPa]	Bending strength R_g [MPa]	Young's modulus E [GPa]
Al_2O_3	23	1650	4.2–6.0	3500	350	380
SSiC	24,5	2540	4.0	> 2500	400	430
100Cr6	–	800	15.4–18.7	–	–	212

The nature of the operation of precision pairs, i.e. sliding contact, imposes high demands on their surface resistance to various types of wear. The condition of the surface structure of products plays a key role in the issue of abrasion. Roughness is also important, but in the case of engineering ceramics, there are some limitations in this respect. The reason is the occurrence of "losses" of the material, i.e. voids, pores, etc., which significantly change the distribution of the surface layer. However, the description of the surface is made possible by other parameters related to load capacity, lubricant capacity (R_{pk}, R_k, R_{vk}), etc. The study of ceramic wear shows the conclusion [4] that the final surface treatment is an important aspect, significantly influencing the roughness. The structure of aluminum oxide depends on the sintering process, the average grain diameter is about 7.5 µm. On the other hand, for SSiC, this value is at the level of about 1.9 µm, so Al_2O_3 is characterized by greater roughness. At the same time, however, both materials show relatively deep defects due to grain tearing, although the number of defect cavities is smaller on the surface of the alumina subjected to polishing.

The parameter determining the quality of the surface is, among others, the coefficient of friction, which plays an important role in the fitting of elements of precision pairs. In common rail injection pumps, a long surface cover is used, which significantly affects the tightness of the node and reduces losses. Unfortunately, the accuracy of the fit increases the contact area of the surfaces and the resistance to movement, and also causes the occurrence of increased phenomena such as heat release. The presence of liquid in the mating pair is also important aspect. The use of ceramic materials should also be considered in above mentioned areas. It is important to reduce the coefficient of friction, which increases the efficiency of the system, but also minimizes the possibility of wear.

The hardness of the surface has a significant impact on the elements in the friction node. Increasing the value of this parameter minimizes the negative effects of tribological processes, including abrasion. The use of ceramic materials leads to the elimination of tribochemical wear, so no adhesive bonds are leading to seizing of the piston-cylinder friction node.

Another issue worth mentioning concerning the use of engineering ceramics in high-pressure injection systems is their chemical and corrosion resistance. Ceramic materials achieve significant resistance even at high operating temperatures, which becomes important in various demanding applications. What is important then is the oxidation process. However, in this system, there is only elevated temperature, because the diesel fuel in the injection pump reaches temperatures of 60°C.

4. Simulation of precision pair operation with results

In the initial preparation for the simulation, the piston-cylinder system of the Bosch CP3 and CP4 pumps was analysed. The difference between the two is the way the motion is transmitted to the piston. In the CP3 pump (Fig. 6), the reciprocating movement is forced by an eccentric on the glass tappet mechanism. In CP4, the movement is forced by a roller (Fig. 7).

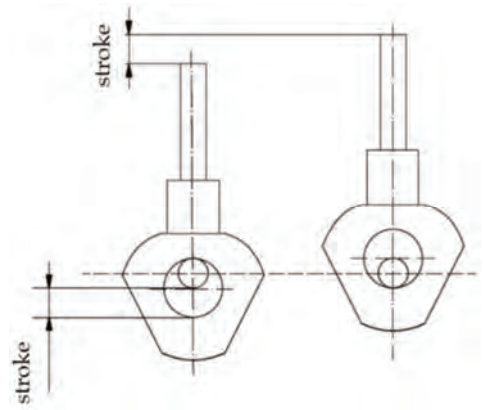

Fig. 6. Principle of operation of the pumping section of the CP3 pump

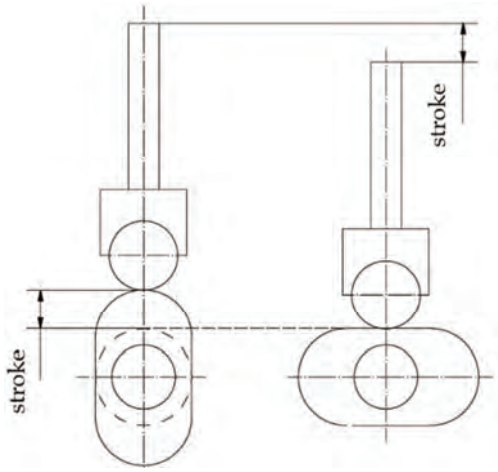

Fig. 7. Principle of operation of the pumping section of the CP4 pump

The course of the piston lift during the entire operating period is variable with some momentary constant values during the supply of fuel to the cylinder's working volume (Fig. 8).

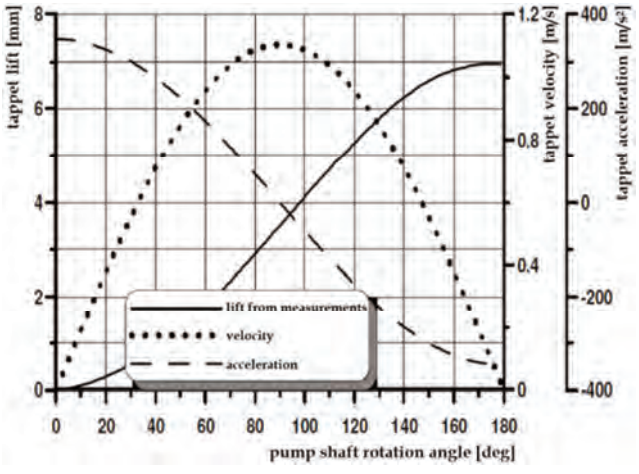

Fig. 8. Diagram of the dependence of lift, velocity and acceleration of the tappet on the angle of rotation of the CP3 pump shaft [6]

It moves from the inlet valve to the bottom dead center, below the high-pressure outlet valve. Thus, the volume of the pumped fuel depends geometrically on the position of the piston during its operation – for the assumed typical dimensions of the section, it varies from 100 to 250 mm^3.

During full load, after a certain period, the initial volume is already approx. 123 mm^3 [6]. The movement of the piston enables the generation of pressures in the CP3 pump up to approx. 180 MPa. The maximum value is reached at the initial pressure resulting from the operation of the feeding pump is about 0.7 MPa. The newer generation of the pump already can generate a pressure of about 200 MPa. The design of the piston must withstand such high pressure loads. Both pumps are devoid of construction defects that occurred in the CP1 generation discussed in Chapter 2. A roller or bucket tappet mechanism avoided the occurrence of forces transverse to the piston axis caused by a sliding plate tappet. This resulted in wear on the lateral surfaces, including the cylinder. Ceramic materials, which are not resistant to bending and are prone to fracture, may not have fulfilled their role in this application [13].

The geometry of the CP4 pump head was used for further finite element analysis. A schematic of the pump model including the components (head, piston, cylinder) is shown in Fig. 9.

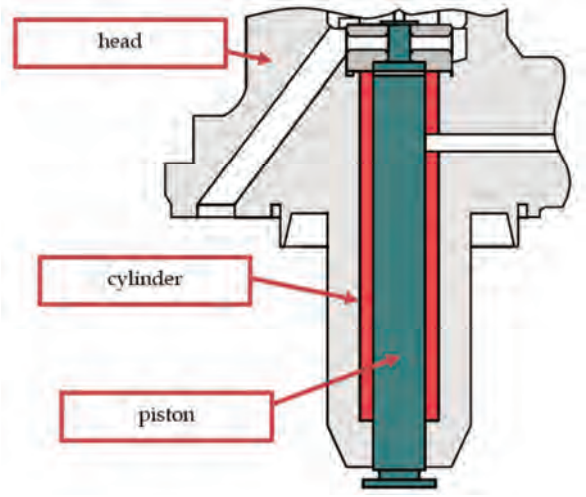

Fig. 9. Model of a CP4 pump

This assumed the use of ceramic materials in the piston-cylinder junction as respectively made junction pairs: Al_2O_3/Al_2O_3 or, in the second variant, SSiC/SSiC. It was further assumed that both components were made by powder metallurgy methods – sintering, while the mating surfaces themselves were subjected to grinding, achieving low surface roughness. The piston and cylinder model used for the simulation, is shown in Fig. 10.

The CAD model of the pump piston used in the simulations was made in the Autodesk Inventor environment. The simulation in this area, using FEM, was realised in the Nastran In Cad package. The discretisation of the piston allowed the model to be divided into finite elements and nodes, by determining a finite element size reduction run for the entire geometry. The model was divided into 35,584 finite elements and 55,426 nodes (Fig. 11).

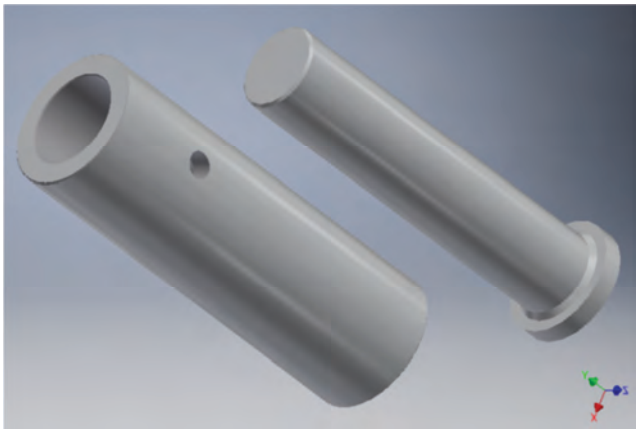

Fig. 10. Piston and cylinder model used for the simulation

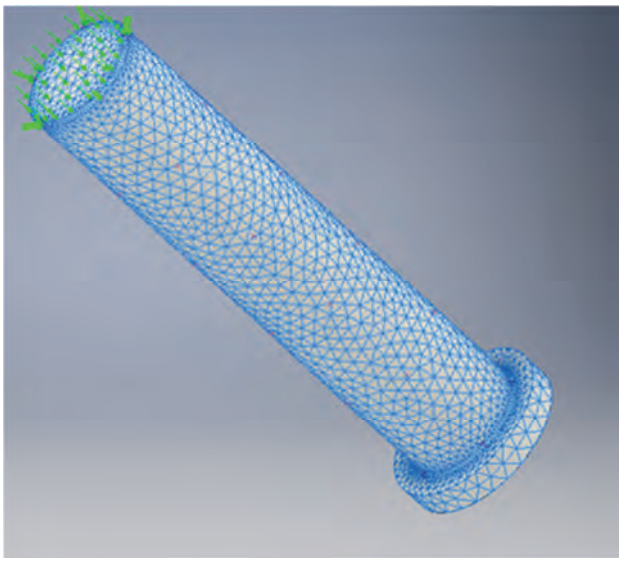

Fig. 11. Piston model discretised into finite elements

It was assumed that the analysis would replicate the conditions prevailing at maximum load, however, the effects of the cylinder/pump head were ignored. For this reason, the piston is subjected to a higher load than the actual load. The interaction of the spring thrust plate with the piston shoe has also been omitted – so the main focus is on the pressure action and its effects. Accordingly, the piston was subjected to the highest possible pressure that was assumed to exist in the pump, i.e. 180 MPa at the end of the compression stroke. The pressure force was applied to the top surface of the piston and the bottom surface of the bead was restrained. The simulation was carried out for three variations of the component design. The first material was corundum the second material was silicon carbide (solid-state sintered) – SSiC, the third material was 100Cr6 alloy-bearing steel.

The material properties were determined based on reference materials [2, 7]. It was decided to collect the results at the moment of the highest discharge pressure, with the assumed course of its variation, as this is a variable load analysis for the moment 0.02 s when the maximum was reached.

An example of simulation results for a component made of sintered silicon carbide is presented in Fig. 12 and 13.

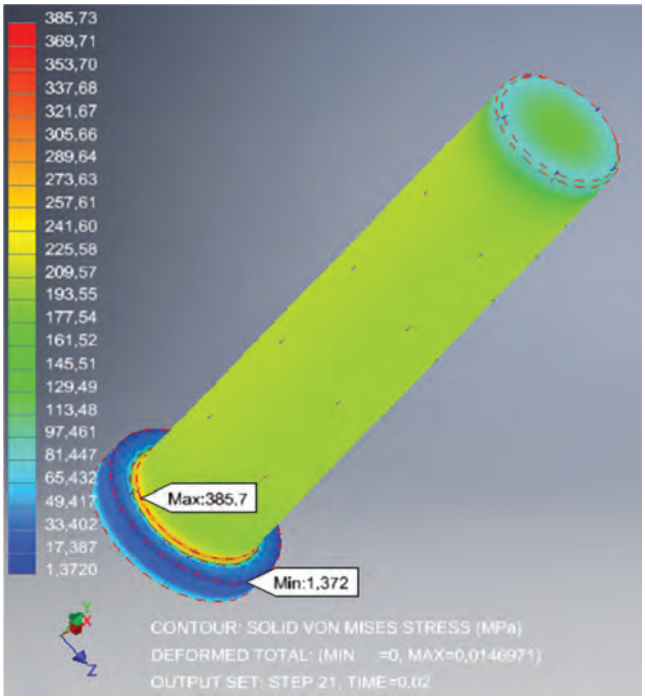

Fig. 12. Huber-Misses reduced stress distribution [MPa] for a component made of made of SSiC

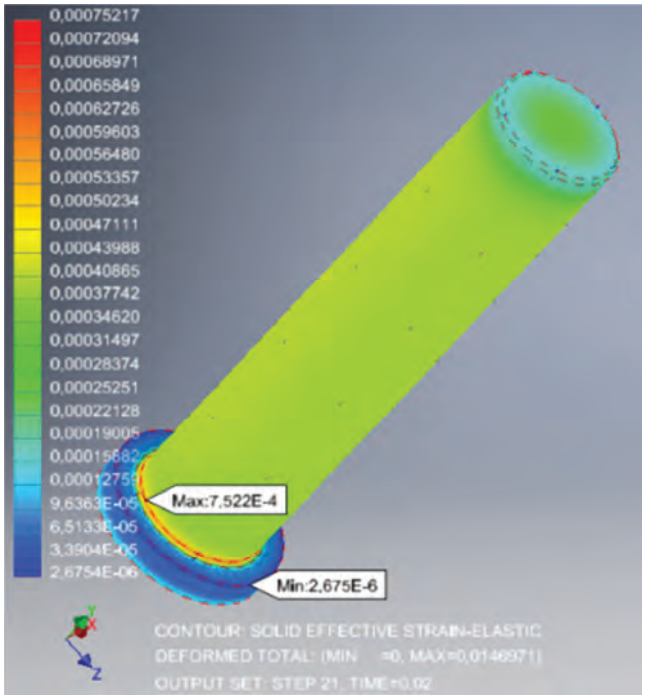

Fig. 13. Strain distribution [-] for a component made of SSiC

Through the finite element computational environment, the feasibility of using Al_2O_3 and SSiC ceramic materials and 100Cr6 steel was analysed. The time-varying load analysis was generalised as a static compression test, thus a strictly strength simulation, and this was adopted in further inference. The set of results is illustrated in Table 2.

The concentration of the maximum stress results for all variants of the component design falls within the area of geometric change. For bearing steel, the smallest maximum reduced stress was obtained, as metals, unlike ceramics, are characterised by elastic and plastic periods. In contrast, as in the other cases, the clustering of the highest stresses and strains occurs just at the transition of the piston geometry to its bead. In this case, the reduced stresses exceed the value of the allowable stresses calculated analytically according to relation (1).

$$\sigma_{dop} = (0.55 - 0.65)R_e \tag{1}$$

Table 2. Results of the analyses

	Al_2O_3	SSiC	100Cr6
Huber-Misses maximum reduced stresses [MPa]	373.4	385.7	372.8
Maximum strain [–]	0.000852	0.000752	0.001539

For compression, the parameter R_e has approximate values determined from the tensile test. In the analysis, a yield strength of 400 MPa was determined for 100Cr6 steel, for which, according to the above relationship, the allowable stress is in the range 220–260 MPa. The maximum simulation result was 372.8 MPa, and condition (2) was not met.

$$\sigma_{red} < \sigma_{dop} \tag{2}$$

The occurrence of maximum stresses in this area of the component can cause the structure to weaken, and the maximum deformation with respect to the entire component indicates that this area is subject to some plastic deformation. This is confirmed by numerous examples of piston damage. Most often, material swelling occurs in this area as a result of plastic deformation caused by the generation of pressures up to their maximum value and the cyclic nature of these pressures – the internal stresses then exceed the permissible values. The resulting load cycles cause fatigue, which can result in cracks forming in the plasticisation zone. It is clear that plastic deformation can result from friction between piston and cylinder, inhomogeneities in material strengthening, uneven temperature distribution and the influence of strain rate. The effects of such a process are changes in the properties of the structure, and (under appropriate geometric conditions) swelling. This may result in slight changes in the diameter of the piston, which directly affects its function – the friction of the mating surfaces. It should be noted, however, that the yield strength considered to illustrate an example of this type of bearing steel can be higher, for example, when hardening is applied. R_e then reaches a value of approximately 1300 MPa.

5. Summary

The paper compares selected ceramic materials Al_2O_3 and SSiC with 100Cr6 steel. Particular attention was paid to the use of the above materials in the precision pairs of a common rail injection pump. A simulation was carried out using FEM by inducing a load on the upper part of the piston, which was assigned the properties of the three compared materials.

The results of the example simulation show that the level of deformation in ceramic components is lower than in metal. In ceramics, plastic deformation does not occur under load, and failure occurs through brittle fracture. The

strain level of Al_2O_3 and SSiC ceramics in this analysis was smaller by an order of magnitude.

Taking the compressive strength as equivalent to the tensile strength (such a simplification is reasonable when describing elastic-plastic materials), a significant advantage of ceramics over steel is noted. The compressive strength of Al_2O_3 and SSiC is higher than that of 100Cr6 steel, even when subjected to processes that increase the overall strength parameters. It is also possible to determine analytically the allowable stresses if the yield strength (Re) is replaced by the compressive strength in formula (1). In this way, the clear limit of the value after which failure (fracture) of the material will occur is much higher than those presented by metals. On the other hand, the fracture itself may occur below the allowable stress values – with regard to ceramics, this is a particularly noteworthy strength aspect.

The results of the analysis mainly depend on the adopted elasticity constants of the material: Young's modulus (E) and Poisson's number. For a constant surface perpendicular to the applied pressure, and therefore for a constant piston diameter, the deformation in the test depends on the longitudinal modulus of elasticity. The greater its value, the smaller the deformation will be and the more rigid the component. For ceramics, this modulus is significantly higher than for steel, as can be seen in the analysis results.

The inhomogeneous structure of ceramics, or more precisely, the pores present in them, is the reason for the appearance of notches, where stresses are concentrated to varying degrees. The simulation does not take into account the presence of defects in the structure, i.e. cracks, pores, voids. It should be emphasized that the analysis carried out is a certain simplification, as parts with a more complex structure and irregular pores may have different stress and strain field distributions that are more difficult to determine properly. This simplification was made because stress concentrations caused by the presence of structural defects are not taken into account for compressive stresses. This means that a component such as a piston subjected mainly to a compressive force is not affected by internal defects, because with such an actual condition the pores are closing and not opening [18].

Nomenclature

SSiC	sintered silicon carbide	FEM	finite element method
HFRR	high frequency reciprocating rig		

Bibliography

[1] Bajerlein M, Bor M, Karpiuk W, Smolec R, Spadlo M. Strength analysis of critical components of high-pressure fuel pump with hypocycloid drive. B Pol Acad Sci Tech. 2020;68(6):1341-1350. https://doi.org/10.24425/bpasts.2020.135380

[2] Blicharski M. Material engineering (PL original: Inżynieria materiałowa). WNT. Warsaw 2019.

[3] Clifton B. Ultracoatings: Enabling energy and power solutions in high contact stress environments through next-generation nanocoatings. CRADA Final Report 2012.

[4] Dulias U, Zum Gahr K-H. Investigation of Al_2O_3 and SSiC-ceramic under lubricated, reciprocating sliding contact and cavitation erosion. Materialwiss Werkst. 2005;36(3-4):140-147. https://doi.org/10.1002/mawe.200500860

[5] Falkowski H, Krępeć T. Maintenance and repair of diesel engine fuel apparatus. WKiL. Warsaw 1973.

[6] Gancarczyk T, Knefel T. Model analysis of the high pressure pump of a common rail system. Mechanik. 2013;86.

[7] Golewski GL. Stress intensity factor as a basic parameter for assessing the fracture toughness of concrete composites. Drogownictwo. 2010;1:31-35.

[8] Ji R, Yao Z, Zhang Y, Wang R. Effects of nano-ceramic coatings on the thermal structure of ω-type pistons. Chinese Intern Combust Engine Eng. 2023;44(2):51-57. https://doi.org/10.13949/j.cnki.nrjgc.2023.02.007

[9] Kaczorowski M, Krzyńska A. Structural metallic, ceramic and composite materials. 2nd ed. Warsaw Technical University Publishing House. Warsaw 2017.

[10] Karpiuk W. Study of the design of a hypocycloidal injection pump. Poznan University of Technology Publishing House. Poznan 2022.

[11] Kruczyński S, Chrupek B. Malfunctions of the common rail fuel system of modern compression-ignition engines Zeszyty Naukowe Instytutu Pojazdów. Warsaw 2014.

[12] Li R, Chen Q, Ouyang L, Ding Y. Adhesion strength and bonding mechanism of γ-Fe (111)/α-Al_2O_3 (0001) interfaces with different terminations. J Alloy Compd. 2021;870:159529. https://doi.org/10.1016/j.jallcom.2021.159529

[13] Magryta P, Pietrykowski K. Crankshaft geometry modification and strength simulations for a new design of diesel opposed-piston engine. Combustion Engines. 2023;194(3):123-128. https://doi.org/10.19206/CE-169371

[14] Majeed EA, Rashid HK, Hussain MK. Review of ceramic materials that used as a thermal barrier in diesel engine pistons. J Phys Conf Ser. 2021;1973:012125. https://doi.org/10.1088/1742-6596/1973/1/012125

[15] Matizamhuka WR. Advanced ceramics – the new frontier in modern-day technology: Part I. J S Afr I Min Metall. 2018;118:757-764. https://doi.org/10.17159/2411-9717/2018/v118n7a9

[16] Mercier JP, Zambelli G, Kurz W. Introduction to Materials Science. Elsevier 2003. https://doi.org/10.1016/C2009-0-29148-3

[17] Merkisz J, Idzior M, Lijewski P, Fuc P, Karpiuk W. The analysis of the quality of fuel spraying in relation to selected rapeseed oil fuels for the common rail system. Proceedings of the Ninth Asia-Pacific International Symposium on Combustion and Energy Utilization. 2008.

[18] Mohd Tamam MQ, Omi MRT, Yahya WJ, Ithnin AM, Abdul Rahman H, Rahman MM et al. Engine performance and emissions evaluation of surfactant-free B30 biodiesel–diesel/water emulsion as alternative fuel. Sci Rep. 2023;13(1):10599. https://doi.org/10.1038/s41598-023-37662-4

[19] Nie G, Li Y, Sheng P, Zuo F, Wu H, Liu L et al. Microstructure refinement-homogenization and flexural strength improvement of Al_2O_3 ceramics fabricated by DLP-stereolithography integrated with chemical precipitation coating process. J Adv Ceram. 2021;10:790-808. https://doi.org/10.21203/rs.3.rs-86507/v1

[20] Niezgoda T, Małachowski J, Szymczyk W. Numerical modelling of the microstructure of ceramics. WNT. Warsaw 2005.
[21] PN-EN 590+A1:2017-06, Automotive fuels – Diesel fuels – Requirements and test methods.
[22] Training materials. Automotive Training Centre, "Autoelectronics Kędzia".
[23] Vengatesan S, Yadav P, Varuvel EG. Effect of alloying elements and ceramic coating on the surface temperature of an aluminum piston in a diesel engine. J Nanomater. 2022; 9916742. https://doi.org/10.1155/2022/9916742
[24] Your Source for Materials Information. MatWeb. www.matweb.com (accessed on 15.09.2023).
[25] Zhang J, Xiao G, Yi M, Chen Z, Zhang J, Chen H et al. Mechanical properties of ZrB2/SiC/WC ceramic tool materials from room temperature to 1100°C and cutting performance. Int J Refract Hard Met. 2021;101:1-7. https://doi.org/10.1016/j.ijrmhm.2021.105697

Prof. Marek Idzior, DSc., DEng. – Faculty of Civil and Transport Engineering, Poznan University of Technology, Poland.
e-mail: *marek.idzior@put.poznan.pl*

Wojciech Karpiuk, DSc., DEng. – Faculty of Civil and Transport Engineering, Poznan University of Technology, Poland.
e-mail: *wojciech.karpiuk@put.poznan.pl*

Rafał Smolec, MEng. – Faculty of Civil and Transport Engineering, Poznan University of Technology, Poland.
e-mail: *rafal.smolec@put.poznan.pl*

Article citation info:
Sawczuk W, Rilo Cañás AM, Kołodziejski S. Thermal imaging of the disc brake and drive train in an electric locomotive in field conditions. Combustion Engines. 2024;196(1):161-168. https://doi.org/10.19206/CE-174320

Wojciech SAWCZUK
Armando Miguel RILO CAÑÁS
Sławomir KOŁODZIEJSKI

Combustion Engines
Polish Scientific Society of Combustion Engines

Thermal imaging of the disc brake and drive train in an electric locomotive in field conditions

ARTICLE INFO

Received: 28 July 2023
Revised: 22 September 2023
Accepted: 19 October 2023
Available online: 25 November 2023

The article presents the results of thermovision tests of the disc brake and the drive system components located in its vicinity on the 111Ed electric locomotive in field conditions. For this locomotive, tests were carried out on a test track to measure the temperature of the disc and the temperature of other devices that were installed close to the brake disc. These tests were performed pointwise, i.e. before and after the test, and continuously throughout the braking process. The article presents the methodology of thermal imaging research and the preparation of the camera for outdoor research with objects with different emissivity. Due to the rotating brake disc, it was decided to measure using an IR camera because measurements using thermocouples were very difficult and complex. In exceptional situations, temperature measurement using thermocouples is used, but it requires an extensive additional measurement system and signal recording, which is more expensive. Correct configuration of the IR camera to real conditions is extremely important because it directly translates into the increase in measurement error.

Key words: *thermal imaging, emissivity, disc brake, electric locomotive, drive train system*

1. Introduction

The thermal imaging camera enables indirect measurement (non-contact at a distance) by recording in the lens the infrared radiation emitted by the tested element in the electromagnetic wavelength range. Each body that has a temperature higher than absolute zero, i.e. 0 K, emits energy in the form of infrared radiation, however, it should be noted that the radiation energy coming from the tested element depends on the length of the electromagnetic wave and the temperature of this object [2, 4, 6]. The IR camera has a built-in infrared detector to convert the energy coming from incident infrared photons from the tested device (element) into an electrical signal. The value of this signal is directly proportional to the temperature of the tested object [3, 12]. Electrical signals in the form of color images are converted into thermograms. This is due to the fact that the tested objects emit radiation of a certain power, which is called luminance. Different intensities of infrared radiation translate into the temperature distribution visible in the thermal image (thermogram).

Fig. 1. View and construction of the FLIR e60 thermal imaging card used in later studies: 1 – lens, 2 – control buttons, 3 – trigger, 4 – camera handle, 5 – laser, 6 – display [11]

The general structure of a thermal imaging camera is shown in Fig. 1. The cameras can be used as portable devices with a handle under the operator's hand (inspection cameras) or as research cameras mounted on a tripod [15].

The division of cameras is diverse. Inspection and research cameras were mentioned earlier, but IR cameras are also divided into devices only for observing objects and related temperature distribution and cameras for simultaneous observation and measurement of temperature values. Detectors that are built into cameras as measurement transducers determine their further division. It should be noted that bolometric cameras are most often used due to the widest range of recorded infrared wavelengths [6, 18]. These types of cameras are used in construction, the power industry or testing machines, and internal combustion engines, as presented in [16, 19].

2. Emissivity determination methods

The thermal imaging camera requires configuration of settings to the conditions that prevail during the tests. Particular attention should be paid to the emissivity (ε factor) setting. The other parameters set in the IR camera, besides emissivity, are ambient temperature, air humidity, and reflected temperature. These parameters, if entered incorrectly during configuration, cause a slight increase in the measurement error by approximately 1–2°C [8]. The emissivity recorded in the camera has the greatest impact on the measurement error (several dozen percent). This is a parameter related to the ability of the tested body to emit real radiation related to the emission from a black body.

$$\varepsilon = \frac{W_{CR}}{W_{DC}} \tag{1}$$

where: W_{DC} – black body radiation, W_{CR} – real body radiation.

It is also defined as the ratio of the intensity of real radiation to the infrared radiation of a black body at the same

temperature as the tested object and the perfect black body, which shows the relationship (1) [9].

The value of the coefficient depends on such factors as the type of body, its temperature, the wavelength of the radiation as well as the condition of the surface [12]. Depending on the surface (polished or rough), the emissivity coefficient may vary from 0.1 to 0.98. Test objects with polished surfaces have an emissivity coefficient even below 0.1 because they reflect approximately 99% of external radiation. All infrared radiation does not reach the camera lens. Rough and black surfaces mean that all the radiation reaches the IR camera lens (ε above 0.9) [2].

There are three ways to determine the emissivity in thermal imaging. It is a calorimetric, reflection and reference body method. The emissivity coefficient in the calorimetric method can be calculated using two methods.

The first method involves using a camera that measures spectral existence. Emissivity is determined by measuring the temperature from a thermocouple. The second method is based on the calculation of spectral existence based on relation (2) [10].

$$M(T) = \varepsilon M_c(T_o) + (1 - \varepsilon)M_\alpha(T_\alpha) \quad (2)$$

where: $Mc(T_o)$ – the existence of a blackbody at the temperature of the object T_o, $M\alpha(T_\alpha)$ – background existences about temperature T_α.

On the basis of the Stefan-Boltzmann law, it is possible to determine the value of existence knowing the temperatures of the object T_o and the ambient (background) temperature T_α, respectively [6]. Then the actual emissivity coefficient is calculated based on equation (3) [9].

$$\varepsilon = \frac{T^4 - T_\alpha^4}{T_o^4 - T_\alpha^4} \quad (3)$$

where: T – temperature value when ε = 1.

The reflection method uses two heat sources, i.e. Z1 and Z2, whose temperatures are different. The following radiation then reaches the camera lens:

- two heat sources Z_1 and Z_2
- reflected from the tested object $(1 - \varepsilon)M_{Z1}$ or $(1 - \varepsilon)M_{Z2}$
- reflected from the mirror M_{Z1} or M_{Z2}
- own properties of the tested object $\varepsilon Mc(T_0)$.

In the reflection method, the emissivity coefficient is calculated based on equation (4) [11]:

$$\varepsilon - 1 = \frac{M_1 - M_2}{M_{Z1} - M_{Z2}} \quad (4)$$

where: M_1, M_2 – existence of the test body illuminated by the source Z_1 and Z_2, M_{Z1}, M_{Z2} – existence of the first and second light sources.

The method with a reference body requires the use of two objects, one of which has a known emissivity ε_r. Both objects, i.e. the tested and reference objects, are located next to each other so that the impact of the environment is the same. This will make the temperature T0 for both objects the same. The next step is to determine the existence of both objects. The actual emissivity of the tested object is calculated in equation (5) [10].

$$\varepsilon = \varepsilon_r \frac{M_1 - M_\alpha}{M_2 - M_\alpha} \quad (5)$$

where: M_1, M_2 – the existence of the test body and the reference one, M_α – ambient radiation energy using a mirror covering the object and with a reflection coefficient of ρ = 1 [9], ε_r – emissivity of the reference body.

In the practice of thermal imaging measurements of mechanical objects, the calorimetric method is most often used. People measuring with an IR camera use thermocouples anyway when configuring the camera, which is carried out so long that the temperature from the thermocouple and the IR camera is the same. In this method, special attention should be paid to the background temperature [11]. However, in thermal imaging measurements in buildings and engineering structures, the method with a reference body is a popular method. Method with a reference body is similar to the calorimetric method because two measurements are performed simultaneously, i.e. a reference and a real object. In the camera settings, the emissivity value is changed for such a long time to obtain the same temperature values in the examined objects [8].

3. Research methodology

3.1. Purpose and object of thermovision research

The aim of the tests was to determine the temperature distribution of the brake disc and elements in its surroundings during braking on the 111Ed-004 electric locomotive (Fig. 2) for compliance with the requirements of UIC and TSI Loc&Pas [1, 7]. The locomotive is equipped with a friction disc brake [17].

Fig. 2. View of the electric locomotive 111Ed-004 on the experimental track in Żmigród

The object of the tests was the Knorr-Bremse (KB) disc brake assembly located on the bogie of the electric locomotive (Fig. 3a and 3b) and the drive system components located in its vicinity [3, 16, 20].

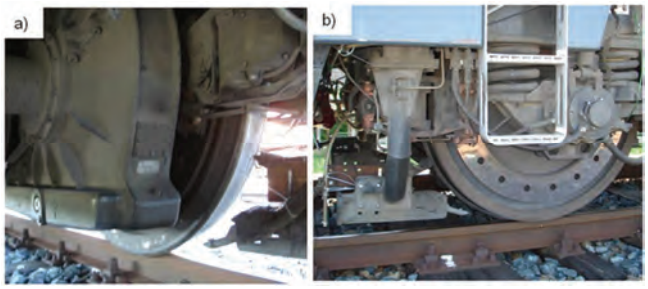

Fig. 3. Object of thermal imaging tests: a) view of the disc braking system and drive gear from the locomotive chassis, b) view of the braking mechanism outside the locomotive

In addition, after a series of emergency and service braking, the temperature increments of the components located in the immediate vicinity of the brake disc, such as the drive gear, springs of the first degree of suspension, the bogie frame, the bearing housing and the rim of the railway wheel, were determined [10]. The influence of the temperature increase (local overheating) on the increase in stresses in the material and its deformations is described in more detail in [1, 14]. The temperature values of the mentioned elements were referred to the initial state before starting the temperature tests.

3.2. Research method

The tests of the temperature distribution of the brake disc were carried out using a FLIR e60 microbolometer camera. The tests were carried out in field conditions on the test track of the Railway Institute in Żmigród.

The thermovision tests were preceded by the initial configuration of the camera settings to the conditions that occurred during the test on the locomotive chassis. The parameters necessary to make settings in the IR camera are air temperature, reflected temperature, humidity, and distance from the tested object. The camera was mounted in a housing attached to the opposite side of the tested brake disc, with elements located in its immediate vicinity, as shown in Fig. 4.

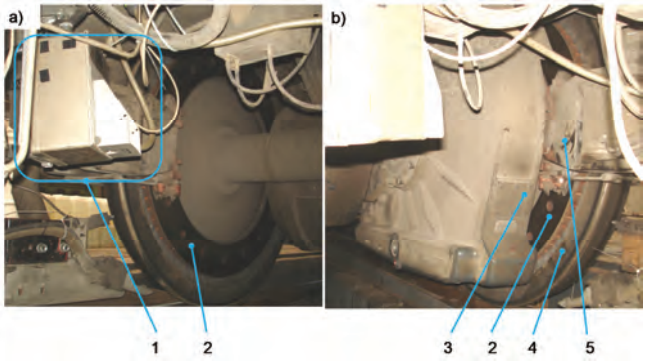

Fig. 4. View from the locomotive chassis with the tested objects: a) view of the housing with a thermal imaging camera mounted (1) at the left wheel of the wheelset, b) view of the tested elements with a thermal imaging camera: 2 – brake disc, 3 – drive gear housing, 4 – drive wheel rim, 5 – disc brake caliper

In the process of configuring the camera for the conditions that existed before the tests, special attention was paid to determining the emissivity coefficient ε.

In the case of testing the temperature distribution of the elements around the brake disc, as shown in Fig. 3b, it was possible to determine one common value of the coefficient ε. These elements are characterized by low reflectivity due to the rough and dark surface, which translates into a high value of the emissivity coefficient. However, in the case of the brake disc itself with a luminous (polished) friction surface characterized by high reflectivity (reflection coefficient), a low value of the emissivity coefficient is introduced. During thermal imaging studies of objects characterized by high reflectivity, using the calorimetric method described in [2, 6], it was possible to determine the actual emissivity coefficient. However, in the case of testing the temperature distribution of rail vehicle components during braking, characterized by different values of the emissivity coefficient, it was necessary to assume one value of the ε coefficient as for most low-reflectivity components, and in the case of a highly reflective object, such as a brake disc, it is necessary to determine correction factors. For this purpose, the method of comparing the temperature result obtained from the thermal imaging camera with the result obtained from the sheathed thermocouple is used. Figure 5 shows the view of temperature measurement from the brake disc with a sheathed thermocouple in order to determine the correction factor. The same method was used to determine the actual temperature values of vehicle components located in the vicinity of the brake disc. The next step in configuring the thermal imaging camera was to gradually change the emissivity coefficient value to obtain the same temperature value read from the IR camera and from the thermocouple.

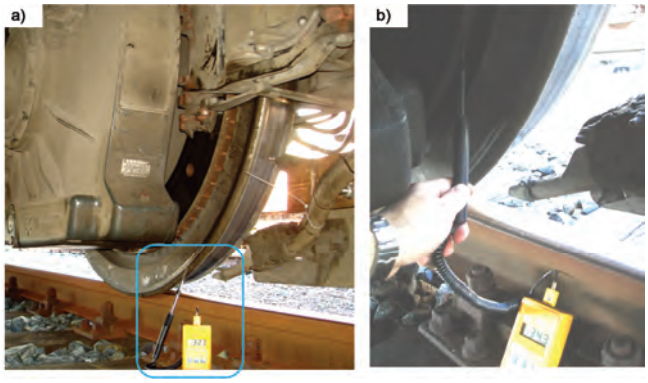

Fig. 5. View of the GTH 1179 temperature sensor with a sheathed probe when measuring the actual temperature of: a) railway wheel, b) brake disc

In the case of testing the temperature distribution on such locomotive elements as the frame, the housing of wheel set bearings, and springs of the first degree of suspension, a thermovision measurement was carried out before the test and after a series of emergency and service braking from the set braking speeds of the locomotive. Figure 5 shows the view of the tested vehicle elements located in the vicinity of the brake discs. The thermal images recorded using a thermal imaging camera were then analyzed in the FLIR Tools program. Figure 6 shows an example thermogram of a disc from a brake disc with measuring points Sp1, Sp2 and Sp3 inserted. These points made it possible to measure the temperature values on three radii of the brake disc. This was necessary to determine the correction factor to calculate the actual brake disc temperature.

Then, according to the relationship (6), the correction factor was determined based on [2] the thermovision measurement in relation to the measurement using a thermocouple.

$$K_{(...)} = \frac{T_{TC}}{T_{IR}} \tag{6}$$

where: T_{TC} – temperature value in °C obtained when measured with a sheathed thermocouple, T_{IR} – temperature value in °C obtained when measuring with a thermal imaging camera.

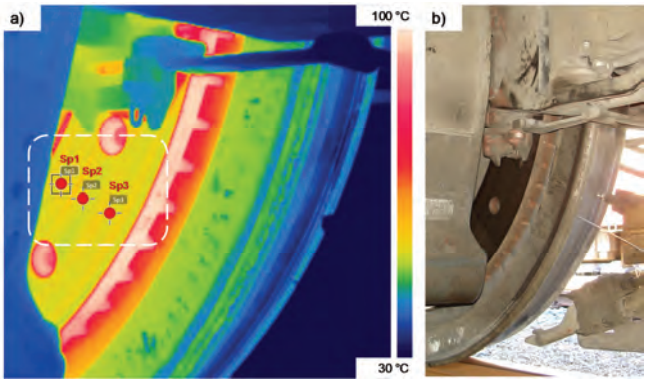

Fig. 6. a) image from a thermal imaging camera of a wheel with a brake disc with measuring points Sp1, Sp2 and Sp3, b) view from the locomotive chassis of a fragment of a wheel with a brake disc in the process of configuring the thermal imaging camera for testing

Then, the actual temperature value of the tested element using the non-contact method using a thermal imaging camera during the locomotive braking was determined in accordance with the following relationship (7):

$$T_{rz\,(\ldots)} = K_{(\ldots)} \cdot T_{IR} \tag{7}$$

where: $T_{rz(\ldots)}$ – the actual value of the temperature of the disc in °C or of the tested locomotive element located in the vicinity of the brake disc.

On the basis of dependencies (6) and (7), correction factors were determined (Table 1) for testing the temperature distribution on the brake disc in motion and on such elements in its vicinity as the brake caliper, wheel and gear housing.

Table 1. Values of correction factors in temperature tests

Tested object	Temperature in °C		Correction factor
	Thermocouple measurement	Measurement with an IR camera	
Brake disc	205.0	90.0	2.278
Wheel	52.0	51.0	1.019
Brake caliper	39.8	35.6	1.118
Drive gear	41.7	41.0	1.017

Table 2. Parameter values of the thermal imaging camera configured for the purpose of testing the temperature distribution of the brake and elements in its surroundings

No.	Parameter	Value
1	Emissivity for objects in the vicinity of the brake disc	0.97
2	Emissivity for the brake disc	0.31
3	Reflected apparent temperature	31°C
4	Distance	1 m
5	Relative humidity	50%
6	Air temperature	31°C
7	External optics temperature	20°C
8	Transmission of the external optical system	1.0

Based on the evaluation of the temperature values determined by the contact and non-contact methods, the actual emissivity coefficients were determined, which, together with the other parameters for the camera configuration, are included in Table 2. Temperature changes in the tested objects on the locomotive chassis were observed from the driver's cab using a Video Grabber converter connected to a camera located under the vehicle. Real-time observation was possible using the Visual Studio 10 software installed on the laptop and a long cable connecting the camera to the laptop via the USB port. The converter allowed for recording analog signals from the camera into digital form on the laptop's hard drive.

4. The course and results of thermal imaging tests

Due to the mounting of the thermal imaging camera on the locomotive chassis, it was not possible to measure the temperature on such elements as the bogie frame, wheel set bearing housings or first-stage springs. Mounting the camera outside the vehicle was not possible due to exceeding the rolling stock gauge. Thermovision measurement of a larger number of elements involves moving the camera away from the tested objects by more than 1 meter so that the radiation emitted by the tested elements is concentrated in the optical system of the camera, and consequently in the camera detector. Therefore, the study of the temperature distribution on the locomotive chassis components was divided into a test in motion and a static test when the locomotive was stopped. The test in motion (during braking) included such elements as the brake disc, wheel, disc brake caliper and drive gear housing). The tangential test (at the moment of stopping the locomotive) was carried out on the frame, bearing housing, springs of the first spring rate, brake caliper and on the wheel (measurement on the wheel disc and wheel rim). Table 3 presents the results of temperature measurements of the disc and elements in its vicinity before the motion tests.

Table 3. Summary of temperature values before testing

Tested object	Wheel 1	Wheel 2
Brake disc	39.9	45.6
Axle bearing housing	37.3	42.6
Railway wheel wreath	40.0	44.7
Trolley frame	34.2	36.9
Ambient temperature T_o = 30.9°C		

Continuous thermovision images were recorded for sudden braking at speeds of v = 100, 120, 140 and 160 km/h. Selected images from the recording of the disc temperature distribution during braking from the speed of v = 160 km/h are shown in Fig. 7.

Example graphs of the peak values of the brake disc temperature recorded from the beginning of braking to stopping the electric locomotive during emergency braking from speeds of v = 120, 140 and 160 km/h as a function of braking time are shown in Fig. 8. The graphs were prepared on the basis of thermal images from a camera located on the locomotive chassis.

On the other hand, Fig. 9 shows the distribution of temperature on such elements located on the vehicle chassis as the housing of the wheel set drive gear, disc brake caliper and wheel rim from the inside during emergency braking from different speeds. The temperature values of the brake disc and other elements of the locomotive were corrected by the coefficient recorded in Table 1.

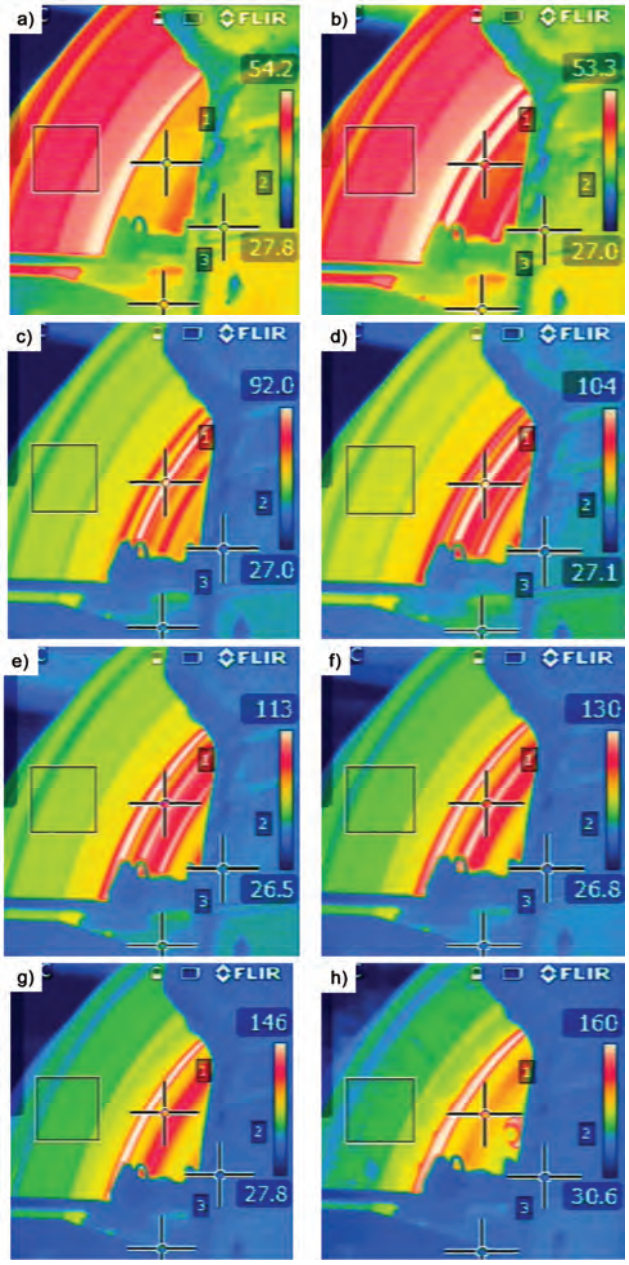

Fig. 7. Selected thermovision photos of the temperature distribution of the brake disc and its surroundings during emergency braking from a speed of 160 km/h; a) before braking, b) 5 seconds of braking, c) 8 seconds, d) 12 seconds, e) 18 seconds, f) 24 seconds, g) 34 seconds, h) stopping

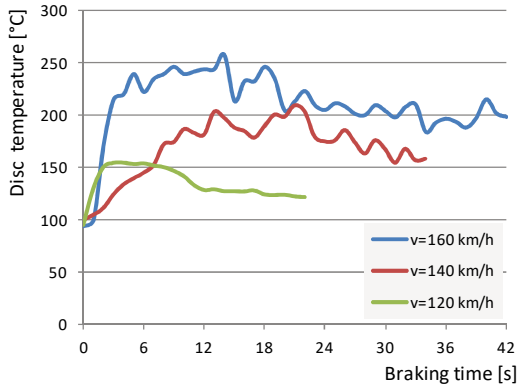

Fig. 8. Temperature distribution on the brake disc during braking from the speed of v = 120, 140 and 160 km/h, emergency (emergency) braking

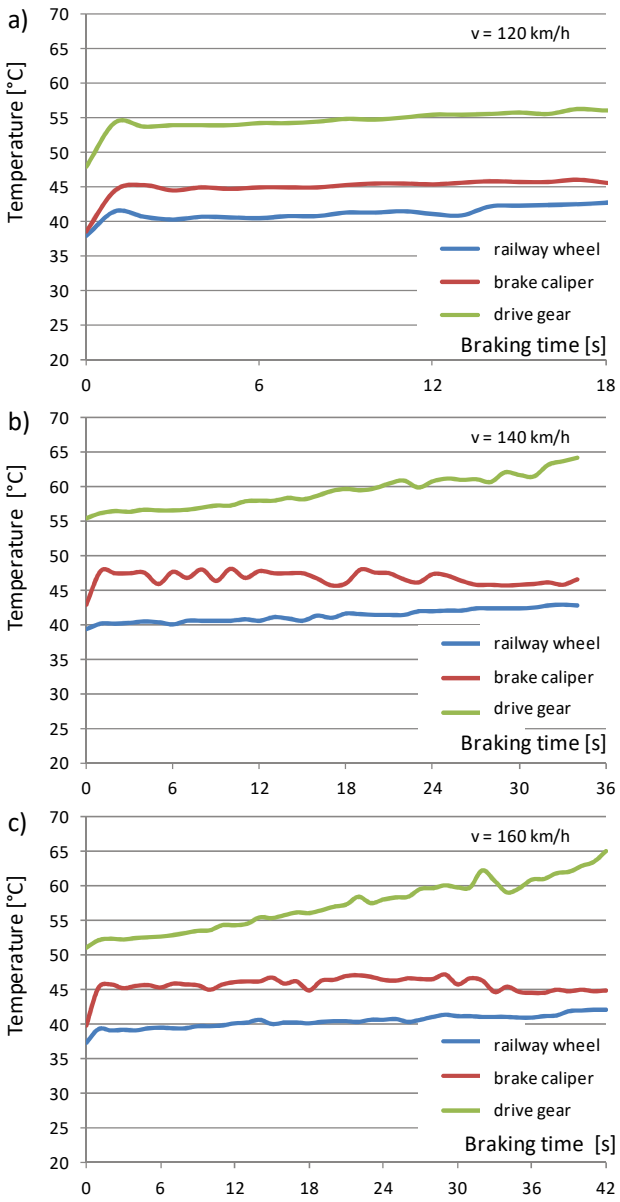

Fig. 9. Temperature distribution on the elements in the vicinity of the brake disc, i.e. the inner side of the wheel, the disc brake caliper and the wheel set drive gear, during braking from the speed of: a) v = 120 km/h, b) v = 140 km/h, c) v = 160 km/h, emergency braking

Figure 10 shows the peak values of the temperature of the disc (I) and the elements in its vicinity for several selected braking speeds (v = 140 and 160 km/h). The blue bars show the temperature before the tests, while the red bars show the temperature after the tests.

Figures 11, on the other hand, show an exemplary combination of both thermal and digital images with the temperature distribution of the disc and elements in its vicinity for one of the wheels of the locomotive. The measurement was carried out in two stages, i.e. before the start of the tests and after a series of 14 brakings.

Figure 12 shows the temperature distribution on the locomotive chassis in order to identify areas with the highest temperature in the vicinity of the brake disc.

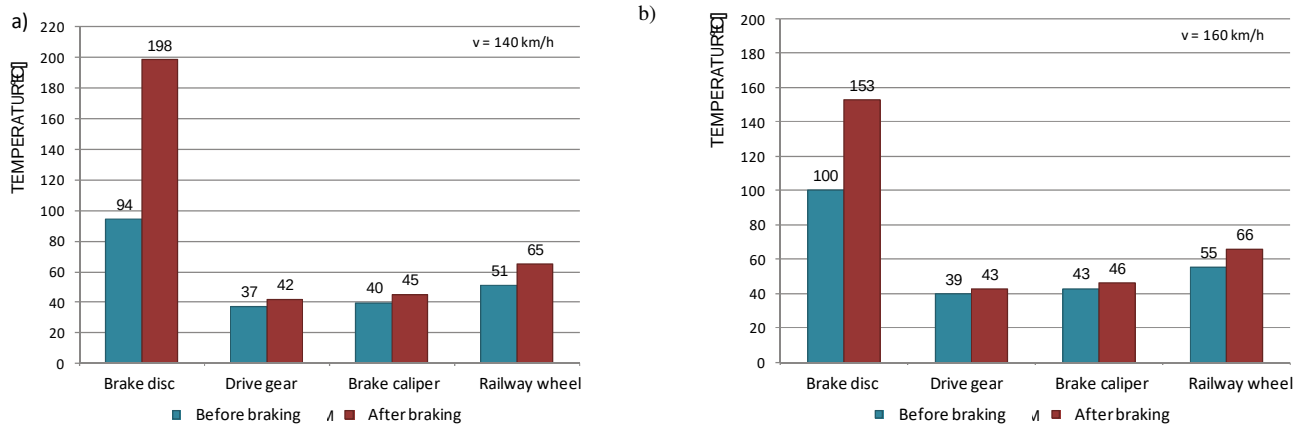

Fig. 10. Temperature increase of the brake disc and elements in its vicinity before and after braking from the speed of: a) v = 140 km/h, emergency braking, b) v = 160 km/h, emergency braking)

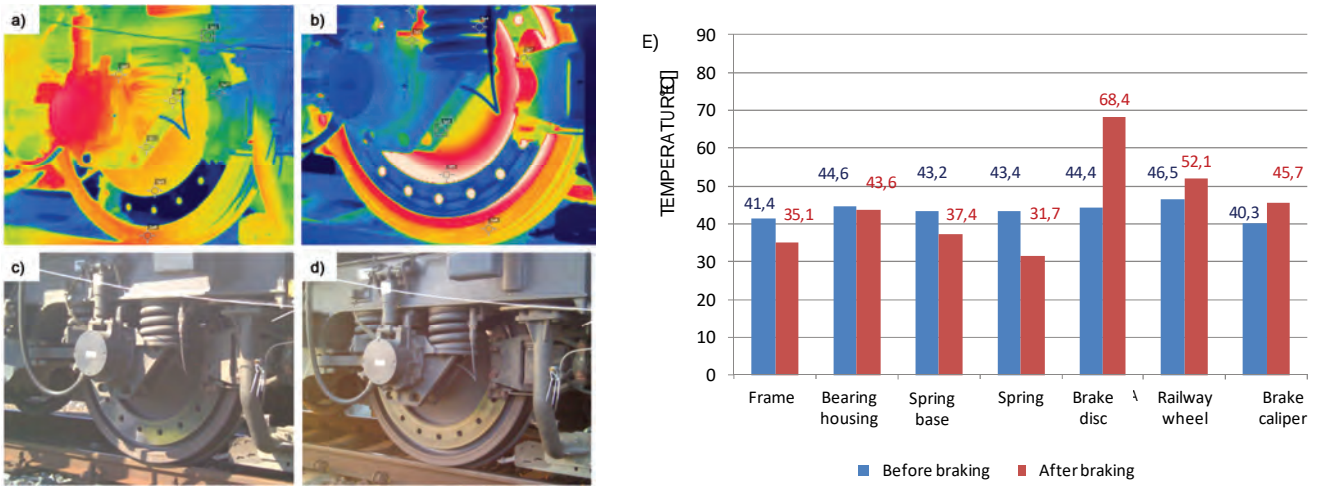

Fig. 11. Temperature distribution in the vicinity of wheel No. 1: a) IR photo before the tests, b) IR photo after the tests, c) digital photo before the tests, d) digital photo after the tests, e) diagram of the maximum temperature distribution of the brake disc and its components environment

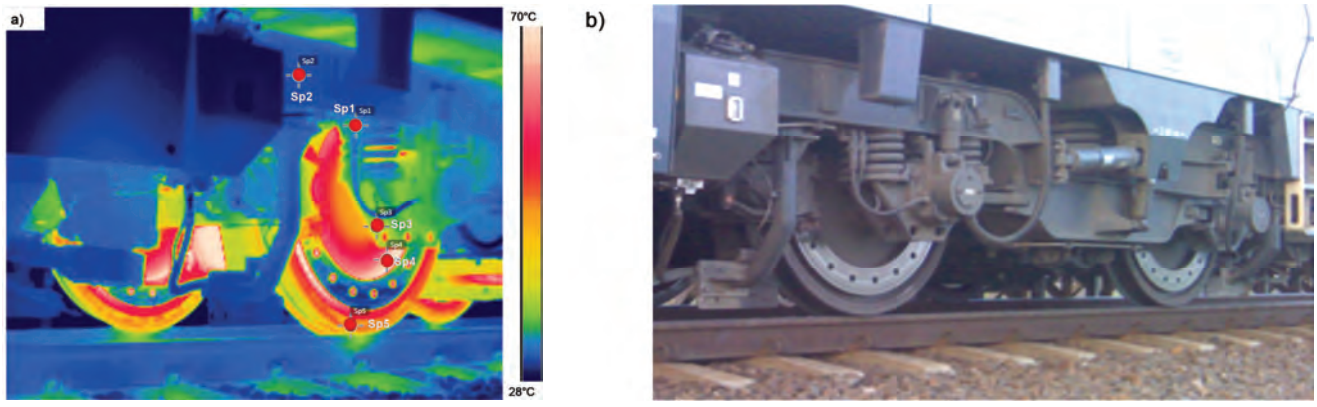

Fig. 12. Temperature distribution on the locomotive chassis after tests on the experimental track after a series of 14 brakings: a) IR photo after all tests, c) digital photo: Sp1 – bogie frame above the brake disc, Sp2 – bogie frame (string member), Sp3 – bearing housing base and springs, Sp4 – wheel disc, Sp5 – wheel rim

The final summary of the maximum values of the temperatures of the brake disc and its surroundings after a series of 14 brakings at various speeds is presented in Table 4. Static tests (vehicle stopped) were carried out in two stages, i.e. in pre-test conditions and also in fixed conditions after a series of braking.

Analyzing the obtained maximum values of the elements located in the immediate vicinity of the brake disc under the locomotive, it was found that the highest temperature increase was observed on the wheel disc (increase by about 33°C (306.15 K) compared to the state before the tests), wheel rim (increase by 15°C (288.15 K)), disc brake caliper (increase by about 34°C (307.15 K)) and the gear

housing of the wheelset drive – increase by 6°C (279.15 K). The brake disc, both during tests in motion and static at speeds of 100, 120, 140 and 160 km/h, does not exceed the value of 400°C (673.15 K) when braking on organic friction linings in accordance with the UIC 541-3 card.

Table 4. Summary of the maximum temperature values after the tests

Point designation	The name of the tested item	Temperature in [ºC]
Sp1	The frame of the trolley surrounded by the brake disc	34.7
Sp2	Bogie frame (string member) above the brake disc	31.3
Sp3	The base of the housing of bearings and springs	38.1
Sp4	Wheel disc	67.3
Sp5	Railway wheel wreath	51.6
Ambient temperature T_o = 26.0°C		

5. Conclusions

Based on the thermovision tests of the temperature distribution of the brake disc and its surroundings in real conditions on the chassis of the 111Ed locomotive, it was found:

a) that individual braking, both service and emergency, do not significantly affect the increase in temperature of components and devices located on the chassis of the tested locomotive. In the test of continuous recording of the temperature distribution with a thermal imaging camera, the maximum temperature increase after emergency braking from a speed of 160 km/h was 5°C (278.15 K) for the gear housing and brake caliper (increase by 12% compared to the temperature before braking) and 14.5°C (287.65 K) for the wheel rim of the wheelset (increase by 23%)
b) in the static test with the use of a thermal imaging camera, after recording the IR image of the locomotive chassis before and after braking, no temperature increases were found on such elements as the frame near the brake disc, springs of the first degree of springing or the housing of wheel set axle bearings (measurement at two points i.e. directly above the bearing and spring support housing). The temperature increase occurred only on the wheel disc, wheel rim and disc brake caliper. The maximum temperature increase values were 40°C (313.15 K) for the wheel disc, 18°C (291.15 K) for the wheel rim and 8°C (281.15 K) for the brake caliper. Under the locomotive, the temperature rise on the wheel was about 33°C (306.15 K), the wheel rim was 15°C (288.15 K), the disc brake caliper was 34°C (307.15 K) and the gear housing was 6°C (279.15 K)
c) the maximum permissible disc temperature was not exceeded after emergency and service braking according to card [1, 6]. Braking from a speed of 160 km/h increases the maximum disc temperature to about 260°C (533.15 K) during braking and about 200°C (473.15 K) when stopping.

Acknowledgements

The investigations were carried out within the Implementation Doctorate Program of the Ministry of Education and Science realized in the years 2021–2025.

Nomenclature

UIC	Union Internationale des Chemins de fer	Ed	electric locomotive with a diesel shunting engine
TSI	Technische Spezifikation für die Interoperabilität	KB	Knorr-Bremse brake system

Bibliography

[1] Czapp S, Szultka S, Ratkowski F, Tomaszewski A. Risk of power cables insulation failure due to the thermal effect of solar radiation. Eksploat Niezawodn. 2020;22(2):232-240. https://doi.org/10.17531/ein.2020.2.6

[2] Karabacak YE, Özmen NG, Gümüşel L. Worm gear condition monitoring and fault detection from thermal images via deep learning method. Eksploat Niezawodn. 2020;22(3): 544-556. https://doi.org/10.17531/ein.2020.3.18

[3] Matusiak K, Goliwąs D, Kaluba M. Adsorption dryer for use in railways. Rail Vehicles/Pojazdy Szynowe. 2022;(1-2):77-85. https://doi.org/10.53502/RAIL-152486

[4] Miao Z, Tu R, Kai Y, Huan G, Kang L, Zhou X. A novel method based on thermal image to predict the personal thermal comfort in the vehicle. Case Studies in Thermal Engineering. 2023;45:102952. https://doi.org/10.1016/j.csite.2023.102952

[5] Ortega-Farias S, Esteban-Condori W, Riveros-Burgos C, Fuentes-Peñailillo F, Bardeen M. Evaluation of a two-source patch model to estimate vineyard energy balance using high-resolution thermal images acquired by an unmanned aerial vehicle (UAV). Agr Forest Meteorol. 2021;304-305(15): 108433. https://doi.org/10.1016/j.agrformet.2021.108433

[6] Pathmanaban P, Gnanavel BK, Anandan SS. Comprehensive guava fruit data set: digital and thermal images for analysis and classification. Data in Brief. 2023;50:109486. https://doi.org/10.1016/j.dib.2023.109486

[7] Rooj S, Routray A, Mandal MK. Feature based analysis of thermal images for emotion recognition. Eng Appl Artif Intel. 2023;120:105809. https://doi.org/10.1016/j.engappai.2022.105809

[8] Ramani V, Martin M, Arjunan P, Chong A, Poolla K, Miller C. Longitudinal thermal imaging for scalable non-residential HVAC and occupant behaviour characterization. Energ Buildings. 2023;287:112997. https://doi.org/10.1016/j.enbuild.2023.112997

[9] Sawczuk W, Pagórek B. Compatibility of the λ-Kolmogorov test of the brake disc emissivity factor distribution in thermal imaging studies. Measurement Automation Monitoring. 2016;2:56-61.

[10] Sawczuk W, Rilo Cañás AM. The issues of hot-spots type in the railway disc brake. Rail Vehicles/Pojazdy Szynowe. 2021;1:33-43. https://doi.org/10.53502/RAIL-138492

[11] Sawczuk W, Rilo Cañás AM. Thermal imaging test of the disk brake of a diesel multiple unit in field conditions. Rail Vehicles/Pojazdy Szynowe. 2020;3:28-36. https://doi.org/10.53502/RAIL-138554

[12] Sangnoree A, Chamnongthai K. Thermal-image processing and statistical analysis for vehicle category in nighttime traffic. J Vis Commun Image R. 2017;48:88-109. https://doi.org/10.1016/j.jvcir.2017.06.006
[13] Song B, Park K, Kim SH, Park G. Comparison of an unmaned aerial vehicle based physical environment with thermal properties from in-situ measurements: Campus of Changwon National University, South Korea. Sustain Cities Soc. 2023;98:104836. https://doi.org/10.1016/j.scs.2023.104836
[14] Stoukatch S, Dupont F, Laurent P, Redouté JM. Package design thermal optimization for metal-oxide gas sensors by finite element modeling and infra-red imaging characterization. Materials. 2023;16(18):6202. https://doi.org/10.3390/ma16186202
[15] Sun H, Zhu HY, Han J, Fu Ch, Chen MM, Wang K. Energy and infrared radiation characteristics of the sandstone damage evolution process. Materials. 2023;16(12):4342. https://doi.org/10.3390/ma16124342
[16] Wu J, Liu J, Zhao J, Su Y. Influencing assessment of different heating modes on thermal comfort in electric vehicle cabin. Energy and Built Environment. 2023. https://doi.org/10.1016/j.enbenv.2023.04.005
[17] Zemlik M, Dziubek M, Pyka D, Konat Ł. Case study of accelerated wear of brake discs made of grey cast iron characterized by increased thermal stability. Combustion Engines. 2022;190(3):45-49. https://doi.org/10.19206/CE-146698
[18] Worsztynowicz B, Uhryński A. The analysis of heating process of catalytic converter using thermo-vision. Combustion Engines. 2015;162(3):41-51. https://doi.org/10.19206/CE-116864
[19] Worsztynowicz B, Uhryński A, Borkowski B, Pluta M. The analysis of thermal state of catalytic converter depending on fuel supply and engine load using thermo-vision. Combustion Engines. 2017;170(3):30-36. https://doi.org/10.19206/CE-2017-305
[20] Zhu H, Lian S, Jin M, Wang Y, Yang S, Lu Q et al. Review of research on the influence of vibration and thermal fatigue crack of brake disc on rail vehicles. Eng Fail Anal. 2023; 153:107603. https://doi.org/10.1016/j.engfailanal.2023.107603

Prof. Wojciech Sawczuk, DSc., DEng. – Faculty of Civil and Transport Engineering, Poznan University of Technology, Poznan, Poland.
e-mail: *wojciech.sawczuk@put.poznan.pl*

Dipl.-Ing. Armando Miguel Rilo Cañás – Faculty of Civil and Transport Engineering, Doctoral School of Poznan University of Technology, Poznan, Poland.
e-mail: *armando.rilocanas@doctorate.put.poznan.pl*

Sławomir Kołodziejski, MEng. – Faculty of Civil and Transport Engineering, Doctoral School of Poznan University of Technology, Poznan, Poland.
e-mail:
slawomir.kolodziejski@doctorate.put.poznan.pl

AIR FORCE INSTITUTE OF TECHNOLOGY
INSTYTUT TECHNICZNY WOJSK LOTNICZYCH

ul. Księcia Bolesława 6, 01-494 Warszawa, Poland
tel.: +48 261 851 300; fax: +48 261 851 313
www.itwl.pl e-mail: poczta@itwl.pl

SUPPORTING OPERATIONS & MAINTENANCE OF AERONAUTICAL ENGINEERING:

- tribological diagnostics of lubrication systems in power units and hydraulic systems
- endoscopic examinations of power units
- measurements of operation parameters of power units using one's own and company systems and their analysis

DEVISING AND DEVELOPING NEW DIAGNOSTIC METHODS:

- CT examinations – V/tome/X CT system
- blade vibration measurements using the tip-timing method

NEW TECHNOLOGIES FOR UNMANNED AERIAL VEHICLES:

- technical condition monitoring system of mini jet engine
- hybrid drive of unmanned aerial vehicle

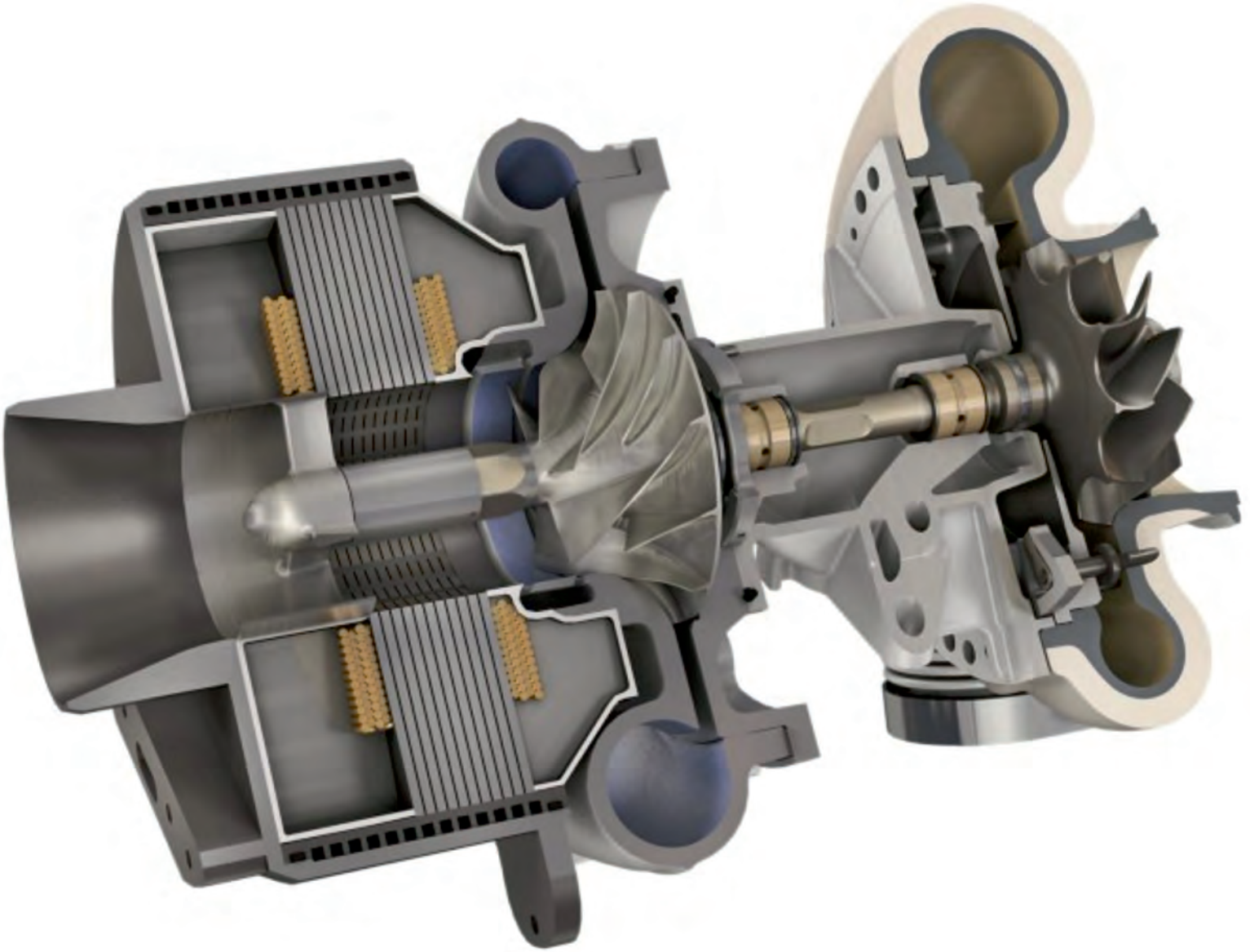

Publisher:

Polish Scientific Society of Combustion Engines

ISSN: 2300-9896
eISSN: 2658-1442

Combustion Engines

Polskie Towarzystwo Naukowe Silników Spalinowych

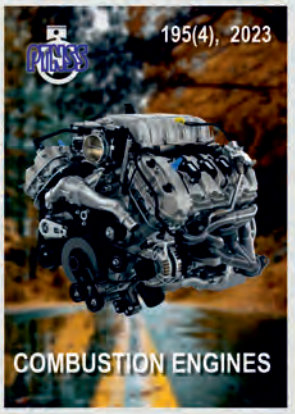

www.combustion-engines.eu